HAL
open science

Synthesis and characterization of bimetallic Pt/Ni particles for the application of catalysis

Noor Hana Hanif Abu Bakar

To cite this version:

Noor Hana Hanif Abu Bakar. Synthesis and characterization of bimetallic Pt/Ni particles for the application of catalysis. Other. Université Henri Poincaré - Nancy 1, 2010. English. NNT : 2010NAN10013 . tel-01748212

HAL Id: tel-01748212

https://hal.univ-lorraine.fr/tel-01748212v1

Submitted on 29 Mar 2018

HAL is a multi-disciplinary open access archive for the deposit and dissemination of scientific research documents, whether they are published or not. The documents may come from teaching and research institutions in France or abroad, or from public or private research centers.

L'archive ouverte pluridisciplinaire **HAL**, est destinée au dépôt et à la diffusion de documents scientifiques de niveau recherche, publiés ou non, émanant des établissements d'enseignement et de recherche français ou étrangers, des laboratoires publics ou privés.

UNIVERSITÉ DE LORRAINE

AVERTISSEMENT

Ce document est le fruit d'un long travail approuvé par le jury de soutenance et mis à disposition de l'ensemble de la communauté universitaire élargie.

Il est soumis à la propriété intellectuelle de l'auteur. Ceci implique une obligation de citation et de référencement lors de l'utilisation de ce document.

D'autre part, toute contrefaçon, plagiat, reproduction illicite encourt une poursuite pénale.

Contact : ddoc-theses-contact@univ-lorraine.fr

LIENS

Code de la Propriété Intellectuelle. articles L 122. 4
Code de la Propriété Intellectuelle. articles L 335.2- L 335.10
http://www.cfcopies.com/V2/leg/leg_droi.php
http://www.culture.gouv.fr/culture/infos-pratiques/droits/protection.htm

U.F.R. STMP
Ecole Doctorale : SESAMES
Chimie et Physico-Chimie Moléculaires et Théorique

Thèse en Co-tutelle UHP-USM

présentée pour l'obtention du titre de

Docteur de l'Université Henri Poincaré, Nancy-I

en Chimie et Physico-Chimie Moléculaires

par NOOR HANA HANIF ABU BAKAR

PARTICULES BIMETALLIQUES. SYNTHESE, CARACTERISATION ET PROPRIETES CATALYTIQUES.

SYNTHESIS AND CHARACTERIZATION OF BIMETALLIC PtNi PARTICLES FOR THE APPLICATION OF CATALYSTS

Soutenue le 2 Mars 2010 à Penang

Membres du jury

Rapporteurs : Abdul Rahman bin Mohamed, Universiti Sains Malaysia, Penang
Prof. Antoine Aboukais, Université du Littoral, Dunkerque
Examinateurs : Wan Ahmad Kamil, Professeur, Universiti Sains Malaysia, Penang
Mohamad Abu Bakar, Maître de Conférences, Universiti Sains Malaysia, Penang (Directeur de Thèse)
Orfan Zahraa, Maître de Conférences, ENSIC, Nancy
Mohammed M. Bettahar, Professeur, Université Henri Poincaré.H.P., Nancy (Directeur de Thèse)

Laboratoire Structure et Réactivité des Structures Moléculaires Complexes
Catalyse Hétérogène (SOR)
Faculté des Sciences & Techniques-54500 Vandoeuvre-lès-Nancy

SYNTHESIS AND CHARACTERIZATION OF BIMETALLIC PtNi PARTICLES FOR THE APPLICATION OF CATALYSTS

by

NOOR HANA HANIF ABU BAKAR

Thesis submitted in fulfillment of the requirements for the degree of Doctor of Philosophy

March 2010

ACKNOWLEDGEMENT

I am grateful to many people who have made it possible for me to complete this thesis. It is with this thought in mind that I would like to take this opportunity to thank them.

First and foremost, I would like to like to express my appreciation to my supervisors, Professor Mohammed M. Bettahar and Associate Professor Dr. Mohamad Abu Bakar as well as my co-superviosors, Dr. Serge Monteverdi and Prof Jamil Ismail for their consistent support, guidance and advice throughout the completion of this work.

My sincere gratitude also goes to Dr. Michel Mercy from the Heterogeneous Catalysis Laboratory in Université Henri Poincaré for his consistent help in accomplishing this work. Thank you also to En. Muthu, Miss Jamilah, Mr. Johari and Mrs. Faezah from the Electron Microscope Department, USM, Dr. Jaafar Ghanbaja from the Electron Microscope and Microanalysis Department, UHP, Mr. Ali as well as the staff from the School of Chemical Sciences, USM. A special thanks to all of them for their much appreciated help.

I would also like to acknowledge the financial support from Universiti Sains Malaysia, Communauté Urbaine du Grand Nancy, Université Henri Poincarée as well as the French and Malaysian governments for the Co-tutelle and ASTS scholarship.

Finally, my heartfelt appreciation goes to my friends and family, who have assisted me in various aspects and have continuously given me much needed support and encouragement. Thank you to all of you.

TABLE OF CONTENTS

Acknowledgement ii

Table of Contents iv

List of Tables xi

List of Figures xii

List of Abbreviations xvii

Abstrak xx

Abstrait xxi

Abstract xxiii

CHAPTER 1 – INTRODUCTION

1.1 A Brief Overview 1

1.2 Problem Statements 2

1.3 Research Objectives 2

1.4 Scope of Study 3

1.5 Thesis Layout 4

1.6 References 5

CHAPTER 2 – LITERATURE REVIEW

2.1 Nanoparticles 6

2.2 Bimetallic Nanoparticles 7

2.2.1 Non-alloyed Bimetallic Nanoparticles 8

2.2.2 Alloyed Bimetallic Nanoparticles 10

2.2.3 Ensemble and Ligand Effects of Bimetallic Particles 13

2.3 Preparation of Catalysts 14

2.3.1 Classical Methods 14

2.3.1.1 Precipitation Technique 15

2.3.1.2 Impregnation Technique 15

2.3.2 Non-classical Methods 17

2.3.2.1 Chemical Reduction 17

2.3.2.2 Microwave Reduction 17

2.3.2.3 Mechanical Attrition 18

2.4 Supports 18

2.4.1 Silicon (IV) Dioxide (SiO_2) 19

2.4.2 MCM-41 20

2.5 Characterization Techniques 21

2.5.1 Temperature Programmed Reduction 21

2.5.2 Temperature Programmed Desorption 22

2.5.3 X-ray Diffraction 25

2.5.4 X-ray Photoelectron Spectroscopy 27

2.5.5 Transmission Electron Microscopy 29

2.6 Application 30

2.6.1 Energy 30

2.6.2 Environment 33

2.6.3 Industries 34

2.7 Bimetallic PtNi Nanoparticles 35

2.8 Benzene 36

2.8.1 Hydrogenation of Benzene 36

2.9 References 39

CHAPTER 3 – EXPERIMENTAL

3.1 Materials 45

3.2 Methods 46

3.2.1 Preparation of Stock Solutions 46

3.2.1.1 Pt/Ni Supported Crystalline Silica Catalysts 46

3.2.1.2 Pt/Ni Stabilized Oleic Acid (Pt/Ni-OA) 46

3.2.1.3 Pt/Ni –OA Supported Crystalline Silica Catalysts (Pt/Ni-OA/Silica) 47

3.2.1.4 Pt/Ni Supported MCM-41 Catalysts (Pt/Ni-MCM) 47

3.2.2 Synthesis of Pt/Ni Supported Crystalline Silica via Co-precipitation. 47

3.2.3 Synthesis of Pt/Ni Supported Crystalline Silica via Co-impregnation 48

3.2.4 Synthesis of Pt/Ni Supported Crystalline Silica via Step-impregnation 49

3.2.5 Synthesis of Pt/Ni Stabilized Oleic Acid Particles 49

3.2.5.1 Effect of Various Concentrations of Oleic Acid 50

3.2.5.2 Effect of Various Reaction Temperatures 50

3.2.6 Preparation of Pt/Ni-OA/Silica Catalysts 50

3.2.7 Preparation of Pt/Ni-MCM Catalysts via Non-classical Method 51

3.2.8 Preparation of Pt/Ni-MCM via Classical Methods 52

3.3 Characterization Techniques 52

3.3.1 H_2-Temperature Reduction (H_2-TPR) 52

3.3.2 H_2-Chemisorption and H_2-Temperature Desorption (H_2-TPD) 53

3.3.2.1 Non-classical Catalysts 53

3.3.2.2 Classical Catalysts 54

3.3.3 Temperature Programmed Surface Reaction (TPSR) 54

3.3.4 O_2-Chemisorption 54

3.3.5 Transmission Electron Microscopy 55

3.3.6 Powder X-ray Diffraction 55

3.3.7 Fourier Transform Infrared (FTIR) 55

3.3.8 X-ray Photoelectron Spectroscopy (XPS) 56

3.4 Calculation Methods 56

3.4.1 Determination of Fractal Dimension 56

3.4.2 Determination of Metal Dispersion 56

3.4.2.1 Borodzinski and Banarowska Method 56

3.4.2.2 H_2-Chemisorption Method 57

3.4.3 Total Surface Area of Metal Phase 58

3.4.4 Particle Size 59

3.4.4.1 H_2-Chemisorption Method 59

3.4.4.2 XRD Technique 59

3.4.5 Degree of Reduction 60

3.5 Catalytic Reaction 60

3.6 Kinetic Studies 62

3.6.1 Determination of Reaction Orders 62

3.6.2 Determination of Energy of Activation 63

3.7 References 64

CHAPTER 4 - THE SYNTHESIS AND CATALYTIC PROPERTIES OF Pt/Ni SUPPORTED SILICA CATALYSTS PREPARED VIA NON-CLASSICAL METHODS

4.1 Introduction 65

4.2 Structural studies 67

4.3 Surface Characteristics 76

4.3.1 H_2-TPR Profiles 76

4.3.2 H_2-Chemisorption 78

4.3.3 H2-TPD Analysis 79

4.3.4 XPS 84

4.4 Effect of Borohydride Reduction 87

4.5 Hydrogenation of Benzene 88

4.6 Summary 90

4.7 References 92

CHAPTER 5 – EFFECT OF IMPREGNATION TECHNIQUE FOR CATALYSTS PREPARED VIA NON-CLASSICAL METHODS

5.1 Introduction 95

5.2 Surface Characteristics 97

5.2.1 H_2-TPR Analysis 97

5.2.2 H_2-Chemisorption 101

5.2.3 H_2-TPD Analysis 102

5.3 TEM Analysis 105

5.4 Catalytic Activity 109

5.5 Characteristics of $Pt_{55}Ni_{45}$-CI Catalyst 113

5.6 Summary 118

5.7 References 120

CHAPTER 6 - CATALYTIC STUDIES OF Pt/Ni STABILIZED OLEIC ACID BIMETALLIC PARTICLES INCORPORATED ONTO SILICA

6.1 Introduction 122

6.2 Formation of Pt/Ni Bimetallic Nanoparticles 123

6.3 Alloying of Pt/Ni Bimetallic Nanoparticles 123

6.4 Morphology 127

6.4.1 Effect of Oleic Acid Concentration 127

6.4.2 Effect of Reaction Temperature 130

6.5 Pt/Ni Interaction with Oleic Acid 131

6.6 Oleic Acid Stabilized Pt/Ni Deposited on Silica 132

6.6.1 Morphology of Active Phase in the Pt/Ni-OA/Silica Catalysts 132

6.6.2 Surface Characteristics 134

6.6.2.1 H_2-TPR Analysis 134

6.6.2.2 H_2-Chemisorption 136

6.6.2.3 H_2-TPD Analysis 136

6.6.3 Benzene Hydrogenation 139

6.7 Summary 141

6.8 References 143

CHAPTER 7 – EFFECT OF REDUCTION CONDITIONS

7.1 Introduction 145

7.2 H_2-TPR Profiles 146

7.3 Effect of Reduction Temperature 146

7.4 Effect of $NaBH_4$ Concentration 151

7.5 Effect of Reduction Medium 155

7.6 Comparison with Monometallic Catalysts at Optimum Conditions 158

7.7 Summary 161

7.8 References 162

CHAPTER 8 - Pt/Ni SUPPORTED MCM-41 CATALYSTS PREPARED VIA CLASSICAL METHODS

8.1 Introduction 163

8.2 Effect of Activation Conditions 165

8.3 O_2-Chemisorption 166

8.4 Surface Characteristics 168

8.4.1 H_2-TPR Analysis 168

8.4.2 H_2-Chemisorption Studies 171

8.4.3 H_2-TPD Profiles 172

8.5 Structural Properties 174

8.6 Morphological Studies 176

8.7 Catalytic Activity 181

8.8 Kinetic Investigations 184

8.9 Classical vs Non-classical Catalysts 187

8.10 Summary 191

8.11 References 192

CHAPTER 9 – CONCLUSIONS

9.1 Conclusion 194

9.2 Recommendations for Future Work 198

LIST OF PUBLICATIONS AND PRESENTATIONS 200

APPENDIX

LIST OF TABLES

Table 3.1: Preparation parameters of PtNi supported MCM-41 catalysts prepared via non-classical methods using co-impregnation technique. 51

Table 4.1: Average particle size, H_2-chemisorption and H_2-TPD studies. 79

Table 5.1: Amounts of H_2 chemisorbed, production and desorbed from H_2-chemisorption, H_2-TPR and H_2-TPD analysis. 103

Table 5.2: Physico-chemical characteristics of supported silica catalysts. 108

Table 6.1: Lattice parameters of PtNi alloys prepared at different ratios 126

Table 8.1: Maximum conversions and temperatures at maximum conversion of the $Pt_{50}Ni_{50}$-MCMC catalyst activated at various conditions. 166

Table 8.2: The degree of reduction of the PtNi catalysts supported MCM-41. 168

Table 8.3: H_2-Chemisorption, dispersion and average particle size of the PtNi catalysts supported MCM-41. 171

Table 8.4: Average particle sizes and distribution of particle shapes of the metallic phase in the PtNi catalysts (a) before and (b) after hydrogenation reactions. 177

Table 8.5: Percentage of conversion, specific rates and TOF values of the PtNi supported MCM-41 catalysts prepared with various PtNi ratios. 184

Table 8.6: Specific rates of the $Pt_{50}Ni_{50}$ and Pt_{100} catalysts supported on MCM-41 prepared via classical and non-classical methods. Catalysts activated at 473 K for duration of 15 minutes in 100 ml/min pure hydrogen. 190

LIST OF FIGURES

Figure 2.1: The influence of particle size on the number of surface, defect and face atoms. 7

Figure 2.2: The effect of the various types of atoms on the conversion of allyl alcohol to propanol. 7

Figure 2.3: Graphical plot of the overall excess of free energy as a function of cluster size, r for heterogeneous and homogeneous nucleation 8

Figure 2.4: Illustrations of typical bimetallic models (a) core-shell morphology; (b) random model and (c) separated model. 9

Figure 2.5: Schematic diagram of the growth mechanism of core shell bimetallic particles. 10

Figure 2.6: Graphical plot of the overall excess of Gibbs free energy, ΔG_r as a function of cluster size, r for alloys and the corresponding monometals. 11

Figure 2.7: Schematic representation of three types of alloys, (a) random, (b) clustered and (c) ordered. 12

Figure 2.8: CO-TPD of PdCo supported Al_2O_3 catalysts prepared with various PdCo ratios. 24

Figure 2.9: XRD diffractograms of (a) $Pt_{core}Cu_{shell}$ (b) $Pt_{core}Cu_{shell}$ after annealing (c) $Cu_{core}Pt_{shell}$ and (d) $Cu_{core}Pt_{shell}$ after annealing. 27

Figure 2.10: The energetics of an x-ray photoemission experiment. 28

Figure 2.11: TEM image of bimetallic particles with core-shell morphology. 30

Figure 2.12: Schematic diagram of a typical fuel cell process for a DMFC. 32

Figure 2.13: Illustration of the hydrogenation of benzene via hydrogen spillover on a support 38

Figure 3.1: Apparatus setup for H_2-TPR, H_2-Chemisorption, H_2-TPD and O_2-chemisorption studies. 53

Figure 3.2: Setup for hydrogenation of benzene. 61

Figure 4.1: XRD diffractograms of (a) the crystalline silica and fresh catalysts and (b) the respective Pt peaks deconvolution. 68

Figure 4.2: XRD diffractograms of crystalline silica, activated catalysts and the respective Pt peaks deconvolution. 69

Figure 4.3: TEM images and particle size histograms of (a) Ni_{100}-P (b) Pt_{100}-P and (c) $Pt_{90}Ni_{10}$-CP catalysts supported on crystalline silica. 71

Figure 4.4: Electron diffraction of (a) Ni_{100}-P (b) Pt_{100}-P (c) $Pt_{90}Ni_{10}$-CP catalysts. 74

Figure 4.5: Line profiles of $Pt_{90}Ni_{10}$-CP supported on crystalline silica. 75

Figure 4.6: H_2-TPR profiles of the various fresh PtNi catalysts supported on crystalline silica. 77

Figure 4.7: H_2-TPD profiles of the various PtNi catalysts supported on crystalline silica. 80

Figure 4.8: H_2-TPD profiles of $Pt_{47}Ni_{53}$-CP without and after activation 83

Figure 4.9: XPS spectra of (a) Pt 4f of Pt_{100}-P (b) Ni 2p of Ni_{100}-P and (c) Pt 4f of $Pt_{90}Ni_{10}$-CP. 85

Figure 4.10: Profiles of the reaction rate of hydrogenation of benzene to cyclohexane for various PtNi catalysts supported on crystalline silica relative to the reaction temperature. 89

Figure 5.1: TPR profiles of (a) Pt_{100}-I and Ni_{100}-I catalysts as well as catalysts prepared via (b) CI and (c) SI technique. 98

Figure 5.2: TPD profiles of (a) Pt_{100}-I and Ni_{100}-I catalysts as well as PtNi catalysts supported on silica prepared via (a) CI and (b) SI technique. 103

Figure 5.3: TEM micrographs of (a) Pt_{100}-I (b) Ni_{100}-I (c) $Pt_{48}Ni_{52}$-SI and (d) $Pt_{55}Ni_{45}$-CI and their corresponding histograms on size distribution. 106

Figure 5.4: Reaction rates of hydrogenation of benzene for (a) Pt_{100}-I and Ni_{100}-I as well as PtNi catalysts prepared via (b) CI and (c) SI techniques. 110

Figure 5.5: (a) SEM micrographs of $Pt_{55}Ni_{45}$-CI and corresponding distributions of (b) Si, (c) O, (d) Pt and (e) Ni. 114

Figure 5.6: XRD diffractograms of Pt_{100}-I and $Pt_{55}Ni_{45}$-CI catalysts prepared via co-impregnation. Diffractograms are obtained after subtraction of the silica peaks. 115

Figure 5.7: XPS profiles of (a) Pt_{100}-I (b) Ni_{100}-I (c) $Pt_{55}Ni_{45}$-CI 116

Figure 6.1: XRD diffractograms of PtNi alloys with different ratios prepared at 80 ºC with 0.02 M oleic acid (a) Pt_{100}; (b) $Pt_{93}Ni_{7}$; (c) $Pt_{78}Ni_{22}$; (d) $Pt_{61}Ni_{39}$ and (e) $Pt_{31}Ni_{69}$. 124

Figure 6.2: XRD diffractograms of PtNi alloys with different ratios prepared using 0.02 oleic acid at 80 ºC (a) Ni_{100} and (b) $Pt_{15}Ni_{85}$. 126

Figure 6.3: Relationship between lattice parameter of PtNi nanoalloys with EDX composition. 127

Figure 6.4: Typical TEM micrographs of (a) aggregated and (b) network formed $Pt_{78}Ni_{22}$ nanoparticles prepared at 353 K stabilized oleic acid. 129

Figure 6.5: FTIR spectra of (a) pure oleic acid and (b) PtNi stabilized oleic acid. 132

Figure 6.6: H_2-TPR profiles of the PtNi-OA/Silica catalysts prepared using various PtNi ratios. 135

Figure 6.7: H_2-TPD profiles of the PtNi-OA/Silica catalysts prepared using various PtNi ratios. 137

Figure 6.8: Reaction rates of the hydrogenation of benzene for the PtNi-OA/Silica catalysts as a function of temperature. 141

Figure 7.1: Typical H_2-TPR profiles of fresh $Pt_{50}Ni_{50}$-MCM-41 catalysts prepared in various conditions. 147

Figure 7.2: TEM images of $Pt_{50}Ni_{50}$-MCM-41 catalysts prepared with 0.2 M $NaBH_4$ in distilled water at reduction temperatures of (a) 273 K and (b) 313 K. 147

Figure 7.3: Reaction rates for the hydrogenation of benzene by $Pt_{50}Ni_{50}$ supported MCM-41 catalysts prepared using 0.2 M $NaBH_4$ in distilled water at various reduction temperatures. 149

Figure 7.4: (a) SEM images of $Pt_{50}Ni_{50}$–MCM-41 prepared at 273 K using 0.2 M $NaBH_4$ in distilled water and line profiles of (b) Si and O and (c) Pt and Ni. 150

Figure 7.5: TEM images of the $Pt_{50}Ni_{50}$ catalysts supported on MCM-41 prepared at 273 K using 0.3 M $NaBH_4$ prepared in (a) mixtures of distil water and ethanol and (b) distil water. 150

Figure 7.6: H_2-TPD profiles of $Pt_{50}Ni_{50}$-MCM-41 prepared at 273 K using various $NaBH_4$ concentrations. 153

Figure 7.7: Effect of $NaBH_4$ concentration on the reaction rate of benzene hydrogenation. $Pt_{50}Ni_{50}$ – MCM-41 prepared at 273 K in mixtures of distil water and ethanol. 155

Figure 7.8: Effect of ethanol on the reaction rate of hydrogenation of benzene by $Pt_{50}Ni_{50}$ catalysts supported on MCM prepared using 0.3 M $NaBH_4$ at 273 K. 158

Figure 7.9: H_2-TPD profiles of Pt_{100}, Ni_{100} and $Pt_{50}Ni_{50}$ and MCM-41 prepared at 273 K using 0.3 M $NaBH_4$ in ethanol. 159

Figure 7.10: Reaction rates of hydrogenation of benzene by Pt_{100}, Ni_{100} and $Pt_{50}Ni_{50}$ catalysts supported on MCM prepared using 0.3 M $NaBH_4$ at 273 K in ethanol. 160

Figure 8.1: H_2-TPR profiles of PtNi supported MCM-41 catalysts prepared at various PtNi ratios. 169

Figure 8.2: H_2-TPD profiles of PtNi supported MCM-41 catalysts prepared at various PtNi ratios. 173

Figure 8.3: XRD diffractograms of (a) Pt_{100}-MCM-C and (b) $Pt_{90}Ni_{10}$-MCM-C before as well as (c) Pt_{100}-MCM-C and (d) $Pt_{90}Ni_{10}$-MCM-C after benzene hydrogenation reactions. 175

Figure 8.4: Typical images of the various morphologies (a) spherical (b) mixtures of spherical and rectangular and (c) rectangular nanoparticles in the catalysts. 178

Figure 8.5: TEM images of typical areas in the (a) Ni_{100}-MCM-C and (b) Pt_{100}-MCM-C catalysts as well as their corresponding EDX analysis. 180

Figure 8.6: Profiles of the reaction rate of hydrogenation of benzene to cyclohexane for various PtNi catalysts supported on MCM-41 relative to the reaction temperature. 182

Figure 8.7: The dependence of the reaction rate on the partial pressure of (a) hydrogen (b) benzene. 186

Figure 8.8: Hydrogenation of benzene profiles of the Pt_{100} and $Pt_{50}Ni_{50}$ catalysts prepared via (a) non-classical synthesized at optimum conditions and (b) classical methods. 189

LIST OF ABBREVIATIONS

A	Pre-exponential factor
AAS	Atomic Adsorption Spectroscopy
Ar	Argon
ASA	Silica-Alumina
Bz	Benzene
C	Classical
C_o	Initial conversion
CI	Co-impregnation
CP	Co-precipitation
D	Dispersion
D_F	Fractal dimension
d	diameter
d_{at}	Atomic diameter
$d_{rel(VS)}$	Relative volume surface mean diameter
Ea	Energy of activation
EDAX/EDS	Energy dispersive x-ray spectroscopy
FTIR	Fourier Transform Infrared Spectroscopy
H_2	Hydrogen
He	Helium
I	Impregnation
k	Rate constant
K_B	Chemisorption constant for benzene
K_E	Equilibrium constant

K_H	Chemisorption constant for hydrogen
$NaBH_4$	Sodium borohydride
m	Partial order of hydrogen
MCM-41	Mesotructured aluminosilicate
n	Partial order of benzene
N_A	Avogadro number
Ni	Nickel
O_2	Oxygen
OA	Oleic acid
P	Precipitation
P_{Bz}	Partial pressure of benzene
P_H	Partial pressure of hydrogen
Pt	Platinum
R	Gas constant
r	Rate
S	Total surface area
SiO_2	Silica
SEM	Scanning Electron Microscopy
SI	Step-impregnation
TEM	Transmission Electron Microscopy
TPD	Temperature Programmed Desorption
TPR	Temperature Programmed Reduction
XPS	X-ray Photoelectron Spectroscopy
XRD	X-ray diffraction

Sintesis dan Pencirian Zarah Dwi-Logam PtNi untuk Aplikasi Sebagai Mangkin

Abstrak

Sintesis mangkin zarah dwi-logam PtNi yang disokong oleh silika, disediakan melalui kaedah bukan klasik, dengan menggunakan natrium borohidrat ($NaBH_4$) sebagai agen penurun, telah dikaji secara terperinci. Penyokong silika yang digunakan bagi penyelidikan ini dihadkan kepada silika berhablur dan aluminosilikat mesoporos (MCM-41). Pelbagai teknik penyediaan dan parameter penurunan dikaji bagi memahami bagaimana faktor-faktor ini mempengaruhi struktur akhir zarah PtNi yang disokong oleh silika serta reaktiviti pemangkinan terhadap penghidrogenan benzena kepada sikloheksana. Didapati bahawa kaedah penurunan ini dapat menurunkan sepenuhnya garam-garam logam semasa peringkat penyediaan mangkin. Penggunaan hidrogen ditentukan menggunakan analisis H_2-TPR, yang mana sebahagian besarnya disebabkan oleh permukaan fasa logam yang teroksida semasa penyimpanan.

Kajian terhadap kesan daripada teknik penyediaan menunjukkan bahawa permukaan dan sifat pemangkinan adalah sangat dipengaruhi oleh nisbah PtNi serta kaedah bagaimana garam logam diperkenalkan ke atas penyokong. Mangkin yang disediakan melalui teknik ko-impregnasi umumnya mempamerkan reaktiviti pemangkinan yang lebih baik berbanding yang disediakan melalui teknik ko-pemendakan dan impregnasi berperingkat. Seterusnya, mangkin yang mengandungi kandungan Ni yang tinggi menunjukkan kecenderungan terhadap reaktiviti yang rendah berbanding dengan mangkin yang mengandungi kandungan Pt yang tinggi. Beberapa mangkin mempamerkan reaktiviti yang lebih baik berbanding dengan mangkin monologam Pt. Kajian menunjukkan bahawa reaktiviti yang lebih baik ini disebabkan oleh pengaloian Pt dan Ni serta diikuti pemisahan permukaan oleh Pt.

Bagi memperbaiki reaktiviti pemangkinan, zarah PtNi yang distabilkan oleh asid oleik telah disintesis sebelum diterap ke atas penyokong silika. Kajian ini bertujuan untuk mendapatkan kawalan yang lebih baik ke atas penyelerakan dan pengaloian antara zarah PtNi. Keputusan menunjukkan bahawa walaupun penyelerakan aloi yang lebih baik diperolehi, aktiviti yang sangat rendah diperhatikan. Pemisahan permukaan oleh Ni besar kemungkinan disebabkan oleh kehadiran oksigen daripada asid oleik.

Kesan daripada pelbagai parameter juga dikaji untuk meningkatkan reaktiviti pemangkinan. Suhu penurunan, kepekatan $NaBH_4$ dan medium di mana penurunan dilakukan dipelbagaikan. Kepelbagaian parameter ini mempengaruhi morfologi zarah dan penyelerakan zarah PtNi. Reaktiviti pemangkinan yang optimum diperolehi apabila zarah PtNi yang kecil berselerak terbentuk pada suhu 273 K menggunakan 0.3 M $NaBH_4$ di dalam medium etanol.

Kaedah klasik juga digunakan untuk mensintesis mangkin PtNi yang disokong. Dalam kajian ini, zarah PtNi terbentuk menggunakan H_2 sebagai agen penurun. Beberapa mangkin menunjukkan reaktiviti yang meningkat. Kajian menunjukkan ia disebabkan oleh kesan penambatan ion Ni^{2+} yang menambat Pt kepada penyokong lalu membentuk zarah Pt yang halus dan berselerak yang dapat digunakan bagi tindak balas pemangkinan.

Secara umumnya, adalah jelas bahawa zarah aloi dan bukan aloi dwi-logam yang disokong oleh silika boleh meningkatkan tindak balas penghidrogenan jika dibandingkan dengan masing-masing mangkin mono-logam. Namun demikian, nisbah PtNi, teknik penyediaan, persekitaran di mana zarah diturunkan dan penyokong mempengaruhi struktur fasa logam mangkin ini. Oleh itu pemahaman yang menyeluruh ke atas parameter ini adalah penting untuk mensintesis mangkin dengan ciri-ciri tertentu yang diingini.

Synthèse et Caractérisation de Particule Bi-métallique PtNi pour l'Application de la Catalyse

Abstrait

La synthèse des catalyseurs bi-métalliques de PtNi supportées sur silice préparés par une méthode non-classique a été étudiée de manière approfondie en utilisant le borohydrure de sodium ($NaBH_4$) comme réducteur du précurseur métallique. Les supports silice utilisés ont été limités à la silice cristallisée et à l'aluminosilicate mesoporeux MCM-41. Diverses techniques de préparation et divers paramètres de réduction ont été étudiés pour déterminer l'effet de structure des particules bi-métalliques PtNi supportées, ainsi que leurs propriétés catalytiques pour l'hydrogénation du benzène en cyclohexane en phase gazeuse. On a montré que cette méthode permettait la réduction totale des sels métalliques pendant l'étape de préparation des catalyseurs. La consommation de l'hydrogène par ces catalyseurs, mesurée par réduction en température programmée, a été attribuée à l'oxydation de la surface de métal pendant leur stockage.

Les études de l'effet des différentes techniques de préparation, ont montré que les propriétés de la surface et les propriétés catalytiques sont influencées par le rapport de PtNi et par la méthode de dépôt des précurseurs métalliques sur la surface du support. En général, les catalyseurs qui ont été préparés par la technique de co-imprégnation donnent une meilleure réactivité catalytique comparée à celles donnée par la co-précipitation et par l'imprégnation par étapes. Par ailleurs, les catalyseurs qui contiennent plus de Ni ont montré une plus faible réactivité, contrairement aux catalyseurs plus riches en Pt, plus réactifs. Plusieurs catalyseurs bimetalliques ont démontré une meilleure réactivité que le catalyseur mono-métallique Pt. Les recherches ont prouvé que l'amélioration de la réactivité peut être attribuée à la formation d'alliage de Pt et Ni accompagnée de la ségrégation du Pt sur l'alliage.

Pour l'amélioration de la réactivité, des particules bi-métallique PtNi stabilisées d'acide oléique ont été synthétisées avant l'incorporation sur le support de silice. Cette méthode a pour but une meilleure dispersion pour la fabrication de l'alliage PtNi. Les résultats montrent, en effet, une meilleure dispersion des particules dans les alliages formés mais la réactivité est très faible. La ségrégation du Ni sur la surface de la particule d'alliage, qui se produit en raison de la présence des oxygènes de l'acide oléique, est la cause de la faible réactivité de l'hydrogénation du benzène.

L'effet de plusieurs paramètres de réduction a été également étudié pour augmenter la réactivité catalytique. Trois paramètres ont été étudiés, la température de la réduction, la concentration de $NaBH_4$ et l'environnement dans lequel la réduction a été effectuée. Les variations de ces paramètres affectent la morphologie et la dispersion des particules PtNi. La réactivité catalytique optimum a été obtenue lors de la formation de petites particules PtNi dispersées à la température de 273 K avec 0.3 M de $NaBH_4$ en solution dans l'éthanol.

Les méthodes classiques aussi ont été utilisées pour la synthèse des catalyseurs PtNi supportés. Dans cette étude les particules de PtNi ont été formées la en phase gazeuse en utilisant un traitement thermique sous hydrogène du précurseur métallique calciné. Plusieurs des catalyseurs ont montré une meilleure réactivité que le platine. On a trouvé qu'elle est attribuable à l'effet d'ancrage des ions de Ni^{2+} sur le support et la fixation du Pt sur ces ions. Dans ce cas, les particules de Pt sont très petites, bien dispersées et disponibles pour la réaction catalytique.

En conclusion, il apparaît dans ce travail que les particules bimétalliques supportées, combinées en alliage ou non, peuvent donner lieu à une meilleure réactivité que les catalyseurs monométalliques. Cependant, le rapport de PtNi, la technique de préparation, l'environnement dans lequel les particules sont réduites et le support

affectent la surface de la phase métallique des catalyseurs. Par conséquent, nos résultats montrent qu'il est impératif de comprendre et de contrôler ces paramètres pour synthétiser les catalyseurs possédant les meilleures propriétés.

Synthesis and Characterization of Bimetallic PtNi Particles for the Application of Catalysts

Abstract

The synthesis of PtNi bimetallic particles supported silica catalysts, prepared via non-classical methods using sodium borohydride ($NaBH_4$) as a reducing agent, was studied in detail. The silica supports employed in this work is limited to crystalline silica and mesoporous aluminosilicate (MCM-41). Various preparation techniques as well as reduction parameters were investigated to gain an insight on how these factors influenced the final structure of the PtNi particles on the silica support and their catalytic reactivity towards the hydrogenation of benzene to cyclohexane. It was found that this reduction method enabled total reduction of the metal salts during the preparation stage of the catalysts. Hydrogen consumptions which were detected using H_2-TPR analysis were mainly attributed to surface oxidation of the metal phase during storage.

Studies on the effect of preparation techniques showed that the surface and catalytic properties of the catalysts are largely affected by the PtNi ratio as well as the method in which the metal salts are introduced onto the support. Catalysts prepared via co-impregnation technique generally exhibited better catalytic reactivity when compared to those prepared via co-precipitation and step-impregnation techniques. Further, catalysts with higher Ni content showed a tendency towards lower reactivity in contrast to those with high Pt content. Several catalysts demonstrated enhanced reactivity when compared to the monometallic Pt catalysts. Investigations showed that the improved reactivity can be attributed to alloying of the Pt and Ni accompanied by surface segregation of Pt.

As a means to improve catalytic reactivity, PtNi stabilized oleic acid particles were synthesized prior to incorporation onto a silica support. The intention of this study is to allow better control of the dispersion and alloying between the PtNi particles. Results show that though better dispersed alloys were obtained, very low activity was observed. Nickel surface segregation is likely to be the cause of this due to the presence of oxygen from oleic acid.

The effect of several reduction parameters was also investigated to enhance catalytic reactivity. The reduction temperature, $NaBH_4$ concentration and medium in which reduction was carried out were varied. Variations in these parameters affected the particle morphology and dispersion of the PtNi particles. Optimum catalytic reactivity was obtained when small dispersed PtNi particles were formed at 273 K using 0.3 M $NaBH_4$ in a medium of ethanol.

Classical methods were also used for the synthesis of PtNi supported catalysts. In this study the PtNi particles were formed using H_2 gas as the reducing agent. Several catalysts showed improved reactivity. Investigations show that this is attributed to the anchoring effect of Ni^{2+} ions which anchors Pt to the support, forming fine dispersed Pt particles available for catalytic reaction.

In general, it is obvious that alloyed and non – alloyed bimetallic particles supported on silica can lead to the enhancement of hydrogenation reactions when compared to the respective monometallic catalysts. However, the PtNi ratios, preparation techniques, environment in which the particles are reduced and support influences the structure of the metallic phase of these catalysts. Therefore it is imperative to gain a thorough understanding on these parameters, in order to synthesize catalysts with desired properties.

CHAPTER 1

INTRODUCTION

1.1 A Brief Overview

The term ‘catalyst’ is not novel in today’s society. In fact, the term was first used by Berzelius as early as in the 1800’s [1]. Since then, numerous catalytic processes have been developed to meet the requirements of a particular era. From the production of bulk explosives during World War I to the generation of hydrogen to produce energy as well as environmental catalysts to reduce pollution in our modern civilization, the applications of catalysts has changed with time. Though without a doubt, catalysts are important necessities as they exist in every aspect of our lives, it is undeniable that the main reason research in this area has been kept alive until now, is its tremendous economic benefits.

In recent times, much attention has been devoted to understanding catalysts and their synthesis, to enable the development of catalysts with better efficiency. Increasing interest has been placed on heterogeneous catalysis as they can be regenerated and used frequently, indirectly making them cost effective. With this in mind, various metals, supports and synthesis conditions have been investigated. This has inadvertently brought about the increasing attention in supported bimetallic catalysts especially when in the nanoscale. Nevertheless, these catalyst materials still lack comprehensive fundamental understanding. For

this reason, much work has been focused on studying not only the properties of these materials but also on their synthesis conditions.

1.2 Problem Statements

- The synthesis of supported bimetallic nanoparticles has gained tremendous attention as catalysts as they are known to promote enhanced reaction rates when compared to their monometallic catalysts. Although extensive work has been carried out on PtNi supported catalysts for oxidation reduction reactions, very few have focused on PtNi supported catalysts for hydrogenation reactions.
- A very limited work on PtNi supported silica based catalysts prepared via non-classical techniques exists. The lack of understanding of this particular system disables the design of potential catalysts for hydrogenation reactions.

1.3 Research Objectives

To overcome the above problems, the aims of this study have been to focus on the following:

- To investigate the influence of preparation techniques on the properties and reactivity of the PtNi supported crystalline silica catalysts prepared via non-classical methods.
- To study the effect of pre-stabilized PtNi nanoparticles on the synthesis of supported PtNi catalysts.
- To gain a comprehensive understanding on how to manipulate the reduction parameters of the non-classical method, in order to control the morphology of the PtNi particles on the MCM-41 support.

- To comprehend the nature in which the PtNi exists when prepared via classical catalysts and to compare its characteristics and reactivity with those prepared via non-classical methods.

1.4 Scope of Study

This study has been limited to the synthesis of PtNi bimetallic nanoparticles on silica supports. Both low and high surface area supports namely crystalline silica and aluminosilicate, mesostructured hexagonal framework, MCM-41 were used. Although the main intention of these supports is to control the morphology and nature in which the PtNi bimetallic particles existed, the effect of oleic acid as a stabilizer for the synthesis of PtNi bimetallic particles which were then incorporated onto crystalline silica was also investigated.

Non-classical reduction methods were mainly employed in this study. Sodium borohydride ($NaBH_4$) was used as the reducing agent for the formation of the bimetallic PtNi nanoparticles. Several techniques in relation to how the metal salts were introduced onto the support as well as the influence of various reduction parameters were investigated. For comparison purposes, classical methods whereby hydrogen (H_2) acted as a reducing agent, was also studied.

The surface of the resulting catalysts were mainly characterized using flow methods such as H_2 temperature programmed reduction (H_2-TPR), H_2-chemisorption and H_2 temperature programmed desorption (H_2-TPD). X-ray photoelectron spectroscopy (XPS) was also employed. Other characterization techniques include the transmission electron microscopy (TEM) and scanning electron microscopy (SEM), both equipped with energy dispersive x-ray

spectroscopy (EDAX/EDS) and electron diffraction as well as powder x-ray diffraction (XRD).

1.5 Thesis Layout

This thesis consists of nine chapters. The first chapter is an overview of this thesis. It highlights the research justification, problem statements, research objectives and the scope of this thesis. Chapter two provides a literature survey, which will cover the development in the field related to the subject of this thesis. In chapter three, the detail experimental procedures and techniques are described. The findings of this research are divided into several chapters. Chapter 4 to 7 focuses on the catalysts prepared via non-classical methods while the sole chapter on catalysts prepared via classical methods is presented in Chapter 8. In Chapter 4 and 5, the synthesis, characterization and reactivity of the PtNi supported crystalline silica catalysts prepared via precipitation and impregnation techniques respectively are discussed in detail. The results and discussion in both these chapters have been published in Journal of Molecular Catalysis A and Journal of Catalysis respectively. The following chapter then focuses on the effect of oleic acid stabilized PtNi nanoparticles incorporated onto crystalline silica as potential catalysts. This is followed by a detailed study on the influence of several reduction parameters on the properties and reactivity of the PtNi bimetallic particles supported on MCM-41 in Chapter 7, which has been published in Catalysis Letters. For comparison purposes, the PtNi supported MCM-41 catalysts prepared via classical methods is then presented in Chapter 8. Finally, Chapter 9 provides a conclusion and recommendations for future work in this field.

1.6 References

1. R. A. van Santen, P. W. N. M. van Leeuwen, J. A. Moulijn, B. A. Averill, Studies Surf. Sci. Catal. Vol. 123. 1999, Netherlands: Elsevier Science B. V, pg 3-28.

CHAPTER 2

LITERATURE REVIEW

2.1 Nanoparticles

Nanoparticles are particles that fall in the 'nano' regime which ranges between 1 - 100 nm. In terms of size, these particles bridge between atoms or molecules and bulk materials. Hence, their electronic and geometric properties differ from the two. Nanoparticles exhibit 'quantum effects' whereby the energy levels are an intermediate between both the atoms or molecules and bulk materials [1]. Therefore this creates a bandgap energy unlike the bulk material and atoms/molecules which are continuous and large correspondingly. Metal nanoparticles also posses' unique properties such as an increase in the number of kinks, corners and edges with dangling bonds (unattached atoms that extend out of a surface) [2, 3]. An example of this occurrence is seen in Figure 2.1, where the number of surface and defect atoms increase with the decrease in particle size while face atoms decrease with decreasing particle size [4]. Generally, both the changes in electronic and geometric properties when nanoparticles are formed can be beneficial in catalytic reactions. A demonstration on the influence of the geometric effect of nanoparticles is shown in Figure 2.2. Here it is observed that the hydrogenation of allyl alcohol to propanol on Pd nanoparticles, prefers face atoms of larger particles (1.5-1.9 nm) when compared to other active sites [4].

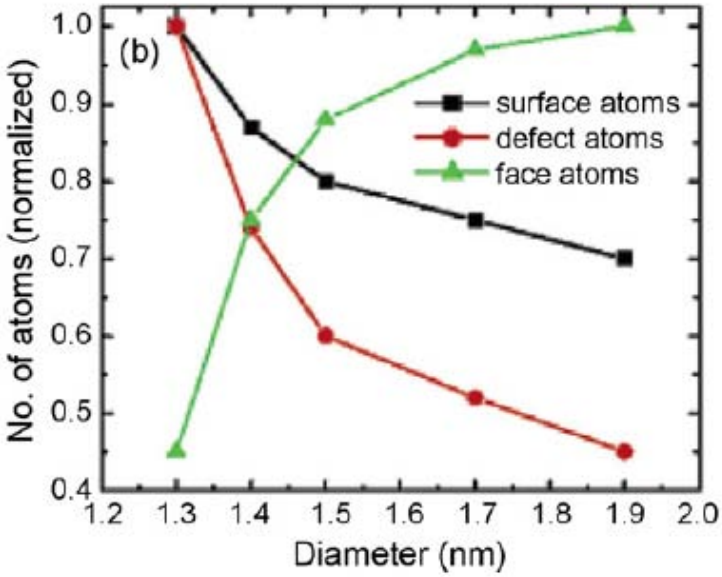

Figure 2.1: The influence of particle size on the number of surface, defect and face atoms [4].

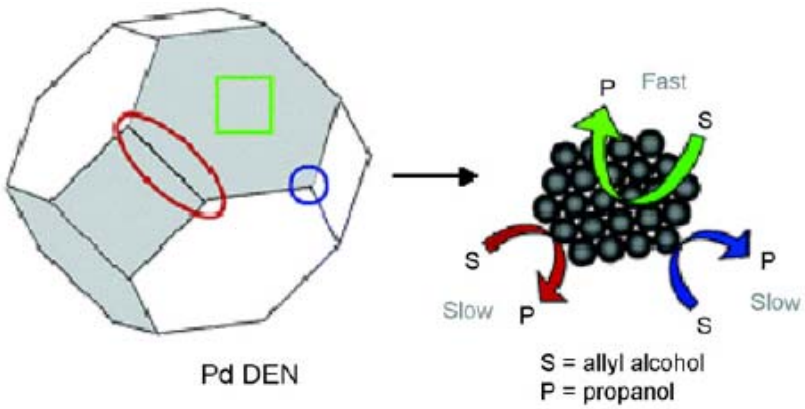

Figure 2.2: The effect of the various types of atoms on the conversion of allyl alcohol to propanol [4].

2.2 Bimetallic Nanoparticles

Bimetallic nanoparticles are formed via the incorporation of two or more metals in a system. Generally they can be categorized as alloyed or non-alloyed bimetallic nanoparticles. The alloyed particles may adopt a random alloy or intermetallic structure while non-alloyed particles result as, cluster in cluster

(atoms of a metal, grouping together) or core-shell structures [5]. A fine line exists between differentiating the existence of alloyed or non-alloyed bimetallic particles. Though several authors have attempted to clarify the differences between the two [6], the question whether a difference between the two exists, is still frequently debated upon.

2.2.1 Non-alloyed Bimetallic Nanoparticles

Generally, the formation of non-alloyed bimetallic particles is governed by the nucleation and growth rates of the metals involved. When two metals exist in a system, the energy required for nucleation of the metals to occur is minimized when compared to a system that contains only one metal. This is illustrated in Figure 2.3 which relates the free energy of a system containing either a type of metal (a homogeneous system) or more than one metal (a heterogeneous system) with the average particle size of the metal particles formed.

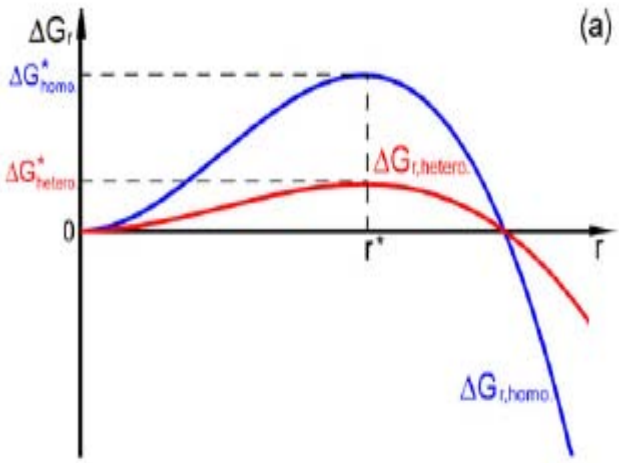

Figure 2.3: Graphical plot of the overall excess of free energy as a function of cluster size, r for heterogeneous and homogeneous nucleation [6].

Various structures of non-alloyed bimetallic particles have been reported. Among them are those that exhibit core-shell, random, separated as well as cluster in cluster morphologies. Some of these structures are illustrated in Figure 2.4.

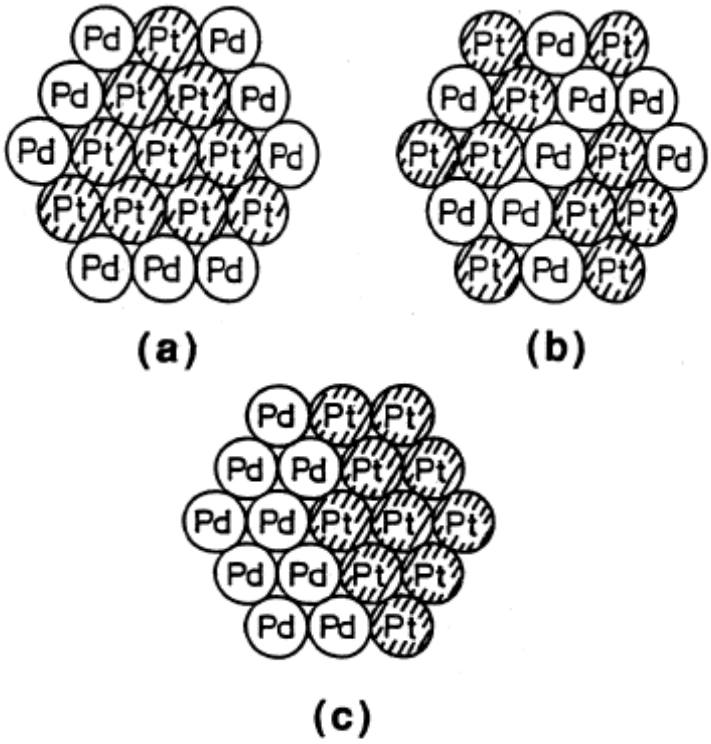

Figure 2.4: Illustrations of typical bimetallic models (a) core-shell morphology; (b) random model and (c) separated model [5].

The formation of either of these structures depends on several factors such as the preparation method and metals involved. Typically, bimetallic particles which exhibit core-shell morphologies consist of a metal forming a core with another metal element surrounding the core to form a shell. A variety of factors influence its mechanism of formation. Among them are the reduction potential of the metals involved [7] as well as the method in which the metals are introduced into a system. Even so, a general mechanism of formation of this bimetallic

structure takes place in two steps. In the first stage, metal ions are reduced to form atoms, which subsequently aggregate into small clusters and grow at the expense of other metal ions. When metal ions of another metal are available, these ions will adsorb onto the surface of the first metal. Successive reduction in a suitable environment will result in a shell surrounding the first metal [8]. A schematic diagram of the growth mechanism is shown in Figure 2.5. Various techniques have been used to prepare bimetallic particles with these structures. Among them are the deposition technique used to prepare RePd and NiPt particles [9] and the chemical reduction technique to synthesize $PtFe_2O_3$ particles [10].

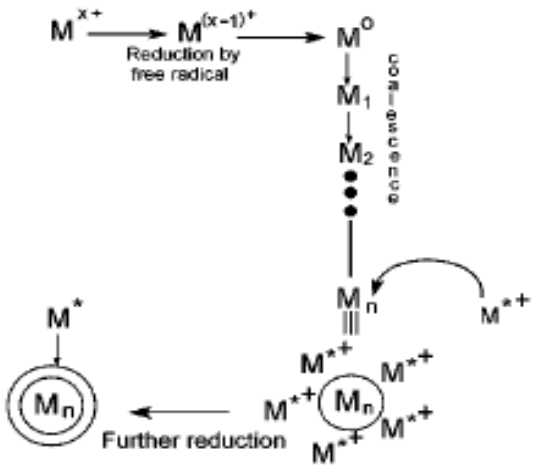

Figure 2.5: Schematic diagram of the growth mechanism of core shell bimetallic particles [8].

2.2.2 Alloyed Bimetallic Nanoparticles

Alloys have been identified as a metallic system consisting of two or more components irrespective of the nature in which the metals are mixed [11, 12]. The formation of these bimetallic particles can best be described in terms of thermodynamics. A simplified explanation is based on the understanding that

alloys occur when the excess of free energy, of the metals involved (ΔG), is negative. Therefore, the enthalpy and entropy of mixing for an alloy can take various values. Typically, most alloys occur spontaneously upon mixing of the metals. In this case, the system has a negative enthalpy of mixing ($\Delta H < 0$) and a positive entropy of mixing ($\Delta S > 0$) [6, 13]. In contrast when the mixing of metals is endothermic, in other words the enthalpy of mixing is positive ($\Delta H > 0$), alloys are formed only at high temperatures as this will lead to a higher contribution from the entropy when compared to the enthalpy of mixing [6, 13]. At low temperatures, the contribution of the entropy of mixing is lower than that of the enthalpy of mixing. Hence, the excess of free energy of mixing is positive. Under these conditions, alloys are not formed as the metals are immiscible [6,13].

The difference in the volume free energy of monometals and alloys formed from these monometals as a function of particle radius gives a good description of the effect of alloying. As shown in Figure 2.6, the volume free energy of alloys is lower than that of monometals.

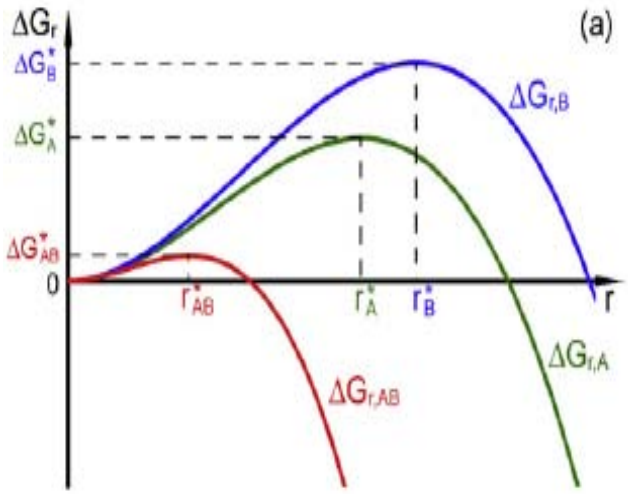

Figure 2.6: Graphical plot of the overall excess of Gibbs free energy, ΔG_r as a function of cluster size, r for alloys and the corresponding monometals [6]

Typically alloys can either take the form of monophasic or biphasic alloys. By definition, monophasic alloys are solid solutions whereby the metals involved exist as a homogeneous phase. In contrast, biphasic alloys occurs when the metals exist in two phases [11]. In this sense, only partial solid solutions are formed. An example of this type of alloy is the segregation of one of the metals to the surface of the alloy. This phenomenon has frequently been reported and its occurrence is dependent on factors such as the enthalpy of mixing, the atomic size of the metals as well as the surface free energies [14].

In addition, alloys can also be classified based on their crystalline order. Three different alloy structures which are known as random, clustered and ordered alloys exist [6]. Typical illustrations of the different types of alloys are presented in Figure 2.7.

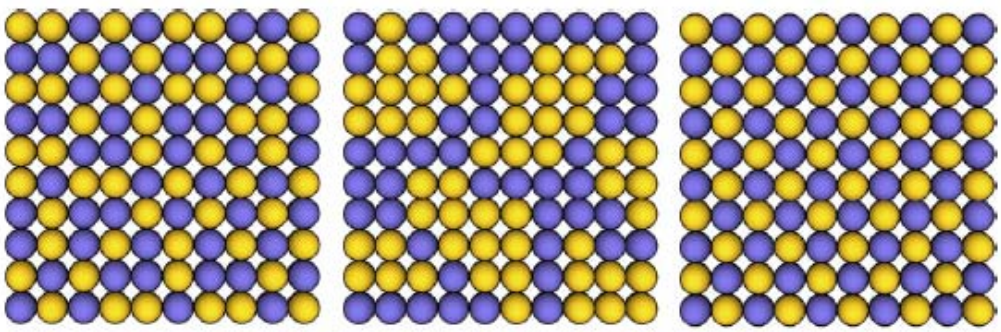

(a) (b) (c)

Figure 2.7: Schematic representation of three types of alloys, (a) random, (b) clustered and (c) ordered [6].

2.2.3 Ensemble and Ligand Effects of Bimetallic Particles

As catalysts, the formation of bimetallic particles has generated a lot of attention due to the benefits they present. Apart from the enhanced reactivity it can exhibit when compared to their respective monometallic catalysts [15], these particles may also demonstrate better selectivity [16] as well as resistance towards deactivation. Much interest has been given to understand how bimetallic nanoparticles influence these properties. Hence, the ensemble and ligand effects have been put forward to better explain these phenomenons.

The ligand effect which is also termed as the electronic effect refers to the modification in electronic interactions that occur between metals in bimetallic systems [17]. This involves electrons in the d band of transition metals. The ensemble effect (also known as the geometric effects) on the other hand explains the enhanced catalytic properties of alloys, in terms of the number of active sites on a surface that is necessary for a reaction to occur [17]. In other words, the selectivity of a reaction can be altered by blocking certain active sites that favor another reaction [14]. Some researches have expressed this as the dilution of actives sites in a metal with a second inert metal [18].

Several authors have attempted to ascribe the enhanced activity and selectivity of catalysts using the ligand and ensemble effects [19]. However, it has been established that the two effects correlate with each other [11, 20]. As an example, when an atom or several atoms of a metal A is placed in an environment of another metal B, such an occurrence cannot be considered solely as an ensemble effect as either metal may have an electronic effect on the other metal due to its close proximity [11].

2.3 Preparation of Catalysts

The preparation of supported metal catalysts can generally be prepared using one of two methods. These methods are widely known as the classical and non-classical methods. In both methods, the techniques in which the metal salts are introduced onto the supports are similar. The variation between the methods lies more in the reduction stage of the metal salts.

2.3.1 Classical Methods

The classical method is frequently used for its simplicity. It also has the advantage in eliminating chemical compounds such as sulfur and chlorine available in the metal salts, which can be poisonous in the final catalytic reaction. Generally, this method is a three step procedure that involves the incorporation of metal salts onto a support, calcinations and finally the reduction of the metal oxides to metal particles in a flow of hydrogen at elevated temperatures. Each step plays a significant role in determining the final properties of the catalyst. As an example, though the aim of the calcinations step is to oxidize the metal ions and to remove poisonous compounds, the temperature at which calcination is conducted can induce changes in the metal particle size as well as the support. In terms of the support, it has been reported that γ-Al_2O_3 changes to α-Al_2O_3 at calcination temperatures of 1300 K [21]. The reduction step can also influence the support. This particularly occurs when reducible oxides such as TiO_2 and CeO_2 are used as supports. For instance, CeO_2 can be reduced to Ce_2O_3 [22]. Even though the calcination and reduction steps are important when preparing catalysts via classical methods, it is no doubt that the technique in which the metal salts are introduced onto the support also plays a crucial role. Basically,

three types of techniques, the deposition, impregnation and precipitation are often employed.

2.3.1.1 Precipitation Technique

This technique entails the formation of an insoluble metal hydroxide or carbonate precipitate upon the addition of a solvent or an acid or base to a metal salt solution. The precipitate can then later be converted to metal oxides via calcinations [23]**.** One or more metals can be precipitated in a system. When two or more metals are involved, sequential or co- precipitation can occur. Sequential precipitation often arises as a result of a large difference in the solubility of the products formed from the original components concerned. Hence, co-precipitation requires a good solubility between the components. Though various metal salt solutions are mixed with the intention of carrying out co-precipitation, sequential precipitation may also occur [24]. This often leads to an inhomogeneity of the metal phase at a macroscopic level [24], which is the main disadvantage of the co-precipitation technique. Contrary to this, if co-precipitation is achieved, very small particles which are beneficial in catalytic reactions can be formed [23].

2.3.1.2 Impregnation Technique

The impregnation of metal salts into a support is typically carried out by mixing an excess of a metal salt solution with a support. The main objective is to occlude the solution into the pores or to allow it to adsorb onto the pore surface of the support [23]. After mixing for a certain duration of time, the catalysts are then dried and subsequently calcined.

The incorporation of large amounts of metal salts is preferable. However, several factors such as the mixing time, temperature, concentration of the metal salt solution and type of metal salt employed during impregnation can influence the final amount of metal salt incorporated into or onto the support. These preparation parameters have been studied extensively by various research groups.

Frequently, longer durations of impregnation time can increase the amount of impregnated metal salt. Though increasing the mixing time is effective, a major drawback of this technique is its extremely long preparation procedure. To overcome this, other researchers have carried out impregnation in several stages. In this technique, a metal salt solution is mixed with the support for a certain time before drying. This procedure is then repeated several times to increase the amount of impregnated metal salts [25]. Subsequently, to further optimize the amount of impregnated metal salt, higher temperatures have also been used during the mixing stage. Gayen et al. [26] used this technique in order to increase the solubility of the metal salt. As a result, they found that higher amounts of Ni nitrate can be impregnated indirectly reducing the number of impregnation stages required.

The impregnation of two or more metal salts onto a support can also be carried out simultaneously (co-impregnation) or subsequently (step-impregnation). In the prior technique, it is important to consider that the affinity of different metal salt solutions to adsorb onto a support varies. Therefore a consequence of utilizing this technique of impregnation is that the final ratio of the different components impregnated may not be the same as that in the metal salt solutions prepared [23].

2.3.2 Non - classical Methods

Non-classical preparation methods generally include those that do not involve calcinations followed by activations at high temperatures for long durations of time. This type of method includes those prepared via physical as well as chemical methods also known as the top-down and bottom-up methods correspondingly. Basically, the main purpose of these methods is to obtain an alternative route to synthesizing catalysts with small metal particles. A variety of non-classical methods have been put forward. However, methods which can be categorized as chemical methods remains the most popular.

2.3.2.1 Chemical Reduction

The chemical method usually involves the use of chemical reagents to reduce the metal salts. This may eliminate the need for a calcinations step and creates an opportunity to reduce the length of activation time. Several chemical reagents such as hydrazine [27], borohydride [28, 29] and alcohols [30] have been used for the preparation of bimetallic catalysts. The variation in reducing strength for the different chemical reagents results in different nucleation and growth rates of the metal particles [31]. This can indirectly influence the final properties of the catalysts formed.

2.3.2.2 Microwave Irradiation

The microwave irradiation technique is a potential reduction method for the formation of metallic particles. This is mainly due to its rapid and uniform heating nature which can lead to particle sizes with a narrow distribution [32]. This reduction technique has been used to prepare several catalysts such as Pd supported silica and alumina [33], PtRu [34] and PtNi [35] supported carbon

catalysts, as well as Pt supported carbon [36, 37]. Generally most of the studies show that metal supported catalysts prepared via microwave irradiation gave rise to small sized particles when compared to other reduction methods [35, 37]. Even so, there exist systems where the metal particles formed by microwave irradiation are larger than that formed via conventional heating [33]. Though the microwave reduction technique demonstrated contrary effects on the particle size, a general enhanced activity was observed for these catalysts when compared to those prepared via other techniques in these studies [33, 35].

2.3.2.3 Mechanical Attrition

This physical preparation method has commonly been employed to prepare alloys, hence is well known as the mechanical alloying technique. In this technique, the particles are formed via structural decomposition of coarser grained structures [38]. Examples of the application of this technique are the preparation of NiB-MgNi composites [39] and CoNi alloys for oxygen reduction reactions [40]. Though this method has been reported to be popular for the formation of nanocrystalline materials [38], one of its drawbacks is its difficulty in obtaining a narrow size distribution of the particles as well as controlling the particle size so that small sized particles are formed.

2.4 Supports

An early concept of typical supports is that this carrier for metal species is a non-reactive compound that is thermally stable even at high temperatures. Today, this perception of supports has altered. It is now well known that supports can also be involved in catalytic reactions. Generally, the choice of support can modify the behavior of a metal in numerous ways. It not only provides a means in

controlling particle morphology in terms of both shape as well as size, but also changes the reducibility of a metal. The use of mesoporous supports can lead to the synthesis of small sized particles provided that growth of the particles occurs in the pores of these supports [41]. In contrast, the reducibility of metal ions or oxides on the other hand is dependent on the strength of metal support interaction. It has been shown that reducible supports can lead to strong metal support interaction [42]. Furthermore, supports can also contribute to the selectivity and catalytic activity directly via spillover species on the support or by the availability of certain sites necessary for a reaction [43]. All these factors can indirectly influence catalytic activity.

2.4.1 Silicon (IV) Dioxide (SiO_2)

Silicon dioxide or better known as silica is composed of a silicon (Si), the second most available element on earth and two atoms of oxygen (O) [44]. It exists naturally in the form of quartz or sand. Silica can form both crystalline as well as amorphous structures. Among the various crystalline forms known are quartz, tridymite and cristobalite. The majority of the crystalline silica is composed of repeating tetrahedron SiO_4 units, which are bound together by their tops hence sharing an oxygen atom [45]. In contrast to crystalline silica, the amorphous state exists as anhydrous glass and hydrated colloidal silica [45].

Silica has long since been used as supports for metal particles as they are chemically inert and have high thermal stability. Among the numerous metals supported on this carrier are NiCu [46], Ni [47, 48] and NiB [49]. Though this support has been widely used due to its low cost, current trends are now turning

to the use of mesoporous silica as this category of silica provides a larger surface area when compared to the traditional silica.

2.4.2 MCM-41

This mesoporous ordered silica material was discovered in 1992 by researches from the Mobile Central Research Laboratory [50, 51]. Its structure is composed of hexagonal shaped pore walls that are amorphous. Even so, the ordered nature of these pores results in the material adopting a long-range crystallinity characteristic [52]. Typically the pore sizes range in the nano regime of 1.5-10 nm, hence this provides the material with a high specific surface area of approximately 1000 m^2 g^{-1} [53]. Though this feature as well as its enhanced thermal stability is advantageous as a catalyst support, its poor acidity and redox properties limit its potential in several catalytic reactions [54]. Other established characteristics of siliceous MCM-41 is it's hydrophobic nature as well as its small amounts of OH sites on its surface including three types of silanol groups. These silanol groups are significant in surface modification reactions such as silylation [51]. These materials only show weak acidity hence are only promising for reactions that do not require strong acidity. This inconvenience has been overcome by incorporating metal species into the silica framework. Though this can cause deterioration in the long range ordered structure, it creates active centers which can improve catalytic behavior. For instance, incorporation of aluminium in the MCM-41 framework is known to form acid sites that can be advantageous for reactions that require strong acidity [55].

2.5 Characterization Techniques

In the early 1900s, a lack of fundamental understanding of the surface properties of supported metal catalysts especially bimetallic catalysts existed mainly due to the limitation in characterization tools. During this era, techniques such as magnetic moments and electrical conductivity measurements were mainly employed [12]. Better understanding of catalysts was only obtained from the 1950's when spectroscopic techniques were introduced as a means to investigate properties such as the surface of catalysts [56]. Since then, numerous characterization tools have been established, enabling researches to gain better insight on the properties of catalysts.

2.5.1 Temperature Programmed Reduction (TPR)

Temperature programmed reduction is a dynamic flow technique that provides information on the reducibility of metal oxides or metal ions in catalysts which are prepared via classical methods. It also gives an insight on the extent of reduction of the metal phase for catalysts synthesized using non-classical methods. The basic principle of this technique involves flowing diluted H_2 through a sample, while increasing its temperature at a predetermined rate. Metal oxides or metal ions available in the catalysts will consume hydrogen forming metal nanoparticles in a reduced state. Generally, the position of the peak at which H_2 consumption occurs, gives information on the temperature at which the metals can be reduced, the state in which the metals exist whether as ions or oxides, the strength of metal-support interaction as well as the size of the metal particles. For bimetallic supported catalysts, this surface characterization technique indirectly demonstrates how the addition of a second metal to a metal

supported catalyst, influences these characteristics. For instance, a study on silica-alumina (ASA) supported nickel catalysts demonstrates that the metal-support interaction decreases with increasing Ni content in the sample or as a result of the addition of Pd in the catalyst. This is elucidated by the decrease in temperature at which H_2 consumption for the NiO occurs [57]. Further, upon the addition of Li to the Ni/ASA catalyst, different metal species are observed. Peaks arising at 670, 720 and 820 K are indicative of various nickel oxides while the peak at 944 K corresponds to nickel in a cationic form [57]. Other research groups have also described the use of this characterization technique to comprehend similar characteristics of various catalysts [58, 59].

2.5.2 Temperature Programmed Desorption (TPD)

This dynamic flow method was originally applied to evaluate the strength of interactions between a surface and an adsorbed species as well as the reaction sites available on a catalyst [60, 61]. Its concept is based on the availability of sufficient thermal energy to break bonds between an adsorbent and its adsorbate. This is accomplished by applying a temperature ramp to the sample. Samples which are initially treated in a reactive gas such as H_2, desorbs the reactive gas into a passing non-reactive gas. The amount of adsorbate desorbed as a function of temperature is followed giving rise to desorption peaks. The peak positions and intensity are dependent on several factors such as the support and metal involved, the adsorbate as well as the pretreatment conditions [43]. The application of this technique to characterize the surface of catalysts has been demonstrated by Li and coworkers [62]. They described the desorption of H_2 from PtNi supported on carbon nanotube catalysts. It was shown that the

temperature at which desorption occurs shifted to lower temperatures with the addition of Ni to Pt. This is due to hydrogen spillover and suggests a strong interaction between Pt and Ni.

Further, the surface composition of bimetallic catalysts can also be evaluated using carbon monoxide (CO) TPD. This reactive gas is frequently employed to investigate the different surface adsorption sites available especially when Pd is involved. This is due to the fact that CO favors different adsorption sites on Pd when compared to other metals. As an example, this reactive gas has been employed for the investigations of PdCo bimetallic catalysts [63]. On Pd, CO adsorption mainly occurs on threefold hollow sites followed by bridge and atop sites. In contrast, adsorption of CO on Co occurs favorably on atop sites. Hence, the CO TPD for pure Pd/Al_2O_3 exhibits a desorption peak at 450 K (three fold hollow sites) while pure Co/Al_2O_3 gives rise to a peak mainly at 390 K (atop sites) with a shoulder at 280 K (bridge sites). When bimetallic $PdCo/Al_2O_3$ catalysts were formed by depositing Pd onto the support followed by Co, changes in the surface properties can clearly be seen with increasing deposition of Co. This is illustrated in Figure 2.8. Based on this knowledge, specific adsorption sites which promote a catalytic reaction can be identified.

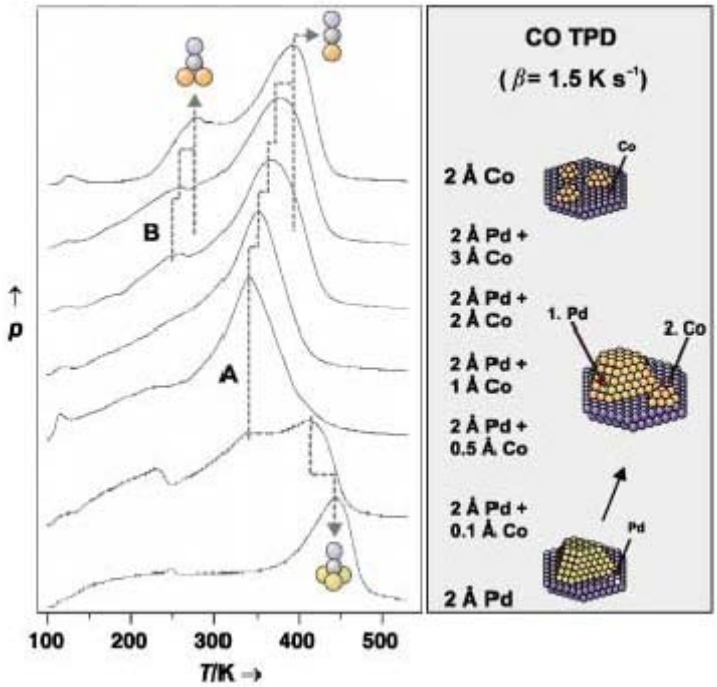

Figure 2.8: CO-TPD of PdCo supported Al_2O_3 catalysts prepared with various PdCo ratios [63].

This technique has also been expanded to characterize other characteristics. Among them is the acidity of the catalysts or their supports. Molecules such as pyridine are used as probes for the detection of acid sites due to their small size, good thermal stability and high basicity [64]. Other molecules such as ammonia [65, 66] and benzene have also been employed for similar purposes. This characterization technique gives an insight on the strength and number of acid sites available on a support or catalyst. However, its main disadvantage is its inability to differentiate Bronsted acid sites from Lewis acid sites. For this reason, this method has at times been supported by characterization methods such as pyridine FTIR.

The acidity of bimetallic catalysts has been studied by several research groups [65, 66]. As an example, valuable information on how the addition of Ni,

to Pt supported zeolite and modernite decreases the acidity of the catalysts irrespective of the preparation technique employed has been obtained [65]. Further, when the acidity of a range of alumina supports were investigated using ammonia TPD, studies showed that γ-alumina, extrudates and tablets show higher ammonia desorption when compared to α-alumina as well as trans-alumina. This is indicative of larger amounts of acid sites available on the earlier supports compared to the latter [67].

Furthermore this characterization tool can also be used to determine the distribution of activation energy for the desorption of hydrogen. This has been described for Ni supported silica catalysts using hydrogen as the probe molecule [68].

2.5.3 X-ray Diffraction

This x-ray technique is employed to comprehend the structure of nanoparticles and gain qualitative elemental information [5]. The basic principle of this characterization method is based on the generation of monochromatic x-rays from a cathode ray tube. These x-rays are directed to a sample resulting in the emission of scattered waves from the atoms. A diffracted radiation is formed when these waves interfere with each other. Its intensity is largely influenced by the structure of the elements analyzed [69]. Hence this enables the determination of the geometric structure of the particles as well as their average particle size.

In the case of bimetallic particles, this technique is advantageous as it enables discrimination between physical mixtures of different metal particles as well as alloys. In catalysts where mixtures of two or more types of metal particles are present, XRD patterns demonstrate the presence of diffraction peaks for both

the metal particles. In contrast, diffraction patterns of alloys display a different characteristic altogether. Only the reflections of one metal component are usually observed. However their positions are shifted to higher 2θ values when compared to the monometallic metal. This was well demonstrated by Zhou and coworkers who investigated systems composed of Pt and Cu [70]. The XRD diffractograms obtained by this research group is presented in Figure 2.9. As can be seen in Figure 2.9(a), when $Pt_{core}Cu_{shell}$ particles were prepared, the XRD patterns indicated the presence of a Pt core (solid vertical line) as well as a $Pt_{0.2}Cu_{0.8}$ alloy shell (peaks denoted with an asterisk). However, subsequent annealing of this sample led to the formation of PtCu alloys (Figure 2.9(b)). Only the Pt peaks which are slightly shifted to higher 2θ values are observed, as it is believed that the Cu atoms are incorporated into the Pt structure. In comparison, when $Cu_{core}Pt_{shells}$ are synthesized, both Pt and Cu (dotted lines) exist separately as shown in Figure 2.9(c). Annealing of this sample results in a Cu rich $Pt_{1-x}Cu_x$ core with a Pt shell (Figure 2.9(d)).

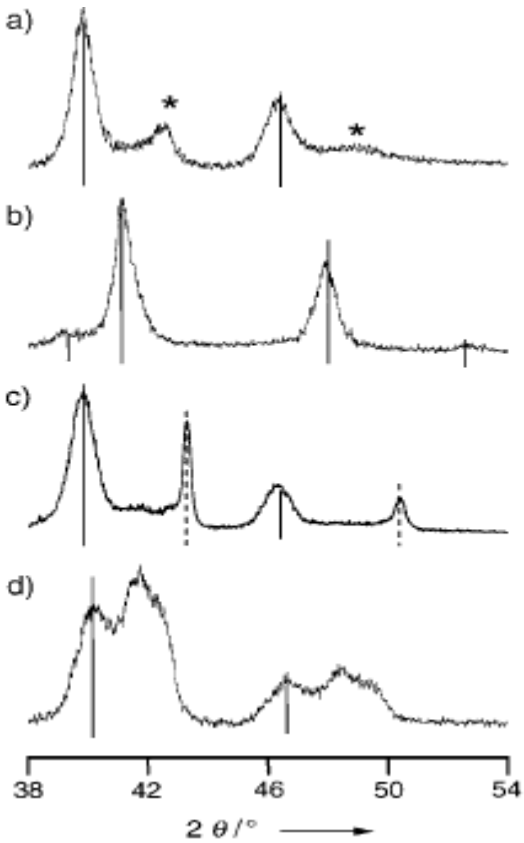

Figure 2.9: XRD diffractograms of (a) $Pt_{core}Cu_{shell}$ (b) $Pt_{core}Cu_{shell}$ after annealing (c) $Cu_{core}Pt_{shell}$ and (d) $Cu_{core}Pt_{shell}$ after annealing [70].

2.5.4 X-ray Photoelectron Spectroscopy

X-ray photoelectron spectroscopy (XPS) is a powerful characterization tool employed to study the surface of solids. It is beneficial in determining the surface composition of a catalysts active phase which usually differs from its bulk. The general theory on how this instrument works can be understood by considering the emission of electrons from a solid induced by a photon energy greater than the work function, Φ (the minimum energy needed to excite an electron from the highest occupied energy level (HOMO) into a vacuum level (that is beyond the lowest unoccupied molecular orbital (LUMO))) of the solid [61]. Electrons from the core and valence bands are emitted. Typically, the core

electrons are insensitive towards its surrounding and maintain binding energies characteristic of the solid. In contrast, the valence electrons which participate in chemical bonding gives rise to peaks characteristic of these interactions [61]. An illustrated description of this process is depicted in Figure 2.10.

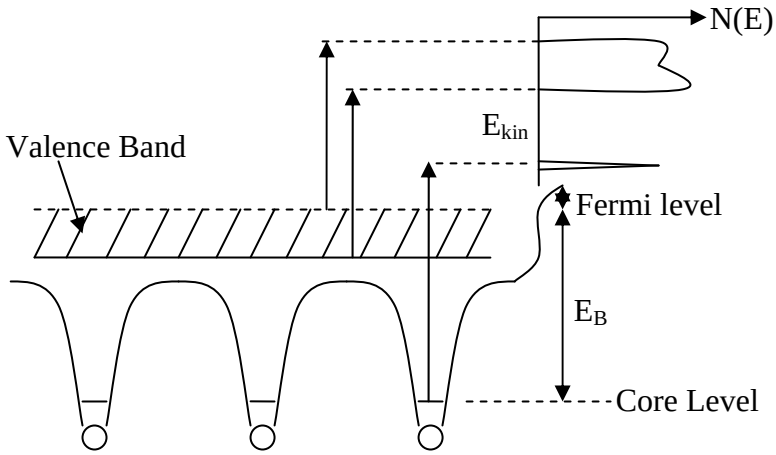

Figure 2.10: The energetics of an x-ray photoemission experiment [61].

The XPS was designed not only to identify elements on the outer most atomic layers of a bimetallic structure but also to detect chemical shifts which are related to the valence state of the elements in question [71]. This technique has been used to analyze various bimetallic structures whether alloyed or non-alloyed. In general alloys are characterized by a shift in the binding energy of an element. This was demonstrated by Park et al. [72] for a series of PtNi alloys. It was shown that the extent in which the energy of the Pt 4f shifted, is influenced by the degree of alloying between Pt and Ni. Though it has been proven that the XPS is a powerful tool for characterizing alloys, it is believed that in some cases, a clear discrimination between the two is difficult. For instance, when AgAu

core-shell bimetallic structures are investigated, XPS profiles show that the main signal observed is of Ag [7]. This indicates that Ag forms a shell surrounding Au. Similarly, segregation of an element in an alloy can also result in intensities of one element. This has been described by other researches [73].

2.5.5 Transmission Electron Microscopy

The transmission electron microscopy (TEM) is an imaging technique which is commonly used to study particle morphology both in terms of shape and size. Its basic principle is based on the penetration of metals by electron beams which are accelerated at certain energy [74]. The extent of electrons which penetrates an element in a sample depends on its molecular weight. Low atomic weight elements allow higher penetration of the electrons giving lighter images while elements with higher atomic weight results in darker images. Indirectly this can facilitate the determination of the different types of bimetallic particles which exist. As an example, Teng and Yang [8] clearly showed the formation of $Pt_{core}Fe_2O_{3shell}$ particles formed via sequential synthesis. This is exhibited in Figure 2.11. Even though this characterization technique has frequently been employed in imaging bimetallic particles, its sole use cannot be extended for the determination of alloyed bimetallic nanoparticles.

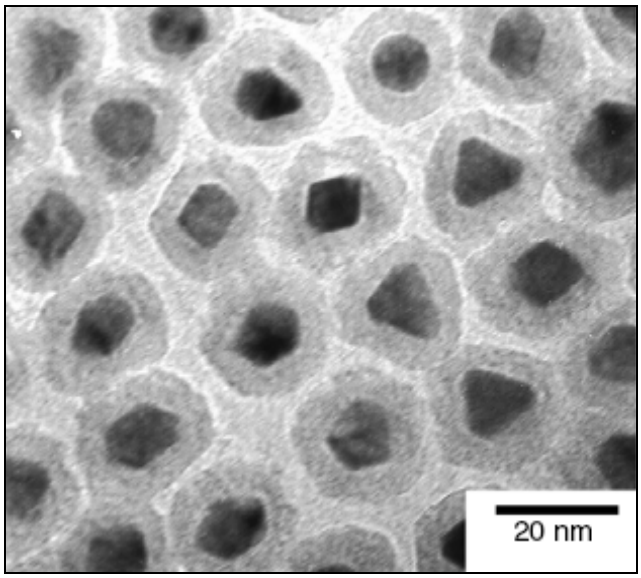

Figure 2.11: TEM image of bimetallic particles with core-shell morphology [8].

2.6 Application

The development of bimetallic catalysts has created opportunities for new technologies as well as the improvement of conventional applications. Bimetallic catalysts can be designed specifically to meet the requirements of various fields. Metals which exhibit different properties can be combined to give rise to catalysts with novel characteristics. Further, with the advancement of nanotechnology, it is hoped that the synthesis of bimetallic catalysts can be controlled to form nanometer scale structures with unique size and shapes for a variety of applications.

2.6.1 Energy

The demands for energy whether for transportation or the generation of electricity has increased steadily over the past decade and will continue to rise with industrial development especially in Asian countries. Efforts have been put forward to reduce the dependency on non-renewable energy sources due to its

diminishing availability as well as the environmental hazards it induces. Hence, this has created a demand for renewable energies.

To date, tremendous attention has been generated towards biofuels as well as fuel cells. Biofuels which at large, are derived from vegetable oils, are traditionally formed via the transesterification process using alkali catalysts such as sodium hydroxide or potassium hydroxide [75]. Though these catalysts efficiently transform the triglycerides to fatty acid methyl esters (FAME), their tendency to form soap (also known as saponification) as a result of the presence of water, has lead researches to find alternative catalysts. Though some have reported the use of metallic catalysts such as FeZn double cyanide metal complexes [76], studies along these lines are still few.

In contrast to biofuels, the application of bimetallic catalysts in fuel cells has been given widespread attention. Both the conventional polymer electrolyte membrane fuel cells (PEMFC) and direct methanol fuel cells (DMFC) employ platinum as catalysts. Generally, these catalysts aid the generation of energy via separating the electron and proton components of fuels such as hydrogen and methanol at the anode. The proton migrates through an electrolyte membrane to the cathode which acts as an insulator for the electrons. This causes the electrons to pass through an external electrical circuit resulting in the production of energy [77]. An illustration of the process is depicted in Figure 2.12 for a typical DMFC [78]. In general, this technology is by far the most promising renewable source of energy. This is because, the supply of fuels such as hydrogen is unlimited and the by-products which are water or water and CO_2 depending on the fuel employed, cause no environmental implications. Even so, one of the most challenging issues in this technology is its high prices due to the platinum catalysts. For this reason,

numerous research groups have actively been working on bimetallic catalysts which may serve as a better option when compared to the Pt catalysts. Practically, the majority of the bimetallic systems investigated to meet the requirements for this technology are Pt based. Among those are the PtCo [79, 80], PtNi [80] and PtCr [80] bimetallic systems.

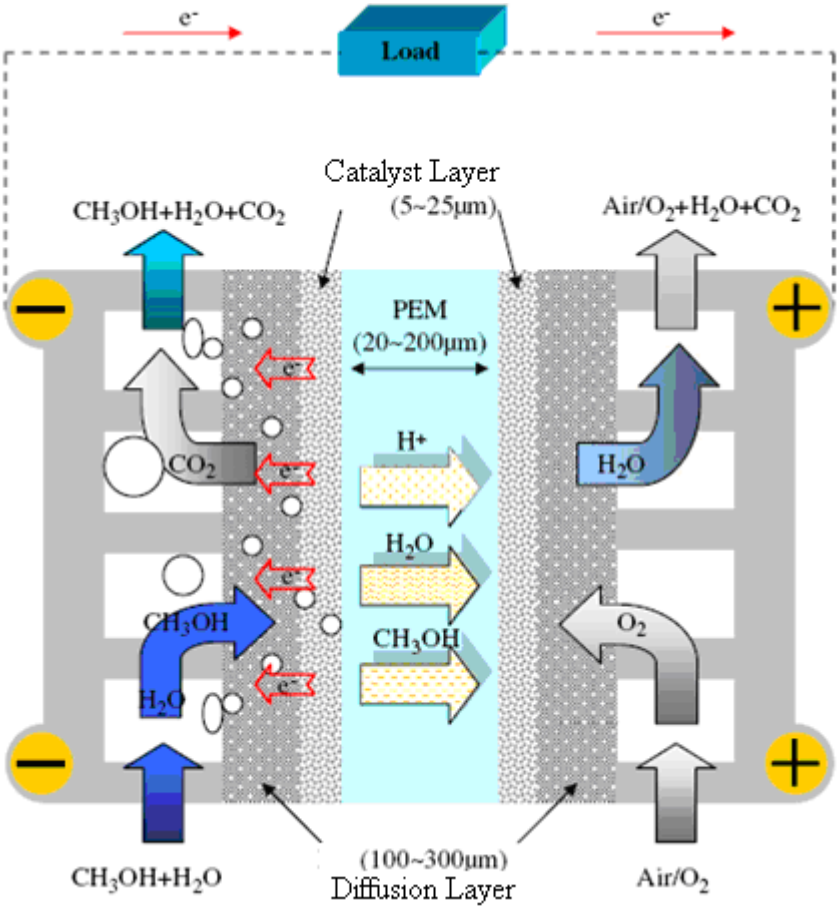

Figure 2.12: Schematic diagram of a typical fuel cell process for a DMFC [78].

2.6.2 Environment

The awareness on environmental issues such as global warming and green house effects have increased considerably over the years. More and more people are being educated regarding its impact on the environment. Knowledge of these threats has forced not only the public to make changes in their everyday life but has also inclined manufacturing and processing companies to ensure that their wastes are free from toxics which can permanently disrupt the food chain. One of the steps towards achieving this is by turning to renewable energy sources, in which bimetallic catalysts play a significant role as explained in section 2.6.1.

Besides this, bimetallic catalysts such as PdFe [81] and PdMg [82] have also been employed for the dechlorination of chlorinated compounds such as hexachlorobenzene (HCB) and polychlorinated biphenyl (PCB). As an example, HCB which is frequently used in chemical industries as well as in agricultural sectors is known to be carcinogenic, hence efficient removal is necessary. Monometallic catalysts such as Fe have been used for this purpose. However, it has been shown that bimetallic Pd/Fe reduces HCB more rapidly. This has been explained as a characteristic of the bifunctional catalyst [81].

Subsequently, bimetallic catalysts have also been employed for waste water treatments. Dyes which are released from textile companies are considered hazardous as they have a high chemical oxygen demand (COD) and can prevent light penetration which can endanger aquatic life [83]. For this reason, Cu/Fe clay catalysts have been developed. In contrast to the original photo Fenton reactions used to address this problem, Cu/Fe clay catalysts are less sensitive towards pH when assisting the degradation of organic dyes such as Acid Black 1 [84].

Volatile organic compounds (VOC) such as benzene, toluene and xylene are another series of chemicals that have posed a risk towards the quality of life. Damage to the ozone layer and its carcinogenic effect on human health are among hazards related to VOC's. Common methods for the removal of VOC's involve their oxidation using bimetallic catalysts such as CuCo supported on Al_2O_3. The catalysts were prepared via polyol process and it was shown that catalysts with high CuCo ratios are easily deactivated. Better activities were observed for the $Cu_{1.25}Co_{3.75}$ supported Al_2O_3 catalysts [85].

2.6.3 Industries

The application of catalysts in industrial processes is not a novel phenomenon. This vital technology has been used in various stages throughout numerous industrial processes for economical as well as environmental purposes. In terms of the economical benefits, various monometallic and bimetallic catalysts have been employed in a variety of industries. The choice of catalyst, depending on the reaction involved.

Bimetallic catalysts have been studied for the conversion of natural gas to methanol or ammonia. Production of methanol normally occurs via steam reforming of methane. This involves a number of catalysts as the whole process is composed of four main stages. Among the stages, the hydrodesulphurization stage employs catalysts such as CoMo [86] and PtNi [87]. The steam reforming stage itself on the other hand traditionally employs Ni as a catalyst [86]. However, this reaction has been tested using NiPt catalysts supported on spinal ($MgAl_2O_4$) [58].

Bimetallic catalysts have also been investigated for application in several other industries. Mingshu et al. [88] demonstrated the potential of PdAu supported silica catalyst for the synthesis of vinyl acetate (VA), which is a well known chemical intermediate used for the production of paints and adhesives. Other studies related to the synthesis of VA using similar catalyst have been presented elsewhere [89, 90]. In contrast, PdPt and PdAu [91] has been described for the formation of hydrogen peroxide (H_2O_2), an oxidizing agent for the production of fine and bulk chemicals. The application of bimetallic catalysts in the few examples described here clearly illustrates the significance of bimetallic catalysts in industries.

2.7 PtNi Bimetallic Nanoparticles

Interest in the application of Pt in bimetallic catalysts stems not only from its active nature for numerous reactions such as hydrogenation and dehydrogenation but also due to its high cost. As an effort to discover a more active catalyst which is cost effective, attention has been given to the development of Pt based bimetallic catalysts, among them PtNi.

PtNi bimetallic catalysts have mainly been employed for reactions such as the oxidative steam reforming of methane [57, 92], oxidation reduction reactions (ORR) [80, 93], hydroisomerisation of n-heptane [94] as well as the hydrogenation of α, β - unsaturated aldehydes [16] and chloronitrobenzene [95]. In most cases the addition of Pt to Ni has shown an increase in the catalytic reactivity, regardless of the reaction employed. Generally, researches have described this enhanced activity as due to the formation of alloys which is known to effectively, shorten the Pt-Pt distance which is favorable for oxygen adsorption

in ORR [80], promote surface segregation of Pt [92] or cause an improved resistance to CO poisoning during methanol oxidation reaction [96].

Though PtNi based systems have been studied for a wide range of reactions, very few studies have given attention to the hydrogenation of benzene. The sulfur tolerance of PtNi supported on H-Mordenite (H-MOR) catalysts [97], as well as low temperature hydrogenation reactions using this bimetallic phase supported on γ-Al_2O_3 in flow and batch reactors [98] have been investigated in detail. In both cases the PtNi catalysts showed lower or slightly higher activity when compared to the monometallic Pt catalyst.

2.8 Benzene

Benzene is a colorless, hazardous substance which is carcinogenic. This volatile organic compound can be found in various industries and appliances including paint, tobacco smoke, automobile exhaust emissions and printing offices. Hence strict regulations have been enforced to ensure low concentrations of this substance is released into the surrounding environment [99]. Among the technologies which have been employed to control the concentration of this pollutant is the catalytic oxidation of benzene [100] as well as the hydrogenation of this substance. The hydrogenation of benzene is well studied. This is not only due to its potential as a means to reduce the amount of benzene in the environment, but also as a model for other hydrogenation reactions.

2.8.1 Hydrogenation of Benzene

Numerous works have been dedicated to understanding the hydrogenation of this compound over the past 40 years. Early studies were mainly focused on monometallic catalysts such as Pd [101], Fe [102], Ni [103, 104] and Pt [105].

However, interests in bimetallic systems such as NiCu [106], NiAg [27, 107] as well as PtNi and PtCo [98] have increased over the years. Several aspects ranging from the effect of supports [108] to the reaction mechanisms for this reaction [101, 102] has been investigated. These studies have led to numerous conclusions. Most of them varying depending on the system studied. However, several works have come to similar conclusions whereby better reaction rates are obtained when metals are supported on acidic supports as compared to nonacidic supports [108]. This has been explained as due to the hydrogen spillover phenomenon which results in the protons produced, activating benzene molecules to form carbonium ions and their subsequent hydrogenation to cyclohexane [103]. The process is illustrated in Figure 2.13. Even so, contradicting results were obtained regarding the structure sensitivity of this reaction. While some have shown that the hydrogenation of benzene is structure sensitive [106], others have shown otherwise [109].

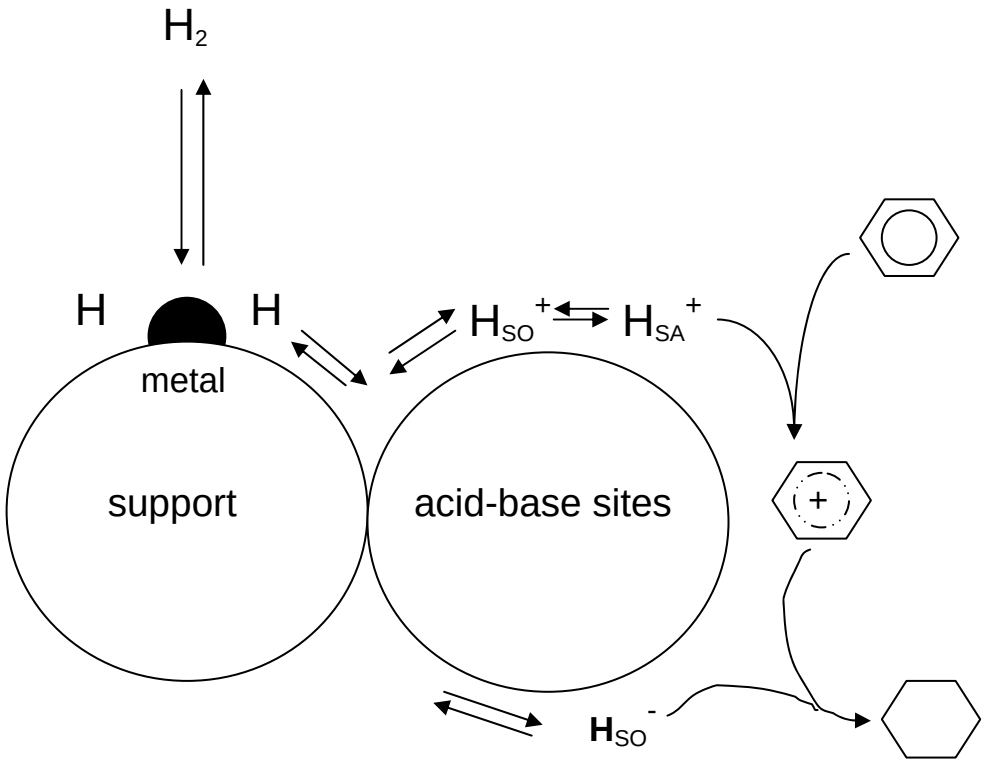

Figure 2.13: Illustration of the hydrogenation of benzene via hydrogen spillover on a support [110]. The denotations H_{SO}^{+}, H_{SO}^{-} and H_{SA}^{+} refers to spiltover hydrogen cations, spiltover hydrogen anions and adsorbed hydrogen cations respectively.

2.9 References

[1] L. M. Liz-Marzan, A. P Philipse, J. Phys. Chem. 99 (1995) 15120.

[2] A. Beck, A. Horvath, A. Sarkany, L. Guczi, Current Appl. Phys. 6 (2006) 200.

[3] G. Schmid, V. Mainack, F. Lautermann, S. Peschel, J. Chem. Soc. Dalton Trans., (1996) 589.

[4] O. M. Wilson, M. R. Knecht, J. C. Garcia-Martinez, R. M. Crooks, J. Am. Chem. Soc. 128 (2006) 4510.

[5] N. Toshima, T. Yonezawa, New J. Chem., (1998) 1179.

[6] Z. Peng, H. Yang, Nano Today, 4 (2009) 143.

[7] L. Qian, X. Yang, Colloids and Surfaces A: Physicochem. Eng. Aspects 260 (2005) 79.

[8] K. Mallik, M. Mandal, N. Pradhan, T. Pal, Nano Lett., 1 (2001) 319.

[9] M. P. Latusek, R. M. Heimerl, B. P. Spigarelli, J. H. Holles, App. Catal. A: Gen. 358 (2009) 79.

[10] X. Teng, H. Yang, Nanotechnology 16 (2005) S554.

[11] V. Ponec, Appl. Catal. A: Gen, 222 (2001) 31.

[12] V. Ponec, G. C. Bond, 1995. Catalysis by metals and alloys. Studies in Surface Science and Catalysis, B. Delmon, J.T. Yates (Eds) Vol. 95. Netherlands: Elsevier Science B. V.

[13] E. Ma, Progress in Mater. Sci., 50 (2005) 413.

[14] J. A. Rodriguez, Surf. Sci. Reports, 24 (1996) 223.

[15] N. H. H. Abu Bakar, M. M. Bettahar, M. Abu Bakar, S. Monteverdi, J. Ismail, M. Alnot, J. Catal. 265 (2009) 63.

[16] X. Han, R. Zhou, B. Yue, X. Zheng, Catal. Lett. 109 (2006) 157.

[17] J. A. Rodriguez, D.W. Goodman, J. Phys. Chem., 95 (1991) 4196.

[18] W. M. H. Sachtler, R. A. van Santen, Adv. Catal. 26 (1977) 69.

[19] H. Xie, J. Y. Howe, V. Schwartz, J. R. Monnier, C. T. Williams, H. J. Ploehn, J. Catal., 259 (2008) 111.

[20] B. Coq, F. Figueras, J. Mol. Catal. A: Chem., 173 (2001) 117.

[21] D. Gao, C. Zhang, S. Wang, Z. Yuan, S. Wang, Catal. Comm. 9 (2008) 2583.

[22] S. Chettibi, R.Wojcieszak, E. H. Boudjennad, J. Belloni, M. M. Bettahar, N. Keghouche, Catal. Today. 113 (2006) 157.

[23] C. N. Satterfield, 1991. Heterogeneous Catalysis in Industrial Practice, 2nd Edition, New York, McGraw-Hill Inc.

[24] J. A. Schwarz, C. Contescu, A. Contescu, Chem. Rev., 95 (1995) 477.

[25] M. Skoglundh, H. Johansson, L. Lijwendahl, K. Jansson, L. Dahl, B. Hirschauer, Appl. Catal. B: Environ. 7 (1996) 299.

[26] P. Gayan, C. Dueso, A. Abad, J. Adanez, L. F. De Diego, F. G. Labiano, Fuel 88 (2009) 1016.

[27] M. M. Bettahar, R. Wojcieszak, S. Monteverdi, J. Coll. Inter. Sci. 332 (2009) 416.

[28] Y. Li, Z. G. Li, R. X. Zhou, J. Mol. Catal. A: Chem. 279 (2008) 140.

[29] N. H. H. Abu Bakar, M. M. Bettahar, M. Abu Bakar, S. Monteverdi, J. Ismail, Catal. Lett. 130 (2009) 440.

[30] H. Nitani, T. Nakagawa, H. Daimon, Y. Kurobe, T. Ono, Y. Honda, A. Koizumi, S. Seino, T. A. Yamamoto, Appl. Catal. A: Gen. 326 (2007) 194.

[31] P. K. Khanna, P. V. More, J. P. Jawalkan, B. G. Bharate, Mater. Lett., 63 (2009) 1384.

[32] K. Patel, S. Kapoor, D. P. Dave, T. Mukherjee, J. Chem. Sci., 117 (2005) 53.

[33] P.S. Prasad, N. Lingaiah, P. K. Rao, F. J. Berry, L. E. Smart, Catal. Lett. 35 (1995) 345.

[34] Z. Liu, X.Y. Ling, J. Y. Lee, X. Su, L. M. Gan, J. Mater. Chem. 13 (2003) 3049.

[35] T. C. Deivaraj, W. Chen, J.Y. Lee, J. Mater. Chem. 13 (2003) 2555.

[36] W. X. Chen, J. Y. Lee, Z. Liu, Chem. Commun. (2002) 2588.

[37] J. Zeng, J. Y. Lee, W. Zhou, Appl. Catal. A: Gen. 308 (2006) 99.

[38] C. C. Koch, NanoStructured Mater., 9 (1997) 13.

[39] Y. Feng, Y. Li, H. Yuan, J. Alloys Comp., 468 (2008) 575.

[40] M. A. Garcia-Contreras, S. M. Fernandez-Valverde, J. R. Vargas-Garcia, J. Alloys Comp., 434-435 (2007) 522.

[41] M. S. Moreno, M. Weyland, P. A. Midgley, J. F. Bengoa, M. V. Cagnoli, N. G. Gallegos, A. M. Alvarez, S. G. Marchetti, Micron, 37 (2006) 52.

[42] P. Weerachawanasak, O. Mekasuwandumrong, M. Arai, S. I. Fujita, P. Praserthdam, J. Panpranot, J. Catal., 262 (2009) 199.

[43] S. A. Stevenson, G. B. Raupp, J. A. Dumesic, S. J. Tauster, R. T. K. Baker, 1987. Metal support Interactions in Catalysis, Sintering and Redispersion, S. A. Stevenson, J. A. Dumesic, .T. K. Baker, E. Euckenstein (Eds.), New York, Van Nostrand Reinhold Company Inc

[44] R. F. Hamilton Jr., S. A. Thakur, A. Holian, Free Radical Bio. Med., 44 (2008) 1246.

[45] A. P. Legrand, 1998. The surface properties of silica, Chichester, John Wiley and Sons.

[46] A. G. Boudjahem, M. Pietrwski, S. Monteverdi, M. Mercy, M. M. Bettahar, J. Mater. Sci., 41 (2006) 2025.

[47] M. A. Keane, J. Catal., 166 (1997) 347.

[48] A.G. Boudjahem, S. Monteverdi, M. Mercy, M. M. Bettahar, J. Catal., 221 (2004) 325.

[49] H. Li, H. Li, J. F. Deng, Catal. Today, 74 (2002) 53.

[50] C. T. Kresge, M. E. Leonowicz, W. J. Roth, J. C. Vartuli, J. S. Beck, Nature 359 (1992) 710.

[51] J. S. Beck, J. C. Vartuli, W. J. Roth, M. E. Leonowicz, C. T. Kresge, K. D. Schmitt, C. T-W. Chu, D. H. Olson, E. W. Sheppard, S. B. McCullen, J. B. Higgins, J. L. Schlenkert, J. Am. Chem. Soc. 114 (1992) 10834.

[52] M. J. Verhoef, P. J. Kooyman, J. A. Peters, H. V. Bekkum, Microporous Mesoporous Mater., 27 (1999) 365.

[53] C. G. Sonwane, S. K. Bhatia, Langmuir, 15 (1999) 2809.

[54] J. Silvestre-Albero, J. C. Serrano-Ruiz, A. S. Escribano, F. Rodriguez-Reinoso, Appl. Catal. A: Gen., 351 (2008) 16.

[55] K.-C. Park, D.-J. Yim, S.-K. Ihm, Catal. Today 74 (2002) 281.

[56] J. W. Niemantsverdriet, 2000. Spectroscopy in Catalysis: An Introduction, 2nd Ed., Weinham, Wiley-VCH.

[57] B. Pawelec, P. Castano, J. M. Arandes, J. Bilbao, S. Thomas, M. A. Pena, J. L. G. Fierro, Appl. Catal. A: Gen., 317 (2007) 20.

[58] B. Li, S. Kado, Y. Mukainakano, M. Nurunnabi, T. Miyao, S. Naito, K. Kunimori, K. Tomishige, Appl. Catal. A: Gen., 304 (2006) 62.

[59] E. L. Foletto, R. W. Alves, S. L. Jahn, J. Power Sources, 161 (2006) 531.

[60] J. F. Falconer, J. A. Schwarz, Catal. Rev.-Sci. Eng., 25 (1983) 147.

[61] G. Attard, C. Barnes, 1998. Surfaces, R.G. Compton (Ed), Vol. 59. Great Britain: Oxford Science Publications.

[62] Y. Li, G.-H. Lai, R.-X. Zhou, Appl. Surf. Sci., 253 (2007) 4978.

[63] M. Heemeier, A. F. Carlsson, M. Naschitzki, M. Schmal, M. Baumer, H. J. Freund, Angew. Chem. Int. Ed., 41 (2002) 4073.

[64] L. Pribylova, Bohumir Dvorak, J. Chromatography A, 1216 (2009) 4046.

[65] A. G. Bhavani, A. Pandurangan, J. Mol. Catal. A: Chem., 267 (2007) 209.

[66] I. Eswaramoorthi, N. Linggapan, Appl. Catal. A: Gen., 245 (2003) 119.

[67] J. Lif, I. Odenbrand, M. Skoglundh, Appl. Catal. A: Gen., 317 (2007) 62.

[68] M. Arai, Y. Nishiyama, T. Masuda, K. Hashimoto, Appl. Surf. Sci., 89 (1995) 11.

[69] A. Guinier, 1963. X – Ray Diffraction, San Francisco: W. H. Freman and Company.

[70] S. Zhou, B. Varughese, B. Eichhorn, G. Jackson, and K. McIlwrath, Angew. Chem. Int. Ed., 44 (2005) 4539.

[71] J. J. F. Scholten, A. P. Pijpers, A. M. L. Hustings, Catal. Rev.- Sci. Eng., 27 (1985) 151.

[72] K.–W. Park, J.-H. Choi, Y.-E. Sung, J. Phys. Chem. B, 107 (2003) 5851.

[73] N. H. H. Abu Bakar, M. M. Bettahar, M. Abu Bakar, S. Monteverdi, J. Ismail, M. Alnot, J. Mol. Catal. A: Chem., 308 (2009) 87.

[74] R. L. Johnston, 2002. Atomic and Molecular Clusters, London: Taylor & Francis. 204

[75] U. Rashid, F. Anwar, Fuels 87 (2008) 265.

[76] P.S. Sreeprasanth, R. Srivastava, D. Srinivas, P. Ratnasamy, Appl. Catal. A: Gen. 314 (2006) 148.

[77] A. Kirubakaran, Shailendra Jain, R. K. Nema, Renewable Sustainable Energy Rev., 13 (2009) 2430.

[78] T.S. Zhao, C. Xu, R. Chen, W.W. Yang, Progress in Energy Combustion Sci., 35 (2009) 275.

[79] J. R.C. Salgado, E. Antolini, E. R. Gonzalez, J. Power Sources, 141 (2005) 13.

[80] M.-K. Min, J. Cho, K. Cho, H. Kim, Electrochim. Acta 45 (2000) 4211.

[81] Y-S. Shih, Y-C. Chen, M-Y. Chen, Y-T. Tai, C-P. Tso, Coll. Surf. A: Physicochem. Eng. Aspects, 332 (2009) 84.

[82] R.DeVor, K. C. Knighton, B. Atken, P. Maloney, E. Holland, L. Talalaj, R. Fidler, S. Elsheimer, C. A. Clausen, C. L. Geiger, Chemosphere 73 (2008) 896.

[83] S. F. Kang, C. H. Liao, H. P. Hung, J. Hazardous Mater. 65 (1999) 317.

[84] A. C. K. Yip, F. L. Y. Lam, X. Hu, Chem. Eng. Sci. 62 (2007) 5150.

[85] C. Y. Lu, H. H. Tseng, M. Y. Wey, L. Y. Liu, J. H. Kuo, K. H Chuang, Fuel 88 (2009) 340.

[86] M. Bowker, 1998. The Basis and Application of Heterogeneous Catalysis. R.G. Compton (Ed.), New York, Oxford University Press Inc. 1-90.

[87] N. A. Khan, H. H. Hwu, J. G. Chen, J. Catal. 205 (2002) 259.

[88] C. Mingshu, D. W. Goodman, Chin. J. Catal., 29 (2008) 1178.

[89] N. Macleod, J. M. Keel, R. M. Lambert, Appl. Catal. A: Gen. 261 (2004) 37.

[90] M. M. Pohl, J. Radnik, M. Schneider, U. Bentrup, D. Linke, A. Brückner, E. Ferguson, J. Catal. 262 (2009) 314.

[91] G. Bernardotto, F. Menegazzo, F. Pinna, M. Signoretto, G. Cruciani, G. Strukul, Appl. Catal. A: Gen. 358 (2009) 129.

[92] Y. Mukaikano, K. Yoshida, S. Kado, K. Okumura, K. Kunimori K. Tomishige, Chem. Eng. Sci. 63 (2008) 4891.

[93] J. F. Drillet, A. Ea, J. Friedamann, R. Kotz, B. Schnyder, V. M. Schmidt, Electrochim. Acta 47 (2002) 1983.

[94] I. Eswararamoorthi, A. G. Bhavani, N. Linggapan, Appl. Catal. A: Gen. 253 (2003) 469.

[95] X-X. Han, R-X. Zhou, G.-H. Lai, X.-M. Zheng, React. Kin. Catal. Lett. 83 (2004) 55.

[96] Y. Zhao, E. Yifeng, L. Fan, Y. Qiu, S. Yang, Electrochem. Acta 52 (2007) 5873.

[97] L. J. Simon, P. J. Kooyman, J. G. van Ommen, J. A. Lercher, Appl. Catal. A: Gen., 252 (2003) 283.

[98] S. Lu, W. W. Lonergan, J. P. Bosco, S. Wang, Y. Zhu, Y. Xie, J. G. Chen, J. Catal., 259 (2008) 260.

[99] T. Duong, N. Phan, M. B. Song, E. W. Shin, J. Hazardous Mater., 167 (2008) 75.

[100] S. Zuo, Q. Huang, R. Zhou, Catal. Today, 139 (2008) 88.

[101] P. Chou, M. A. Venice, J. Catal., 107 (1987) 140.

[102] K. J. Yoon, M. A. Venice, J. Catal., 82 (1983) 457.

[103] R. Molina, G. Poncelot, J. Catal. 199 (2001) 162.

[104] R. Z. C. van Meerten, J. W. Coenen, J. Catal., 46 (1977) 13.

[105] A. G. A.Ali, L. I. Ali, S. M. Aboul Fotouh, A. K. Aboul Gheit, Appl. Catal. A: Gen., 170 (1998) 285.

[106] G. A. Martin, J. A. Dalmon, J. Catal., 75 (1982) 233.

[107] R. Wojcieszak, S. Monteverdi, J. Ghanbaja M. M. Bettahar, J. Coll. Inter. Sci., 317 (2008) 166.

[108] S. D. Lin, M. A. Venice, J. Catal., 143 (1993) 563.

[109] S. D. Lin, M. A. Venice J. Catal. 143 (1993) 539.

[110] R. Wojciesjak, 2006. Study of Supported Nickel Catalysts Prepared by Aqueous Hydrazene Method. Hydrogenation Properties and Hydrogen Storage. Support and Silver Effect. PhD Thesis, Nancy, France.

CHAPTER 3

EXPERIMENTAL

3.1 Materials

All materials were used as received. The supports, crystalline silica (99.99 %) was obtained from Chempure and aluminosilicate, mesostructured hexagonal framework, MCM-41 from Aldrich. Hydrated and non-hydrated hexachloroplatinic acid ($H_2PtCl_6.H_2O$; MW = 517.90, H_2PtCl_6; MW = 409.69) was purchased from Sigma, nickel (II) sulphate ($NiSO_4.6H_2O$) acquired from R & M Chemicals, oleic acid (GC standard) obtained from Fluka Chimika and sodium borohydride ($NaBH_4$) from Riedel de Haen. The solvent, absolute ethanol was obtained from Riedal de Haen while benzene (C_6H_6) $\geq$ 99.5 % was purchased from Merck.

All gases were purchased from Air Liquide. Hydrogen (H_2) 99.995 %, argon (Ar) 99.995 %, 500 ppm H_2/Ar 99.999 % and helium (He) 99.999 % were passed through a manganese oxytrap supplied by Engelhardt to ensure that all traces of oxygen were eliminated before flowing to the reactor. In contrast, 1000 ppm oxygen/argon (O_2/Ar) 99.999 % was used as obtained.

3.2 Methods

3.2.1 Preparation of Stock Solutions

3.2.1.1 PtNi Supported Crystalline Silica Catalysts

As much as 0.66 g of the Pt salt was weighed and dissolved in 25 ml of distilled water to obtain a stock solution of 0.05 M $H_2PtCl_6.H_2O$. The stock solution of 0.08 M $NiSO_4.6H_2O$ was prepared by weighing and dissolving 2.21 g of the Ni salt in 100 ml of distilled water. Fresh cold $NaBH_4$ was obtained by dissolving an amount of 0.19 g of the reducing agent in 25 ml of distilled water to obtain a final concentration of 0.2 M. The $NaBH_4$ stock solution was chilled before use.

3.2.1.2 PtNi Stabilized Oleic Acid (PtNi-OA)

Stock solutions of H_2PtCl_6 and $NiSO_4.6H_2O$ were prepared by dissolving 0.10 and 0.14 g of the metal salts in 25 ml of distilled water respectively. This was to obtain separate stock solutions of 0.01 M and 0.02 M correspondingly. Several stock solutions of oleic acid were prepared. The concentrations of the oleic acid stock solutions are 0.02, 0.05, 0.15, 0.20 and 0.50 M. As much as 0.06, 0.14, 0.42, 0.56 and 1.41 g of the pure oleic acid was diluted in 10 ml of ethanol to attain the corresponding stock solutions. Sodium borohydride was employed as a reducing agent. Here, 0.19 g of the chemical was weighed and dissolved in 25 ml of distilled water. Final concentration of the reducing agent is 0.2 M. The stock solution was chilled before being used.

3.2.1.3 PtNi –OA Supported Crystalline Silica Catalysts (PtNi-OA/Silica)

The $H_2PtCl_6.H_2O$ and $NiSO_4.6H_2O$ stock solutions were prepared to attain stock solutions with a concentration of 0.05 M and 0.08 M correspondingly. As much as 0.66 g and 2.21 g of the of the Pt and Ni salts were weighed and dissolved in 25 and 100 ml of distilled water correspondingly. An oleic acid stock solution with a concentration of 0.15 M was obtained by diluting 1.06 g of the pure oleic acid with 25 ml of ethanol. The $NaBH_4$ with a concentration of 0.2 M was prepared by dissolving 0.19 g of the reducing agent in 25 ml of distilled water. This stock solution was chilled before use.

3.2.1.4 PtNi Supported MCM-41 Catalysts (PtNi-MCM-41 and PtNi-MCM-C)

A stock solution of the Pt salt was obtained by dissolving 0.66 g of $H_2PtCl_6.H_2O$ in 25 ml of distilled water. Final concentration of the stock solution is 0.05 M. On the other hand, as much as 1.12 g of $NiSO_4.6H_2O$ dissolved in 25 ml of distilled water was used to prepare 0.17 M of a Ni salt solution. Fresh cold $NaBH_4$ was prepared according to the concentrations required. An amount of 0.19 g, 0.28 g, 0.38 g and 0.47 g of the reducing agent was weighed and dissolved in 25 ml of distilled water to obtain a concentration of 0.20, 0.30, 0.40 and 0.50 M of $NaBH_4$ correspondingly. The $NaBH_4$ stock solutions were chilled before use.

3.2.2 Synthesis of PtNi Supported Crystalline Silica via Co-precipitation

Catalysts were prepared via non-classical methods using crystalline silica as support. Approximately 2.5 g of silica support was suspended in a mixture of 30 ml distilled water and 8 ml ethanol. The suspension was purged with argon at 353 K. Subsequently, various amounts of Pt and Ni salt stock solutions were

added to the suspension to obtain a PtNi weight ratio of Pt_{100}, $Pt_{90}Ni_{10}$, $Pt_{47}Ni_{53}$, $Pt_{22}Ni_{78}$ and Ni_{100}, where total metal content is approximately 3 wt % (calculated based on AAS analysis). In all cases, the Ni salt solution was added prior to the Pt salt solution. The resultant mixtures were homogenized for duration of 10 minutes before the addition of 8 ml of 0.2 M fresh cold $NaBH_4$. The reaction was allowed to continue for an additional 15 minutes before filtering and washing with distilled water. The catalysts were denoted as CP (co-precipitation).

3.2.3 Synthesis of PtNi Supported Crystalline Silica via Co-impregnation

Crystalline silica was employed to prepare the catalysts using the non-classical methods. In the co-impregnation technique various volumes of the Ni and Pt salt solutions were incorporated in an argon purged colloidal mixture of 2.5 g silica and 30 ml distilled water. The Pt and Ni salt solutions were added to obtain catalysts with a PtNi weight ratio of $Pt_{17}Ni_{83}$, $Pt_{55}Ni_{45}$ and $Pt_{92}Ni_{8}$ (determined via AAS analysis). Total metal content of the catalysts is about 3 wt %. The mixture was then homogenized for 15 minutes before evaporating the liquid phase and drying the residue under vacuum. The silica–metal salt cake was ground and redispersed in a mixture of 30 ml distilled water and 8 ml ethanol. The colloid was than purged with argon at 353 K for 10 minutes before the addition of 8 ml of 0.2 M fresh cold $NaBH_4$. Finally the sample was filtered and washed before drying under vacuum. These catalysts are denoted as CI (co-impregnation).

3.2.4 Synthesis of PtNi Supported Crystalline Silica via Step-impregnation

Approximately 2.5 g of silica support mixed with 30 ml distilled water was bubbled with argon at room temperature for duration of 10 minutes before the addition of a certain volume of Ni salt stock solution. The colloid was then homogenized for another 15 minutes. Subsequently, the liquid phase was evaporated and dried under vacuum. The residue was then ground and immersed in a mixture of 30 ml distilled water and 8 ml ethanol. As much as 5 ml of fresh cold 0.2 M $NaBH_4$ was added to the mixture in an inert condition at 353 K. The reaction was allowed to continue for duration of 15 minutes. The liquid phase was then evaporated and the mixture dried in vacuum. The Ni catalyst supported on silica was then redispersed in 30 ml of distilled water. A volume of the previously prepared Pt stock solution was subsequently impregnated and reduced using 3 ml of fresh cold 0.2 M $NaBH_4$ as described for the Ni. Catalysts with a total metal content of approximately 3 wt % and PtNi weight ratios of $Pt_{22}Ni_{78}$, $Pt_{48}Ni_{52}$ and $Pt_{72}Ni_{28}$ were prepared and denoted as SI.

3.2.5 Synthesis of Oleic Acid Stabilized PtNi Particles

Samples were prepared by mixing various amounts of the Pt ion stock solutions with the Ni ion stock solutions to obtain PtNi weight ratios of approximately Pt_{100}, $Pt_{93}Ni_{7}$, $Pt_{78}Ni_{22}$, $Pt_{61}Ni_{39}$, $Pt_{31}Ni_{69}$, $Pt_{15}Ni_{85}$ and Ni_{100}. As much as 2 ml of 0.02 M of oleic acid previously dissolved in ethanol was then added to the mixture and homogenized under nitrogen atmosphere for 10 minutes at 353 K. Subsequently, 2 ml of fresh cold 0.2 M $NaBH_4$ was added to the solution. Homogenization was continued for another 15 minutes before the

reaction mixture was centrifuged and the solid sample separated and cleaned with ethanol. The cleaned samples were then dried in a vacuum oven.

3.2.5.1 Effect of Various Concentrations of Oleic Acid

The bimetallic sample with a weight ratio of $Pt_{78}Ni_{22}$ was chosen to study the influence of various concentrations of oleic acid. As much as 2 ml of the oleic acid stock solution with a concentration of 0.05, 0.15, 0.20 or 0.50 M was employed to prepare the oleic acid stabilized PtNi particles. The preparation was carried out as described in section 3.2.4.

3.2.5.2 Effect of Various Reaction Temperatures

This parameter was studied using samples with a weight ratio $Pt_{78}Ni_{22}$. Synthesis procedures are as explained in section 3.2.4 above. A concentration of 0.15 M oleic acid was used instead of 0.02 M. However, the reaction temperature was varied. Temperatures of 313, 373 and 413 K were employed.

3.2.6 Preparation of PtNi-OA/Silica Catalysts

Catalysts with a PtNi weight ratio of approximately Pt_{100}, $Pt_{79}Ni_{21}$, $Pt_{58}Ni_{42}$ and $Pt_{24}Ni_{76}$ and Ni_{100} were synthesized. Samples were prepared to obtain catalysts with a total metal loading of approximately 3 wt %. The stabilized oleic acid particles were first prepared. Certain amounts of the Pt and Ni ion stock solutions were added to a round bottom flask. As much as 8 ml of 0.15 M oleic acid was then added. The mixture was homogenized under nitrogen atmosphere for 10 minutes at 353 K. Subsequently, 8 ml of fresh cold 0.2 M $NaBH_4$ was added to the solution. Reaction was allowed to continue for 15 minutes. Approximately 2.5 g crystalline silica was then added to the solution

and this was mixed for duration of 15 minutes under argon atmosphere at room temperature. The obtained oleic acid-stabilized PtNi supported on silica (PtNi-OA/Silica) was then filtered, washed and dried under vacuum.

3.2.7 Preparation of PtNi-MCM-41 Catalysts via Non-classical Method

Catalysts were prepared via the co-impregnation technique, using MCM-41 as the support. Certain amounts of $H_2PtCl_4.6H_2O$ and $NiSO_4.6H_2O$ stock solutions were added to a suspension of the 5.0 g of support and 50 ml of distilled water to obtain a PtNi weight ratio of 50:50 and total metal content of 1 wt %. The mixture was mixed for 15 minutes and then dried under inert conditions at 373 K before redispersing it in a certain reduction medium. A flow of argon was bubbled through the mixture for a duration of 10 minutes at a certain temperature followed by the addition of 8 ml fresh cold $NaBH_4$. Reaction was allowed to continue for another 15 minutes before filtering, washing and drying the sample under vacuum conditions. The different reduction temperature, $NaBH_4$ concentration and reduction medium employed are tabulated in Table 3.1. The real metal content and the PtNi wt ratios were determined via AAS analysis.

Table 3.1: Preparation parameters of PtNi supported MCM-41 catalysts prepared via non-classical methods using co-impregnation technique.

PtNi Weight Ratio	Reduction Temperature (K)	Reduction Medium	$NaBH_4$ Concentration (M)
50:50	353	EtOH + H_2O	0.2
50:50	313	EtOH + H_2O	0.2
50:50	273	EtOH + H_2O	0.2
50:50	273	EtOH + H_2O	0.3
50:50	273	EtOH + H_2O	0.4
50:50	273	EtOH + H_2O	0.5
50:50	273	EtOH	0.3
50:50	273	H_2O	0.3

3.2.8 Preparation of PtNi-MCM-41 via Classical Method

All catalysts were prepared via co-impregnation technique using MCM-41 as the support. As much as 5.0 g of the support was weighed and suspended in 50 ml of distilled water. Argon gas was flowed through the suspension to achieve an inert atmosphere. Subsequently, an amount of Ni stock solution was added followed by the Pt stock solution. The mixture was homogenized for another 15 minutes before evaporating the aqueous phase until the PtNi ion mixture was completely dry in an atmosphere of N_2 at 363 - 373 K. Several PtNi catalysts were prepared with a total metal content of about 1 wt %. These are Pt_{100}, $Pt_{90}Ni_{10}$, $Pt_{50}Ni_{50}$, $Pt_{90}Ni_{10}$ and Ni_{100}. The actual metal content was determined using AAS analysis.

The PtNi ion mixture was then calcined in air to oxidize the metal ions and remove impurities. Samples were placed in a U shaped reactor and heated to 373 K at a heating rate of 5 K min^{-1} in a flow of 300 ml min^{-1} air. Treatment was allowed to continue at this temperature for 1 hour before increasing the temperature to 773 K at a heating rate of 30 K min^{-1}. Samples were than calcined for another 4 hours before cooling to room temperature. These catalysts are denoted as C (classical).

3.3 Characterization Techniques

3.3.1 H_2-Temperature Reduction (H_2-TPR)

Experiments were performed on all of the fresh catalysts. As much as 50 mg of the catalyst was weighed and placed in a U tube reactor. The catalyst was heated at a constant rate of 5 K min^{-1} from room temperature to 1123 K while purging with a mixture of hydrogen and argon (1000 ppm H_2). The total gas flow

rate was previously determined as 90 ml min^{-1}. The resultant effluent gas was analyzed on line using an Agilent G2890A microchromatograph operated at 333 K. A typical scheme of the set-up used is shown in Figure 3.1

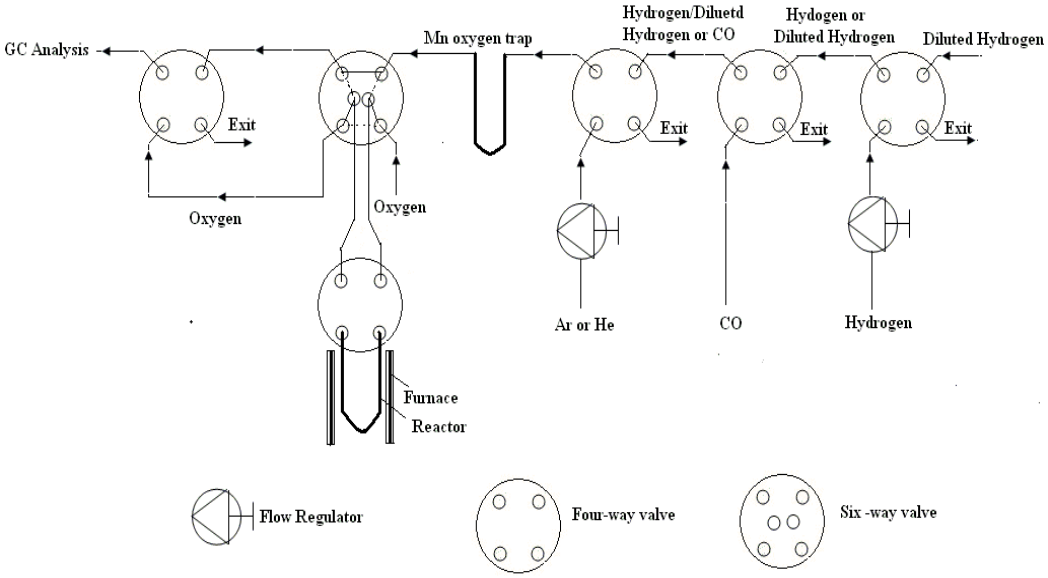

Figure 3.1: Apparatus setup for H_2-TPR, H_2-Chemisorption, H_2-TPD and O_2-chemisorption studies.

3.3.2 H_2 Chemisorption and H_2-Temperature Desorption (H_2-TPD)

3.3.2.1 Non-classical Catalysts

Typically, 50 mg of a catalyst was placed into a U tube reactor. This was then activated at 473 K in pure hydrogen for the duration of 15 minutes. Subsequently, samples were purged with argon (100 ml min^{-1}) for approximately 45 minutes at similar temperature before cooling to room temperature. The gas was then switched to diluted hydrogen (100 ppm) and H_2-chemisorption studies were carried out. The amount of H_2 was detected at an interval of 2 minutes using an Agilent G2890A microchromatograph operated at 333 K. Upon saturation, the

samples were purged with argon before H_2-TPD analysis was carried out in a flow of argon (100 ml min^{-1}). A similar temperature program and detection as the TPR analysis described in section 3.3.1 was employed.

3.3.2.2 Classical Catalysts

Similar procedures as in section 3.3.2.1 were employed. However, catalysts were activated at 373 K in pure hydrogen for duration of 3 hours.

3.3.3 Temperature Programmed Surface Reaction (TPSR)

An amount of 25 mg of a classical catalyst was weighed and placed in a reactor. The sample was activated in a flow of 50 ml min^{-1} of pure H_2 from room temperature to 373 K at a heating ramp of 10 K min^{-1}. After maintaining the temperature of the catalyst at 373 K for duration of 3 hours, the sample was cooled to 323 K and the hydrogenation of benzene was carried out in a reaction flow of 5/50/145 ml min^{-1} of $C_6H_6/H_2/He$. Following this, the sample was cooled to room temperature while helium was passed through the reactor for duration of 1 hour. Temperatures were then increased at a rate of 2 K min^{-1} and in a flow of 2/48 ml min^{-1} H_2/He.

3.3.4 O_2 Chemisorption

Analysis was conducted using 50 mg of the fresh catalysts prepared via classical methods. The samples were weighed and placed in a reactor before activation. Temperature was increased from room temperature to 373 K at 10 K min^{-1} in a flow of 100 ml min^{-1} of pure H_2. Upon reaching 373 K, the temperature was maintained for 3 hours. Following this, the gas flow was switched to 100 ml

min^{-1} of argon. Samples were purged for 1 hour to ensure that all loosely adsorbed hydrogen was desorbed. The temperature was then further increased to 673 K at a ramp of 10 K min^{-1} in argon. Upon reaching 673 K, the gas flow was switched to diluted oxygen (100 ppm O_2) with a flow rate of 100 ml min^{-1}. The chemisorption of O_2 was analyzed every 2 minutes using an Agilent G2890A microchromatograph operated at 333 K until a constant concentration of O_2 was obtained.

3.3.5 Transmission Electron Microscopy (TEM)

All samples were prepared similarly. The samples were dispersed in ethanol and sonicated for 10 minutes before placing a drop of the solution onto carbon coated copper grids. Images were obtained using a CM20 Philips TEM operating at 20kV or a CM12 Philips TEM operating at 80kV.

3.3.6 Powder X-ray Diffraction (XRD)

All samples were used without further treatment. The XRD spectra were recorded using a SIEMENS D5000 XRD or a Philips X'Pert Pro diffractometer in the 2θ range of 10-100º with a Cu Kα radiation.

3.3.7 Fourier Transform Infrared (FTIR)

The Pt/Ni stabilized oleic acid samples were mixed with potassium bromide (KBr) and then pressed into thin pellets. These pellets were subjected to analysis using a Perkin Elmer System Model 2000 from 600 – 4000 cm^{-1}.

3.3.8 X-ray Photoelectron Spectroscopy (XPS)

The fresh catalysts were used without further treatment. XPS measurements for C 1s, Si 2p, O 1s, Ni 2p and Pt 4f were conducted using an ESCALAB MK II VG with Mg Kα and Al Kα radiations.

3.4 Calculation Methods

3.4.1 Determination of Fractal Dimension

The particles dispersion onto and within the crystalline silica support is evaluated using the fractal technique. Fractal dimensions, D_F, of the samples were determined based on the method described by Liang [1]. This approach involves choosing several center points in a TEM image of a sample and drawing circles with a radius of $r_1, r_2, r_3 \ldots r_i$. Following this, the micrograph is manually digitized using ones and blanks to indicate the presence and absence of particles respectively. The number of ones (M_i) within a circle of a certain radius is calculated and an average is obtained. Subsequently, by plotting ln M vs ln r, the D_F value is obtained from the slope of the plot.

3.4.2 Determination of Metal Dispersion

3.4.2.1 Borodzinski and Bonarowska Method

Metal dispersion in the catalysts were determined using the mathematical approach proposed by Borodzinski and Bonarowska [2]. The mathematical expressions developed relate the average particle size and their dispersions. For metal particles where $d_i > 24d_{at}$, (where '*at*' is atomic) the dispersion (D) is expressed as in equation (3.1)

$$D = \frac{\left(5.01 d_{at} \sum n_i d_i^{\,2}\right)}{\sum n_i d_i^{\,3}} \tag{3.1}$$

while for metal particles with an average particle size of $d_i \leq 24.0 d_{at}$, D_M can be calculated according to equation (3.2)

$$D = \frac{2.64}{d_{rel(VS)}^{\;0.81}} \tag{3.2}$$

where $d_{rel(VS)}$ is the relative volume surface mean diameter which can be calculated based on equation (3.3) and (3.4).

$$d_{rel(VS)} = \left(\frac{\sum n_i d_i^{\,3}}{\sum n_i d_i^{\,2.19}}\right)^{1.23} \tag{3.3}$$

3.4.2.2 H_2-Chemisorption Method

Dispersion of the metal phase is obtained based on the quantity of H_2 adsorbed and the stoichiometry of H_2 chemisorption on the Pt and Ni respectively. Values were calculated assuming that the Pt/H stoichiometry is 1 and Ni/H stoichiometry is 2. The equation employed is as follows [3]:

$$D = \frac{100 \cdot V \cdot n \cdot M}{22414 \cdot m \cdot wt} \tag{3.4}$$

where, V is the volume adsorbed (cm^3)

n is the stoichimetric factor

22414 is the molar gas volume (cm^3 mol^{-1})

m is the sample weight (g)

wt is the metal content (wt %)

M is the metal atomic weight (g mol^{-1})

3.4.3 Total Surface Area of Metal Phase

Total surface area of the metal phase is determined based on the D values calculated using equation 3.4. The following equation is employed to obtain this surface area [3].

$$S = \frac{a_m \cdot N_A \cdot D}{M} \tag{3.5}$$

where, S is the total surface area

a_m is the surface covered by one metal atom (Pt = 8.07 x 10^{-20} m^2; Ni = 6. 51 x 10^{-20} m^2)

N_A is the Avogadro number (6.023 x 10^{23} mol^{-1})

3.4.4 Particle Size

3.4.4.1 H_2-Chemisorption Method

Particle size can be determined based on the total surface area of the metal obtained from equation (3.6).

$$d = \frac{6000}{S \cdot \rho} \tag{3.6}$$

where, S is the total surface area

ρ is the metal density

3.4.4.2 XRD Technique

Average particle size based on XRD results can be determined based on the following equation.

$$d = \frac{K\lambda}{\beta \cos\theta} \tag{3.7}$$

where, K is the Scherrer's constant (0.89)

λ is the wavelength of the x-ray

β is the peak width at half the maximum intensity (radians)

θ is the angle of the peak

3.4.5 Degree of Reduction

The degree of reduction was calculated based on the O_2 chemisorption analysis. The following reactions are assumed to occur depending on the catalyst.

$$Pt° + ½\ O_2 \rightarrow PtO$$

$$Ni° + ½\ O_2 \rightarrow NiO$$

Hence, the degree of reduction was calculated by dividing the total mol of oxygen involved in the reaction with the total mol of metal content.

3.5 Catalytic Reaction

Typically as much as 50 mg of the samples were weighed and placed in a U-shaped reactor. The catalysts were then activated in a flow of 100 ml min^{-1} of pure H_2. Samples were heated to 473 K at a heating rate of 10 K min^{-1}. Upon reaching 473 K, the samples were maintained at the same temperature for another 15 minutes. Catalysts were then cooled to room temperature and the catalytic activity measurements were conducted by contacting the catalysts with a reaction mixture of 10/40/150 ml min^{-1} benzene/hydrogen/helium. The extent of dilution of the reaction mixture with helium was previously chosen to enable comparison of catalytic activity of the prepared catalysts. The reaction products were fed into a 5730A Hewlett-Packard gas chromatography equipped with a flame ionization detector and 8 m molecular sieve column. A typical scheme of the set-up employed is illustrated in Figure 3.2. Various other temperatures were studied to evaluate the catalytic activity. Reaction rates were calculated according to equation (3.8), which is suitable for dilute reactants at low conversion.

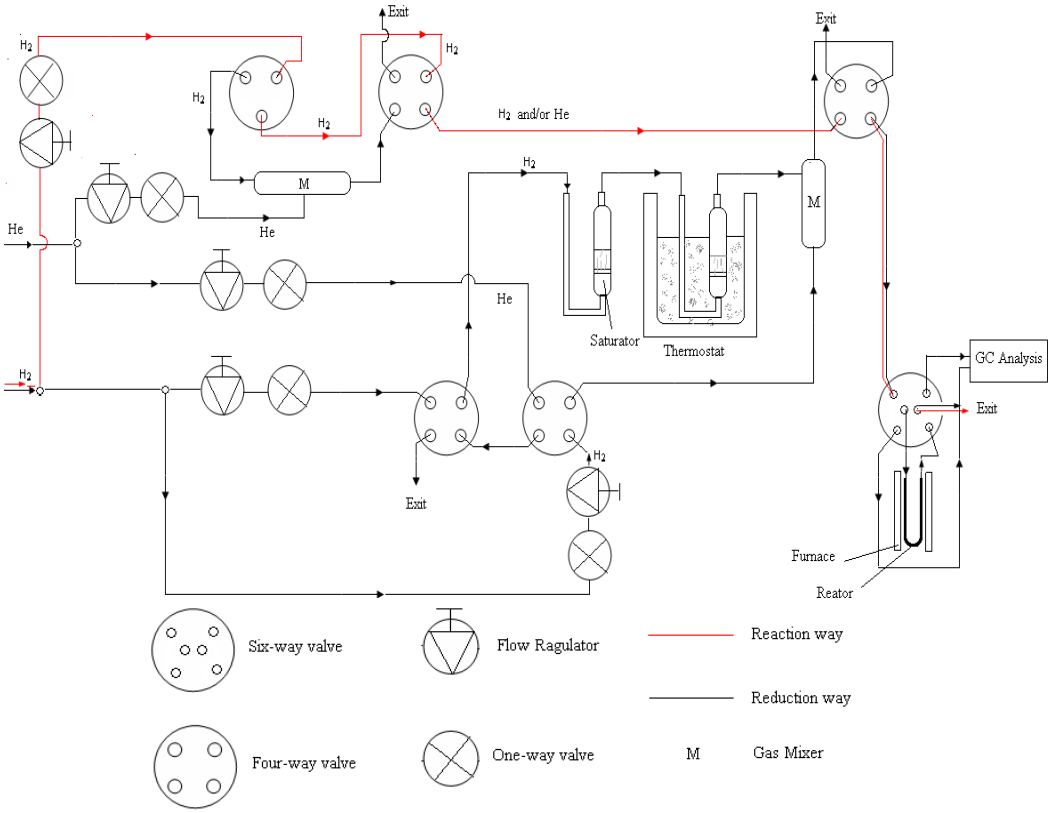

Figure 3.2: Set-up for hydrogenation of benzene.

$$\text{Reaction Rate} = \frac{C_o \times [Bz] \times Flw}{M_{met}} \tag{3.8}$$

Where, C_o = Initial conversion of cyclohexane

[Bz] = Concentration of benzene, (mol m^{-3})

Flw = Total flow rate of reaction mixture, (m^3 min^{-1})

M_{met} = Total mass of active phase (g)

3.6 Kinetic Studies

3.6.1 Determination of Reaction Orders

As much as 25 mg of a catalyst was weighed and placed into a U-tube reactor. The catalyst was activated in a flow of 50 ml min^{-1} of pure hydrogen from room temperature to 373 K and then kept at constant temperature for duration of 3 hours. Subsequently, the temperature was decreased to 358 K and catalytic reactions were carried to obtain a conversion of less then 10 %. Total flow rate of the reaction mixture is 200 ml min^{-1} and consisted of a mixture of benzene, hydrogen and helium.

In the first series of catalytic reactions, the flow rate of hydrogen was kept constant at 50 ml min^{-1}, obtaining a partial pressure of 0.25 atm. The flow rate of benzene was varied from 7.0 to 20.3 ml min^{-1} to obtain partial pressures ranging from 0.035 to 0.10 atm. After carrying out the reaction at each partial pressure, hydrogen was allowed to pass through the reactor while increasing the temperature to 373 K. Catalysts were reactivated for 20 minutes before reducing the temperature to 353 K and conducting the catalytic reaction with the subsequent reaction mixture.

In the second series of catalytic reactions, the flow rate of benzene was kept constant (10 ml min^{-1}) to obtain a constant partial pressure of approximately 0.05 atm. Partial pressures of hydrogen was varied by regulating the hydrogen flow rate between 25 and 48 ml min^{-1} to obtain pressures between 0.13 and 0.24 atm. Similar treatments were carried out on the catalysts after each flow rate as mentioned in the first series.

The reaction order was calculated based on equation (3.9).

$$r = kP_{Bz}^{m}P_{H_2}^{n} \tag{3.9}$$

Where, r = Reaction rate

k = Rate constant

P_{Bz} = Partial pressure of benzene (atm)

P_{H_2} = Partial pressure of hydrogen (atm)

m = reaction order of benzene

n = reaction order of hydrogen

3.6.2 Determination of Energy of Activation

As much as 25 mg of catalyst was placed into a reactor and activated in 50 ml min^{-1} pure hydrogen for duration of 3 hours at 373 K. The catalysts were then cooled to 323 K and catalytic reactions were carried out at various temperatures ranging from 323 – 498 K in a flow of 9/50/141 ml min^{-1} benzene/hydrogen/helium. Catalytic conversions were kept at less than 10 %. A plot of 1/T (K) vs ln k was obtained and energy of activation was calculated based on (3.10).

$$\ln k = \frac{-E_a}{R}\left(\frac{1}{T}\right) + \ln A \tag{3.10}$$

Where, k = Rate constant

E_a = Energy of activation (J mol^{-1})

R = Gas constant (8.314 J K^{-1} mol^{-1})

T = Temperature (K)

A = Pre-exponential factor

3.7 References

[1] J. Z. Liang, Compos. Part A: Appl. Sci. Manuf. 38 (2007) 1502.

[2] A. Borodzinski, M. Bonarowska, Langmuir 13 (1997) 5613.

[3] G. Bergeret, P. Gallezot, Handbook of Heterogeneous Catalysis, Vol 2, Wiley-VCH, Weinham, 1997, pg. 439.

CHAPTER 4

SYNTHESIS AND CATALYTIC PROPERTIES OF PtNi SUPPORTED SILICA CATALYSTS PREPARED VIA NON-CLASSICAL METHODS

4.1 Introduction

The non-classical methods for the synthesis of catalysts have been increasingly popular in recent years as reducing agents such as borohydrides [1-5], hydrazine [6-8], formaldehyde [9-10] and alcohols [10-12] allow better control of the metal particle morphology even at low temperatures. Small sized particles can be formed due to a balance between the reduction rate of the precursors and the support or stabilizer employed. For bimetallic nanoparticles, although this method is capable of efficiently synthesizing the particles, it does not guarantee the formation of crystalline alloys. Hence, many researchers have employed thermal treatments at high temperatures for long durations even after reduction of the metal salts [3, 8, 13]. As an example, Teng and Yang [14] reported the synthesis of non-alloyed bimetallic particles with core-shell morphology while other researches [7, 15] demonstrated the formation of alloyed bimetallic nanoparticles with similar morphology. In general, though the non-classical method may prove to be advantageous due to its shorter preparation times and metal particles can be designed to meet the requirements of a catalytic reaction, the thermal treatments used may hinder the actual potential of the catalyst due to the increase in particle size during alloy formation as previously

mentioned. Therefore understanding the factors that govern the metal particle structure and their manipulation is significant.

Various works have revealed that the size, structure, and metal support interaction of supported metal particles prepared by chemical reduction method, depends on factors such as the reduction conditions [2], the nature of the support [16,17] and the presence of a metal additive [18]. By using hydrazine as the reducing agent, it is found that crystalline silica promoted the reduction of nickel [17] while amorphous silica inhibits the nickel reduction by giving rise to Ni ion-silica surface species [16]. In a similar chemical reduction method [18], whereby the bimetallic system is silver (Ag) and Ni, the presence of Ag sharply increased the catalytic activity of Ni. Although Ag is known as an inactive catalyst it was found that the NiAg core-shell groupings formed, leads to an increase in metallic surface area of Ni and consequently to a sharp increase in catalytic activity.

The preparation technique which refers to the technique in which metal salts are incorporated onto a support is also significant. Impregnation or precipitation techniques are frequently used for the preparation of catalysts. The choice of technique can significantly influence factors related to the surface and catalytic properties of catalysts as those mentioned above [19, 20]. It is undeniable that it is difficult to fully understand how the preparation techniques influence these factors as many other aspects play a role in determining the final characteristics of a catalyst. Hence, the effect of the preparation techniques varies depending on a system. For this reason, studies on diverse systems for example, Pt/SBA-15 [21], Ni/SiO_2 [22] and WO_3/ZrO_2 [23] have been carried out.

To date, no work on PtNi supported silica catalysts prepared using $NaBH_4$ as a reducing agent has been investigated. Considering that PtNi supported

bimetallic particles hold potential as catalysts, a detail study on this system prepared via co-precipitation technique is presented. In this chapter, it is shown that long thermal treatments at high temperatures are not required to form alloys. Further, the nature of the Pt and Ni phases in the bimetallic catalysts are examined and their affects on the catalytic activity for the hydrogenation of benzene are described.

4.2 Structural Studies

The XRD analysis of the crystalline silica exhibits peaks at 2θ values of approximately 39.5º, 40.3º, 42.4º and 45.7º. This is shown in Figure 4.1 and 4.2 which exhibits the fresh and activated catalysts respectively. The main peaks for Pt are also positioned at around similar values (39.8 and 46.3) and hence make the determination of the metallic phase of Pt in the samples difficult. The metal particle size which may be small and the low metal content with respect to the silica may have also contributed to the inability to determine the existence of these peaks. Interestingly, the Pt peaks are a little more prominent, after catalyst activation, in both the Pt_{100}-CP and $Pt_{90}Ni_{10}$-CP catalysts. Deconvolutions of these peaks indicate that a slight shift of the Pt peaks occurs in the $Pt_{90}Ni_{10}$-CP catalysts when compared to that of Pt_{100}-CP. The Ni_{100}-CP, on the other hand, exhibits no peaks that indicate the formation of Ni or NiO. The unavailability of Ni and NiO peaks is quite surprising considering the nature of Ni which easily agglomerates hence should give rise to strong signals. Even so, this phenomenon may be due to the arrangement of the Ni atoms that forms amorphous Ni or NiO. Similar occurrences have been reported elsewhere for Ni [24]. The Pt peaks shift

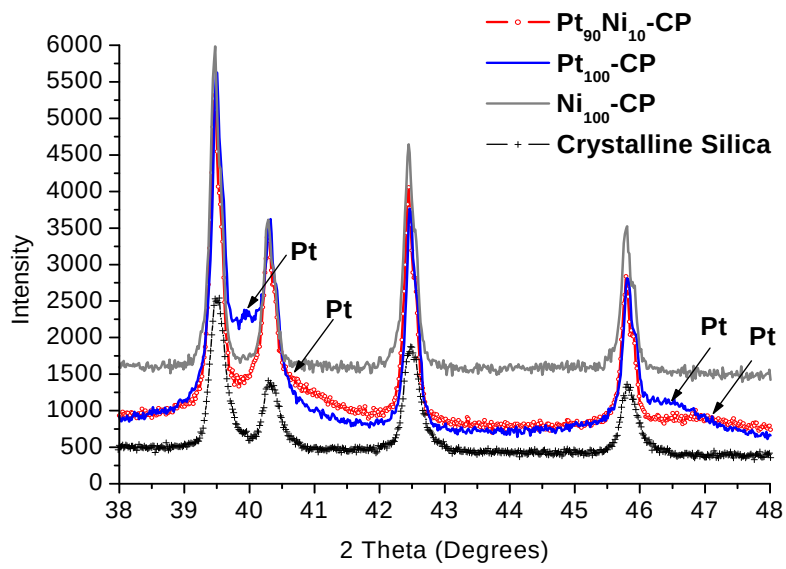

(a)

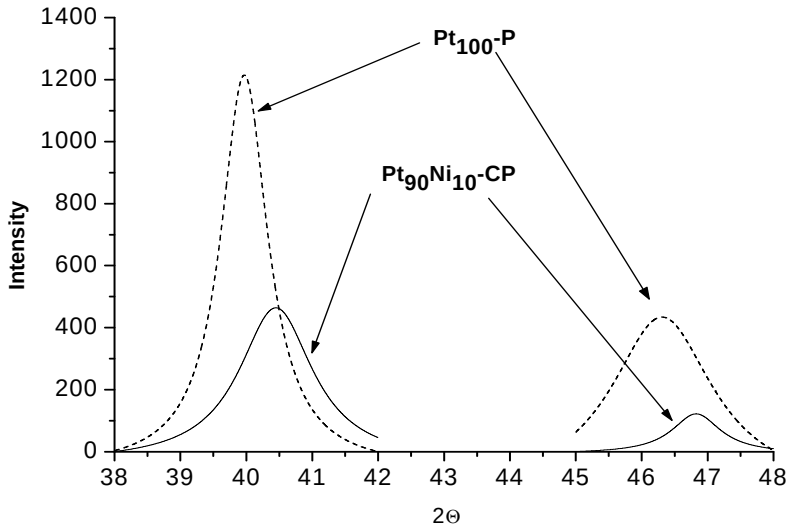

(b)

Figure 4.1: XRD diffractograms of (a) the crystalline silica and fresh catalysts and (b) the respective Pt peaks deconvolution.

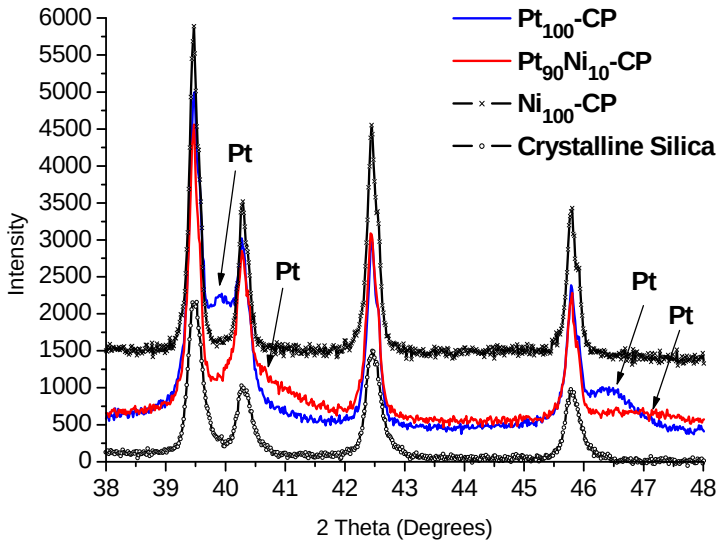

(a)

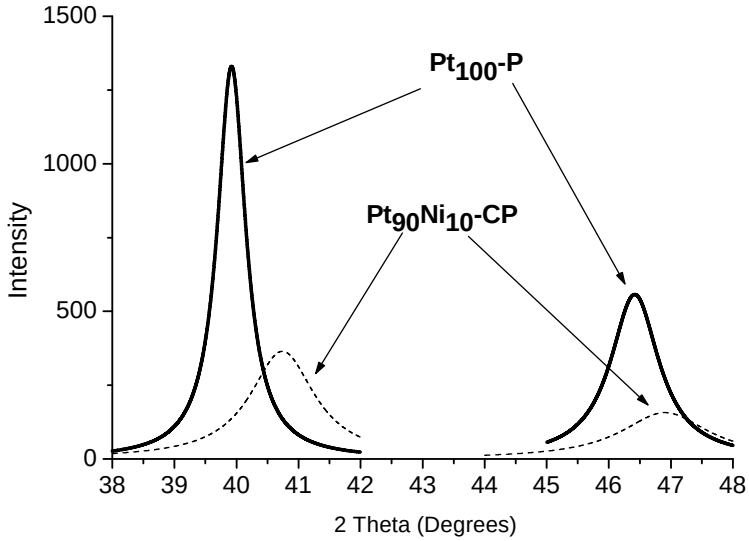

(b)

Figure 4.2: XRD diffractograms of (a) crystalline silica and activated catalysts and (b) the respective Pt peaks deconvolution.

can be correlated to lattice distortions which arise as a result of the variation in the atomic size of the elements involved. This may lead to the occurrence of surface segregation or to the formation of alloys. Several researches have also attributed the occurrence of surface segregation in PtNi alloys to lattice distortion [25, 26] while others indicated the peak shift owing to alloying between Pt and Ni [27, 28]. In the latter, Ni atoms are incorporated into the fcc structure of Pt. Similar observations have been reported for the formation of PtCo alloys using $NaBH_4$ as a reducing agent at temperatures below 373 K [2].

TEM images of the Ni_{100}-CP, Pt_{100}-CP and $Pt_{90}Ni_{10}$-CP are shown in the respective Figure 4.3(a) – (c). It is observed that in all samples, most of the particle formation did not occur on the support but instead the particles occurred surrounding the crystalline silica forming fractal structures. This occurrence can be attributed to the low surface area of the support which limits incorporation of the metal salts along with its solvation in the aqueous phase during the reduction stage. Li et al. [29] also reported possible Ni leaching during reduction with KBH_4 in aqueous solutions, for catalysts calcined at low temperatures prior to the chemical reduction. This is due to the poor interaction between the Ni species and the support which may also have caused the fractal formation surrounding silica in this case. Formation of such morphologies is due to non-equilibrium growth of the particles [30]. This implies that the structure grows in different directions at different rates. Such morphologies exhibit unique properties that differ from their bulk or isolated particles [31]. These fractal structures have a fractal dimension (D_F) of 2.46, 1.85 and 1.97 for the Ni_{100}-CP, Pt_{100}-CP and $Pt_{90}Ni_{10}$-CP respectively. According to previous studies, fractals with different D_F values indicate the nature in which the fractals exist. In general, those with a value of 2

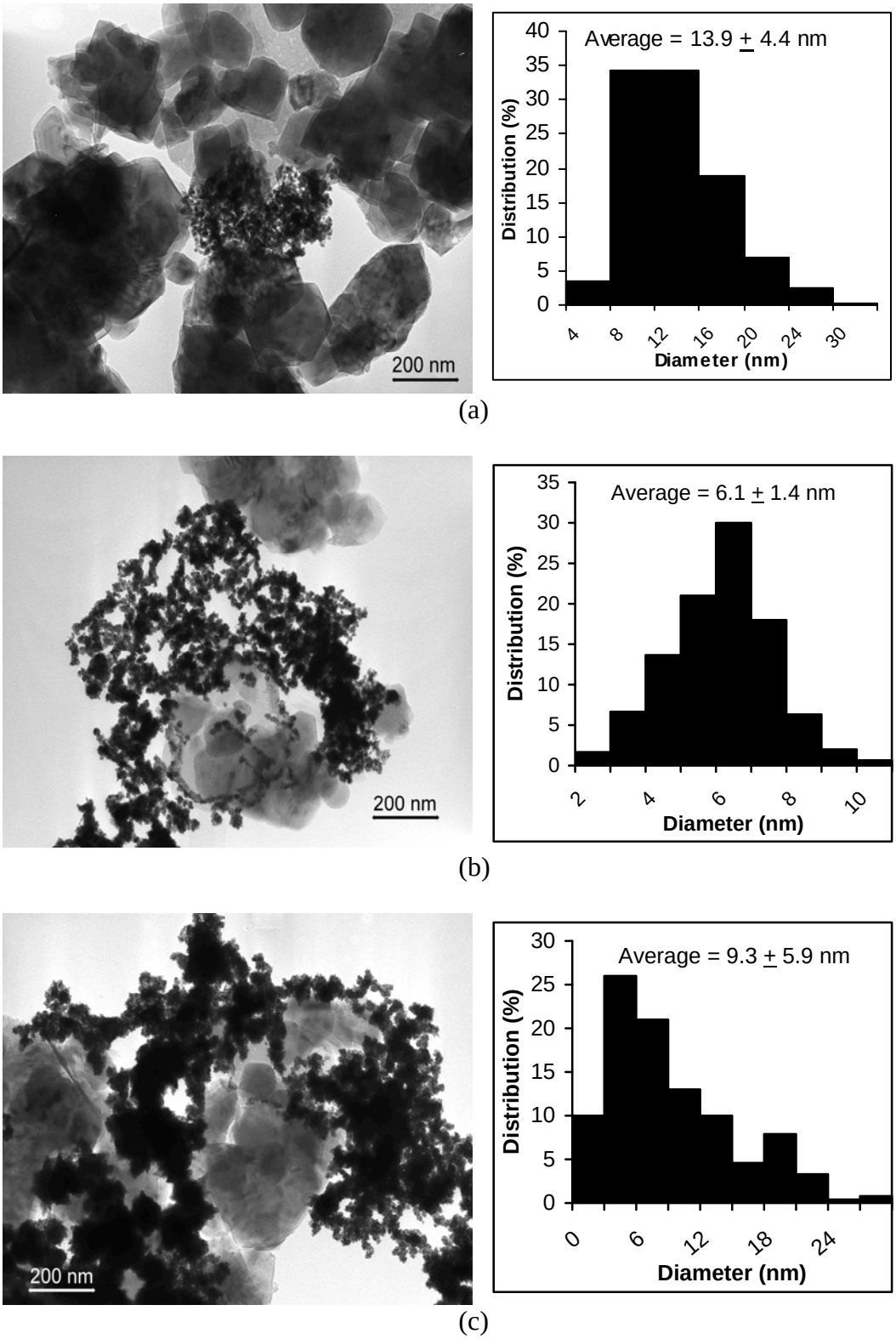

Figure 4.3: TEM images and particle size histograms of (a) Ni_{100}-CP (b) Pt_{100}-CP and (c) $Pt_{90}Ni_{10}$-CP catalysts supported on crystalline silica.

refer to the formation of smooth surfaces while fractals with a D value of more than 2 and less than 2, indicate that rough continuous surfaces and surfaces which are chemically active exist respectively [32, 33]. Based on the D_F values, the Ni_{100}-CP fractals exist as corrugated continuous surfaces. This means that the metal phase is present as large structures of an uneven surface. The type of irregularities in the metal structure can be in the form of humps, cracks, whiskers or even pores [33]. On the other hand, according to Pajkossy and Nyikos [33] both the Pt_{100}-CP and $Pt_{90}Ni_{10}$-CP samples exhibit fractal dimensions that usually correspond to that of catalysts. They reported that two types of fractals with D_F values less than 2 can occur. Typically, continuous fractals usually have partially blocked active surfaces while non-continuous fractals are described as chemically active islands on inactive supports. In this work, the fractal growth did not occur on the crystalline silica support hence the fractals formed are that of partially blocked active surfaces. This phenomenon is described to occur, due to the growth of the fractals that occurs in several dimensions hence may cover some of the active sites available. In contrast, the non-continuous fractals are stabilized by the inactive support that inhibits extensive growth and this enables a maximum exposure of the active sites.

Images of the catalysts at higher magnification (not shown here) show that the fractals are composed of small spherical particles. The average particle size of the nanoparticles is 6.1 ± 1.4, 14.0 ± 4.4 and 9.3 ± 5.9 nm for Pt_{100}-CP, Ni_{100}-CP and $Pt_{90}Ni_{10}$-CP respectively. The size distribution histograms indicate that the Pt_{100} exhibited a narrow size distribution while both Ni_{100}-CP and $Pt_{90}Ni_{10}$-CP demonstrated particles with a wide size distribution. The reduction in particle size with increasing Pt content may be explained as due to the decrease in the total

number of atoms available in the catalysts during the reduction and growth process. The similar total metal content in terms of weight and the higher atomic weight of Pt decreases the number of atoms that can be adsorbed and grow on nucleated metal particles. This results in the smaller particle size. However, the presence of B to a certain extent may also play a role in the reduction of the average particle size as reported previously [34, 35]. Dispersion values of the metal phase in the catalysts, calculated based on the particle sizes obtained via TEM [36], are 46.6 %, 9.9 % and 36.8 % for the Pt_{100}-CP, Ni_{100}-CP and $Pt_{90}Ni_{10}$-CP samples respectively. Comparison of the metal dispersity of these samples with other works [28, 37] showed that similar values were obtained, although different determination methods were used.

The electron diffraction patterns are shown in Figure 4.4. The pattern of Ni_{100}-P as in Figure 4.4(a) is seen to be very diffuse and have less intense rings. Hence this correlates with the XRD results that indeed amorphous Ni occurs in the catalyst. Samples of Pt_{100}-CP and $Pt_{90}Ni_{10}$-CP, on the other hand, exhibit finer rings that are more intense, owing to the polycrystalline nature of the metal particles. Based on these patterns, the d spacings for the Pt_{100}-CP is 2.33, 1.96, 1.40 and 1.19 Å. These values are attributed to the (111), (200), (220) and (311) planes of the fcc structure of Pt [38]. For $Pt_{90}Ni_{10}$-CP, the d spacings are 2.27, 1.96, 1.38 and 1.16 Å. These values are similar to that of Pt_{100}. No additional rings assigned to Ni exists, hence indicates that alloying occurs in the $Pt_{90}Ni_{10}$-CP sample whereby Ni is incorporated into the Pt fcc lattice.

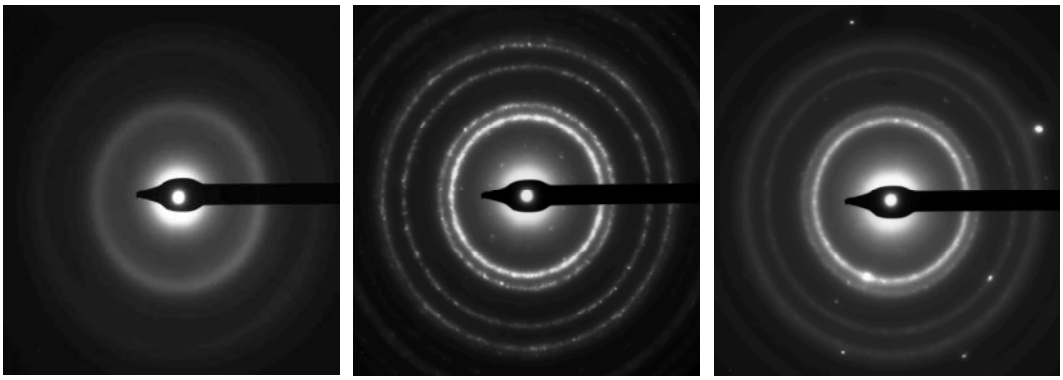

(a) (b) (c)

Figure 4.4: Electron diffraction of (a) Ni_{100}-CP (b) Pt_{100}-CP (c) $Pt_{90}Ni_{10}$-CP catalysts.

The line profiles of the $Pt_{90}Ni_{10}$-CP, as shown in Figure 4.5, also confirmed that most of the metal particles are not incorporated into the crystalline silica support. The profiles of Si and O are similar and thus indicate that only silica and no other metal oxides exist in the samples. The profiles of both the Pt and Ni metals are almost identically matched. Hence, this further elucidates the formation of PtNi alloys in the $Pt_{90}Ni_{10}$-CP catalyst. This reaffirms the result obtained from the SAED analysis previously described.

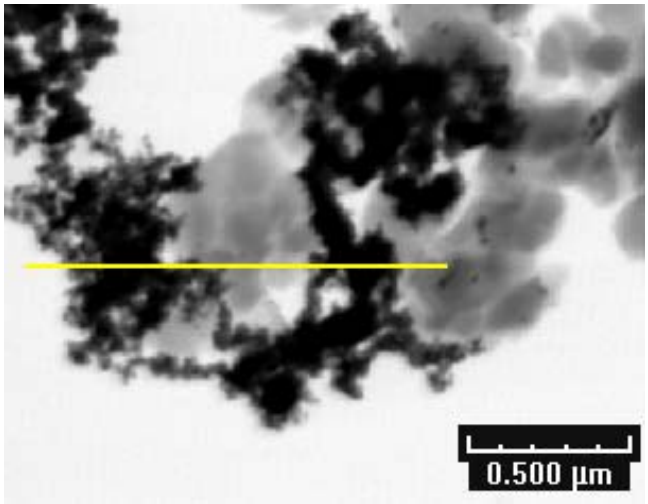

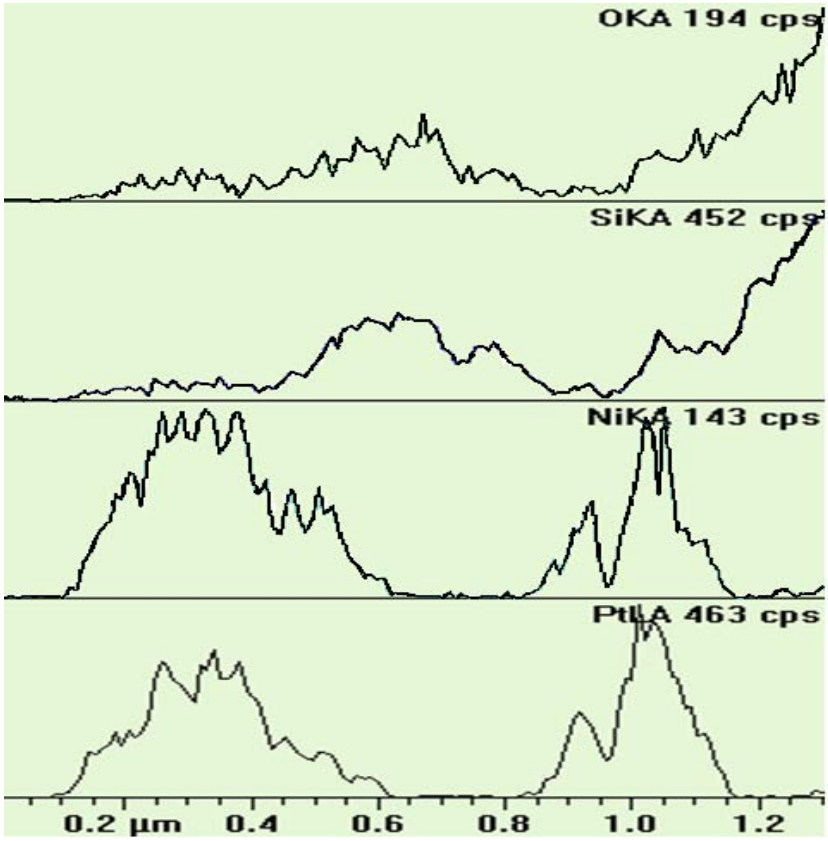

Figure 4.5: Line profiles of $Pt_{90}Ni_{10}$-CP supported on crystalline silica.

4.3 Surface Characteristics

4.3.1 H_2-TPR Profiles

It is expected that all metal particles are in the reduced state following the reduction of the metal ions in inert conditions. However, possible superficial oxidation of the metal phase may have occurred as a result of storing the catalysts in atmospheric conditions. H_2-TPR analysis was conducted to investigate the state of the metallic phase in the fresh catalysts. Figure 4.6 illustrates the H_2-TPR profiles obtained. It is obvious that for all catalysts, the consumption of H_2 does not occur in the temperature range studied. No consumption peaks are observed for Ni oxides although nickel is known to easily oxidize due to its high negative potential. This is indicative of the occurrence of total reduction of the metal ions during the preparation stage and the catalysts are stable towards oxidation even when exposed to air during storage of the samples. This is similarly observed by Li and coworkers [1] who studied the formation of PtNi supported on carbon nanotubes and graphites. However, in their work, they observed the consumption peaks positioned at 243-303 K that are attributed to the formation of PtO. In the present work, such peaks would not have been observed due to the limitations of the equipment.

The profiles of Figure 4.6 indicate the production of hydrogen occurs for samples with high Ni content (i.e. Ni_{100}-CP and $Pt_{22}Ni_{78}$-CP). The production of the hydrogen occurs in the temperature range of 600-760 K and is attributed to H_2 strongly adsorbed onto the metallic surface. As much as 4.1×10^{-3} and 4.8×10^{-3} mol g_{met}^{-1} H_2 were produced by Ni_{100}-CP and $Pt_{22}Ni_{78}$-CP catalysts respectively. This desorption may be explained as due to several factors; the excess of borohydride ions not removed from the catalysts after washing, adsorption of

hydrogen gas during the preparation stage or adsorption of hydrogen during the TPR experiment at low temperature. To determine the contributing factor, a sample containing only silica and $NaBH_4$ was similarly analyzed using H_2-TPR**.** The results showed that no desorption of hydrogen occurred from both materials. Hence it can be summarized that the production of hydrogen from high Ni content catalyst samples is possibly due to the adsorption of the gas molecules during the reaction of metal ions with $NaBH_4$ or at low temperatures during TPR experiment.

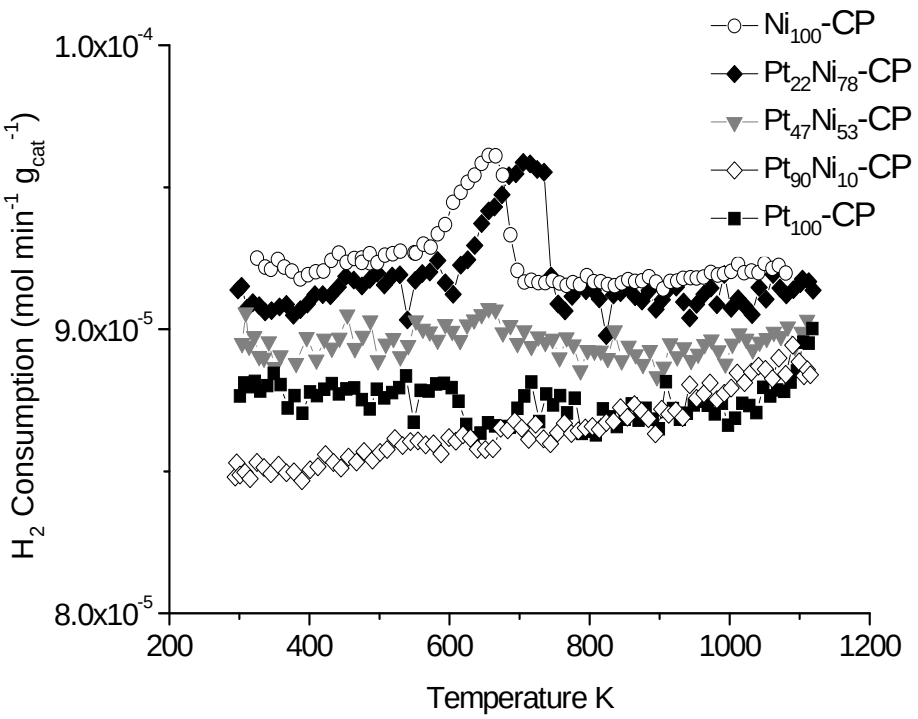

Figure 4.6: H_2-TPR profiles of the various fresh PtNi catalysts supported on crystalline silica.

4.3.2 H_2-Chemisorption

H_2-chemisorption was conducted at room temperature after activating the catalysts. Values are tabulated in Table 4.1. It was found that the Ni_{100}-CP catalyst exhibited low H_2 adsorption properties at room temperature. This can mainly be attributed to the strong interaction of hydrogen atoms adsorbed during activation which stays on the surface even after purging, resulting in very few adsorption sites available during H_2-chemisorption. In addition, the existence of large particles also reduces the surface area of the active phase available for hydrogen adsorption. The calculated active surface area for the Ni_{100}-CP catalyst is 2.81 $m^2 g^{-1}$.

In contrast, the Pt_{100}-CP catalysts show high H_2 adsorption characteristics. H_2-adsorption for this catalyst is 8 times more than the Ni_{100}-CP catalysts. The weaker strength of adsorption between the active sites on the Pt particles and the hydrogen atoms adsorbed during activation as well as the larger surface area of this catalyst which is about 14.00 m^2 g^{-1}, contribute to this higher H_2-chemisorption properties. This indicates the probability of a higher reactivity compared to the monometallic Ni catalyst.

The bimetallic catalysts all show lower H_2 adsorption values when compared to the Pt_{100}-CP catalyst. A general trend is observed for these catalysts whereby adsorption of H_2 increased with increasing amounts of Pt. This depicts that less adsorption sites are available on the bimetallic catalysts when compared to the Pt_{100}-CP catalyst.

The dispersion of the metal phase was calculated from the H_2-chemisorption values. It was found that dispersion ranged between 0.4 – 5.6 % for all the catalysts. The lowest and highest dispersions were exhibited by the

Ni_{100}-CP and Pt_{100}-CP correspondingly. In general, dispersion percentages calculated using this method showed large variations when compared to percentages obtained using the Borodzinksi and Bonarowska method [36]. Considering that the earlier method reflects the whole metal phase of a catalyst while the later method only considers the metal particles which show distinct particle spherical shapes, it is highly likely that the H_2-chemisorption technique gives a better perspective of the percentage of dispersion.

Table 4.1: Average particle size, H_2-chemisorption and H_2-TPD studies.

Catalyst Denotation (mol ratio)	**Total Metal Content (wt %)**	**Metal Content (wt %)**		**Average [a] Particle Size (nm)**	**H_{2ads} at RT [b] (x 10^{-5} mol g_{met}^{-1})**	**H_{2des} [c] (x 10^{-3} mol g_{met}^{-1})**
		Ni	**Pt**			
Ni_{100}-CP	2.50	2.50	-	13.6	3.6	4.6
$Pt_{22}Ni_{78}$-CP	2.98	2.32	0.66	15.7	8.4	6.2
$Pt_{47}Ni_{53}$-CP	2.74	1.44	1.30	11.6	8.2	2.5
$Pt_{47}Ni_{53}$-CP	2.74	1.44	1.30	-	-	0.7[d]
$Pt_{90}Ni_{10}$-CP	2.15	0.22	1.93	9.3	12.7	2.4
Pt_{100}-CP	2.82	-	2.82	6.1	28.6	0.3

[a] Calculations based on TEM analysis
[b] Obtained after H_2-activation at 473 K
[c] Based on H_2-TPD analysis, after H_2-activation at 473 K then H_2-adsorption at room temperature (see Experimental).
[d] Without H_2-activation at 473 K and H_2-adsorption.

4.3.3 H_2-TPD Analysis

Figure 4.7 exhibits the H_2-TPD profiles. These profiles suggest that there exist four distinct types of catalysts, that of Ni_{100}-CP, those with high amounts of Ni content ($Pt_{22}Ni_{78}$-CP and $Pt_{47}Ni_{53}$-CP), Pt_{100}-CP and that with high Pt content ($Pt_{90}Ni_{10}$-CP).

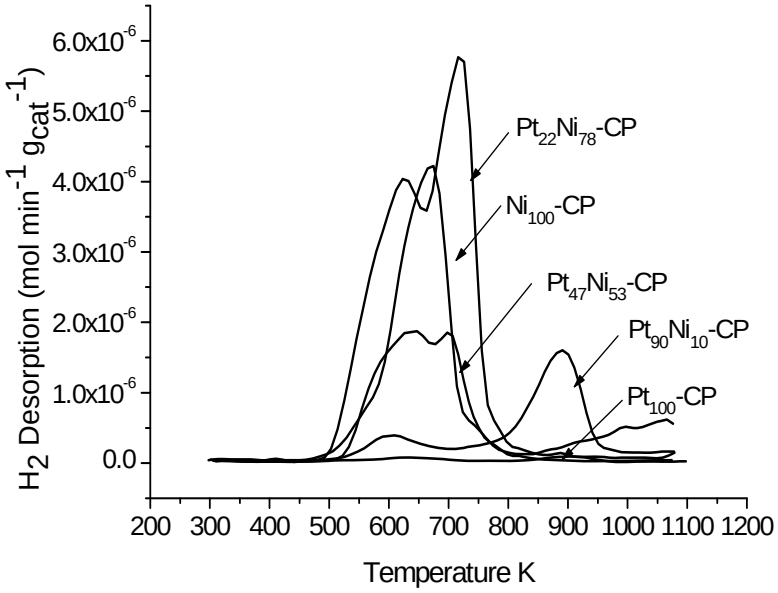

Figure 4.7: H_2-TPD profiles of the various PtNi catalysts supported on crystalline silica.

The first type of catalyst, Ni_{100}-CP, desorbs hydrogen at approximately 500 - 800 K with a maximum at 670 K. The second type of catalyst also desorbed hydrogen in a similar temperature range but the incorporation of Pt resulted in the formation of additional adsorption sites. Deconvolution of peaks of these two types of catalyst demonstrate that both catalysts are comprised of 4 peaks positioned at approximately 570-610 K, 625-640 K, 690-705 K and 700-745 K. Inspection showed that, upon addition of Pt, the Ni peak is shifted from 670 K to a lower temperature range of 625-640 K. Another interesting observation is that the peaks attributed to the Ni_{100}-CP as well as that of $Pt_{22}Ni_{78}$-CP and $Pt_{47}Ni_{53}$-CP catalysts (at 625-745 K) roughly coincide with those of the H_2-TPR profiles of Figure 4.6. Previous work have shown that these peaks arise due to several factors: H_2 strongly bonded to the Ni particles, hydrogen retained at the metal

support interphase or H_2 incorporated in the support as spillover species [39]. Adsorption of H_2 in this case may have occurred during the preparation stage when the metal ions were reduced with $NaBH_4$ or otherwise during the activation step. As for the peaks positioned at lower temperatures, these are explainable as due to H_2 loosely bound to the metal surface. The third type of catalyst, Pt_{100}-CP, exhibits three peaks of different characteristics. The first peak is centered at room temperature and is due to very loosely bound hydrogen atom from dissociated hydrogen molecule. The second peak is positioned at 638 K and is similar to that observed in the second type of catalyst (high to moderate amounts of Ni content) and is ascribed to the moderately adsorbed H atoms on the Pt surface. Finally the third peak at 925 K is due to H-spillover species. Even though these three peaks are discrete, they are less intense and almost flat as compared to those of the first type of catalyst. The final type of catalyst, $Pt_{90}Ni_{10}$-CP, exhibits a different profile when compared to the other catalysts. In this case, two peaks are observed, a small peak at 604 K and a larger peak at 865 K. An interesting observation of this peak is that it occurs at a lower temperature in comparison to the high temperature peak of Pt_{100}-CP. Hence, it is possible to summarize that Ni may have induced a shift in the latter Pt peak to lower temperature. Li et al. [1] attribute this to the strong interaction between the two metals at lower temperature that consequently improves the H_2 adsorption.

All catalysts investigated desorbed larger amounts of H_2 throughout the analysis as compared to the amounts adsorbed at room temperature (between 1.4 x 10^{-5} and 4.5 x 10^{-3} mol g_{met}^{-1}). However, Ni_{100}-CP and $Pt_{22}Ni_{78}$-CP catalysts desorbed the largest quantities of H_2 as tabulated in Table 4.1. It is important to note that a difference in the amounts desorbed from TPD (4.6 x 10^{-3} and 6.2 x 10^{-}

^{3} mol g_{met}^{-1}) and TPR (4.1 x 10^{-3} and 4.8 x 10^{-3} mol g_{met}^{-1} respectively) studies occurs. This difference may be caused by the different experimental conditions employed in both TP analyses. For H_2-TPD, samples were activated with pure hydrogen for 15 minutes, hence would incorporate greater quantities of H_2 when compared to the TPR analysis which was conducted in a more diluted environment of 1% H_2. On the other hand it is observed that a lower amount was desorbed by the Pt_{100}-CP catalyst while a moderate amount was incorporated in the $Pt_{47}Ni_{53}$-CP and $Pt_{90}Ni_{10}$-CP catalysts. These results correlate well with the TPR profiles shown in Figure 4.6.

Further TPD experiments were carried out on the $Pt_{47}Ni_{53}$-CP catalyst without activation in order to understand the above adsorption-desorption phenomenon. Figure 4.8 exhibits the profile in comparison with that obtained after activation. It can be seen that two peaks are observed in the profile. These peaks are centred at 600-640 K and 727 K. They are similar to that observed for the catalyst after activation as well as that of $Pt_{22}Ni_{78}$-CP. This infers that hydrogen adsorbs on similar sites whether it is caused by the reduction process in aqueous media at 353 K or from gaseous hydrogen molecules during the activation process at 473 K. However, additional peaks are observed for the activated catalyst and may be explained as due to the formation of additional Ni^{o} or Pt^{o} sites. Moreover, for $Pt_{90}Ni_{10}$-CP and Pt_{100}-CP catalysts, absence of peak at 670-750 K strongly indicates that no incorporation of hydrogen during reduction with $NaBH_4$ occurred. Hence, samples containing high amounts of Pt (Pt_{100}-CP and $Pt_{90}Ni_{10}$-CP) show desorption that are contributed by the adsorption during the activation stage. The catalyst without activation, on the other hand, desorbed a lower quantity of H_2 i.e. 0.7 x 10^{-3} molg_{met}^{-1}; this is less than 1/3 of the amount

desorbed by the activated sample. This desorbed H_2 represents the amount that is adsorbed by the catalyst during the preparation stage (reduction of metal ions). Similar adsorption phenomenon is observed for the $Pt_{22}Ni_{78}$-CP and Ni_{100}-CP catalysts. This occurrence has also been observed for supported monometallic nickel catalysts where hydrazine was used as a reducing agent. Hydrazine adsorbs on the support during the preparation stage then desorbs as nitrogen and hydrogen [16].

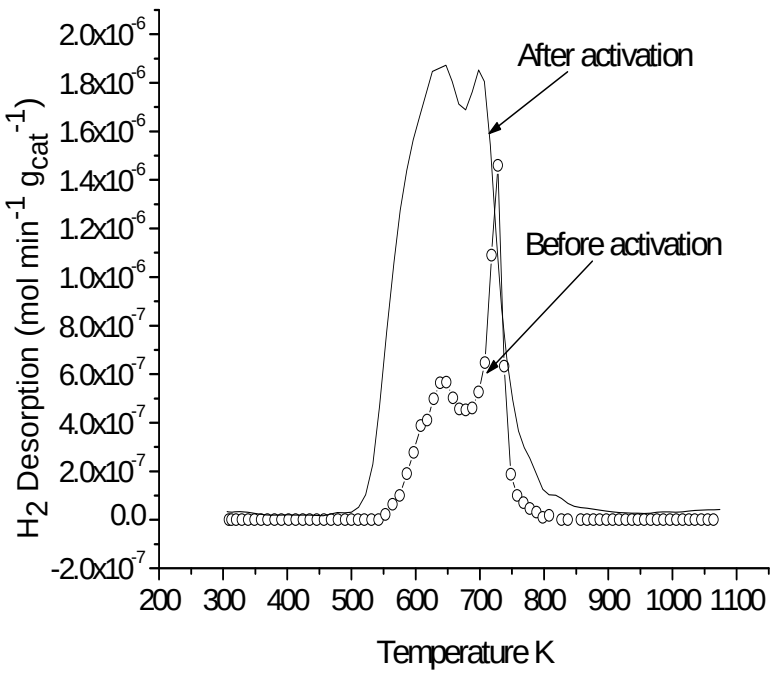

Figure 4.8: H_2-TPD profiles of $Pt_{47}Ni_{53}$-CP before and after activation

.

Thus the obtained temperature profiles suggest that the formation of alloy nanoparticles modify the sorption properties of the individual metallic components. The presence of one component into the other reduce the adsorption of H_2 onto the catalyst and thus decreases the desorption temperature of

hydrogen. Moreover, the bimetallic catalysts seem to indicate the existence of specific sites not observed in the other monometallic catalysts. This occurrence is probably the result of synergistic interaction that occurs between Pt and Ni nanoparticles.

4.3.4 XPS

Figure 4.9(a) shows the XPS spectrum of the Pt 4f of the Pt_{100}-CP sample. Two peaks corresponding to the core levels of $4f_{7/2}$ and $4f_{5/2}$ are observed at 71.6 and 74.9 eV respectively. These values correlate to that of the bulk Pt metal which was previously reported at 71.3 and 74.0 eV [40]. Hence, this indicates that the Pt in Pt_{100}-CP is in the zerovalent state [40]. The Ni 2p core shell spectrum of Ni_{100}-CP is shown in Figure 4.9(b). The Ni $2p_{3/2}$ exhibits two peaks at 856.6 and 862.9 eV. The peak positioned at 856.6 eV can be attributed to the existence of NiO while the peak at 862.9 is identified as a multielectron excitation satellite peak arising from the high binding energy peak at 856.6 eV [41]. Comparison of these results with that obtained from H_2-TPR studies show differences in the states in which the Ni exists. H_2-TPR studies indicate that no oxidation occurred contrary to the results obtained via XPS. It is possible that the NiO observed in the XPS profiles may be due to the formation of slight surface oxidation in the samples while the bulk of the metal phase is composed of Ni in the zerovalent state as shown by H_2-TPR studies. In the XPS spectrum of the $Pt_{90}Ni_{10}$-CP catalyst, similar peaks as to that of the Pt_{100} occurred for the Pt 4f. Here, the $4f_{7/2}$ and $4f_{5/2}$ core levels are positioned at 71.5 and 74.7 eV respectively and are designated to metallic Pt. It is observed that there is a difference of 0.2 eV towards lower binding energies (BE) for the Pt $4f_{7/2}$ core

shell. In addition, no peaks attributed to Ni are observed in the catalyst. These phenomenons are attributed to the occurrence of alloying as well as surface segregation of Pt respectively.

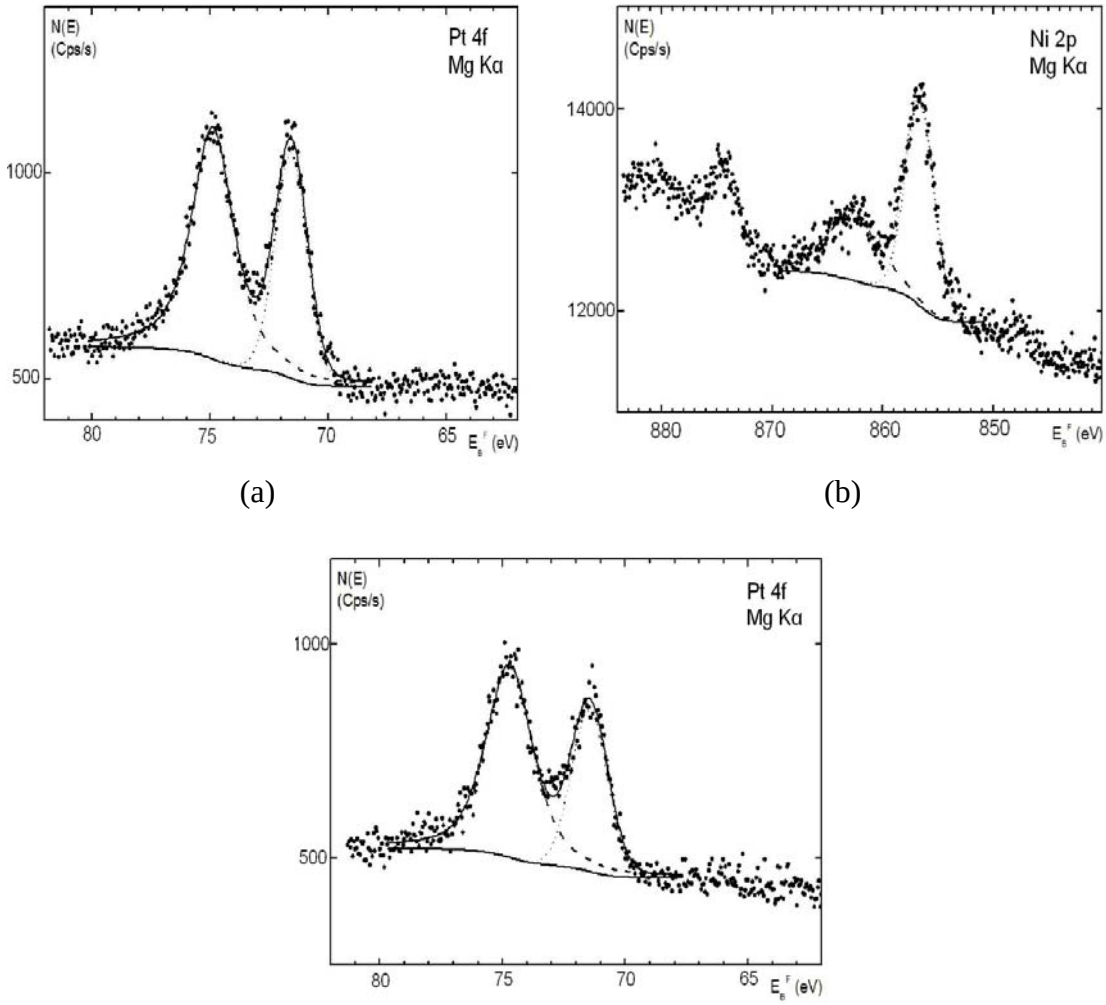

Figure 4.9: XPS spectra of (a) Pt 4f of Pt_{100}-CP (b) Ni 2p of Ni_{100}-CP and (c) Pt 4f of $Pt_{90}Ni_{10}$-CP.

In terms of alloying, the extent to which the peak shifts as a result of alloying is attributed to several factors. Among these factors are the type of interactions that exist between the metals involved and the temperature at which the metals are annealed or activated. Generally, previous works have shown that ionic bonding induces shifts via electron transfer from Ni to Pt [27, 40, 42]. Zhao and coworkers [27] showed that a shift of about 0.3 eV to lower BE occurred in the Pt 4f spectra for PtNi nanoparticle alloys supported on multi-walled carbon nanotubes. Park et al. [40] also obtained similar values. However, other researchers have explained that this shift is attributed to variations in the annealing temperature. As an example, Park and coworkers [43] reported that annealing PtNi electrodes at 300 and 500 ºC showed larger XPS peak shifts compared to annealing at 200 ºC. In their work, annealing at the latter temperature exhibits a shift of 0.1 eV which indicates that less alloying occurred compared to when higher temperatures were applied. In this work a shift of 0.2 eV is observed. It is possible that a weak interaction between the Pt and Ni occurred. Metallic bonds which are weaker than ionic bonds may have been formed leading to the small shift. Even so, the low temperature at which the PtNi catalyst was activated may have also contributed to this slight peak shift. This further proves that alloying occurs in the PtNi system prepared in this work.

Surface segregation of the Pt may also occur in the metal phase of the $Pt_{90}Ni_{10}$-CP catalyst. It is well known that metals with a lower heat of sublimation tend to segregate on the surface of alloys. Considering that the heats of vaporization of Pt and Ni are 509.6 and 370.3 kJ mol^{-1} respectively, such thermodynamic explanation is not applicable in the case of PtNi alloys [40]. Hence, other theories have been put forward to explain this occurrence. One of

the most widely accepted theory is based on the electronic structure of the metals. Hugosson et al. [44] described that the size of atoms play a significant role in the surface segregation in alloys. Larger atoms tend to have a shorter bonding distance with their nearest neighbours compared to smaller atoms. Such structures exhibit lower surface energy. Thus, stable alloys are formed by forcing the larger atoms to the surface where the coordination number is even smaller. In this work, the larger size of the Pt atoms compared to Ni, leads to segregation of the Pt on the PtNi alloy surface. The total Ni content, which is 27.5 atomic %, is retained in the bulk of the PtNi alloy making it undetectable via XPS. Similar finding has been reported elsewhere [25].

4.4 Effect of Borohydride Reduction

The possible formation of NiB or PtB is also another important aspect that requires consideration as the work described employs $NaBH_4$ as the reducing agent. Several authors have reported the formation of NiB via the reduction of Ni salts using KBH_4 [29, 45, 46]. We presume that PtB alloying does not occur due to the stable nature of Pt. Several studies on the incorporation of Pt and B on various supports have reported that only interaction between the support and B occurred [47, 48]. The possible amorphous nature of NiB prevents the determination of this compound via XRD, if it occurs. This gives rise to the possibility of NiB existing in the catalysts. However, the extent in which it is present is unknown. XPS investigations of the Ni $2p_{3/2}$ spectrum show that no peaks signifying the availability of NiB arise at approximately ~ 853 eV. Even so, AAS analysis reveals that only 0.27 wt % of boron exists in the Ni_{100}-CP catalysts. This indicates that the formation of NiB, if any, is limited. Interestingly

the bimetallic catalysts and Pt_{100}-CP exhibits the presence of even less boron content. The Pt_{100}-CP, $Pt_{90}Ni_{10}$-CP, $Pt_{47}Ni_{53}$-CP and $Pt_{22}Ni_{78}$-CP contain 0.01-0.15 wt % of boron. Here, boron content decreases with Ni content. It is well known that unlike Pt, Ni easily forms NiB via the donation of electrons from B to metallic Ni making B electron deficient and Ni electron rich [29]. Hence, this may explain the higher availability of boron in catalysts with high Ni content. These alloys have highly unsaturated coordinative sites that promotes adsorption and surface reactions [49]. Therefore this elucidates the adsorption of H_2 by catalysts with high Ni content upon reduction of the metal ions with $NaBH_4$ as observed via H_2-TPD analysis.

4.5 Hydrogenation of Benzene

The reaction rates for the hydrogenation of benzene to cyclohexane with various PtNi catalysts as a function of temperature were investigated and are illustrated in Figure 4.10. Analysis of the support mixed with $NaBH_4$ (not shown in Figure 4.10) exhibited no activity at all. PtNi catalysts on the other hand showed an increase in reaction rates and a shift towards lower temperatures with increasing Pt content. The Ni_{100}-CP catalyst showed no reaction rates, similar to that of the support mixed with $NaBH_4$ in the temperature range studied. However, incorporation of Pt in the catalysts resulted in drastic increases in the reactions rates. Both $Pt_{22}Ni_{78}$-CP and $Pt_{47}Ni_{53}$-CP exhibited reaction rates of approximately 3.5 x 10^{-3} mol min^{-1} g_{met}^{-1} at 420 K and 397 K respectively. Further increase of the Pt content in the catalyst $Pt_{90}Ni_{10}$-CP demonstrated an even higher reaction rate of 10.7 x 10^{-3} mol min^{-1} g_{met}^{-1} at 368 K. Interestingly this is 4.4 x 10^{-3} mol

min^{-1} g_{met}^{-1} higher than that of the Pt_{100}-CP catalyst which exhibits maximum reaction rates at 400 K.

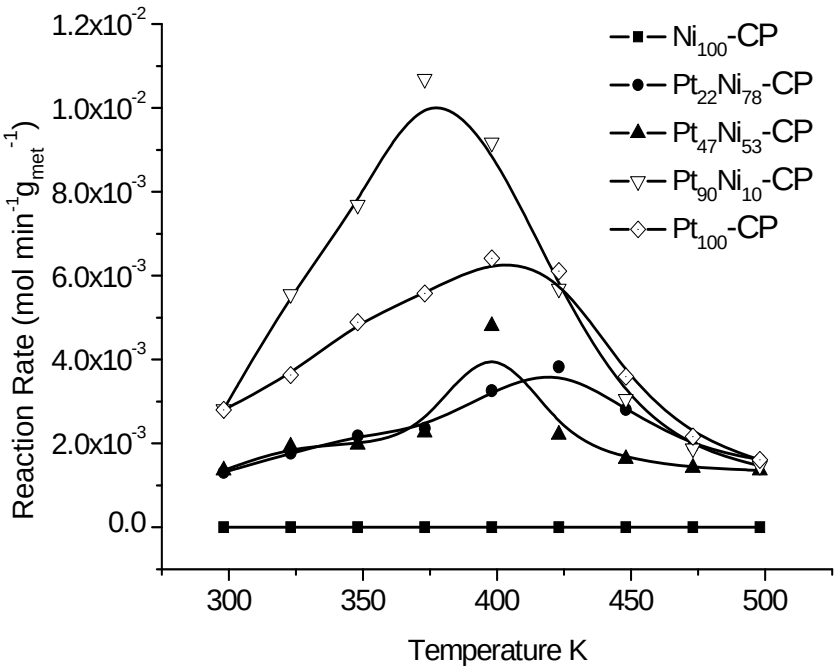

Figure 4.10: Profiles of the reaction rate of hydrogenation of benzene to cyclohexane for various PtNi catalysts supported on crystalline silica relative to the reaction temperature.

High reaction rates are always observed for aromatic hydrogenation over group VIII metal catalysts [50]. Hence, bimetallic catalysts containing a metal from this group have frequently shown high reaction rates. Research on the PtNi systems suggested that the occurrence of synergistic effects between Ni and Pt upon alloying occur [27, 28, 51]. This influences the metals electronic structure and indirectly the chemisorption properties of the molecules/atoms on the metals involved, which leads to changes in the reaction rates. Numerous factors can change the electronic structure as a result of alloying. Among these are the

difference in Pt-Pt bond distance, number of Pt nearest neighbours as well as electron density of the Pt d orbital [52, 28].

In this study, the high reaction rate exhibited by the $Pt_{22}Ni_{78}$-CP and $Pt_{47}Ni_{53}$-CP catalysts as compared to Ni_{100}-CP may be explained as due to the presence of Pt in the bimetallic catalysts. However, the enhanced reaction rate of the $Pt_{90}Ni_{10}$-CP when compared to the Pt_{100}-CP catalysts can be attributed to several factors. Comparison of the average particle sizes of Pt_{100}-CP and $Pt_{90}Ni_{10}$-CP indicates that Pt_{100}-CP particles are smaller however reactivity of the $Pt_{90}Ni_{10}$-CP is much higher. This signifies that the morphology of the metal particles did not affect the reactivity and emphasizes that the reactivity may be attributed to alloying between the Pt and Ni metals. This was shown previously via line analysis and XPS results. Surface segregation of Pt which is more active than Ni atoms, seen in the XPS studies could have also played a role in promoting the reactivity of this catalyst. In this system, contribution of NiB, if any, to the reaction rate is minimal considering Ni_{100}-CP which contains the highest B content exhibits inactivity towards the hydrogenation of benzene to cyclohexane.

4.6 Summary

The present study shows that the catalysts prepared via non-classical method using $NaBH_4$ as the reducing agent facilitates the formation of totally reduced bimetallic metal particles. Hence, activation at high temperatures for long durations is unnecessary. TEM analysis reveals that the metal phase in the Pt_{100}-CP, Ni_{100}-CP and $Pt_{90}Ni_{10}$-CP catalysts exist as fractal morphologies. Enhanced activity is seen for all bimetallic catalysts when compared to Ni_{100}-CP. Even so, the best catalytic activity is seen for the $Pt_{90}Ni_{10}$-CP. Results indicate

that alloying and Pt segregation on the surface of the alloys are factors that lead to the improved conversion of benzene.

4.7 References

[1] Y. Li, G. H. Lai, R-X Zhou, Appl. Surf. Sci. 253 (2007) 4978.

[2] E. Antolini, J. R. C. Salgado, R. M. da Silva, E. R. Gonzalez, Mater. Chem. Phys. 101 (2007) 395.

[3] Z. Xiong, Z. Mi, X. Zhang, Catal. Commun. 8 (2007) 571.

[4] Y. He, M. Qiao, H. Hu, J-F Deng, K. Fan, Appl. Catal. A: Gen. 228 (2002) 29.

[5] K. Torigoe, Y. Nakajima, K. Esumi, J. Phys. Chem. 97 (1993) 8304.

[6] M. Mandal, S. Kundu, S. K. Ghosh, T. K. Sau, S. M. Yusuf, T. Pal, J. Coll. Interf. Sci. 265 (2003) 23.

[7] T. C. Deivaraj, W. Chen, J. Y. Lee, J. Mater. Chem. 13 (2003) 2555.

[8] A-G Boudjahem, M. Pietrowski, S. Monteverdi, M. Mercy, M. M. Bettahar, J. Mater. Sci. 41 (2006) 2025.

[9] M. M. Telkar, J. M. Nadgeri, C. V. Rode, R. V. Chaudhari, Appl. Catal. A: Gen. 295 (2005) 23.

[10] Y. Liang, H. Zhang, B. Yi, Z. Zhang, Z. Tan, Carbon 43 (2005) 3144.

[11] S. Zhou, B. Varghese, B. Eichhorn, G. Jackson, K. McIlwrath, Angew. Chem. 117 (2005) 4539.

[12] S. Sun, C. B. Murray, D. Weller, L. Folks, A. Moser, Science 287 (2000) 1989.

[13] J. Luo, M. M. Maye, V. Petkov, N. N. Kariuki, L. Wang, P. Njoki, D. Mott, Y. Li, C.-J. Zhong, Chem. Mater. 17 (2005) 3086.

[14] X. Teng, H. Yang, Nanotechnology 16 (2005) S554.

[15] H. M. Chen, H.-C Peng, R. S. Liu, S. F. Hu, L.-Y. Jang, Chem. Phys. Lett. 420 (2006) 484.

[16] A. Jasik, R. Wojcieszak, S. Monteverdi, M. Ziolek, M. M. Bettahar, J. Mol. Catal. A: Chem. 242 (2005) 81.

[17] A. G. Boudjahem, S. Monteverdi, M. Mercy, M. M. Bettahar, Langmuir, 20 (2004) 208.

[18] R. Wojcieszak, S. Monteverdi, J. Ghanbaja, M. M. Bettahar, J. Coll. Interf. Sci. 317 (2008) 166.

[19] C. N. Satterfield, 1991. Heterogeneous Catalysis in Industrial Practice, 2nd Ed, USA, McGraw-Hill Inc.

[20] G. Neri et al, Appl. Catal. A: Gen. 356 (2009) 113.

[21] S. Chytil, W. R. Glomm, I. Kvande, Z. Tiejun, and E. A. Blekkan, Studies Surf. Sci. Catal. 162 (2006) 513.

[22] K. Hadjiivanov, M. Mihaylov, D. Klissurski, P. Stefanov, N. Abadjieva, E. Vassileva, L. Mintchev, J. Catal. 185 (1999) 314.

[23] S. Ramu, N. Lingaiah, B.L.A. Prabhavathi Devi, R.B.N. Prasad, I. Suryanarayana, P.S. Sai Prasad, Appl. Catal. A: Gen. 276 (2004) 163.

[24] Y. Koltypin, G. Katabi, X. Cao, R. Prozorov, A. Gedanken, J. Non-Cryst. Solids 201 (1996) 159 .

[25] S.Y. Choi, Y.S. Kwon, S.C. Hong, J.I. Lee, R.Q. Wu, J. Magn. Magn. Mater. 226-230 (2001) 1662.

[26] P. Deurinck, C. Creemers, Surf. Sci. 441 (1999) 493.

[27] Y. Zhao, E. Yifeng**.** L. Fan, Y. Qiu, S. Yang, Electrochim. Acta 52 (2007) 5873.

[28] H. Yang, W. Vogel, C. Lamy, N. Alonso-Vante, J. Phys. Chem. B 108 (2004) 11024.

[29] H. Li, H. Li, J. F. Deng, Catal. Today 74 (2002) 53.

[30] E. Ben-Jacob, P. Garik, Nature 343 (1990) 523.

[31] Z. W. Chen, J. K. L. Lai, C. H. Shek, H. D. Chen, Appl. Surf. Sci. 250 (2005) 3.

[32] E. Nouri, A. Dolati, Mater. Res. Bull. 42 (2007) 1769.

[33] T. Pajkossy, L. Nyikos, Electrochim. Acta 34 (1989) 171.

[34] J. Li, N. J. Coville, Appl. Catal. A: Gen. 181 (1999) 201.

[35] L. Chen, Y. Lua, Q. Hong, J. Lin, F.M. Dautzenberg, Appl. Catal. A: Gen. 292 (2005) 295.

[36] A. Borodzinski, M. Bonarowska, Langmuir 13 (1997) 5613.

[37] U. A. Paulus, A. Wokaun, G. G. Scherer, T. J. Schmidt, V. Stamenkovic, V.

Radmilovic, N. M. Markovic, P. N. Ross, J. Phys. Chem. B 106 (2002) 4181.

[38] P. Sivakumar, R. Ishak, V. Tricoli, Electrochim. Acta 50 (2005) 3312.

[39] S. Chettibi, R. Wojcieszak, E. H. Boudjennad, J. Belloni, M. M. Bettahar, N. Keghouche, Catal. Today 113 (2006) 157.

[40] K-W Park, J. H. Choi, B. K. Kwoon, S-A Lee, Y-E Sung, H-Y Ha, S-A Hong, H. Kim, A. Wieckowski, J. Phys. Chem. B 106 (2002) 1869.

[41] F. Liu, J. Y. Lee, W. Zhou, J. Phys. Chem. B 108 (2004) 17959.

[42] F. Liu, J. Y. Lee, W. J. Zhou, Small 2(1) (2006) 121.

[43] K-W. Park, J-H. Choi, Y-E. Sung, J. Phys. Chem. B 107 (2003) 5851.

[44] H. W. Hugosson, O. Eriksson, U. Jansson, I. A. Abrikosov, Surf. Sci. 585 (2005) 101.

[45] Y. Lu, J. Li, J. Lin, Catal. Lett. 76 (2001) 167.

[46] Y. Feng, Y. Li, H. Yuan, J. Alloys Comp. 468 (2008) 575.

[47] M. Hatano, H. Kinoshita, Appl. Surf. Sci. 121-122 (1997) 278.

[48] D. Hullmann, G. Wendt, U. Šingliar, G. Ziegenbalg, Appl. Catal. A: Gen. 225 (2002) 261.

[49] R. Zhang, F. Li, N. Zhang, Q. Shi, Appl Catal. A: Gen. 239 (2003) 17.

[50] M. A. Keane, J. Catal. 166 (1997) 347.

[51] J. F. Drillet, A. Ea, J. Freidemann, R. Kotz, B. Schnyder, V. M. Schmidt, Electrochim. Acta 47 (2002) 1983.

[52] L. Xiong, A. M. Kannan, A. Manthiram, Electrochem. Commun. 4 (2002) 898.

CHAPTER 5

EFFECT OF IMPREGNATION TECHNIQUE FOR CATALYSTS PREPARED VIA NON-CLASSICAL METHODS

5.1 Introduction

Supported bimetallic nanoparticles have received increasing attention as catalysts, as prices of metals such as Pt have seen a drastic hike over the past decade. As shown in the previous chapter, the addition of a transition metal to an active metal may enhance catalytic reactivity. However, this is influenced by several factors among them the PtNi ratio and its structure. As an example, PtNi supported ZrO_2 catalysts have been employed for reactions such as the hydrogenation of chloronitrobenzene [1] and cinnamaldehyde [2]. In the hydrogenation of chloronitrobenzene the PtNi/ZrO_2 shows low hydrogenation activity but an increase in its yield to form chloroaniline [1]. In contrast, better selectivity towards hydrocinnamaldehyde and higher hydrogenation rates with the amount of Ni is observed for the hydrogenation of cinnamaldehyde [2]. Frequently, these superior characteristics are discussed based on the electronic and/or geometric effects which occur when two or more metals are available.

The incorporation of two metals in a system can form alloyed or non-alloyed bimetallic nanoparticles. The alloyed particles may adopt a random alloy or intermetallic structure while non-alloyed particles may result as, cluster in

cluster or core-shell structures [3]. The formation of these structures is drastically influenced by the conditions in which they are synthesized in. Hence, elaborate understanding of factors such as the choice of metal, stabilizer or support employed as well as the preparation technique is essential to design bimetallic nanoparticles suitable for a certain catalytic reaction. For instance, some works have shown that simultaneous reduction of metal ions such as Pt and Pd in stabilizers such as PVP can generate core shell bimetallic nanoparticles [4], while others have demonstrated that incipient wetness impregnation techniques favour the formation of alloys with a random distribution [5]. This shows the significance of the preparation technique employed. It is also important to understand that the factors mentioned above inter-correlate with each other. Hence, it is difficult to predict the final outcome of the bimetallic particles in a certain system. This has lead to diverse findings even when similar preparation techniques are employed.

Therefore, it is the objective of this chapter to investigate how the preparation techniques affect the properties of PtNi structures supported on silica. For this purpose, the PtNi-silica was prepared via co-impregnation (CI) and step-impregnation (SI) techniques using similar reducing methods as in Chapter 4. The characteristics of the samples are investigated in order to gain a better insight on its surface properties and the as formed structures and their effect on the catalytic reaction.

5.2 Surface Characteristics

5.2.1 H_2-TPR Analysis

The active phase in catalysts plays an important role in catalytic reactions. It acts as sites that allow the adsorption of reactant gas molecules and subsequent reaction and conversion to products. This active phase is usually comprised of transition metals and is most active in its reduced state. In order to gain insight on the state in which these phases exist, H_2-TPR analysis was conducted. H_2-TPR profiles of the Pt_{100}-I and Ni_{100}-I catalysts are shown in Figure 5.1(a). The profile of Pt_{100}-I does not exhibit any H_2 consumption peaks and hence indicates that the catalyst is in its reduced state.

Contrary to this, the Ni_{100}-I catalyst exhibits two hydrogen consumption peaks. These peaks are positioned at 677 and 805 K. The peak positioned at approximately 677 K has frequently been reported to be attributed to the existence of nickel oxides [6, 7]. However, the assignment of the peak positioned at 805 K is controversial. Similar to the peak at 677 K, this peak may signify the presence of Ni^{2+} ions in the form of nickel oxides [7]. It is possible that the nickel oxides originate from the re-oxidation of metallic nickel formed during reduction with $NaBH_4$. Oxidation could have occurred during handling or storage of the samples. Hence, the two peaks may be attributed to the occurrence of metal particles with different sizes [7]. The peak at 805 K may be related to larger particles while the peak arising at 677 K can be attributed to smaller particles. Similar observations were also seen by Rynkowski and co-workers [8].

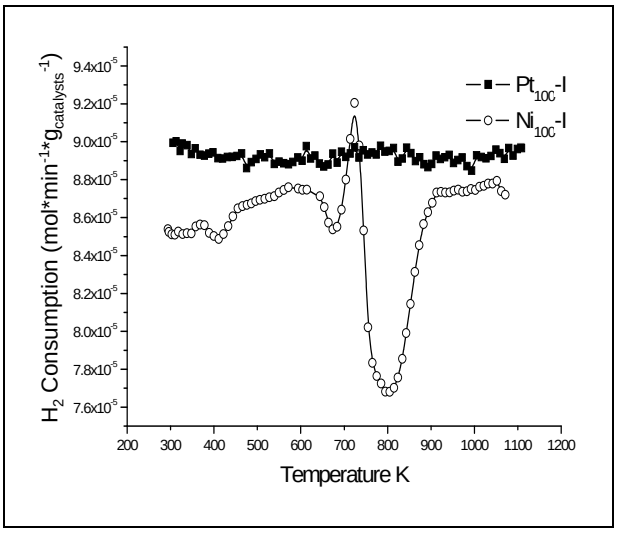

(a)

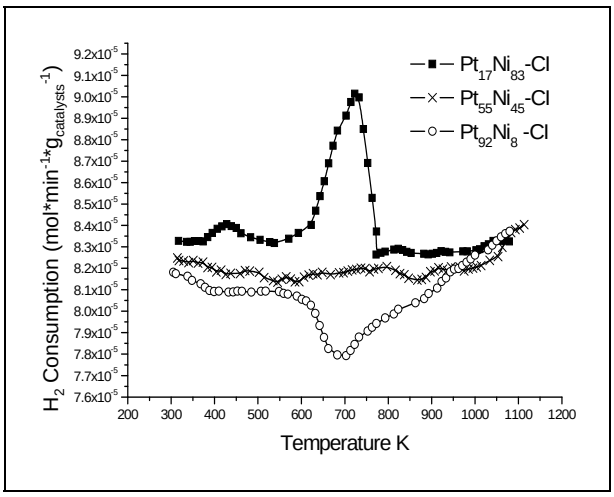

(b)

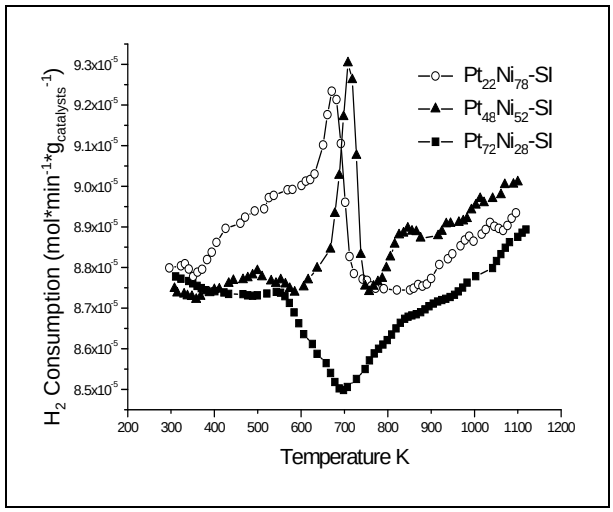

(c)

Figure 5.1: TPR profiles of (a) Pt_{100}-I and Ni_{100}-I catalysts as well as catalysts prepared via (b) CI and (c) SI technique.

Though this might occur in this work, it is important to consider that the peak at 805 K may also identify the availability of phyllosilicates, which is a type of nickel silicate. This compound occurs via strong interaction between the nickel ions and SiO_2 support [9]. Though SiO_2 is an inert support, it is well established that impregnation of Ni salts onto SiO_2 leads to strongly and weakly adsorbed Ni^{2+} ions [9, 10]. The phyllosilicates are obtained by impregnation of the nickel salt followed by washing and subsequent drying of the catalysts at temperatures below 373 K. The washing stage removes free Ni^{2+} ions which would otherwise form weakly adsorbed Ni^{2+} ions [9]. In this work, the Ni_{100} catalyst was prepared by simple impregnation followed by the drying stage. The catalyst was washed only after reduction with $NaBH_4$. Therefore, the weakly attached Ni^{2+} ions should give rise to large Ni metal particles which may reoxidize upon contact with air, the extent of reoxidation depending on the particle size. Phyllosilicates are not expected to form or exists as a minor species if any.

Subsequently, impregnation of Ni in the Pt catalysts resulted in the formation of catalysts with slightly different surface properties. The co-impregnated catalysts (Figure 5.1(b)) containing low to moderate amounts of Pt ($Pt_{17}Ni_{83}$-CI and $Pt_{55}Ni_{45}$-CI) exhibited no hydrogen consumption in the temperature range studied. Similar to the pure Pt catalysts, this signifies that total metal reduction occurred during the reduction stage with $NaBH_4$. In comparison, the catalysts with high Pt content demonstrated a consumption of hydrogen at approximately 679 K. Total H_2 consumption of the $Pt_{92}Ni_8$-CI catalyst is 1.33 x 10^{-3} mol g_{met}^{-1}. This corresponds to 21.7 % of the total mol metal content existing as oxides. In accordance with the peak position, we attribute this H_2 consumption as due to the occurrence of nickel oxide.

The catalysts prepared via step-impregnation technique also showed similar hydrogen consumption trends with those prepared via co-impregnation technique. This is shown in Figure 5.1(c). Both the $Pt_{22}Ni_{78}$-SI and $Pt_{48}Ni_{52}$-SI catalysts showed no hydrogen consumption while catalysts with high Pt content ($Pt_{72}Ni_{28}$-SI) demonstrated a consumption of 4.50 x 10^{-3} mol g_{met}^{-1} at 689 K. This is similar to the hydrogen consumption peak in the pure Ni catalyst and amounts to 52.9 % of the total mol metal content.

The occurrence of metal oxides or more specifically nickel oxides in catalysts with high Pt content, regardless of the preparation method employed, can only be explained as due to the occurrence of Pt and Ni existing as separate entities. The profiles clearly demonstrate that in these catalysts, Pt does not catalyze total reduction of the nickel oxides. This phenomenon is surprising and is yet to be fully understood.

Another interesting feature observed for the Ni_{100}-I catalyst as well as both the co- and step-impregnated catalysts with more than 50 % Ni content, is that a maximum H_2 production is seen at approximately 630 -740 K. Profiles of the Ni_{100}, $Pt_{17}Ni_{83}$-CI as well as $Pt_{22}Ni_{78}$-SI and $Pt_{48}Ni_{52}$-SI catalysts, indicate that maximum H_2 desorbed at temperatures of 735 K (1.73 x 10^{-3} mol g_{met}^{-1}), 727 K (3.63 x 10^{-3} mol g_{met}^{-1}), 679 K (9.10 x 10^{-4} mol g_{met}^{-1}) and 720 K (2.10 x 10^{-3} mol g_{met}^{-1}) for the four catalysts respectively. This shows that similar H_2 adsorption sites exist in the catalysts. Some hydrogen desorption is also seen at higher temperatures. The adsorption of hydrogen may have originated from two possibilities. Primarily, adsorption of H_2 may have occurred during the reduction stage. Hydrogen gas which is produced during the reduction of metal ions with $NaBH_4$ may have adsorbed onto certain phases of the metal structure. Second, the

TPR analysis was preformed in a H_2 atmosphere. Hence, it is possible that H_2 gas adsorbed at lower temperatures are desorbed at higher temperatures. Similar behaviour has been observed for Pd supported SiO_2 catalysts [11]. Palladium can form hydrides, which acts as a reversible storage medium for active hydrogen.

5.2.2 H_2-Chemisorption

H_2-chemisorption was carried out and values are tabulated in Table 5.1. Analysis of the samples show that the Ni_{100}-I catalyst exhibited the lowest amount of adsorbed H_2. In contrast the Pt_{100}-I catalyst adsorbed approximately 32.41 x 10^{-5} mol g_{met}^{-1} of H_2 at room temperature. This is 20 times more than that exhibited by the Ni_{100}-I catalyst. Comparison of the Pt_{100}-I catalyst, with the bimetallic PtNi catalysts also show that the later catalysts exhibit lower H_2-chemisorption properties. Catalysts prepared via step-impregnation show a similar trend to those prepared via co-precipitation technique. Increasing amounts of Pt content increased the amount of H_2-chemisorbed. The catalysts prepared via co-impregnation on the other hand, showed a unique tendency. In this series, a significant increase in the H_2 adsorption is observed when the Pt content is increased from 17 to 55 wt %. H_2-adsorption for the two catalysts are 6.84 x 10^{-5} and 28.2 x 10^{-5} mol g_{met}^{-1} correspondingly. Upon subsequent increase in the Pt content to 92 wt %, it was found that the amount of adsorbed H_2 decreased to 18.25 x 10^{-5} mol g_{met}^{-1}. This suggests that a greater number of similar active sites are available in the $Pt_{55}Ni_{45}$-CI catalyst in comparison to other bimetallic catalysts.

The dispersion of the metal phase in the catalysts was calculated based on the H_2-chemisorption data. It was found that low dispersions were obtained

ranging from 0.2 – 6.3 %. All the bimetallic catalysts showed lower dispersions when compared to the Pt_{100}-I. However, the $Pt_{55}Ni_{45}$-CI catalyst exhibited a dispersion similar to the Pt_{100}-I.

Table 5.1: Amounts of H_2 chemisorbed, production and desorbed from H_2-chemisorption, H_2-TPR and H_2-TPD analysis.

Catalyst	Total Metal Content (wt %)	Metal Content (wt %) Pt	Ni	H_{2ads} at RT [a] (x 10^{-5} mol g_{met}^{-1})	Dispersion [b] (%)
Ni_{100}-I	4.21	-	4.21	1.62	0.2
$Pt_{17}Ni_{83}$-CI	4.40	0.77	3.63	6.84	0.8
$Pt_{55}Ni_{45}$-CI	2.35	1.29	1.06	28.20	5.5
$Pt_{92}Ni_{8}$-CI	2.25	2.06	0.19	18.25	3.6
$Pt_{22}Ni_{78}$-SI	3.58	0.77	2.81	2.74	0.3
$Pt_{48}Ni_{52}$-SI	3.36	1.62	1.74	9.23	1.8
$Pt_{72}Ni_{28}$-SI	2.89	2.07	0.82	19.10	3.7
Pt_{100}-I	2.63	2.63	-	32.41	6.3

[a] at room temperature after activation in H_2/473 K/15 min
[b] calculated based on H_2 chemisorption analysis

5.2.3 H_2-TPD Analysis

The H_2-TPD profiles of the Pt_{100}-I and Ni_{100}-I catalysts are exhibited in Figure 5.2(a). Both catalysts show very different characteristics. The H_2-TPD profile of Ni_{100}-I indicates two main peaks positioned at 621 K and 741 K. These peaks coincide roughly with the H_2-TPR profiles. The peak at 621 K is attributed to H_2 strongly adsorbed onto the Ni surface while the desorption band occurring at 741 K can be explained as due to hydrogen retained at the interphase of the metal support [12]. As much as 2.34 x 10^{-3} mol $g_{(metal)}^{-1}$ hydrogen is desorbed from this catalyst.

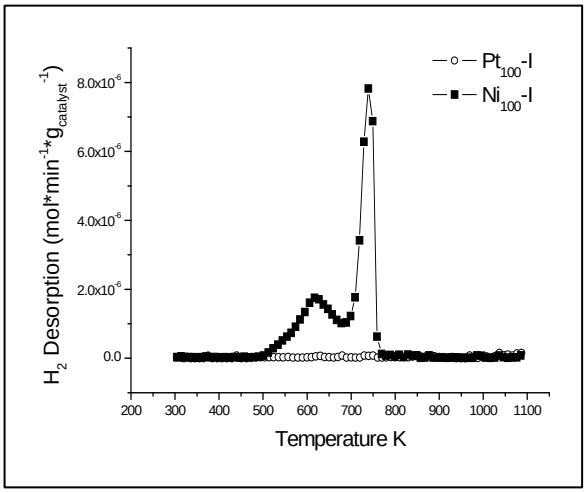

(a)

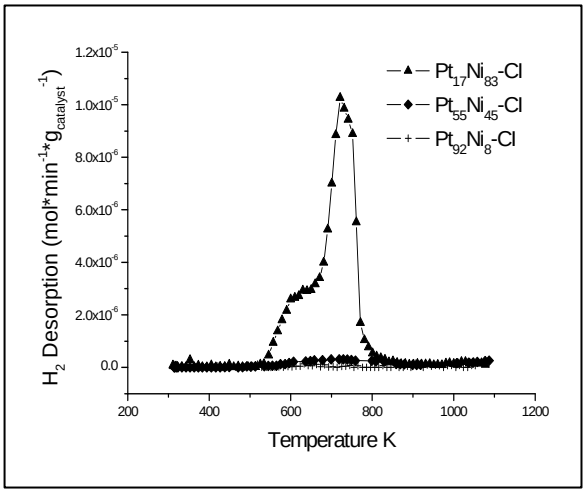

(b)

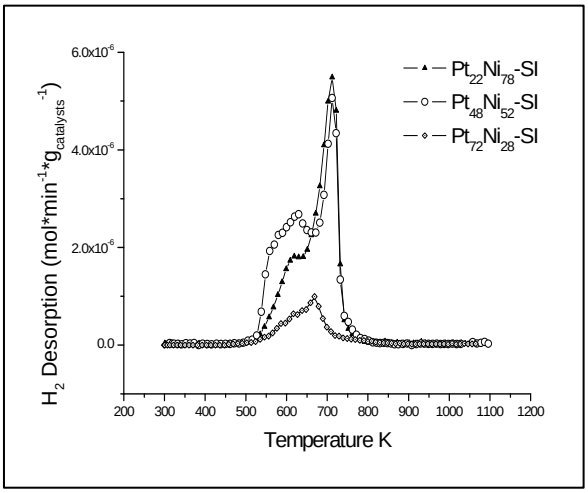

(c)

Figure 5.2: TPD profiles of (a) Pt_{100}-I and Ni_{100}-I catalysts as well as PtNi catalysts supported on silica prepared via (a) CI and (b) SI technique.

In contrast, the H_2-TPD analysis of Pt_{100}-I shows an almost flat profile. It is interesting to note that very little desorption occurred for this catalysts. This occurrence can be explained as due to the hydrogen weakly adsorbed onto the Pt surface when compared to Ni on which hydrogen is more strongly adsorbed. The difference in adsorption characteristics of Pt and Ni can be explained based on their positions in the periodic table. Atoms at the top of the periodic table such as Ni generally have stronger chemisorption characteristics compared to atoms positioned further down such as Pt. This is due to the increase occupancy of the d bands in the Pt atoms. The lower strength of adsorption for Pt_{100}-I may have caused the hydrogen adsorbed during activation to desorb during the purging treatment following the activation. Hence this explains the lack of hydrogen desorption during the H_2-TPD analysis for catalysts with high Pt content.

Subsequently, H_2-TPD profiles of the bimetallic catalysts were investigated. It is observed that CI catalysts exhibit two types of catalysts. The profiles are shown in Figure 5.2 (b). The first type is of $Pt_{17}Ni_{83}$-CI. This catalyst shows similar characteristics to that of Ni_{100}-I. Two peaks positioned at 613 K and 732 K is observed. These peaks are shifted to lower temperatures when compared to Ni_{100}-I. The shifts can be explained as due to the addition of platinum in the samples. Following this, a high amount of H_2 (5.02×10^{-3} mol g_{met}^{-1}) was desorbed from the catalyst when compared to Ni_{100}-I. We attribute this to the incorporation of H_2 during the reduction stage as well as during the activation stage. This correlates well with the H_2-TPR profiles. The second type of catalysts observed is for samples $Pt_{55}Ni_{45}$-CI and $Pt_{91}Ni_{8}$-CI. Both these catalysts can be described as similar to the pure Pt type. Very little desorption is

observed, hence it is possible to summarize that these bimetallic catalysts have similar characteristics to Pt_{100}-I.

The SI catalysts as presented in Figure 5.2 (c) also show two types of catalysts. However, in contrast to the types observed in the CI technique, a separate type of catalyst is also observed. The first type of catalysts includes $Pt_{22}Ni_{78}$-SI and $Pt_{48}Ni_{52}$-SI. These catalysts are comparable to that of Ni_{100}-I and $Pt_{17}Ni_{83}$-CI. It is observed that the desorption peaks for $Pt_{22}Ni_{78}$-SI and $Pt_{48}Ni_{52}$-SI are also shifted to lower temperatures in the range of 620-625 K and 710-715 K. On the other hand, the second type of catalyst is solely of $Pt_{72}Ni_{28}$-SI. This type of catalysts was not observed in the samples prepared via the previous method. Though $Pt_{72}Ni_{28}$-SI exhibits two peaks, both are positioned at temperatures much lower than the first type. Deconvolution of the TPD profiles indicate that the peaks are at 623 K and 667 K. These peaks are characteristic of hydrogen strongly attached to the Ni particle or hydrogen which exists at the metal support interphase [12].

Based on the surface properties investigated, it is found that two main types of catalysts occur; catalysts that are characteristic of Ni_{100}-I and catalysts characteristic of Pt_{100}-I. Only $Pt_{72}Ni_{28}$-SI shows properties unlike the previous two types.

5.3 TEM Analysis

The morphology of the catalysts was studied using TEM analysis. Images of the Pt_{100}-I, Ni_{100}-I and typical images of the bimetallic catalysts are exhibited in Figure 5.3.

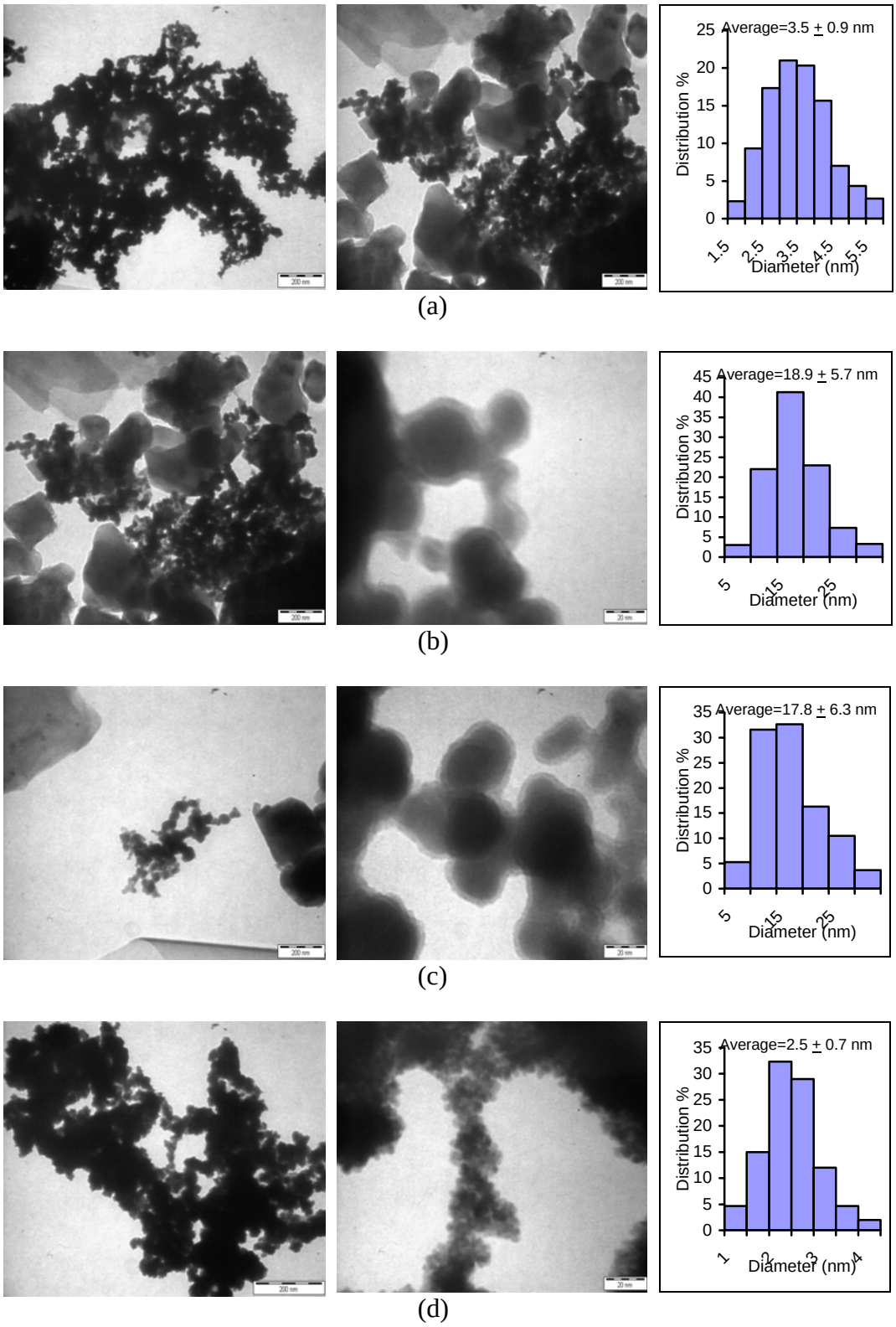

Figure 5.3: TEM micrographs of (a) Pt_{100}-I (b) Ni_{100}-I (c) $Pt_{48}Ni_{52}$-SI and (d) $Pt_{55}Ni_{45}$-CI and their corresponding histograms on size distribution.

As can be seen, all samples demonstrate the formation of fractals. Similar morphologies have been observed elsewhere [13, 14]. These fractals occur due to the agglomeration of smaller metal particles. The images demonstrate that the particles in all samples are spherical in shape. However, an interesting feature in the Ni_{100}-I and $Pt_{48}Ni_{52}$-SI catalysts is that the spherical particles are surrounded by a thin shell. This shell has been described to be a layer of oxide surrounding the metal core [15, 16]. Such a phenomenon was not observed in the Pt_{100}-I and the bimetallic $Pt_{55}Ni_{45}$-CI catalyst. Hence, this shows that oxidation of the Ni_{100}-I and $Pt_{48}Ni_{52}$-SI occurred during the preparation or storage stage. Even so the degree of oxidation in both samples varies. As was observed in the H_2-TPR studies, large hydrogen consumption is observed for the Ni_{100}, hence indicates that extensive oxidation occurred. In contrast, no hydrogen consumption was seen in the TPR profiles of $Pt_{48}Ni_{52}$-SI catalyst. Therefore it is possible that little oxidation occurred in this sample. Such a phenomenon may be explainable as due to the existence of Pt that changes the adsorption properties of the synthesized catalyst.

Following this, average sizes of the particles are obtained and reported in Table 5.2. A comparison of the average particle sizes of Pt_{100}-I and Ni_{100}-I shows that the Ni particles are approximately five times larger than the Pt particles. This may be attributed to the magnetic nature of the Ni catalysts, which promotes particle agglomeration. Upon alloying of the Pt and Ni, it is seen that the average particle size decreased significantly with the increase in Pt content when compared to the Ni_{100}-I catalyst. A comparison of the $Pt_{17}Ni_{83}$-CI and $Pt_{22}Ni_{78}$-SI catalysts show that the average particle size of the particles are 7.3 ± 5.0 and 9.7 ± 5.8 nm respectively. Similarly, the $Pt_{55}Ni_{45}$-CI and $Pt_{48}Ni_{52}$-SI catalysts give

average particle sizes of 2.5 ± 0.6 and 17.9 ± 6.3 nm respectively. The difference in the average particle sizes of the bimetallic nanoparticles, prepared via different techniques but with similar PtNi compositions may indirectly affect the reactivity of the catalysts due to the variation in surface area available for reaction.

Table 5.2: Physico-chemical characteristics of supported silica catalysts.

Catalysts	Atomic Percentage		Average Particle Size (nm)	Dispersion [a] (%)
	Pt	Ni		
Pt_{100}-I	100	-	3.5 ± 0.9	41.3
$Pt_{17}Ni_{83}$ -CI	6.0	94.0	7.3 ± 5.0	11.0
$Pt_{55}Ni_{45}$ -CI	26.8	73.2	2.5 ± 0.7	54.0
$Pt_{92}Ni_{8}$ -CI	76.5	23.5	2.4 ± 0.6	54.1
$Pt_{22}Ni_{78}$-SI	7.6	92.4	9.7 ± 5.8	10.9
$Pt_{48}Ni_{52}$-SI	21.9	78.1	17.8 ± 6.3	8.9
$Pt_{72}Ni_{28}$-SI	43.1	56.9	2.3 ± 0.5	58.0
Ni_{100}-I	-	100	18.9 ± 5.7	7.3

[a] Calculated based on TEM analysis

The dispersion of the metal phase in the catalysts was also calculated based on the size distribution of the nanoparticles using the mathematical model described by Borodzinski and Bonarowska [17]. This technique was also applied by Yang et al. [18] who studied the synthesis of PtNi nanoparticles for catalytic application. Based on this method, the bimetallic $Pt_{55}Ni_{45}$-CI, $Pt_{92}Ni_{8}$-CI and $Pt_{72}Ni_{28}$-SI catalysts showed a high percentage of dispersion. Dispersion of the active phase is 54.0, 54.1 and 58.0 % respectively. This is comparable to the dispersion percentage of Pt_{100}-I which is 41.3 %. Other bimetallic catalysts showed low dispersion values similar to that of the Ni_{100}-I which is 7.3 %. As in the previous chapter, large differences in the dispersion values are obtained when this technique is employed in comparison to the H_2-chemisorption technique.

Similarly, this can be attributed to the fact that the H_2-chemisorption takes into consideration the accessible metal phase while the TEM method even includes particles which are overlapped but still exhibit its spherical shape. The nature in which the particles are attached to each other is not taken into account. Hence, in this chapter, the H_2-chemisorption gives a more likely percentage of dispersion.

5.4 Catalytic Activity

A control sample of silica impregnated with $NaBH_4$ was activated at 473 K in a flow of pure H_2. The sample which was exposed to a reaction stream containing benzene showed that no cyclohexane was detected indicating no conversion. Therefore the support and reducing agent used are inactive towards gas phase hydrogenation of benzene.

Reaction rates of the Pt_{100}-I and Ni_{100}-I catalysts as well as the bimetallic catalysts prepared via CI and SI technique are depicted in Figure 5.4(a)-(c). It was found that the reaction rate is dependant on the PtNi composition, temperature of reaction and preparation method. The Ni_{100}-I catalyst shows a nearly constant reaction rate in the temperature range of 298 to 347 K. The rate of reaction then increases until it reaches a maximum of about 2.14 $x10^{-3}$ mol min^{-1} g_{met}^{-1} at 431 K. In contrast, Pt_{100}-I is active even at low temperatures. The reaction rate at 298 K is 2.56 x 10^{-3} mol min^{-1} g_{met}^{-1} and a maximum reaction rate of 1.18 x 10^{-2} mol min^{-1} g_{met}^{-1} is obtained when temperature reaches 400 K. This is approximately a 5 fold increase over the Ni_{100}-I sample.

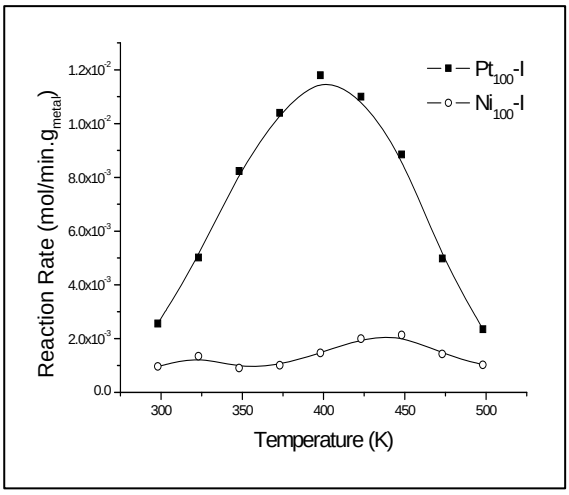

(a)

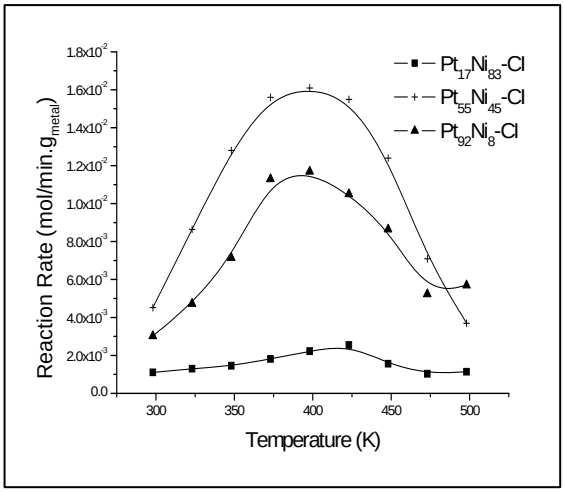

(b)

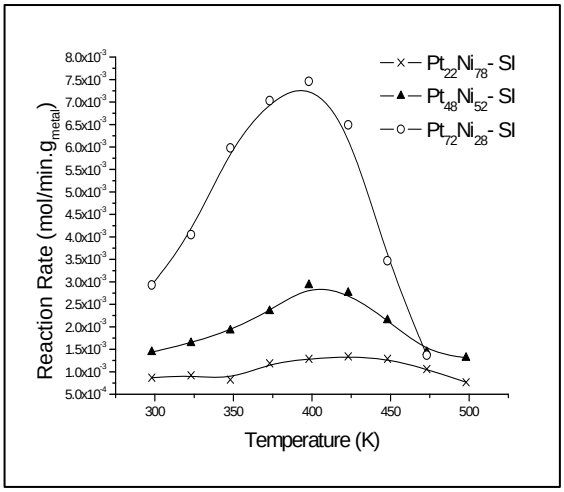

(c)

Figure 5.4: Reaction rates of hydrogenation of benzene for (a) Pt_{100}-I and Ni_{100}-I as well as PtNi catalysts prepared via (b) CI and (c) SI techniques.

Generally, the formation of bimetallic PtNi catalysts improves the reaction rate of benzene hydrogenation when compared to Ni_{100}-I. However, for samples prepared via SI technique, the reaction rate of the catalysts with 22 % of Pt ($Pt_{22}Ni_{78}$-SI) is lower than that of Ni_{100}-I. Only upon addition of the Pt content to 52 % and 72 % is there an improvement in the catalytic activity of the samples. Reaction rates of the catalysts increased to 2.85 x 10^{-3} and 7.30 x 10^{-3} mol min^{-1} g_{met}^{-1} respectively. Here, it can be seen that for this preparation technique, reaction rates increased with the amount of Pt added to the catalysts.

Interestingly, when the bimetallic catalysts were prepared via CI technique, better reaction rates are seen when compared to the SI technique. Comparison of the $Pt_{17}Ni_{83}$-CI catalysts with that of the $Pt_{22}Ni_{78}$-SI catalysts shows that the sample prepared via CI is enhanced by approximately 2 folds. The reaction rate of the $Pt_{17}Ni_{83}$-CI catalyst is 2.55 x 10^{-3} mol min^{-1} g_{met}^{-1}. Addition of Pt to 55 % ($Pt_{55}Ni_{45}$-CI) in the catalysts resulted in a drastic increase in reaction rate. Maximum rate reached 1.59 x 10^{-2} mol min^{-1} g_{met}^{-1} at 397 K. This is approximately 5 times higher than the catalyst with similar PtNi compositions prepared via SI and 25 % more than the reaction rate obtained for Pt_{100}. Even so, upon further increase of the Pt content to 92 % ($Pt_{92}Ni_{8}$-CI), it was observed that the conversion of benzene to cyclohexane decreased to similar reaction rates as that of Pt_{100}-I.

Further comparison of the Pt atomic percentage in the $Pt_{55}Ni_{45}$-CI catalysts shows that only 26.8 atomic % of Pt is available when compared to the Pt_{100} catalysts. The striking enhancement in the hydrogenation of benzene to cyclohexane can be attributed to the synergistic effect which occurs when Pt and Ni are in close proximity to each other. The smaller average PtNi particle size in

$Pt_{55}Ni_{45}$-CI (2.5 $\pm$ 0.6 nm) may also play a role in presenting a larger surface area available for reaction to occur, hence leading to the superior reactivity observed. However, this is not always the case considering that the $Pt_{92}Ni_{8}$-CI (76.5 at %) and $Pt_{72}Ni_{28}$-SI (43.1 at %) catalysts also have similar average particle size but lower reactivity values. Generally speaking, factors such as the method of preparation or PtNi ratio influence the particles size and structure of metal based catalysts. The similar particle sizes are only coincidences. The fractal morphologies evidenced by TEM are roughly different and this may explain the different activities observed. Fractals can be described by their fractal dimensions (D_F) which are characteristic of the porosity of the catalyst. Variations in this porosity can influence the diffusion and reaction phenomenon. Hence, the reactivity of the catalysts depends on the fractals formed. It has been shown that the energy of activation is dependant on the D_F of the catalyst [19]. Though previous works have discussed the reactivity of catalysts in terms of the D_F of metal supported catalysts whereby the support exhibits fractal morphologies [20, 21], we emphasize that in this work the very low surface area of the support and mild reduction conditions may not have played a role in changing the characteristics of the support. In contrast, the fractal nature of the active phase may be responsible for the variation in reactivity observed. A separate study is required to further understand how the D_F of the active phase influences catalytic reactivity.

In general, at high Ni metal loadings the catalytic activity of the catalysts are similar to that of the Ni_{100}-I due to the dominance of the Ni content. However, as the Ni content is reduced, a synergistic effect of the metals involved results in the enhancement in catalytic activity. This effect is then less observed when the

Pt is more dominant in the catalysts. In this case, the PtNi catalyst follows the nature of the Pt_{100}-I catalysts resulting in similar reaction rates.

5.5 Characteristics of $Pt_{55}Ni_{45}$-CI Catalyst

To understand the factors that may have caused the enhanced catalytic activity of the $Pt_{55}Ni_{45}$-CI catalyst, various analyses were carried out. SEM analysis with mapping of the $Pt_{55}Ni_{45}$-CI catalyst was conducted to investigate the distribution of the bimetallic nanoparticles on the silica. The darker area in the image of Figure 5.5(a) is of the silica support. The distribution of the Si is consistent with that of O. The brighter area in the image can be attributed to the metal phase. This correlates well with the distribution of Pt and Ni. Considering that similar distribution is observed for both the metals, it is highly likely that alloying of the metals occurred in the catalyst.

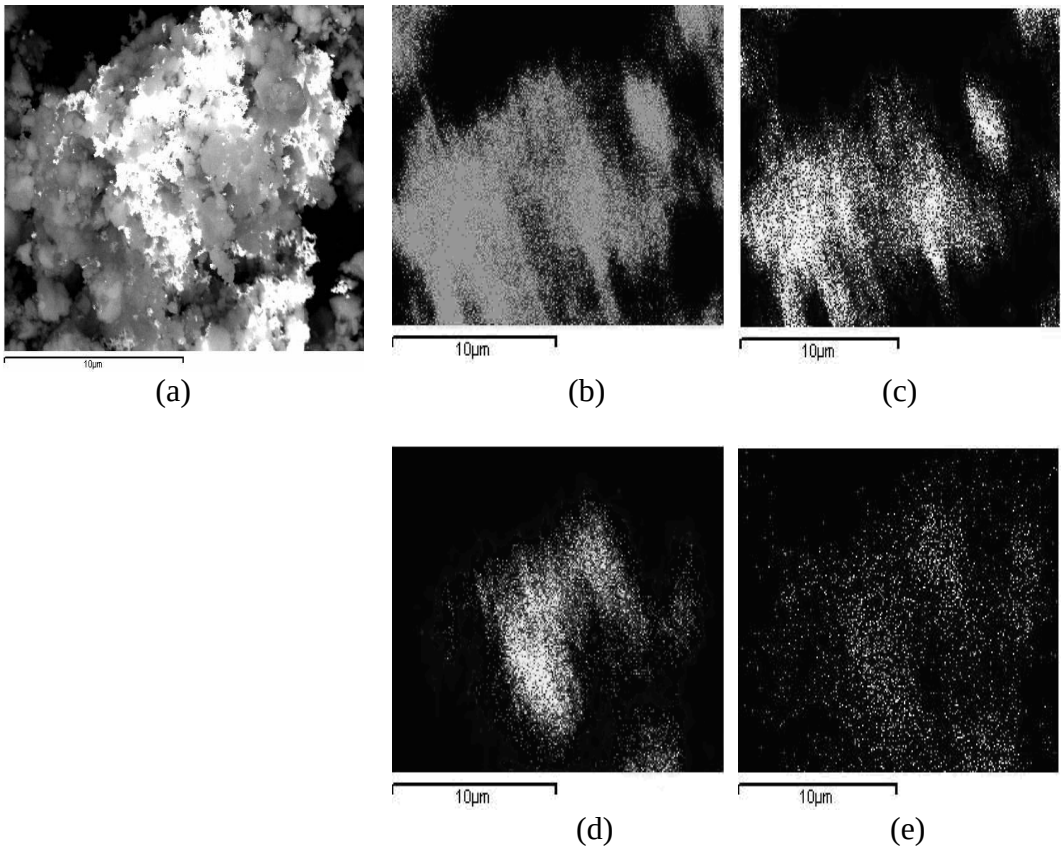

Figure 5.5: (a) SEM micrographs of $Pt_{55}Ni_{45}$-CI and corresponding distributions of (b) Si, (c) O, (d) Pt and (e) Ni.

To confirm the mapping analysis, XRD diffractograms of the fresh Pt_{100}-I, Ni_{100}-I and $Pt_{55}Ni_{45}$-CI catalysts were studied. However, subtraction of the silica diffractograms from the XRD diffractograms of the catalysts and further deconvolutions were necessary as the peaks of crystalline silica were superimposed with that of the Pt peaks. The XRD patterns are depicted in Figure 5.6. As can be seen, Pt_{100}-I shows the existence of peaks positioned at 2θ values of 39.91, 46.31, 67.76 and 81.71. These peaks are indicative of the (111), (200), (220) and (311) planes of the *fcc* crystalline structured Pt particles. Therefore Pt exists in its reduced state in the fresh catalyst. For the Ni_{100}-I supported on silica catalyst, no peaks indicating the existence of Ni are observed. Thus, considering

the large sized particles obtained via size distribution analysis, this shows that the Ni exists in an amorphous phase. Consequently, upon reduction of Ni ions in the presence of Pt, it is found that for $Pt_{55}Ni_{45}$-CI, only Pt peaks were observed, these peaks are shifted to higher 2θ values and are positioned at 40.23, 46.69, 67.98 and 82.26. This shift in the 2θ values is attributed to the alloying of the metals involved. Thus in this work, Ni is incorporated into the Pt structure. In addition, the average particle size of the nanoparticles formed based on the XRD analysis can be calculated using the Scherrer equation [22]. Values of 3.9 and 4.2 nm were obtained for the samples Pt_{100}-I and $Pt_{55}Ni_{45}$-CI respectively. These values differ from that obtained via TEM analysis and can be explained as due to the particle-particle interaction that may occur when particles are positioned close to each other.

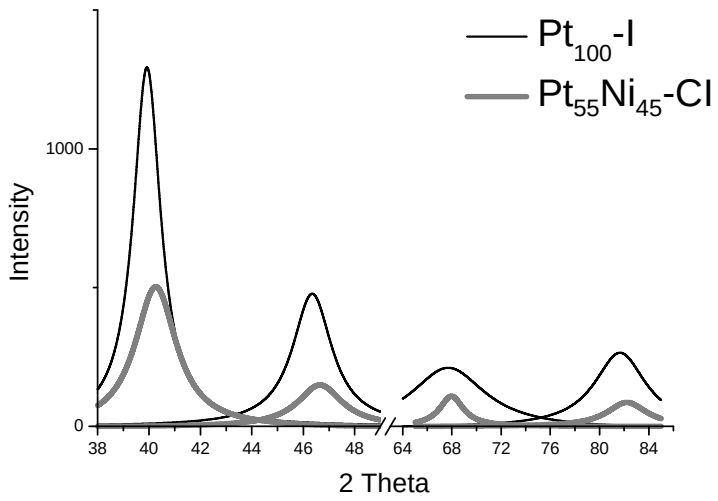

Figure 5.6: XRD diffractograms of Pt_{100}-I and $Pt_{55}Ni_{45}$-CI catalysts prepared via co-impregnation. Diffractograms are obtained after subtraction of the silica peaks.

To further investigate the nature of the catalyst, XPS measurements of the Pt_{100}-I and Ni_{100}-I were investigated and compared with the profile of $Pt_{55}Ni_{45}$-CI catalyst. The profile of the Pt 4f region in Figure 5.7 (a) exhibits doublet peaks at 71.4 and 74.8 eV. These peaks correspond to Pt $4f_{7/2}$ and Pt 4f $_{5/2}$ signals of metallic Pt. This correlates well with the TPR profiles of Pt_{100} as well as the XRD diffractograms.

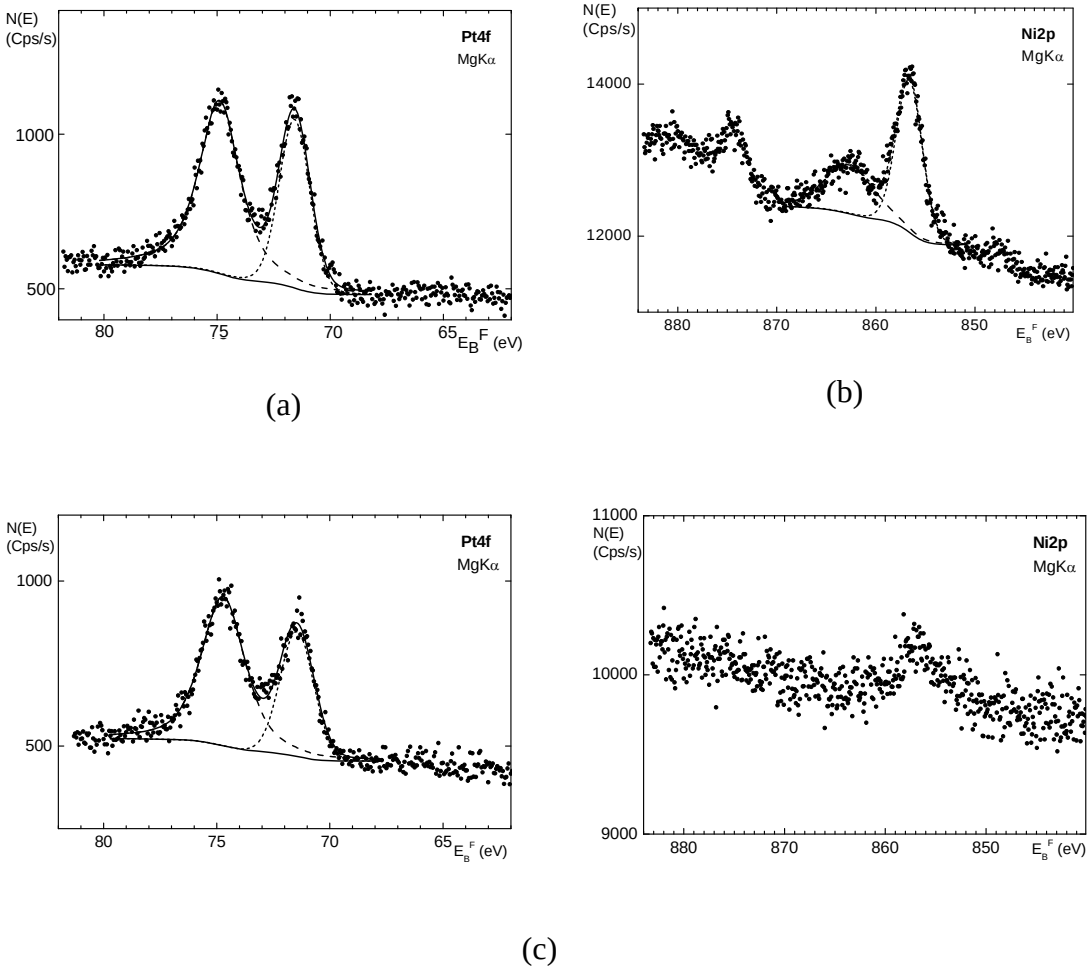

Figure 5.7: XPS profiles of (a) Pt_{100}-I (b) Ni_{100}-I (c) $Pt_{55}Ni_{45}$-CI

Subsequently, analysis of the states in which the nickel exists in the Ni_{100}-I catalyst was studied. Two prominent peaks at 856.9 and 862.4 eV are obtained in the Ni $2p_{3/2}$ spectrum. The peak positioned at 862.4 eV is known as the satellite peak that appears as a result of multielectron excitation [22, 23]. The occurrence of the peak at 856.9 eV on the other hand is ambiguous. In general, various works have reported that this peak can be attributed to the occurrence of Ni hydroxides in the samples and that deconvolution of this peak may give rise to several other peaks that indicate the occurrence of NiO as well as metallic Ni depending on the broadness of the peak [23]. However, it has been shown that for Ni supported on SiO_2 systems this peak can be attributed to the occurrence of nickel silicate ($NiSiO_3$). This indicates the formation of phyllosilicates to some extent. Considering the broadness of the peak which arises starting from 852.9 to 859.6 eV, it is also possible that the NiO or Ni_2O_3 peak overlaps with this peak. Both oxides usually exhibit a maximum at 854.3 eV and 856.0 eV respectively [24]. This corresponds to the H_2-TPR profiles previously discussed.

Investigation of the bimetallic nanoparticles reduced simultaneously reveals that signals indicating the presence of Pt in the Pt 4f spectra are seen. These signals are positioned at BE values of 71.3 and 74.6 eV. The similar positions of the peaks with those of the Pt_{100} catalyst designate that metallic Pt exists in the samples. However, comparison of the BE shows a difference of 0.1 and 0.2 eV respectively. This shift to lower binding energies is due to the formation of metallic bonds or alloying that occurs at low temperatures [25]. Interestingly, no peaks are seen in the Ni 2p spectra. This phenomenon is explainable as due to surface segregation of the Pt metal phase on the surface of the bimetallic nanoparticles.

As a whole, based on the properties of $Pt_{55}Ni_{45}$-CI catalyst, it is obvious that this catalyst exhibit unique properties superior to that of Pt_{100}-I and Ni_{100}-I. Its small particle size combined with surface segregation of Pt on the bimetallic nanoparticles and alloying of the metal phases involved, all contributes to the enhanced catalytic activity of benzene hydrogenation.

5.6 Summary

These findings show that surface and catalytic properties are governed by both the PtNi ratio and the preparation technique. The reduction method employed can facilitate the formation of totally reduced pure metal or bimetallic metal particles. This reduced state is maintained after handling and storage in air for Pt_{100}-I as well as moderate and low Pt content bimetallic catalysts. For Ni_{100}-I and low Ni content bimetallic metal particles, oxidation occurred. Co-impregnated catalysts exhibit enhanced reactivity when compared to step impregnated catalysts. Superior activity compared to Pt_{100}-I is seen when a moderate amount of Pt is incorporated via co-impregnation technique ($Pt_{55}Ni_{45}$-CI catalyst). This improved activity is striking considering that it only contains 26.8 atomic % of Pt when compared to the Pt_{100}-I catalyst. Further investigations on the characteristics of the $Pt_{55}Ni_{45}$-CI using SEM with x-mapping analysis as well as XRD lead to belief that alloying occur in the catalyst. Furthermore, surface segregation of Pt on the alloys as proven by XPS results also contribute to this enhanced reactivity.

In conclusion, these results correlate well with each other showing that the co-impregnation technique used to prepare the catalysts is superior to that of the step-impregnation. In addition, the novelty lie's in the fact that a simple non-

classical method can be employed to prepare alloyed catalysts which can be activated at low temperatures for short durations and still exhibit enhanced reactivity when compared to the Pt_{100}-I catalyst.

5.7 References

[1] X.-X. Han, R.-X. Zhou, G.-H. Lai, X.-M. Zheng, Reac. Kinet. Catal. Lett., 83 (2004) 55.

[2] X. Han, R. Zhou, B. Yue, X. Zheng, Catal. Lett., 109 (2006) 157.

[3] N. Toshima, T. Yonezawa, New J. Chem., 22 (1998) 1179.

[4] N. Toshima, M. Harada, T. Yonezawa, K. Kushibashi, K. Asakurat, J. Phys. Chem. 95 (1991) 7448.

[5] W. Shen, F.E. Huggins, N. Shah, G. Jacobs, Y. Wang, X. Shi, G. P. Huffman, Appl. Catal. A: Gen., 351 (2008) 102.

[6] K. Nagaoka, K. Sato, H. Nishiguchi, Y. Takita, Appl. Catal. A: Gen., 327 (2007) 139.

[7] A. Saadi, R. Merabti, Z. Rassoul, M.M. Bettahar, J. Mol. Catal. A: Chem., 253 (2006) 79.

[8] J. Rynkowski, D. Rajski, I. Szyszka, J. R. Grzechowiak, Catal. Today, 90 (2004) 159.

[9] M. Che, Z. X. Cheng, C. Louis, J. Am. Chem. Soc. 117 (1995) 2008.

[10] C. Louis, Z. X. Cheng, M. Che, J. Phys. Chem., 97 (1993) 5703.

[11] P.S.S. Prasad, N. Lingaiah, P.K. Rao, F.J. Berry, L.E. Smart, Catal. Lett., 35 (1995) 345.

[12] S. Chettibi, R. Wojcieszak, E. H. Boudjennad, J. Belloni, M. M. Bettahar, N. Keghouche, Catal. Today, 113 (2006) 157.

[13] L. Zhang, A. Manthiram, Appl. Phys. Lett., 70 (1997) 2469.

[14] W. Zhang, X. Quan, J. Wang, Z. Zhang, S. Chen, Chemosphere 65 (2006) 58.

[15] Q.A. Pankhurst, A.Y. Martinez, L.F. Barquin, Phys. Rev. B, 69 (2004) 212401.

[16] J.T. Nurmi, P.G. Tratnyek, V. Sarathy, D.R. Baer, J.E. Amonette, K. Pecher, C. Wang, J.C. Linehan, D.W. Matson, R.L. Penn, M.D. Driessen, Environ. Sci. Tech., 39 (2005) 1221.

[17] A. Borodzinski, M. Bonarowska, Langmuir, 13 (1997) 5613.

[18] H. Yang, W. Vogel, C. Lamy, N. Alonso-Vante, J. Phys. Chem. B, 108 (2004) 11024.

[19] A. I. Trypolskyi, T. M. Gurnyk, P. E. Strizhak, Chem. Phys. Lett. 460 (2008) 492.

[20] M. Tatlier, L. K. Minsker, Catal. Comm., 6 (2005) 731.

[21] M. O. Coppens, G. F. Froment, Chem. Eng. Sci., 51 (1996) 2283.

[22] K.-W. Park, J.-H. Choi, B.K. Kwoon, S.-A. Lee, Y.-E. Sung, H.Y. Ha, S.-A. Hong, H. Kim, A. Wieckowski, J. Phys. Chem. B, 106 (2002) 1869.

[23] T.C. Deivaraj, W. Chen, J.Y. Lee, J. Mater. Chem., 13 (2003) 2555.

[24] D. Jo, J. S. Lee, K. H. Lee, J.Mol. Catal. A: Chem., 222 (2004) 199.

[25] K.-W. Park, J.-H. Choi, Y.-E. Sung, J. Phys. Chem. B, 107 (2003) 5851.

CHAPTER 6

CATALYTIC STUDIES OF PtNi STABILIZED OLEIC ACID BIMETALLIC PARTICLES INCORPORATED ONTO SILICA

6.1 Introduction

Metal nanoparticles stabilized by organic or inorganic compounds have attracted widespread attention as they promote the formation of well defined, small sized nanoparticles. When incorporated onto a support, these particles are known to maintain their shape and size hence can show a high reactivity or better selectivity. In most cases, the high activity is obtained with the condition that the compounds are removed from the metal particles [1-4]. In contrast, improved selectivity of the catalysts occurs as a result of a possible bifunctional mechanism when the organic compounds are available together with the active sites of the metal particles [5].

In this chapter, a similar approach as above for the synthesis of bimetallic supported catalysts is employed. The characteristics and catalytic behaviour of originally PtNi stabilized oleic acid bimetallic particles incorporated onto crystalline silica is described. A detail study on the synthesis of the PtNi stabilized oleic acid nanoparticles is first presented. The intention of this part is to determine the optimum conditions to obtain dispersed and alloyed PtNi particles. Subsequently, a study of the properties and reactivity of the PtNi particles incorporated onto the silica support was conducted.

6.2 Formation of PtNi Bimetallic Nanoparticles

The synthesis of the PtNi bimetallic particles resulted in the formation of black precipitates. As a mixture of distilled water and ethanol was used as the solvent to enable the solubility of oleic acid, it is possible that reduction of the PtNi nanoparticles may have occurred via $NaBH_4$ or alcohol reduction. Ethanol acts as a reducing agent due to its reactive α-hydrogen and this reducing property is usually effective at elevated temperatures [6]. However, due to the fact that a small amount of ethanol was used in the preparations and that reaction mixtures were homogenized for only 10 minutes, coupled with the instant formation of metal particles upon addition of the fresh cold $NaBH_4$, it is concluded that the reduction process by $NaBH_4$ is more dominant. The reduction reaction can be expressed according to equations (6.1) and (6.2) below [7, 8].

$$2PtCl_6^{2-} + BH_4^- + 4H_2O \rightarrow 2Pt + B(OH)_4^- + 8H^+ + 12Cl^- \quad (6.1)$$

$$2Ni^{2+} + BH_4^- + 2H_2O \rightarrow 2Ni + BO_2^- + 4H^+ + 2H_2\uparrow \quad (6.2)$$

6.3 Alloying of PtNi Bimetallic Nanoparticles

The XRD diffractograms of the bimetallic PtNi as well as of Pt_{100} and Ni_{100} samples were obtained to investigate the crystallinity of the metal phases. The pattern of the Pt_{100} shown in Figure 6.1(a) indicates the existence of peaks positioned at 2θ values of 39.98º, 46.49º, 67.81º, 81.67º and 85.99º. These peaks are indexed to the (111), (200), (220), (311) and (222) reflections of the face centred cubic (fcc) crystal lattice of platinum. Similar results have been reported by other researches [9, 10]. The diffractogram for Ni_{100} in Figure 6.2(a) on the other hand, exhibits broad peaks. These peaks indicate the possible occurrence of

a mixture of Ni, Ni hydroxides and Ni oxides in the samples. The peaks for Ni are usually positioned at 44.5º, 51.8º and 76.4º corresponding to the Miller indices (111), (200) and (222) [11]. As can be seen the broad peak at approximately 44º may overlap with the second main peak of Ni positioned at 51.8º. Even so, this peak as well as that positioned at 20º also overlaps with main peaks corresponding to Ni oxide and Ni hydroxide. Hence the possibility of these other forms of Ni existing in the sample has to be taken into consideration [12]. Subsequently, another interesting observation is that the broad peaks may signify that this metal phase show amorphous characteristics or that small sized particles exist.

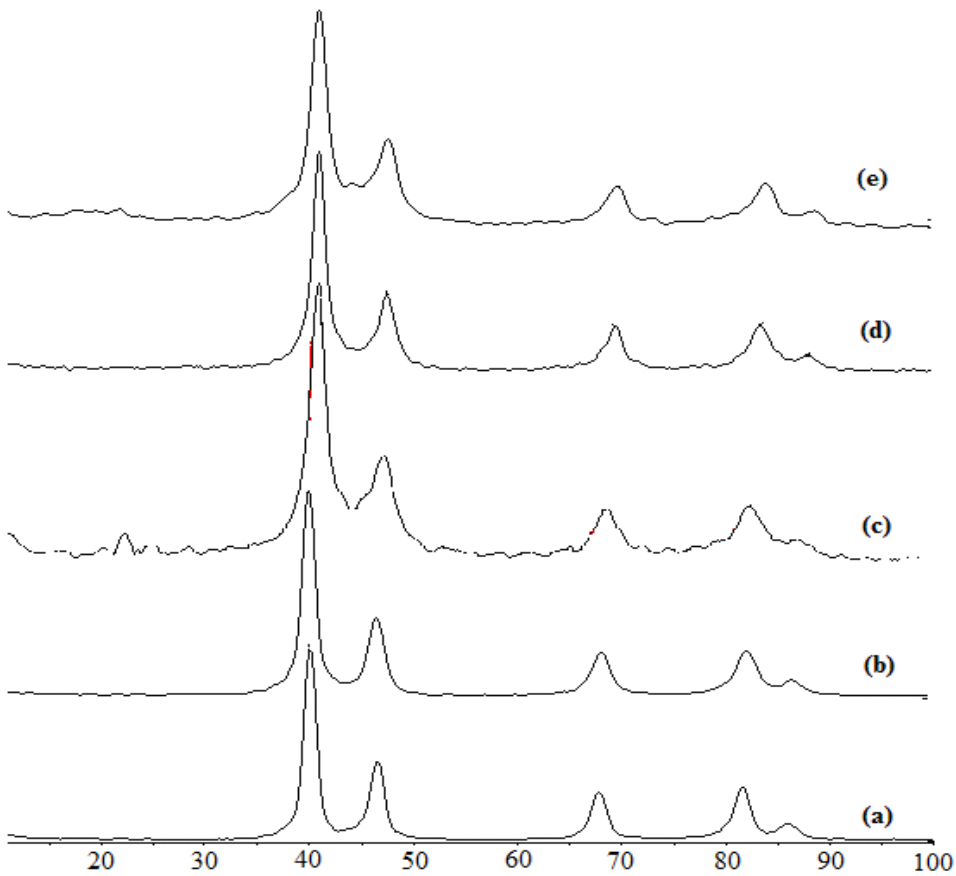

Figure 6.1: XRD diffractograms of PtNi alloys with different ratios prepared at 80 ºC with 0.02 M oleic acid (a) Pt_{100}; (b) $Pt_{93}Ni_{7}$; (c) $Pt_{78}Ni_{22}$; (d) $Pt_{61}Ni_{39}$ and (e) $Pt_{31}Ni_{69}$.

Subsequent analysis of the PtNi samples showed that samples of $Pt_{93}Ni_{7}$, $Pt_{78}Ni_{22}$, $Pt_{61}Ni_{39}$ and $Pt_{31}Ni_{69}$ demonstrated similar trends. The diffractograms illustrated in Figure 6.1(b-e) show that only Pt peaks are observable. However, these peaks are slightly shifted to higher 2θ values as tabulated in Table 6.1. Interestingly, no characteristic peaks indicating the existence of Ni or NiO crystal structures are apparent in these XRD patterns. This is evidence of the formation of Pt/Ni alloys whereby Ni is incorporated into the Pt structure. The lattice parameters of the samples calculated from the d spacing values of the (111) peak, also show a decrease when compared to Pt_{100}. Based on previous reports this decrement is also an indication of the formation of alloys [13]. The lattice parameter values are shown in Table 6.1. In all the XRD patterns obtained, no superlattice lines or satellite peaks are observed. This indicates that ordered alloys whereby Pt and Ni atoms are organized in periodically alternating layers are not formed. Hence, it is possible to summarize that the PtNi obtained are in the form of solid solutions or disordered alloys. For the $Pt_{15}Ni_{85}$, no Pt peaks are observed. Instead, a similar pattern to that of the Ni_{100} diffractogram is seen as shown in Figure 6.2(b). This can be explained as due to the amount of Ni in the sample which is dominant.

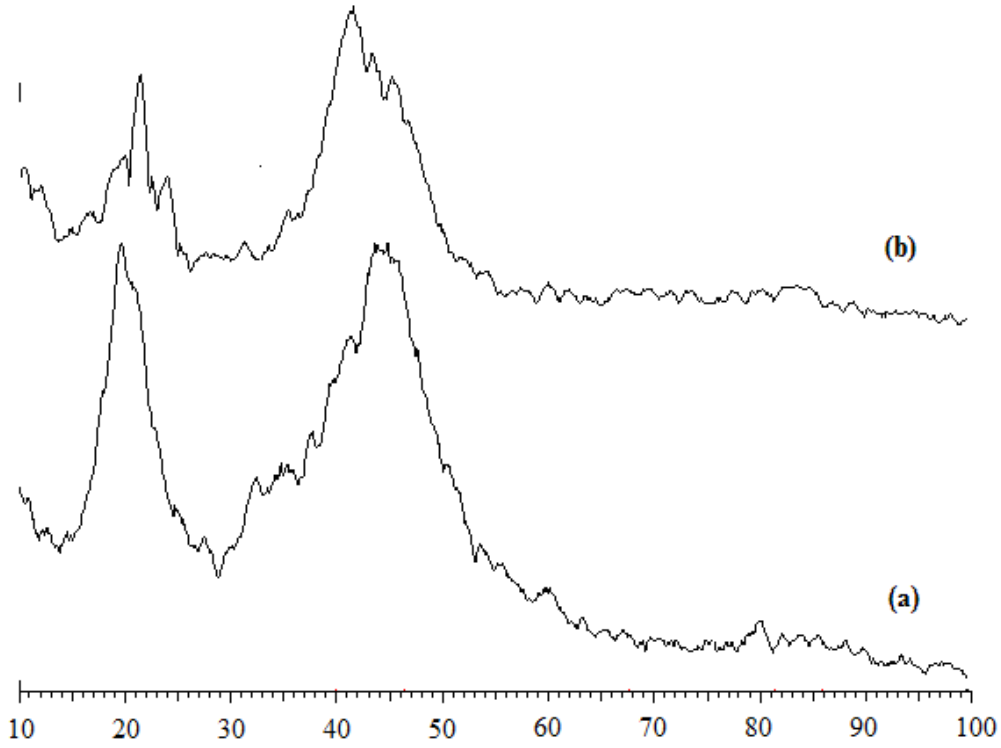

Figure 6.2: XRD diffractograms of PtNi alloys with different ratios prepared using 0.02 oleic acid at 80 ºC (a) Ni_{100} and (b) $Pt_{15}Ni_{85}$.

Table 6.1: Lattice parameters of PtNi alloys prepared at different ratios

Pt:Ni Wt Ratio	2θ Values					Lattice Parameter (nm)	EDX Composition (atomic ratio)
100:0	39.98	46.49	67.81	81.67	85.99	0.3901	100:0
93:7	40.38	46.83	68.51	82.53	86.81	0.3868	80:20
78:22	40.69	47.18	69.25	83.14	87.76	0.3838	45:54
61:39	40.70	47.16	69.12	83.34	87.68	0.3836	41:59
31:69	40.87	47.51	69.63	83.83	88.55	0.3819	28:74
15:85	-	-	-	-	-	-	93:7
0:100	-	-	-	-	-	-	0:100

The extent of alloy formation between Pt and Ni can be determined by investigating the dependence of the lattice parameter on the EDX compositions. This relationship is exhibited as a linear plot, as shown in Figure 6.3. However, linear regression of the plot gives an R^2 value of 0.8443. This demonstrates that the Pt and Ni metal phases are not completely alloyed in the samples. Previous works have also described this phenomenon [14].

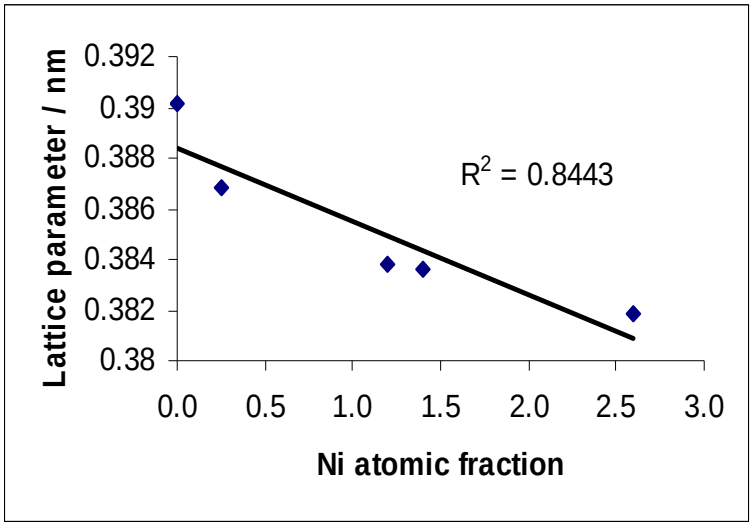

Figure 6.3: Relationship between lattice parameter of PtNi nanoalloys with EDX composition.

6.4 Morphology

6.4.1 Effect of Oleic Acid Concentration

TEM analysis was conducted to study the effect of oleic acid concentration on the morphology of the PtNi alloys. The $Pt_{78}Ni_{22}$ sample prepared at 353 K was employed for this study. As can be seen, at all concentrations of the oleic acid, agglomerations of the metal nanoparticles results in chain like structures. This can be explained as due to the magnetic attraction

exhibited between adjacent Ni particles. Similar phenomenon is observed for Ni-Fe nanoparticles [15]. It is well known that the magnitude of magnetization influences the attractive force between the metal particles. A higher magnitude of magnetization results in a more dense agglomeration of the metal nanoparticles when compared to a lower magnitude of magnetization. However in this work, the variation in the degree of agglomeration can also be attributed to the difference in oleic acid concentration. As depicted in Figure 6.4(a), at a concentration of 0.02 M oleic acid, aggregation of the alloys occurred forming very dense structures. This occurrence is due to the inability of the oleic acid to efficiently adsorb onto the metal particle surface and prevent aggregation. Upon further increase of the oleic acid concentration to 0.05 M, it was revealed that spherical particles with an average particle size of 4.2 ± 2.6 nm surrounded the dense structures. Hence the additional oleic acid is sufficient to stabilize some of the particles. Interestingly, when 0.15 M and 0.2 M of oleic acid are used, network formations are observed instead. Typical images are shown in Figure 6.4(b). These networks are found to be composed of smaller spherical particles whose average particle size is 6.8 ± 2.5 and 4.2 ± 1.3 nm for samples containing 0.15 M and 0.2 M of oleic acid respectively. The formation of these structures in both samples is attributed to the oleic acid that sufficiently interacts with the surface of the metal particles upon particle formations during the reduction process. The organic layer that surrounds the particles forms a barrier that inhibits attraction between the metal nanoparticles. When the concentration of oleic acid is further increased to 0.5 M, aggregation occurred similar to that shown in Figure 6.4(a), whereby no small spherical nanoparticles are observed. This may be due to greater interaction between the oleic acid molecules upon increasing the

oleic acid concentration. The probable increase in inter-oleic acid interactions is at the expense of metal particles stabilization. It is anticipated that the respective metal-metal and acid-acid interactions dominates at the lower and higher concentrations of oleic acid. Thus in the case of the $Pt_{78}Ni_{22}$ sample above, when the oleic acid concentration employed is 0.15 M or 0.2 M, the metal-acid interaction is between these two extremes. This is further discussed in section 6.4 below.

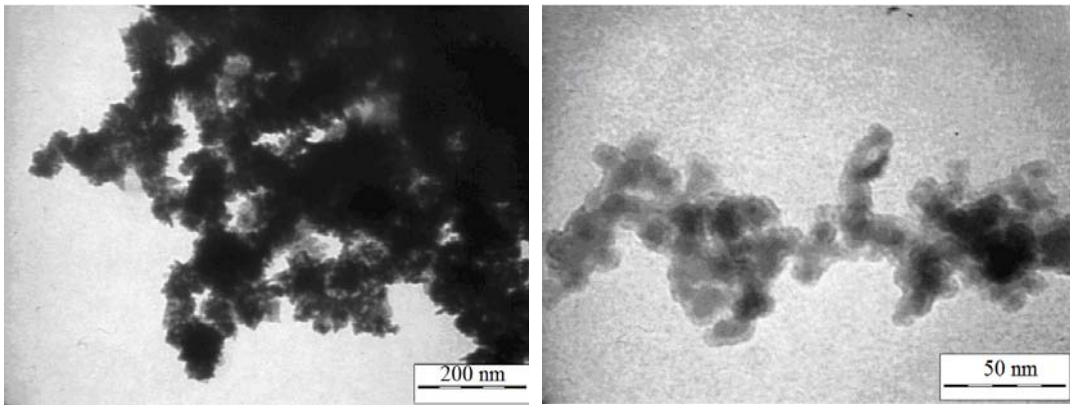

(a)

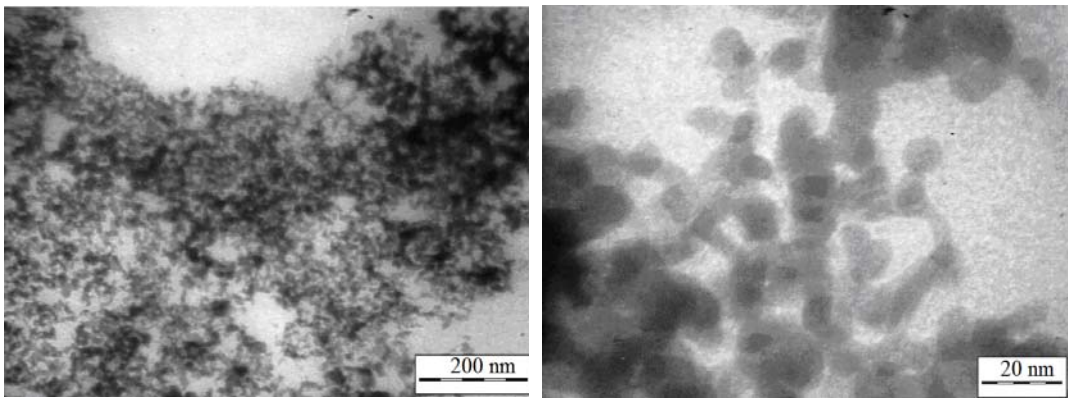

(b)

Figure 6.4: Typical TEM micrographs of (a) aggregated and (b) network formed $Pt_{78}Ni_{22}$ nanoparticles prepared at 353 K stabilized with oleic acid.

6.4.2 Effect of Reaction Temperature

The effect of various temperatures on the morphology of the $Pt_{78}Ni_{22}$ alloys prepared with an oleic acid concentration of 0.15 M was studied. It is observed that for preparation temperatures of 413 and 373 K aggregated morphologies composed of smaller particles are formed similar to that exhibited in Figure 6.4 (a). The average particle sizes of the smaller particles are 4.5 ± 1.8 and 4.1 ± 1.4 nm for samples prepared at 413 and 373 K respectively. Upon reduction of the reaction temperatures to 353 and 313 K, network formations as in Figure 6.4 (b) are observed, though some aggregates co-exist in the samples prepared at 313 K. In these structures the average particle sizes of the nanoparticles are 6.8 ± 2.5 and 1.9 ± 0.4 nm for the samples prepared at 353 and 313 K correspondingly. The large difference in particle size between the sample prepared at 313 K and those prepared at higher temperatures can only be explained as due to the inhomogeneity of the stabilizing effect of oleic acid. Based on these results, it is found that the reaction temperature can exert influence on the PtNi structures. The aggregation behaviour observed at higher temperatures can be explained as due to the increase in reaction rate (and the possible participation of alcohol acting as reducing agent). This causes nucleation and reduction of the metal nanoparticles to occur faster and simultaneously hence leads to the rapid growth of nanoparticles. This rapid growth of the nanoparticles leads to the inability of the oleic acid to adsorb on the nanoparticle surface in time in order to effectively inhibit the particles growth. On the other hand, at lower reaction temperatures, the nucleation and growth of the nanoparticles occur at a slower rate. This allows the oleic acid to adsorb on the surface of the metal particles hence stabilizing the particles to form network structures.

6.5 PtNi Interaction with Oleic Acid

The stabilization mechanism of oleic acid and its interaction with the surface of the alloys was studied via FTIR analysis. A typical FTIR spectrum of the pure oleic acid and Pt/Ni alloy stabilized with oleic acid is depicted in Figure 6.5. Characteristic peaks of oleic acid are positioned at 2922 and 2855 cm^{-1} indicating the asymmetric and symmetric stretching of the $-CH_2$ and terminal $-CH_3$ bands, 1711 cm^{-1} attributed to the C=O band, 1285 cm^{-1} assigned to C-O as well as 1464 cm^{-1} indicating the $–CH_2$ deformation band [16,17]. A comparison of this spectrum with that of the PtNi alloys showed few similarities. In the spectrum presented in Figure 6.6(b), an OH band is apparent at approximately 3414 cm^{-1}. This band is attributed to the adsorbed water molecules that are present in the samples [18]. The HOH peak at 1617 cm^{-1} similarly characterizes the water molecules. A sharp band characteristic of CO_2 also occurs at 2337 cm^{-1}. Adsorption of CO_2 on the metal surface may have occurred during the preparation stage. Another obvious difference is the absence of the C=O band at 1711 cm^{-1}. It has been reported that the disappearance of this band and the appearance of bands at 1560 and 1639 cm^{-1} is indicative of the interaction that occurs between oleic acid and the metal nanoparticles [19]. The two new bands are attributed to the respective asymmetric ν_{as}(COO-) and symmetric ν_s(COO-). According to Zhang et al. [19], the difference (Δ) between the wavenumber of these bands, determine the type of interaction that occurs between the carboxylate and the metal. A large difference (Δ ~200-300 cm^{-1}) signifies a monodentate interaction, whereas a small difference (Δ <110 cm^{-1}) is attributed to the bidentate interaction. Here, the difference between the two bands is 79 cm^{-1}. This indicates that a bidentate interaction between the oleic acids and PtNi particles occur.

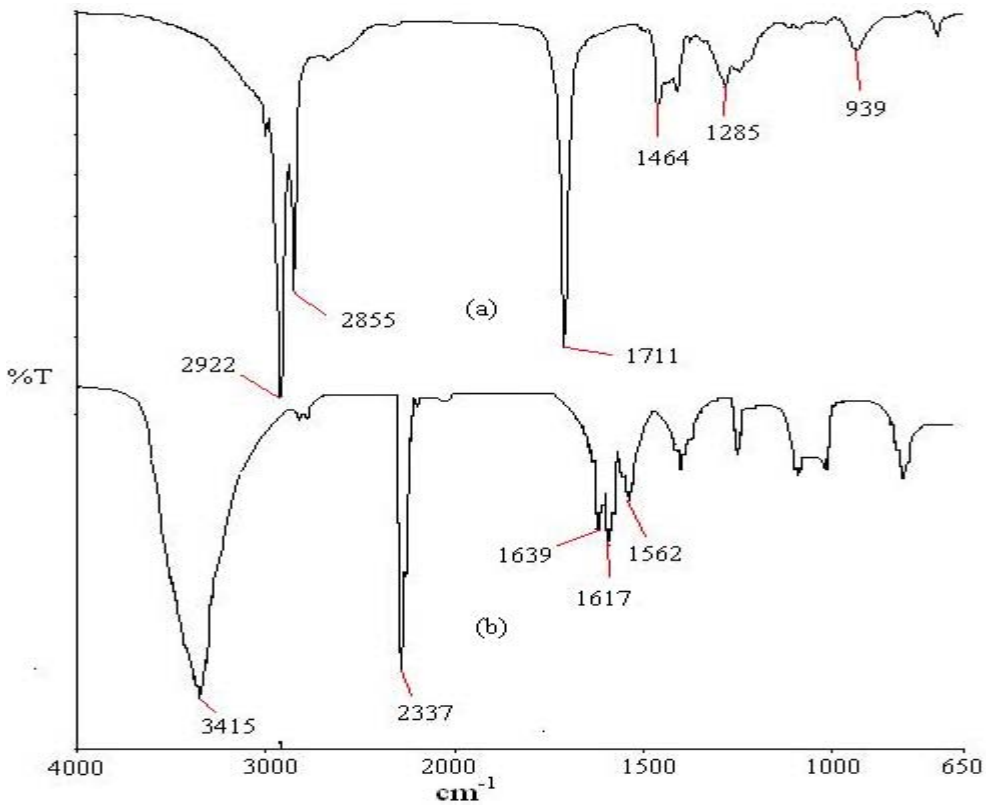

Figure 6.5: FTIR spectra of (a) pure oleic acid and (b) oleic acid stabilized PtNi.

6.6 Oleic Acid Stabilized PtNi Deposited on Silica

PtNi stabilized oleic acid nanoparticles with various ratios were prepared at 353 K in 0.15 M of oleic acid for the following study. The as synthesized oleic acid stabilized PtNi nanoparticles were deposited onto a crystalline silica support to form PtNi-OA/Silica catalysts. The morphology and surface characteristics of the active phase of these catalysts were investigated. In addition, the effectiveness of these catalysts is tested for the hydrogenation of benzene to cyclohexane.

6.6.1 Morphology of Active Phase in the PtNi-OA/Silica Catalysts

The PtNi-OA/Silica catalysts were prepared by mixing the silica support with the as synthesized oleic acid stabilized PtNi particles. Upon washing, clean

PtNi-OA supported on silica is obtained. To gain an insight on the morphological effect of depositing the oleic acid stabilized PtNi particles on the support, TEM analysis was conducted.

The morphology of the PtNi particles in the $Pt_{79}Ni_{21}$-OA/Silica catalyst was investigated and compared to the $Pt_{78}Ni_{22}$ unsupported metal particles. Observations reveal that the metal particle structure is retained upon incorporation on the silica support. The average particle size of the particles in the $Pt_{79}Ni_{21}$-OA/Silica is 6.3 ± 5.4 nm. Though the average particle size is similar to that of the initial unsupported PtNi nanoparticles, it is obvious that the standard deviation for both samples vary by approximately 2.9 nm. A greater range of particle sizes is observed in the supported silica sample. This phenomenon may be attributed to interaction that may occur between oleic acid and silica. According to Blyholder and coworkers [20], oleic acid can adsorb onto silica by formation of hydrogen bonds between the free SiOH groups on silica and the carbonyl group from oleic acid. Single or cyclic double hydrogen bonds can occur [21]. Such an occurrence may indirectly cause destabilization of the metal particles (originally stabilized via oleic acid), which can latter fuse together forming larger particles.

The morphology of the metal phase in the $Pt_{24}Ni_{76}$-OA/Silica and $Pt_{58}Ni_{42}$-OA/Silica samples, were also studied. In these catalysts, the average particle sizes of the metal particles are 10.5 ± 3.6 and 10.0 ± 3.2 nm respectively. Similar phenomenon as in the $Pt_{79}Ni_{21}$-OA/Silica catalysts whereby the oleic acid adsorbs onto the silica resulting in the formation of these large particles is likely to occur.

6.6.2 Surface Characteristics

6.6.2.1 H_2-TPR Analysis

The H_2-TPR profiles of a series of PtNi-OA/Silica catalysts are presented in Figure 6.6. It can be seen that hydrogen consumption and production occurs in the catalysts with high to moderate amounts of Ni.

Both the $Pt_{24}Ni_{76}$-OA/Silica and $Pt_{58}Ni_{42}$-OA/Silica catalysts show a hydrogen consumption starting from room temperature to approximately 470 K. This can be attributed to two occurrences. First is the reduction of platinum oxides and second due to hydrogenation reaction of the oleic acid available in the catalyst. The latter reason is more likely since PtNi supported silica catalysts without oleic acid did not exhibit hydrogen consumption. The hydrogenation of oleic acid is well known to occur over catalysts such as Pt [22] and Ru [23], to form stearic acid. Upon further increase in the temperature, it is observed that two hydrogen production peaks are seen for the $Pt_{24}Ni_{76}$-OA/Silica catalyst. These peaks achieve maximum at approximately 518 and 608 K. It is believed that similar peaks occur in the $Pt_{58}Ni_{42}$-OA/Silica catalyst except that they are less defined.

The production of hydrogen which starts at approximately 470 - 720 K can be attributed to the dehydrogenation of oleic acid catalyzed by the metal phase. According to Perez-Dieste and coworkers [24], dehydrogenation of adsorbed oleic acid commences at a temperature near 673 K for Ni and Co nanoparticles synthesized using super hydride ($LiBEt_3H$) as the reducing agent, prior to depositing on a silicon substrate. In contrast, Roonasi and Holmgren [17] found that dehydrogenation occurred in the temperature range of 553 - 723 K for magnetite nanoparticles coated with sodium oleate. This shows that

dehydrogenation may be influenced by the metal on which oleic acid is adsorbed onto. Hence, for these catalysts a possible synergistic effect between Pt and Ni may have promoted the dehydrogenation of oleic acid at earlier temperatures. Though this phenomenon may have contributed to the production of hydrogen, it is important to bear in mind that hydrogen adsorbed during the reduction stage may also have desorbed during H_2-TPR analysis.

Subsequently, in contrast to the catalysts with high to moderate Ni contents, the $Pt_{79}Ni_{21}$-OA/Silica shows only a hydrogen consumption which occurs in a similar temperature range. This leads to the belief that only hydrogenation reactions of oleic acid and reduction of Pt oxides may have occurred. The lack of dehydrogenation reactions may be related to the different surface properties of the catalysts, which however is not completely understood.

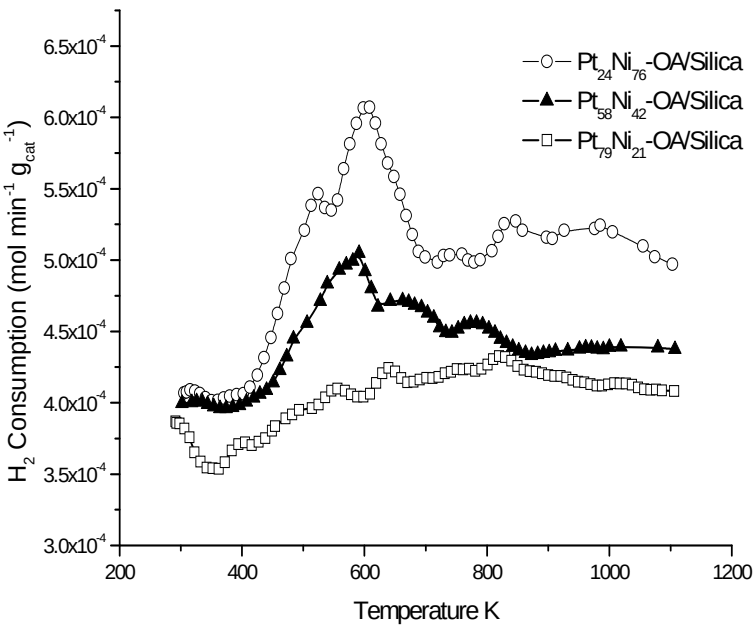

Figure 6.6: H_2-TPR profiles of the PtNi-OA/Silica catalysts prepared using various Pt/Ni ratios.

6.6.2.2 H_2-Chemisorption

H_2-chemisorption studies carried out on the catalysts activated in pure H_2 at 473 K showed that the amount of hydrogen chemisorbed on the surface of the active phase increased with increasing amounts of Pt content in the catalysts. As much as 1.83 x 10^{-5} and 3.70 x 10^{-4} mol g_{met}^{-1} of H_2 were adsorbed for the Ni_{100}-OA/Silica and Pt_{100}-OA/Silica catalysts respectively. The amounts adsorbed for the bimetallic catalysts on the other hand are 4.34 x 10^{-5}, 7.28 x 10^{-5} and 9.55 x 10^{-5} mol g_{met}^{-1} for the $Pt_{24}Ni_{76}$-OA/Silica, $Pt_{58}Ni_{42}$-OA/Silica and $Pt_{79}Ni_{21}$-OA/Silica catalysts correspondingly. As an overall, these catalysts with the exception of Pt_{100}-OA/Silica show low H_2-chemisorption characteristics. Quantities are generally lower than those obtained for the bimetallic catalysts with similar PtNi ratios, prepared without oleic acid irrespective of the preparation technique (section 4.3.2 and 5.2.2). This may have been caused by the larger particles exhibited by these catalysts. However, this reason is not convincing considering that less aggregated metallic phases are obtained in these catalysts. Another possibility is the occurrence of a layer of carbonaceous compounds surrounding the metal particles which may occur upon activation of the catalysts. However, further investigations are required to verify these possibilities.

6.6.2.3 H_2-TPD Analysis

H_2-TPD analysis was carried out to understand the surface properties of the silica supported PtNi stabilized oleic acid catalysts. Plots of the amount of desorbed H_2 as a function of temperature are presented in Figure 6.7. The Pt_{100}-OA/Silica catalyst demonstrates an almost flat profile. However, inspection of the

profile at a lower scale reveals that it consists of two peaks. These peaks arise at approximately 609 and 886 K. The earlier peak can be related to H atoms moderately adsorbed onto the Pt surface while the latter to H-spillover species. Investigations of the Ni_{100}-OA/Silica catalyst on the other hand gives rise to only one broad peak ranging from 550-793 K. Maximum H_2 desorption occurred at 699 K.

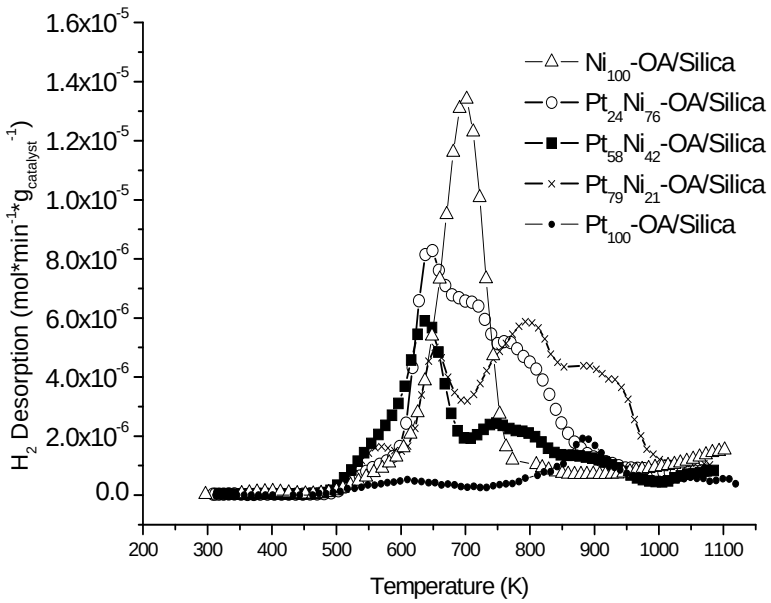

Figure 6.7: H_2-TPD profiles of the PtNi-OA/Silica catalysts prepared using various PtNi ratios.

H_2-TPD analysis of the bimetallic catalysts were conducted and compared to the monometallic catalysts. It can be seen that the $Pt_{24}Ni_{76}$-OA/Silica catalyst also exhibited a broad desorption peak ranging from 480 – 940 K. Deconvolution of this peak showed that it is composed of several desorption peaks positioned at approximately 566, 630, 656, 700 and 772 K. Similar peaks are also seen in the $Pt_{58}Ni_{42}$-OA/Silica and $Pt_{79}Ni_{21}$-OA/Silica catalysts. The $Pt_{58}Ni_{42}$-OA/Silica gives

rise to only one distinct peak in the temperature range of 560-650 K. However the broad tail towards lower temperatures strongly indicates the possibility of another peak. In comparison, these two peaks are clearly observed in the $Pt_{79}Ni_{21}$-OA/Silica catalyst. Further observations of these profiles indicate that two peaks arise at higher temperatures. The peak positioned at approximately 760-770 K is similar to that observed in the $Pt_{24}Ni_{76}$-OA/Silica positioned at 772 K, while another peak at about 880-900 K is only seen in catalysts with high to moderate amounts of Pt.

Indeed, a comparison with the Ni_{100}-OA/Silica catalyst clearly demonstrates that in all the bimetallic catalysts, the main Ni peak positioned at approximately 699 K shifts to lower temperatures of about ~ 640 - 650 K. However, it is obvious that in the bimetallic catalyst with high Ni content ($Pt_{24}Ni_{76}$-OA/Silica), Ni sites which are not influenced by the presence of Pt in the catalyst still exist as a strong peak arising at 700 K. These peaks identify with hydrogen strongly adsorbed onto the Ni surface or due to hydrogen retained at the interface of the metal support. Further comparison of the bimetallic catalysts with that of the Pt_{100}-OA/Silica also indicates the possibility of Pt active sites available on the surface of the catalysts. This is due to the occurrence of the existence of a peak at approximately 560 K in all the bimetallic catalysts which is similar to the peak at 609 K in the Pt_{100}-OA/Silica catalyst as well as peaks in the temperature range of 800 - 900 K attributed to spillover of hydrogen in catalysts with high to moderate contents of Pt. Only the peaks observed in the temperature range of 760 – 770 K which may also occurs as a result of hydrogen spillover are not related to Ni or Pt active sites. This additional peak marks the occurrence of sites that exist as a result of the availability of PtNi in the catalyst. Even so, desorption

properties of all the catalysts clearly shows that characteristics of the Ni_{100}-OA/Silica is dominant. In fact, the intensity of the major peak for Ni active sites at about ~ 630 K only decreases slightly with increasing Pt content. This is surprising especially for the catalysts with higher Pt contents. Similar trends were not seen in the series of catalysts prepared without oleic acid. This phenomenon indicates the possibility of Ni segregation on the surface of the alloys. It is uncertain whether segregation occurred prior or after incorporation of the Pt/Ni particles on the silica support. However, it is well known that in the presence of oxygen species (which may have originated from the oleic acid structure), Ni tends to segregate to the surface [25]. TPD analysis of these samples correlates well, as slight desorptions of methane and carbon monoxide was seen during analysis. This finding may indirectly explain the lower H_2-chemisorption amounts obtained for this series of bimetallic Pt/Ni catalysts in comparison to those presented in the previous chapters.

6.6.3 Benzene Hydrogenation

The hydrogenation of benzene to cyclohexane was carried out to investigate the reactivity of the Pt/Ni alloys incorporated onto crystalline silica. Generally the profiles in Figure 6.8 show that reactivity increased with the addition of Pt content. The $Pt_{24}Ni_{76}$-OA/Silica showed only a slight reactivity where a maximum reaction rate of 1.38 x 10^{-3} mol min^{-1} g_{met}^{-1} was reached at 378 K. Upon further addition of Pt content, reactivity increased though only slight variations were found for the $Pt_{58}Ni_{42}$-OA/Silica and $Pt_{79}Ni_{21}$-OA/Silica catalysts. The maximum reactivity for the catalysts are 5.10 x 10^{-3} and 5.77 x 10^{-3} mol min^{-1} g_{met}^{-1} respectively. For both catalysts, maximum reactivity was achieved at 388

K. Comparison of the reactivity obtained for the bimetallic catalysts with that of the monometallic catalysts showed that all the catalysts were more active than the Ni_{100}-OA/Silica catalyst which was inactive throughout the catalytic reaction. However, the bimetallic catalysts were less active than the Pt_{100}-OA/Silica catalyst. It was found that the Pt_{100}-OA/Silica catalyst achieved a maximum reaction rate of 15.26 x 10^{-3} mol min^{-1} g_{met}^{-1} at 406 K. This is approximately triple the activity observed for the $Pt_{58}Ni_{42}$-OA/Silica and $Pt_{79}Ni_{21}$-OA/Silica catalysts.

Based on these findings, it is obvious that though the unsupported PtNi stabilized oleic acid nanoparticles exhibited alloying, when supported on silica, no enhancement in the catalytic reactivity when compared to the Pt_{100}-OA/Silica catalyst is observed. This is interesting considering that when alloys are formed in the PtNi supported silica catalysts prepared without oleic acid, improved reactivity with respect to the monometallic Pt catalyst was observed, as discussed in the previous chapters. In fact, further comparison between the bimetallic catalysts with similar ratios indicates that the reactivity of catalysts prepared with oleic acid is generally lower or similar to those prepared without oleic acid. Observations show that only the Pt_{100}-OA/Silica catalyst exhibited a higher reactivity when compared to the Pt_{100}-P (6.28 x10^{-3} mol min^{-1} g_{met}^{-1}) and Pt_{100}-I (11.80 x 10^{-3} mol min^{-1} g_{met}^{-1}) catalyst. This may be explained as due to the stabilizing effect of oleic acid which promotes the availability of a higher surface area of the metallic phase for reaction to occur. This is in good accordance with the H_2-chemisorption studies which show that a higher quantity of H_2 is adsorbed onto the Pt_{100}-OA/Silica catalyst in contrast to those without oleic acid. This emphasizes the role of oleic acid in giving rise to less aggregated metallic particles. Hence, based on these findings it can only be concluded that the low

reactivity seen in the bimetallic catalysts prepared in oleic acid can only be attributed to segregation of the Ni atoms on the surface of the alloys formed as shown by its dominant characteristic in the H_2-TPD profiles. Even so, inhibition of the reactivity due to carbonaceous compounds surrounding the bimetallic particles could also have occurred. This is supported by the desorption of methane and carbon monoxide observed in TPD analysis.

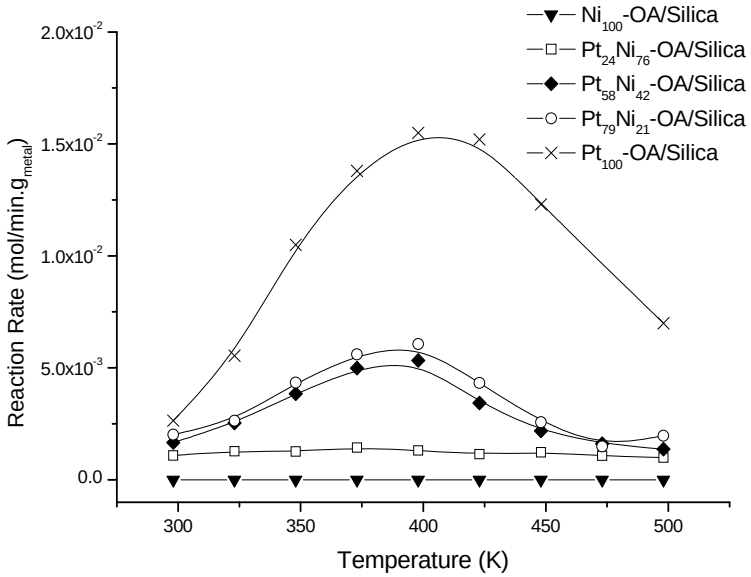

Figure 6.8: Reaction rates of the hydrogenation of benzene for the PtNi-OA/Silica catalysts as a function of temperature.

6.7 Summary

PtNi stabilized oleic acid nanoparticles were synthesized via chemical route using $NaBH_4$ as the reducing agent. The stabilization of the metal nanoparticles occurred via interaction between the oleic acid and the metal particle surfaces which were found to be partially alloyed. The morphology of the alloyed particles formed, were found to be dependent on the oleic acid

concentration and reaction temperatures. The conditions where least aggregated particles are obtained were employed for the preparation of a series of PtNi-OA/Silica catalysts. Though alloyed metal particles were present in these catalysts, enhanced reactivity when compared to the monometallic catalysts was not observed. The major reason for this occurrence can be attributed to availability of Ni active sites on the surface of the alloyed metal particles irrespective of the PtNi ratio. However, the availability of carbonaceous compounds on the surface of the particles may also have inhibited catalytic reactivity to some extent.

6.8 References

[1] A. Horvath, A. Beck, Zs. Koppany, A. Sarkany, L. Guczi, J. Mol. Catal. A: Chem. 182 – 183 (2002) 295.

[2] A. Sarkany, A. Beck, A. Horvath, Zs. Revay, L. Guczi, Appl. Catal. A: Gen. 253 (2003) 283.

[3] W. Yu, M. Liu, H. Liu, X. An, Z. Liu, X. Ma, J. Mol. Catal. A: Chem. 142 (1999) 201.

[4] H. Bönnemann, R. Brinkmann, P. Britz, U. Endruschat, R. Mörtel, U. A. Paulus, G. J. Feldmeyer, T. J. Schmidt, H. A. Gasteiger, R. J. Behm, J. New Mater. Electrochem. Systems, 3 (2000) 199-206.

[5] H. Bonnemann, G. A. Braun, Chem. Eur. J. 3 (1997) 1200-1202.

[6] D. G. Duff, P. P. Edwards, B. F. G. Johnson, J. Phys. Chem. 95 (1995) 15934.

[7] J. Shen, Z. Li, Q. Yan, Y. Chen, J. Phys. Chem. 97 (1993) 8504.

[8] T. C. Deivaraj, J. Y. Lee, J. Power Sources, 142 (2005) 43

[9] C. Y. Du; T. S. Zhao, Z. X. Liang, J. Power Sources, 176 (2008) 9.

[10] Y. Yang, J. Lee, T. C. Deivaraj, H. -P. Too, Coll. Surf. A: Physico. Eng. Aspects 240 (2004) 131.

[11] S.-H. Wu, D.-H. Chen, J. Coll. Interf. Sci., 259 (2003) 282.

[12] B. B. Nayak, S. Vitta, A. K. Nigam, B. Bahadur, Thin Solid Films, 505 (2006) 109.

[13] H. Yang, C. Coutanceau, J.-M. Legar, N. Alonso-Vante, C. Lamy, J. Electroanal. Chem., 576 (2005) 305.

[14] H. Yang, N. Alonso-Vante, J. -M. Legar, C. Lamy, J. Electroanal. Chem. 576 (2005) 305.

[15] W. Zhang, X. Quan, J. Wang, Z. Zhang, S. Chen, Chemosphere, 65 (2006) 58.

[16] N. Wu, L. Fu, M. Su, M. Aslam, K. C. Wong, V. P. Dravid, Nano Lett. 4 (2004) 383.

[17] P. Roonasi, A. Holmgren, Appl. Surf. Sci. 255 (2009) 5891.

[18] L. Wang, M. Zhang, X. Wang, W. Liu, Mater. Res. Bull. 43 (2008) 2220.

[19] L. Zhang; R. He, H.-C. Gu, Appl. Surf. Sci., 253 (2006) 2611.

[20] G. Blyholder, C. Adhikar, A. Proctor, Colloids Surf. A: Physicochem. Eng. Aspects, 105 (1995) 151.

[21] K; Marshall, C. H. Rochester, J. Chem. Soc. Faraday. Trans. I, 71 (1975) 1754.

[22] N. Shukla, E. B. Svedberg, J. Ell, Coll. Surf. A: Physico. Eng. Aspects 301 (2007) 113.

[23] M. J. Mendes, O. O. Santos, E. Jordao, A. M. Silva, Appl. Catal. A: Gen. 217 (2001) 253.

[24] V. Perez-Dieste, O. M. Castellini, J. N. Crain, M. A. Eriksson, A. Kirakosian, J.-L. Lin, J. L. McChesney, F. J. Himpsel, Appl. Phys. Lett. 83 (2003) 5053.

[26] C. A. Menning, H. H. Hwu, J. G. Chen, J. Phys. Chem. B 110 (2006) 15471.

CHAPTER 7

EFFECT OF REDUCTION CONDITIONS

7.1 Introduction

The properties exhibited by catalysts and their reactivity can be manipulated by varying not only the preparation techniques as shown in the previous chapters but also the reduction method employed. The reduction stage is equally as important as the preparation phase. This is because the environment, in which the bimetallic particles are synthesized, whether in colloidal or gas phase, in the presence of a support, gives rise to particles with different characteristics.

In colloidal systems, reducing agents such as borohydrides [1-3], hydrazine [4, 5] and alcohol [6] have been employed with the intention of achieving small, dispersed and alloyed bimetallic particles. Though the choice of reducing agent is critical as its reduction strength directly influences the nucleation and growth of the bimetallic particles, other factors such as the reduction temperature also plays a significant role [2]. For this reason, the influence of various reduction conditions such as reduction temperature, $NaBH_4$ concentration and the medium in which reduction was carried out, on the morphology of the $Pt_{50}Ni_{50}$ bimetallic supported catalysts, which effects catalytic reactivity is presented. Here, MCM-41 is chosen as a support for its porous structure, which contributes to a larger surface area, beneficial for the

incorporation of small bimetallic particles formed, depending on the synthesis conditions employed [7-9].

7.2 H_2–TPR profiles

H_2-TPR experiments were conducted to verify the achievement of the reduction of PtNi particles via $NaBH_4$. Typical profiles of the fresh $Pt_{50}Ni_{50}$-MCM catalysts prepared in various conditions are shown in Figure 7.1. As can be seen, most of the catalysts exhibited nil or very little hydrogen consumption occurring mainly at approximately 350-400 K. Total reduction occurred during the reduction stage with $NaBH_4$ for most samples. Calculations based on the amount of H_2 consumed reveal that almost all catalysts contained approximately 0.24 – 3.75 % of metal oxides. This may be attributed to surface oxidation of the metal phase that occurs during the storage.

7.3 Effect of Reduction Temperature

The effect of reduction temperature on the morphology of the PtNi nanoparticles and its influence on the reaction rates for the hydrogenation of benzene was investigated for the $Pt_{50}Ni_{50}$ catalysts supported on MCM-41. Reductions were preformed using a concentration of 0.2 M $NaBH_4$ in a mixture of distilled water and ethanol at temperatures of 273 K and 313 K. The various morphologies obtained are shown in Figure 7.2.

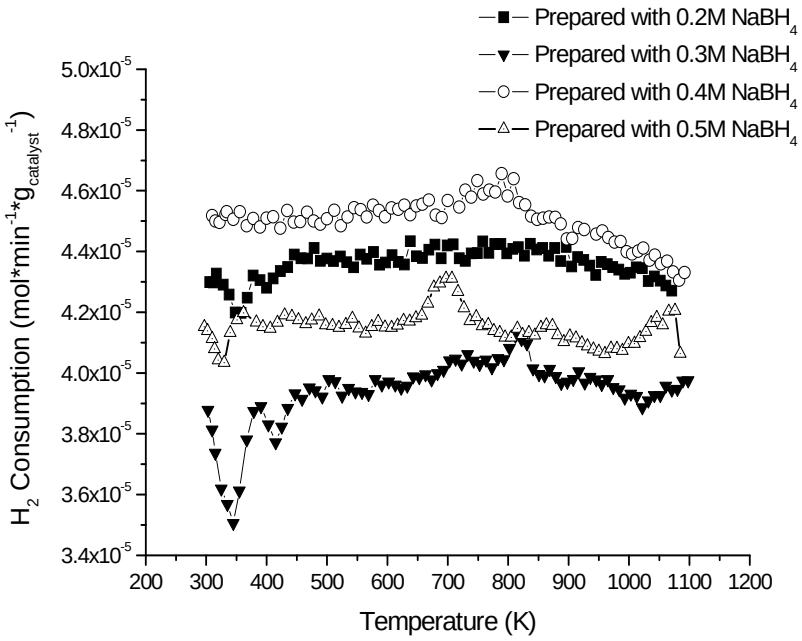

Figure 7.1: Typical H_2-TPR profiles of fresh $Pt_{50}Ni_{50}$-MCM-41 catalysts prepared in various conditions.

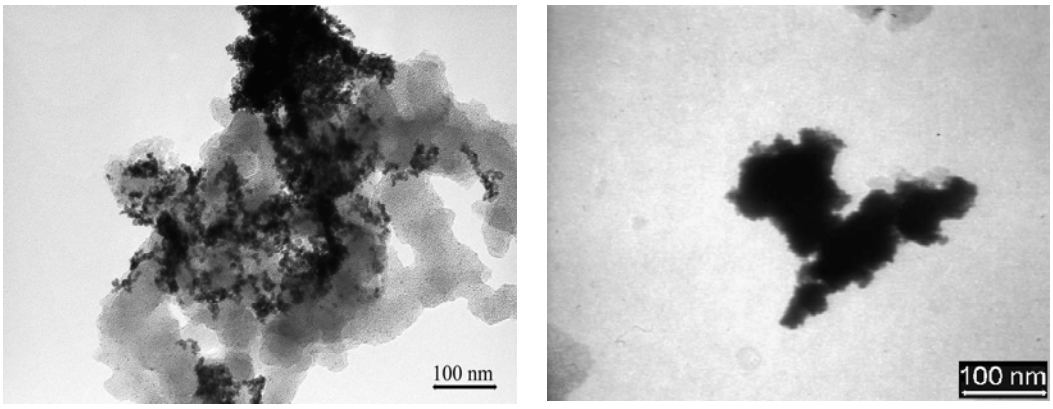

(a) (b)

Figure 7.2: TEM images of $Pt_{50}Ni_{50}$-MCM-41 catalysts prepared with 0.2 M $NaBH_4$ in distilled water at reduction temperatures of (a) 273 K and (b) 313 K.

The morphology of the metal nanoparticles as shown by TEM images in Figure 7.2(a) showed that the reduction of the impregnated Pt and Ni metal salts at 273 K resulted in the formation of a mixture of aggregates and small dispersed nanoparticles with an average particle size of 5.7 $\pm$ 1.6 nm. In comparison, when a higher reduction temperature of 313 was employed, it was found that the majority of the metal phase aggregated (Figure 7.2(b)). The influence of reduction temperature on the particle morphology can be explained as due to the reduction rate of the metal salts. At lower temperatures of 273 K, the slower reduction rates promote the stabilization of the metal nanoparticles on the MCM-41 support. This effectively inhibits particle growth giving rise to the formation of smaller sized nanoparticles. In contrast, the increase in reduction temperature enhances the metal ion reduction rate. This causes the particles to come in contact with each other frequently hence results in aggregation of the particles.

Catalysts prepared at 273 K and 313 K chemisorbed 1.5 x 10^{-4} mol g_{met}^{-1} and no H_2 respectively. The inability of the catalyst prepared at 313 K to adsorbed H_2 correlates well with the aggregated particles observed in the TEM images as compared to that obtained for the catalyst prepared at 273 K.

Figure 7.3 depicts the effect of reduction temperature on the reaction rates of $Pt_{50}Ni_{50}$ catalysts supported on MCM-41. The catalyst prepared at 273 K exhibits the highest activity with maximum reaction rate of 16.1 x 10^{-3} mol min^{-1} g_{met}^{-1} at 400 K. In contrast, the catalyst prepared at 313 K was completely inactive. This correlates well with the inability of the catalyst to adsorb hydrogen as well as with aggregated particles observed in the TEM images.

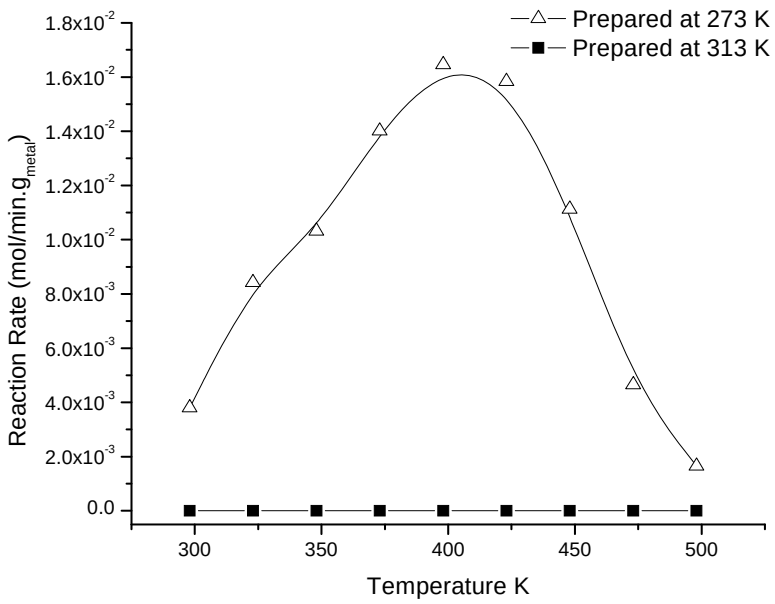

Figure 7.3: Reaction rates for the hydrogenation of benzene by $Pt_{50}Ni_{50}$ supported MCM-41 catalysts prepared using 0.2 M $NaBH_4$ in distilled water at various reduction temperatures.

To further understand the characteristics of the catalyst prepared at 273 K, a line analysis profile of the sample was obtained to gain an insight on the distribution of the elements which exist in the catalyst. Figure 7.4 exhibits the SEM image and the corresponding line profile. The darker area in the image is attributed to the silica support. This is consistent with the distribution of Si and O. The lighter area on the other hand is of the metal phase. As can be seen, both the Pt and Ni profiles are identical. Hence, this indicates that possible alloying may have occurred between Pt and Ni. Furthermore, it is observed that the intensity of Pt is higher than that of Ni. This can be explained as due to Pt segregation on the surface of the metal phase.

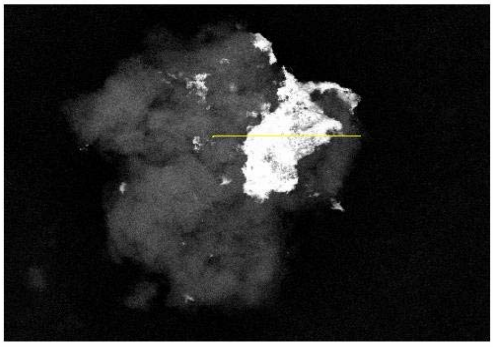

10 µm

(a)

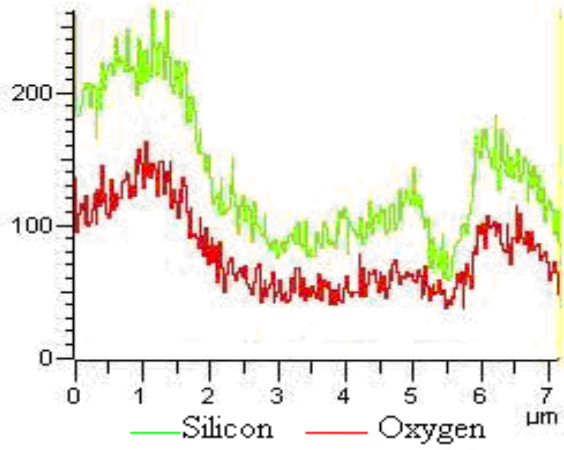

(b)

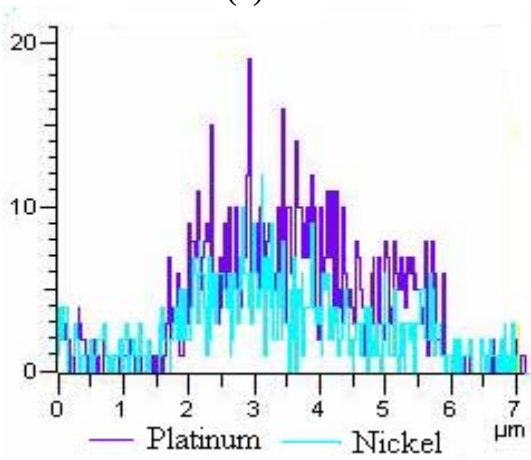

(c)

Figure 7.4: (a) SEM images of $Pt_{50}Ni_{50}$–MCM-41 prepared at 273 K using 0.2 M $NaBH_4$ in distilled water and line profiles of (b) Si and O and (c) Pt and Ni.

7.4 Effect of $NaBH_4$ Concentration

The effect of $NaBH_4$ concentration on the properties of the catalysts was also studied to understand the conditions in which optimum activity is obtainable. Investigations were carried out at 273 K in a mixture of distilled water and ethanol. In general, studies on the morphology of the metal phase reveal that an increase in the $NaBH_4$ concentration resulted in a reduction in the average particle size to a certain extent. However, further increase in the concentration of the reducing agent caused the particles to aggregate. Average particle size of the metal particles produced using 0.2 and 0.3 M of $NaBH_4$ is 5.7 $\pm$ 1.6 and 4.4 $\pm$ 1.3 nm respectively. The decrease in average particle size with increasing $NaBH_4$ concentration is influenced by the nucleation and growth rates of the particles. At low concentrations of $NaBH_4$ (0.2 M), the nucleation rate of the metal particles is slow. This facilitates particle growth as more metal atoms formed in the later stage of the reaction will collide and adsorb on the nuclei and grow [10]. Upon increasing the $NaBH_4$ concentration to 0.3 M, the nucleation rate increases giving rise to larger amounts of nuclei at the early stage of the reaction. Though other metal atoms will collide and adsorb on the nuclei, the drastic decrease in amount of metal ions left after nucleation inhibits growth of the metal nanoparticles [11]. A typical image of the metal particles prepared using 0.3 M of $NaBH_4$ is shown in Figure 7.5(a). Further increase in the concentration of $NaBH_4$ to 0.4 and 0.5 M demonstrated the formation of metal aggregates. In this case, the excess of nuclei's formed at the beginning of the reaction is insufficiently stabilized by the support leading to the formation of larger particles.

H_2-chemisorption studies which were carried out to gain an insight on the surface area available for reaction are consistent with the TEM morphologies

observed. Our findings show that the amount of H_2 adsorbed increased with $NaBH_4$ concentration from 0.2 to 0.3 M, and then decreased with further increases in $NaBH_4$ concentration. The catalyst prepared using 0.3 M of $NaBH_4$ adsorbed 5.2 x 10^{-4} mol g_{met}^{-1} H_2. This is more than double that adsorbed by the catalyst prepared using 0.2 M $NaBH_4$. Upon further increase in $NaBH_4$ concentration, this value decreased reaching 1.7 x 10^{-4} mol g_{met}^{-1} of H_2 for the catalysts prepared using 0.5 M $NaBH_4$.

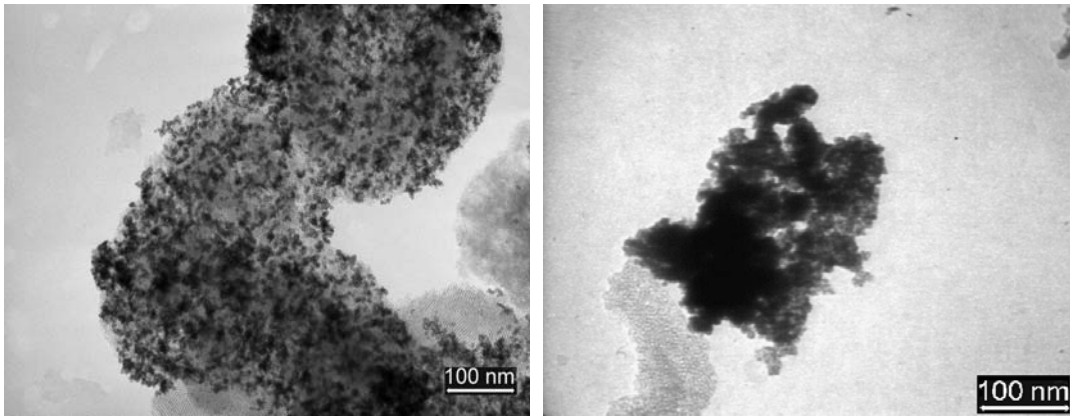

(a) (b)

Figure 7.5: TEM images of the $Pt_{50}Ni_{50}$ catalysts supported on MCM-41 prepared at 273 K using 0.3 M $NaBH_4$ prepared in (a) mixtures of distil water and ethanol and (b) distil water.

H_2-TPD profiles corresponding to the effect of $NaBH_4$ concentration on the prepared catalysts are shown in Figure 7.6. As can be seen, the catalysts synthesized using 0.2, 0.3 and 0.4 M of $NaBH_4$ all show similar adsorption sites where a peak is positioned at approximately 775 – 840 K. In contrast, the sample prepared with 0.5 M of $NaBH_4$ exhibited an additional peak at 706 K. The formation of this site could have been caused by an increase in boron concentration in the catalyst. However, atomic analyses of the B content in the

catalysts were reported as less than 0.05 %. This limits comparison and further explanation on this phenomenon. Even so, both adsorption peaks indicate the presence of hydrogen strongly adsorbed to the metal surface or hydrogen present at the interface between the metal particle and the support or incorporated into the support as spillover species [12, 13]. Generally it is observed that an increase in the $NaBH_4$ concentration resulted in an increase in hydrogen desorption during the TPD studies. Considering that the activation and analysis conditions are identical for all the samples, this trend can only be attributed to the adsorption of hydrogen produced during the reduction of the metal salts with $NaBH_4$ in the preparation stage. The increase in $NaBH_4$ concentration resulted in an increased production of hydrogen. This indirectly led to additional amounts of adsorbed hydrogen on the metal particles.

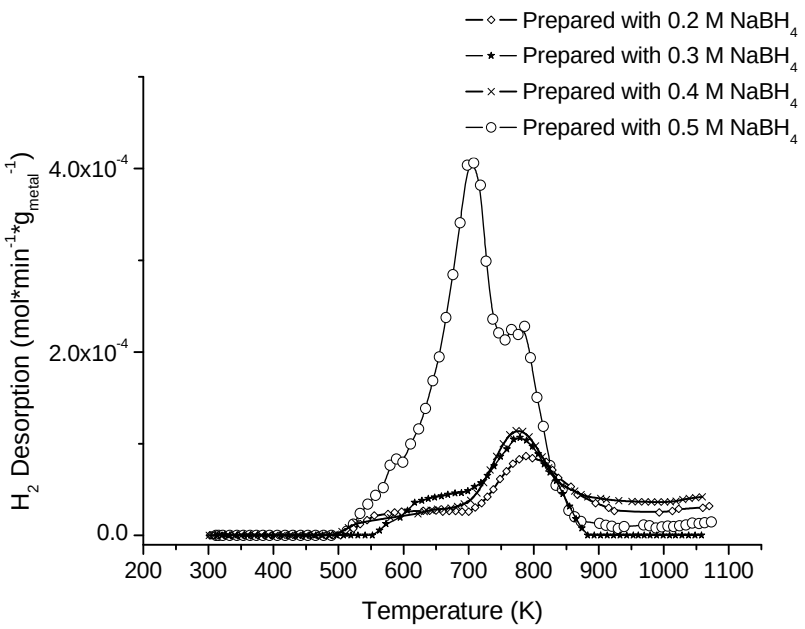

Figure 7.6: H_2-TPD profiles of $Pt_{50}Ni_{50}$-MCM-41 prepared at 273 K using various $NaBH_4$ concentrations.

It is found that reaction rates in benzene hydrogenation to cyclohexane increased to a certain extent and then decreased with increasing $NaBH_4$ concentration. As illustrated in Figure 7.7, the catalyst prepared with 0.2 M of $NaBH_4$ showed a reaction rate with a maximum of 16.2 x 10^{-3} mol min^{-1} g_{met}^{-1} occurring at 404 K. Further increase in the concentration of the reducing agent to 0.3 M resulted in an enhancement in the reaction rate. In this case, the $Pt_{50}Ni_{50}$ catalyst prepared using 0.3 M $NaBH_4$ showed a maximum reaction rate of 25.0 x 10^{-3} mol min^{-1} g_{met}^{-1} at 400 K. Subsequent increase in the concentration of the reducing agent employed showed no further improvement in the reaction rate. The reaction rates decreased to 14.0 x 10^{-3} and 8.3 x 10^{-3} mol min^{-1} g_{met}^{-1} for catalysts prepared with 0.4 and 0.5 M $NaBH_4$ respectively. The increase and decrease in reaction rate with $NaBH_4$ concentration can be explained based on the morphology of the metal phase. At lower and higher concentrations of $NaBH_4$, aggregates are formed and caused a reduced surface area available for reaction. Thus, a low conversion of benzene to cyclohexane is observed. It is found that upon employing 0.3 M of $NaBH_4$, the particle size of the metal particles decreases giving a larger surface area for the reaction to occur. In this case high reaction rates are obtained. H_2-chemisorption studies correlate well with this phenomenon.

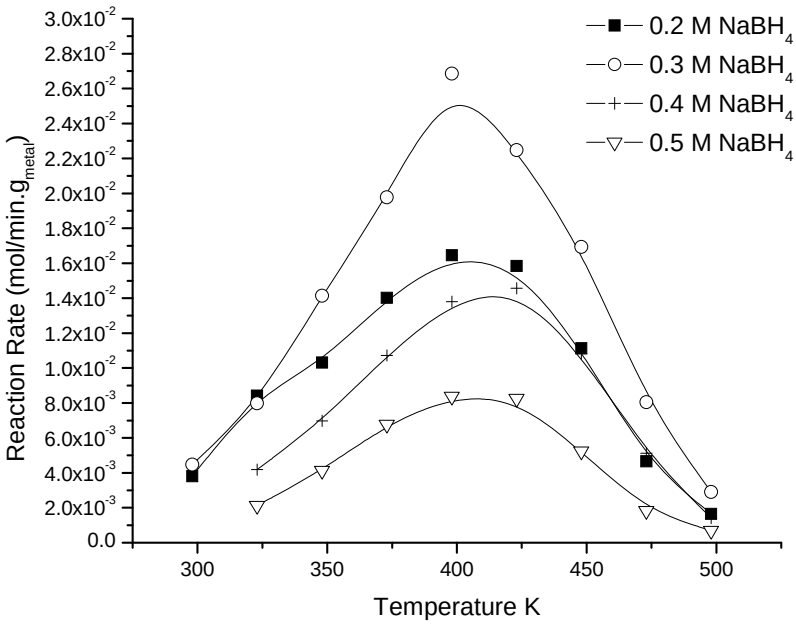

Figure 7.7: Effect of $NaBH_4$ concentration on the reaction rate of benzene hydrogenation. $Pt_{50}Ni_{50}$ – MCM-41 prepared at 273 K in mixtures of distil water and ethanol.

7.5 Effect of Reduction Medium

The effect of various reduction mediums on the reaction rates of $Pt_{50}Ni_{50}$-MCM-41, synthesized using 0.3 M of $NaBH_4$ at 273 K was investigated. Inspections on particle morphology showed that catalysts synthesized in distilled water formed aggregates (Figure 7.5(b)) while those prepared in ethanol exhibited smaller particles. Average particle size of the metal phase obtained from TEM, for catalysts synthesized in mixtures of distilled water and ethanol as well as ethanol is 4.4 $\pm$ 1.3 and 2.8 $\pm$ 1.2 nm respectively. This indicates that the average particle size of the metal particles supported on MCM decreases with increasing amounts of ethanol in the reduction medium. H_2-chemisorption investigations show similar trends to the average particle size of the PtNi nanoparticles. The increase in ethanol in the reduction medium led to higher

amounts of adsorbed H_2 indicating that smaller particles are available. As much as 1.3 x 10^{-4}, 5.2 x 10^{-4} and 19.9 x 10^{-4} mol g_{met}^{-1} H_2 was adsorbed by the catalysts prepared in distilled water, mixtures of distilled water and ethanol as well as ethanol respectively.

Previous studies have shown that the dielectric constants of solvents can affect the surface energy of metal particles [14, 15]. Therefore this can influence particle morphology. In this case, distilled water which has a high dielectric constant of 78.54 caused the metal particles to aggregate. Instability of the particles occurs as a result of the high surface energy of the particles formed upon reduction with $NaBH_4$. The particles aggregate in order to reduce the surface energy. In contrast, the addition of ethanol to the reduction medium reduces the dielectric constant of the solvent medium as ethanol has a dielectric constant of 20.33. This can lower the surface energy of the particles resulting in smaller particles as observed in the TEM images.

Interaction between the solvents and $NaBH_4$ during the reduction of the metal salts is another factor that may affect the morphology of the metal phase. The reduction of the metal salts using $NaBH_4$ in the presence of distilled water leads to the formation of $[B(OH)_4]^-$ or $[BO_2]^-$ according to equations (7.1) and (7.2) [16, 17]. These ionic complexes have lower steric stabilizing properties as compared to the $[B(OC_2H_5)_4]^-$ or $[B(OC_2H_5)_2]^-$ which have longer hydrocarbon chains, formed during the reduction of the metal salts in the presence of ethanol as shown in equations (7.3) and (7.4) [18].

$$PtCl_6^{2-} + BH_4^- + 4H_2O \rightarrow 2Pt + B(OH)_4^- + 8H^+ + 12Cl^- \qquad (7.1)$$

$$2Ni^{2+} + BH_4^- + 2H_2O \rightarrow 2Ni + BO_2^- + 4H^+ + 2H_2 \qquad (7.2)$$

$$2PtCl_6^- + BH_4^- + 4C_2H_5OH \rightarrow 2Pt + B(OC_2H_5)_4^- + 8H^+ + 12Cl^- \quad (7.3)$$

$$2Ni^{2+} + BH_4^- + 2C_2H_5OH \rightarrow 2Ni + B(OC_2H_5)_2^- + 4H^+ + H_2 \quad (7.4)$$

Therefore, the metal particles formed are unstable in distilled water and hence promotes particle aggregation. In mixtures of ethanol-distilled water, a competition between the formation of BO_2^- or $B(OH)_4^-$ and $B(OC_2H_5)_2^-$ or $B(OC_2H_5)_4^-$ occur due to the coexistence of water and ethanol molecules. The interactions between the reducing agent and ethanol produced smaller particles as compared to those formed in water. In ethanol small particles are obtained as competition with water does not arise. Kim et al. [19] reported a similar phenomenon occurring in systems based on distilled water and ethylene glycol.

The effect of solvent medium on the reaction rates of the catalysts are shown in Figure 7.8. It is observed that when distilled water is used, the catalysts demonstrated the lowest reaction rate. In this case, reaction rate increased starting from 298 K reaching a maximum of 18.6 x 10^{-3} mol min^{-1} g_{met}^{-1} at 401 K before declining. Using a mixture of ethanol-distilled water caused the reaction rate to increase. A similar trend was also observed when only ethanol was used. In both cases, maximum reaction rates increased to 25.0 x 10^{-3} mol min^{-1} g_{met}^{-1} and 27.9 x 10^{-3} mol min^{-1} g_{met}^{-1} respectively. The results obtained can be correlated to the average particle size of the PtNi nanoparticles. As shown above alcohol as a solvent favors the formation of smaller metal particles.

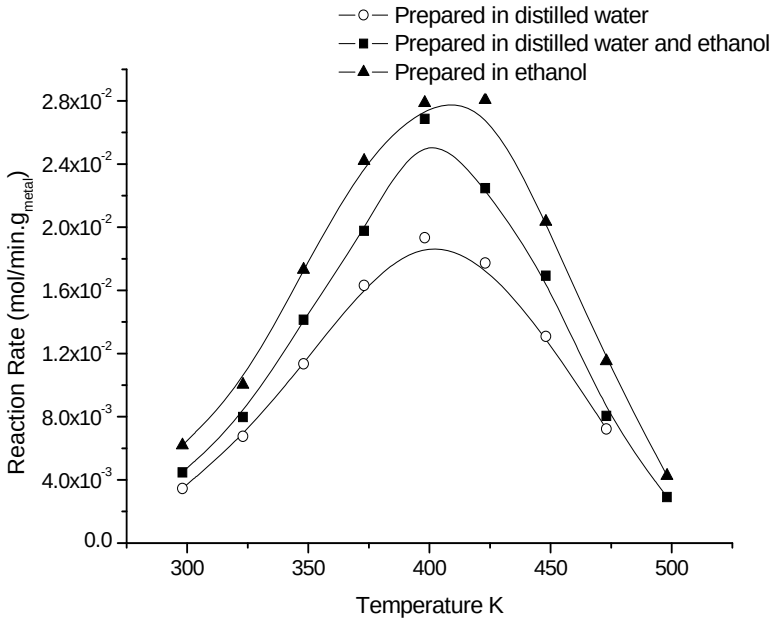

Figure 7.8: Effect of ethanol on the reaction rate of hydrogenation of benzene by $Pt_{50}Ni_{50}$ catalysts supported on MCM-41 prepared using 0.3 M $NaBH_4$ at 273 K.

7.6 Comparison with Monometallic Catalysts at Optimum Conditions

Pure Pt and Ni catalysts were synthesized using the optimum conditions at which, hydrogenation of benzene was most reactive for the $Pt_{50}Ni_{50}$ catalyst. For this study, the Pt and Ni salts impregnated separately in MCM-41 was reduced at 273 K using 0.3 M of $NaBH_4$ in a medium of ethanol.

H_2-chemisorption studies showed that no H_2 was adsorbed by the monometallic Ni_{100} catalyst. In comparison, the monometallic Pt_{100} catalyst as well as the $Pt_{50}Ni_{50}$ catalysts prepared at optimum conditions adsorbed 3.2 x 10^{-4} and 19.9x 10^{-3} mol g_{met}^{-1} H_2 correspondingly. This strongly indicates a high reactivity for the bimetallic catalyst. H_2-TPD profiles are presented in Figure 7.9. Studies of the monometallic Ni catalyst revealed that a desorption peak arises at

approximately 561 K. This is attributed to hydrogen moderately attached to active nickel sites. In contrast, the pure Pt profile exhibits two major peaks positioned at 707 and 900 K. The peak positioned at 707 K is attributed to hydrogen retained at the metal support interphase while the latter peak corresponds to hydrogen spillover species. Further investigations demonstrate that additional active sites are observed for the $Pt_{50}Ni_{50}$ catalyst when compared to the monometallic catalysts. Four peaks arising at 603, 764, 833 and 880 K are seen. The peaks positioned at 603 and 764 K correspond to hydrogen moderately adsorbed onto the metallic surface and retained at the metal support interphase respectively while those positioned at higher temperatures can be correlated to hydrogen spillover onto the support. Differences in the TPD profiles between the pure metals and the bimetallic compound attest to the existence of special PtNi groupings in the latter catalyst.

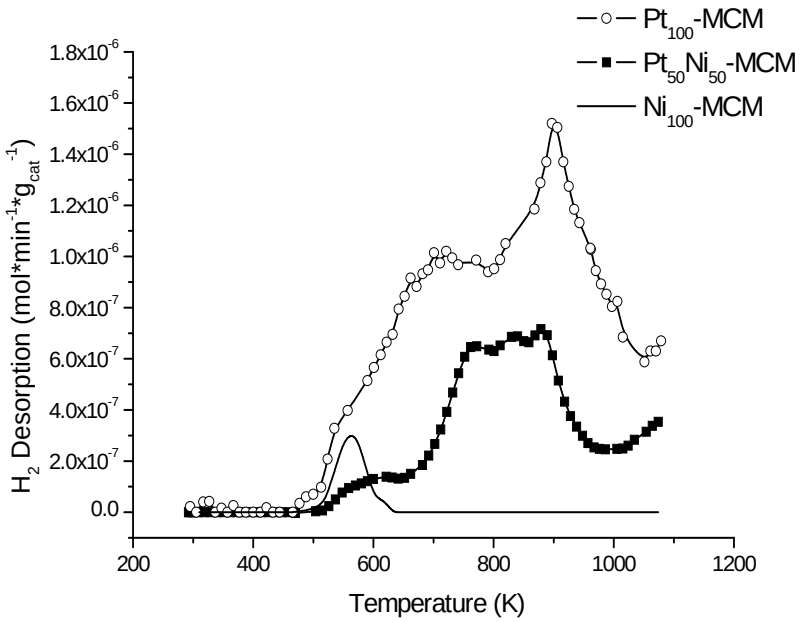

Figure 7.9: H_2-TPD profiles of Pt_{100}, Ni_{100} and $Pt_{50}Ni_{50}$ and MCM-41 prepared at 273 K using 0.3 M $NaBH_4$ in ethanol.

To investigate the reactivity of these catalysts, hydrogenation of benzene was carried out. Figure 7.10 which illustrate the reactivity profiles show that the Ni_{100} catalyst is inactive under the conditions employed. The Pt_{100} catalyst on the other hand is reactive reaching a maximum of 24.7 x 10^{-3} mol min^{-1} g_{met}^{-1} at 414 K. Even so, enhanced reactivity is observed for the $Pt_{50}Ni_{50}$ catalyst whereby a reaction rate of approximately 27.9 x 10^{-3} mol min^{-1} g_{met}^{-1} is obtained at similar temperature. This can be explained due to the synergistic effect in the bimetallic catalyst. Results correlate well with the H_2-chemisorption studies.

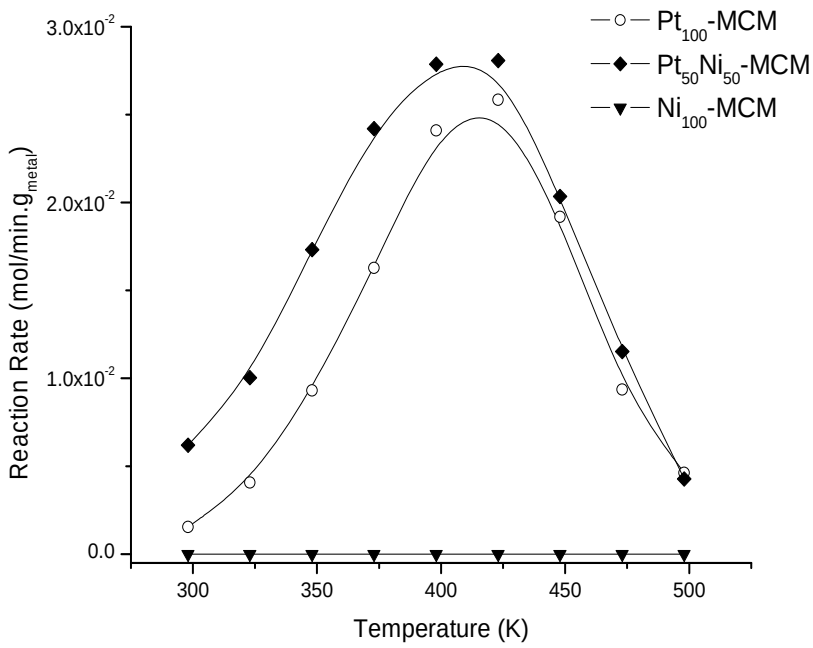

Figure 7.10: Reaction rates of hydrogenation of benzene by Pt_{100}, Ni_{100} and $Pt_{50}Ni_{50}$ catalysts supported on MCM prepared using 0.3 M $NaBH_4$ at 273 K in ethanol.

7.7 Summary

The morphology of the metal phase in the $Pt_{50}Ni_{50}$-MCM-41 catalysts significantly influences the hydrogenation reaction of benzene to cyclohexane. Various factors such as the reduction temperature, concentration of $NaBH_4$ as well as the reduction medium play a role in determining the particle morphology. Our studies show that optimum reaction rates were obtained when catalysts were synthesized at 273 K using 0.3 M $NaBH_4$ in a medium of ethanol. Under these optimum synthesis conditions, a synergistic effect is obtainable in the bimetallic $Pt_{50}Ni_{50}$ supported MCM-41 catalyst whereby superior activity compared to the monometallic catalysts was observed.

7.8 References

[1] Y. Li, G. H. Lai, R. X. Zhou, Appl. Surf. Sci. 253 (2007) 4978.

[2] E. Antolini, J. R. C. Salgado, R. M. da Silva, E. R. Gonzalez, Mater. Chem. Phys. 101 (2007) 395.

[3] Z. Xiong, Z. Mi, X. Zhang, Catal. Commun. 8 (2007) 571.

[4] S. K. Ghosh, M. Mandal, S. Kundu, S. Nath, T. Pal, Appl. Catal. A: Gen. 268 (2004) 61.

[5] A. G. Boudjahem, M. Pietrowski, S. Monteverdi, M. Mercy, M. M. Bettahar, J. Mater. Sci. 41 (2006) 2025.

[6] Y. Liang, H. Zhang, B. Yi, Z. Zhang, Z. Tan, Carbon 43 (2005) 3144.

[7] A. Corma, A. Martinez, V. Martinez-Soria, J. Catal. 169 (1997) 480.

[8] J. N. Armor, Appl. Catal. 112 (1994) N21.

[9] P. V. Adhyapak, P. Karandikar, K. Vijayamohanan, A. A. Athawale, A. J. Chandwodlear, Mater. Lett. 58 (2004) 1168.

[10] S. H. Wu, D. H. Chen, J. Coll. Interf. Sci. 273 (2004) 165.

[11] L. M. Liz-Marzan, A. P. Philipse, J. Phys. Chem. 99 (1995) 15120.

[12] S. Chettibi, R. Wojcieszak, E. H. Boudjennad, J. Belloni, M. M. Bettahar, N. Keghouche, Catal. Today 113 (2006) 157.

[13] A. G. Boudjahem, S. Monteverdi, M. Mercy, D. Ghanbaja, M. M. Bettahar, Catalysis Lett. 84 (2002) 115.

[14] K. H. Kim, Y. B. Lee, S. G. Lee, H. C. Park, S. S. Park, Mater. Sci. Eng. A. 381 (2004) 337.

[15] D. P. Wang, D. B. Sun, H. Y. Yu, H. M. Meng, J. Cryst. Growth 310 (2008) 1195.

[16] J. Shen, Z. Li, Q. Yan, Y. Chen, J. Phys. Chem. 97 (1993) 8504.

[17] T. C. Deivaraj, J. Y. Lee, J. Power Sources 142 (2005) 43.

[18] S. Ege, 1999. Organic Chemistry: Structure and Reactivity, USA, Houghton Mifflin Company.

[19] P. Kim, J. B. Joo, W. Kim, J. Kim, I. K. Song and J. Yi, J. Power Sources 160 (2006) 987.

CHAPTER 8

PtNi SUPPORTED MCM-41 CATALYSTS PREPARED VIA CLASSICAL METHODS

8.1 Introduction

The method employed for the synthesis of supported bimetallic metal particles is crucial as it relates to the subsequent pretreatment conditions which can significantly influence the final properties of a catalyst. In recent years, attention has been channeled to the synthesis of supported bimetallic catalysts prepared via non-classical methods, as this method provides a better means for control over the formation of metal particles. The main reason is to obtain catalysts which not only demonstrate better catalytic performances but are also economical. Even so, catalysts prepared via non-classical methods at times, pose disadvantages in terms of the inhibiting effect of stabilizers and the occurrence of trace elements which can poison catalysts. This occurs due to the inability to effectively remove the two from the catalysts. It is these reasons that promote pretreatments of catalysts. Hence, it is frequently debatable whether the non-classical methods are in fact superior to the classical methods when synthesizing catalysts.

The so called ‘classical’ methods have been reported comprehensively [1, 2]. This approach is recognized for its simplicity and clean resultant materials

which is a result of the pretreatment conditions. These treatments are conducted with the intention to ensure removal of poisoning species, the formation of crystalline alloys (when two or more metals are employed) as well as for drying and activation purposes. Though this method has the advantage of eliminating the existence of elements that can hinder catalytic activity as well as promoting alloy formation which can improve catalytic activity, it may to some extent result in aggregation or sintering of the metals involved. Increase in particle sizes with increasing temperature and heating periods has been observed [3]. This phenomenon largely depends on the temperature in which hydrogen reduction is conducted [4]. Although in some cases, this may cause a loss in catalytic activity, this is not necessary true as the metals and support employed may also play a significant role. As an example, it has been shown that a significant increase in the hydrogenation of benzene is observed when Ni is supported on MCM-41 in contrast to AlMCM-41 [5]. This is due to the higher extent of reduced Ni available on MCM-41 compared to AlMCM-41, which can be correlated to the strength of interaction. In contrast, other works by the same research group showed that similar reactivity can be obtained when higher reduction temperatures are employed. However, the stability of the Ni-MCM-41 catalyst was drastically reduced [6]. Hence indirectly, these works show that the properties of metal supported MCM-41 based catalysts can be influenced by the reduction conditions.

In the previous chapters a thorough study on how catalysts prepared via non-classical methods affect the structure and morphology of supported PtNi particles and in turn their catalytic reactivity has been presented. This method has shown potential for controlling the PtNi morphology, by varying various

preparation techniques and reduction parameters. Although it has been shown that the PtNi alloys exhibit enhanced reactivity when compared to their monometallic catalysts, one question still arises. To what extent are the catalysts prepared via non-classical methods superior when compared to those prepared via classical methods? Hence, this has prompted the investigation of PtNi supported on MCM-41 catalysts prepared via classical methods. In this study, a series of experiments were conducted to investigate the optimum activation conditions for the PtNi catalysts prepared via classical methods. Further, these catalysts were characterized using various techniques to gain a better understanding on how the morphology and structure of the PtNi particles in these catalysts influence the catalytic reactivity. Finally, the reactivity of these catalysts was compared to those prepared via non-classical methods using similar activation conditions.

8.2 Effect of Activation Conditions

The $Pt_{50}Ni_{50}$-MCM-C catalyst was employed to determine the optimum activation conditions for the series of catalysts investigated, as similar amounts of the Pt and Ni metal salt was incorporated in this catalyst. This enabled us to obtain a balance between the conditions required to activate Pt (usually low temperature activation) and Ni (activation at higher temperatures).

The activity of the catalyst was compared at different activation temperatures, time and temperature ramp. Maximum conversion and the temperature at which it is achieved are tabulated in Table 8.1. As can be seen, the catalyst activated at 373 K for duration of 3 hours (100 ml min^{-1}, 10 K min^{-1}) showed the highest conversion of approximately 42.3 % at 458 K. Catalysts

activated at 473 K showed only two thirds the conversion of that activated at 373 K. The drastic decrease in activity as temperature is increased is interesting. It is speculated that this may be due to the formation of aggregates which is well known to occur at higher activation temperatures. Oxygen chemisorption confirmed this assumption (see section 8.3). Also considering that high activation temperatures resulted in lower activity, all catalysts in the following discussions were treated at 373 K for duration of 3 hours (100 ml min^{-1}, 10 K min^{-1}) when activation was required.

Table 8.1: Maximum conversions and temperatures at maximum conversion of the $Pt_{50}Ni_{50}$-MCM-C catalyst activated at various conditions.

Conditions				Maximum Conversion (%)	Temp. at Maximum Conversion (K)
Temp (K)	**Time (Hours)**	**Flow rate (ml min^{-1})**	**Ramp (K min^{-1})**		
373	3	100	10	42.3	458
473	3	100	10	24.7	474
373	2	100	10	35.3	489
373	4	100	10	33.6	439
373	3	200	10	37.2	467
373	3	100	5	33.4	448

8.3 O_2 Chemisorption

O_2-chemisorption studies were carried out to determine the degree of reduction of the metal phase for the $Pt_{50}Ni_{50}$-MCM-C catalysts activated at 373 and 473 K for duration of 3 hours (100 ml min^{-1}, 10 K $^{-1}$min) as well as for the catalysts with different PtNi ratios after activation in pure hydrogen.

The $Pt_{50}Ni_{50}$-MCM-C catalyst activated at 373 and 473 K adsorbed 7.26 x 10^{-3} and 9.42 x 10^{-3} mol g_{met}^{-1} O_2 respectively. This corresponds to 65.7 % and

85.0 % of the metallic phase existing in a reduced state. Indirectly, this suggests the formation of aggregates when higher temperatures were used. This leads to the conclusion that aggregation of the metal particles upon activation gives rise to a lower activity for the catalysts activated at 473 K.

The degree of reduction for catalysts prepared with different PtNi ratios are presented in Table 8.2. It was found that the Ni_{100}-MCM-C catalyst exhibited the lowest degree of reduction. Only 1.17 x 10^{-3} mol g_{met}^{-1} of O_2 was adsorbed attributing to 6.8 % of the Ni phase existing as Ni° after activation. The $Pt_{10}Ni_{90}$-MCM-C catalyst on the other hand showed O_2 adsorption of 1.88 x 10^{-3} mol g_{met}^{-1}. This demonstrates a degree of reduction of 12.0 %. The low degree of reduction in both the Ni_{100}-MCM-C and $Pt_{10}Ni_{90}$-MCM-C catalysts can be described as due to both the low calcinations and activation temperatures. The calcination temperature employed in this work prevents total decomposition of nickel sulfate to nickel oxides. Based on previous works, it has been shown that nickel sulfate is usually decomposed at temperatures of approximately 1003 K and above [7]. This limits the availability of NiO for subsequent reduction with H_2. In addition, the low activation temperature may contribute to insufficient energy for H_2 to reduce the nickel oxides available to Ni metal nanoparticles.

Subsequently, the $Pt_{50}Ni_{50}$-MCM-C catalyst exhibited a medium degree of reduction. An O_2 adsorption of 7.26 x 10^{-3} mol g_{met}^{-1} was obtained resulting in 65.7 % of the metal phase existing in a reduced state. In contrast the Pt_{100}-MCM-C and $Pt_{90}Ni_{10}$-MCM-C catalysts adsorbed 5.36 x 10^{-3} and 7.00 x 10^{-3} mol g_{met}^{-1} respectively. The calculated degree of reduction gives values of 105 and 103 %. In both cases, it is considered that 100 % of the metal phase is reduced after activation.

Table 8.2: The degree of reduction of the PtNi catalysts supported MCM-41.

Catalyst	Total Metal Content (%)	Metal Loading (%)		Degree of metal reduction (%)
		Pt	Ni	
Ni_{100}-MCM-C	0.80	-	0.80	6.8
$Pt_{10}Ni_{90}$-MCM-C	0.90	0.10	0.80	12.0
$Pt_{50}Ni_{50}$-MCM-C	0.90	0.45	0.45	65.7
$Pt_{90}Ni_{10}$-MCM-C	0.70	0.60	0.10	105
Pt_{100}-MCM-C	1.10	1.10	-	103

8.4 Surface Characteristics

8.4.1 H_2-TPR Analysis

H_2-TPR profiles of the catalysts calcined at 773 K are illustrated in Figure 8.1. The profile of Ni_{100}-MCM-C exhibits a strong sharp peak positioned at approximately 800 K. This peak can be attributed to the occurrence of NiO particles [8], nickel silicate [5] or nickel sulfate species [9] in the catalysts which are in strong interaction with the support. In contrast, the Pt_{100} supported MCM-41 catalysts can be characterized by a small peak positioned at 374 K. Decomposition of PtO_2 can occur at temperatures ranging between 553 - 823 K [10, 11]. In this work, calcinations were conducted at 773 K. Hence, decomposition of PtO_2 to form Pt and O_2 may have occurred as previously reported [12]. This may have caused reduction of a majority of the PtO_2 hence resulting in the small peak observed. Previous works have shown that the consumption of hydrogen in this temperature region is explained as due to the reduction of large PtO particles or PtO_2 [13]. The position of this peak varies depending on the support employed as well as the addition of a metal [13, 14]. Further observation of the profile also reveals the presence of another two

different metal particle size or sites in the Pt_{100}-MCM-C catalysts. Interestingly, these two sites which rise at about 693 and 894 K exhibit the production of hydrogen. This phenomenon can be attributed to the desorption of hydrogen incorporated at lower temperatures during H_2-TPR analysis. Hydrogen dissociates at the surface of the Pt particles and then migrates to the MCM-41 support as spillover hydrogen. As the temperature was increased, enough energy was obtained to allow desorption of the hydrogen from the support.

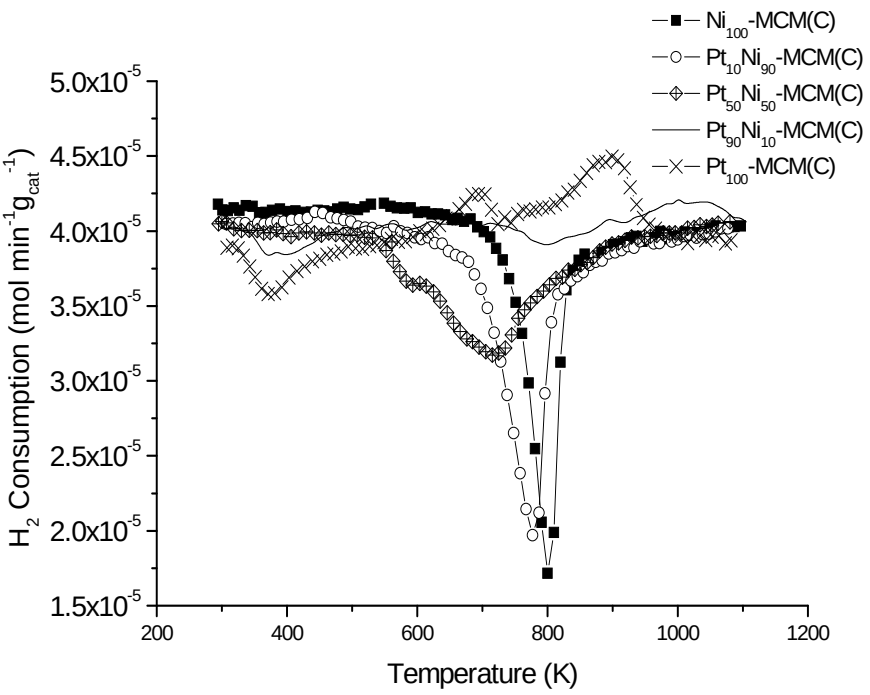

Figure 8.1: H_2-TPR profiles of PtNi supported MCM-41 catalysts prepared at various Pt/Ni ratios.

The surface properties of the bimetallic catalysts after calcinations are dependent on the metal ratios. Typically, they show intermediate characteristics of the pure metal supported MCM-41 catalysts. It can be observed that the $Pt_{10}Ni_{90}$-MCM-C catalyst demonstrates a peak similar to that of the Ni_{100}-MCM-C catalyst. This peak may also arise due to the interaction of nickel oxides or residual nickel sulfate with MCM. However the peak is slightly shifted to a lower temperature of 777 K. The slight shift may be attributed to the hydrogen spillover effect. The spillover species which originates from the Pt particles migrates to the Ni species via the support facilitating the reduction of the nickel species at lower temperatures [15]. In this case, segregates of Pt and Ni species are expected to exist on the support ensuring the transport of hydrogen [16]. A comparable trend is also seen for the $Pt_{50}Ni_{50}$-MCM-C catalysts. Here, a main peak and a shoulder are positioned at 718 and 593 K respectively. The $Pt_{90}Ni_{10}$-MCM-C catalyst on the other hand exhibits characteristics similar to the Pt_{100}–MCM-C catalyst. A slight consumption peak arises at approximately 381 K. In addition, hydrogen spillover occurs at higher temperatures, tough to a lesser extent when compared to the Pt_{100}-MCM-C catalyst.

8.4.2 H_2 - Chemisorption Studies

H_2-chemisorption studies were carried out to obtain information on the dispersion of the metal phase and the total surface area available for reaction. Values are tabulated in Table 8.3 Corrections have been made taking into account the degree of reduction of the catalysts.

Table 8.3: H_2-Chemisorption, dispersion and average particle size of the PtNi catalysts supported MCM-41.

Catalyst	H_2-Adsorption ($x10^{-3}$ mol g_{met}^{-1})	Dispersion [a] (%)	Particle [a] Size (nm)
Ni_{100}-MCM-C	0.13	21.8	4.6
$Pt_{10}Ni_{90}$-MCM-C	0.07	6.8	14.7
$Pt_{50}Ni_{50}$-MCM-C	1.43	42.3	2.7
$Pt_{90}Ni_{10}$-MCM-C	1.96	38.2	2.9
Pt_{100}-MCM-C	1.02	19.9	5.6

[a] Obtained from H_2-chemisorption studies after taking into account the degree of reduction of the catalyst.

As can be seen, catalysts with low quantities of Pt (Ni_{100}-MCM-C and $Pt_{10}Ni_{90}$-MCM-C) exhibit low hydrogen adsorption at room temperature. Upon taking into consideration the degree of reduction, it can be seen that the Ni_{100}-MCM-C catalyst exhibits a dispersion of 21.8 % giving a total metal surface area of 145.6 m^2 g^{-1}. Due to the low degree of reduction, the matrix allowed the stabilization of very small Ni° particles. Low activation temperature prevented their aggregation. The $Pt_{10}Ni_{90}$-MCM-C on the other hand gives rise to a low dispersion. Higher degree of reduction in $Pt_{10}Ni_{90}$-MCM-C led to the excess of Ni° atoms formed which more easily agglomerated than in Ni_{100}-MCM-C.

In contrast, the $Pt_{50}Ni_{50}$-MCM-C catalyst as well as catalysts with high amounts of Pt content ($Pt_{90}Ni_{10}$-MCM-C and Pt_{100}-MCM-C), demonstrate H_2 adsorption of more than 10 times that exhibited by the Ni_{100}-MCM-C catalyst. Dispersion of these catalysts range between 19.0 - 43.0 %. As H_2-chemisorption values are consistent with the calculated dispersions, it is possible that high catalytic activity can occur for these catalysts when compared to the Ni_{100}-MCM-C and $Pt_{10}Ni_{90}$-MCM-C catalysts.

Interestingly, it is observed that both the $Pt_{50}Ni_{50}$-MCM-C and $Pt_{90}Ni_{10}$-MCM-C catalysts exhibit enhanced hydrogen adsorption characteristics when compared to the Pt_{100}-MCM-C catalyst. This may be attributed to the smaller size of the metal particles which can give rise to a larger surface area of the metal phase available for reaction. This promotes hydrogen adsorption. The small sizes can be explained as due to the anchoring effect of the Ni^{2+} ions that aides the formation of well dispersed Pt particles. Less reducible metal acts as anchors for more reducible metals [17]. According to Yermakov et al., [18], Pt particles which can be stabilized by Re ions which acts as anchoring sites on SiO_2. Other researches have also explained this phenomenon in detail [3, 17].

8.4.3 H_2-TPD Profiles

The H_2-TPD curves of the catalysts are presented in Figure 8.2. The profile of the Ni_{100}-MCM-C catalysts shows a very low desorption of hydrogen which reaches a maximum at 494 and 660 K. Both peaks are broad, indicating the availability of a wide range of Ni particle size upon activation in pure hydrogen or the existence of different Ni species with various adsorption strengths. The low quantities of hydrogen desorbed can be attributed to the small number of nickel metallic atoms. Pt_{100}-MCM-C on the other hand reveals very large hydrogen desorption in the temperature range of approximately 400 to 1073 K. Here, optimum desorption occurs at 675 and 800 K. Shoulders which signify the presence of other active sites are also seen at 474 K and after 920 K. Generally, it has been proposed that the shoulder at 474 K can be attributed to hydrogen chemisorbed on the Pt surface [19] while the peak at higher temperatures correspond to the hydrogen species on the support far from the Pt, namely

hydrogen spillover. This correlates well with the H_2-TPR curves. Comparison of the amount of hydrogen desorbed from the Pt_{100}-MCM-C catalyst with that of the Ni_{100}-MCM-C demonstrates that a larger quantity is desorbed from the Pt_{100}-MCMC catalyst. This occurrence can be attributed to a greater number of platinum metallic atoms and a better dispersion of the metal particles in the Pt_{100}-MCM-C catalysts which increases the amounts of hydrogen atoms incorporated on the metal or the support surface as spillover species.

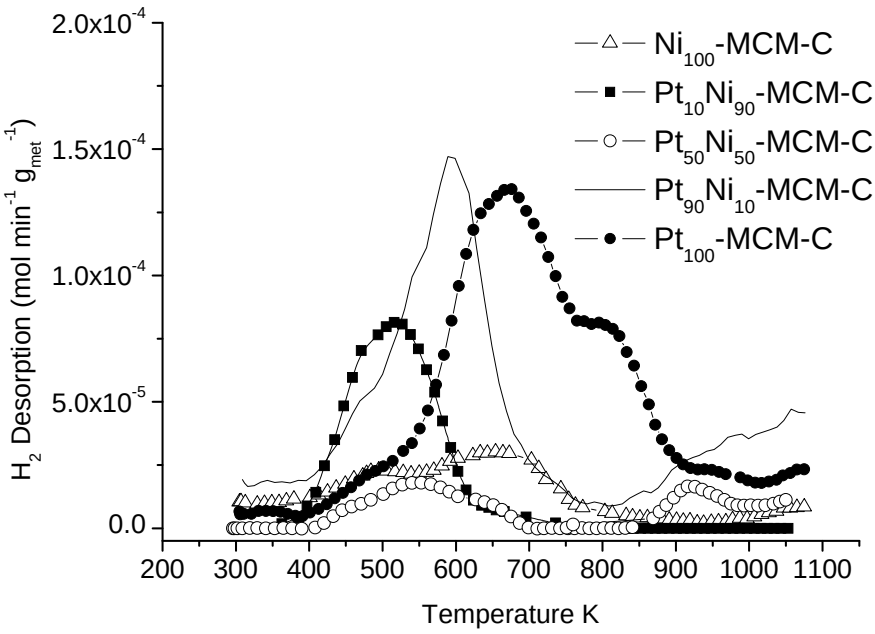

Figure 8.2: H_2-TPD profiles of PtNi supported MCM-41 catalysts prepared at various PtNi ratios.

The profiles of the PtNi supported MCM-41 catalysts are also depicted in Figure 8.2. The $Pt_{10}Ni_{90}$-MCM-C catalyst exhibits a peak at 516 K. In contrast, the $Pt_{50}Ni_{50}$-MCM-C and $Pt_{90}Ni_{10}$-MCM-C catalysts give rise to two peaks positioned as 542 and 918 K as well as 590 and starting at 835 K correspondingly. The peaks positioned in the temperature range of 510 - 590 K in all three bimetallic catalysts are consistent with H_2 moderately attached to the metal surface. It can be seen that the temperature at which maximum desorption occurs in these catalysts, shifts to lower temperatures with increasing Ni content. This demonstrates the synergistic effect between PtNi. Furthermore, except for the $Pt_{50}Ni_{50}$-MCM-C catalyst, it is generally seen that the amount of desorbed hydrogen decreases with increasing Ni content. This demonstrates the decrease of the number of nickel metallic atoms with increasing Ni content, which causes a decrease in the metallic surface area available for adsorption to occur. The exceptional behavior of the $Pt_{50}Ni_{50}$-MCM-C catalyst is not fully understood.

8.5 Structural Properties

XRD analysis was conducted to investigate the nature in which the metallic phase of PtNi exists. Diffractograms of the Pt_{100}-MCM-C and $Pt_{90}Ni_{10}$-MCM-C before and after hydrogenation reaction are exhibited in Figure 8.3. All spectra demonstrate a broad peak positioned at the 2θ value of approximately 23°. This peak is assigned to the MCM-41 support. Further inspections of the spectra reveal that the Pt_{100}-MCM-C and $Pt_{90}Ni_{10}$-MCM-C catalysts before hydrogenation reactions (obtained after calcinations in air) give rise to peaks positioned at ~ 39.77° and ~ 39.83° respectively. These diffraction peaks can be indexed to the (111) phase of the face cubic centered (fcc) structure of metallic

Pt. No peaks indicating the presence of PtO_2 or Pt_3O_4 are available [20]. This can be explained as due to the decomposition of the majority of the platinum oxides during calcinations as previously mentioned. The low content of platinum oxides as shown by H_2-TPR studies may not be observable in the XRD diffractograms. Further inspections show that a slight shift towards higher 2θ values is seen in the spectrums of $Pt_{90}Ni_{10}$-MCM-C when compared to the pure Pt catalysts. This can be explained as due to the occurrence of lattice distortions of the fcc structure of Pt. These lattice distortions have been related to the formation of alloys [21, 22] as well as a variation in particle structure. Comparison of the $Pt_{90}Ni_{10}$-MCM-C and Pt_{100}-MCM-C catalysts supported on MCM-41 after hydrogenation reactions also show similar trends to that of the catalysts obtained before hydrogenation reactions.

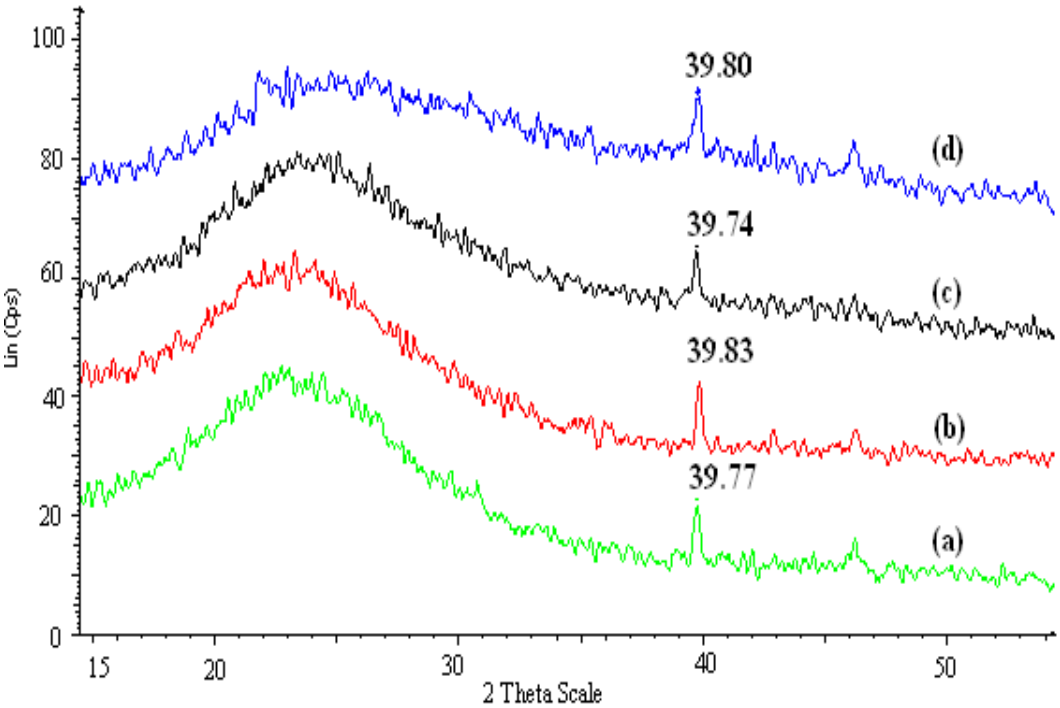

Figure 8.3: XRD diffractograms of (a) Pt_{100}-MCM-C and (b) $Pt_{90}Ni_{10}$-MCM-C before as well as (c) Pt_{100}-MCM-C and (d) $Pt_{90}Ni_{10}$-MCM-C after benzene hydrogenation reactions.

8.6 Morphological Studies

The morphology of the active phase of the PtNi supported MCM-41 catalysts before and after catalytic reactions was investigated via TEM. Images of the catalysts before catalytic reactions were obtained after impregnation of the metal salts as well as after subsequent calcinations in air. Typically, it is observed that fine flat like spherical particles are obtained upon impregnation of the metal salts (figure not shown). These grain-like particles grow upon heat treatment during calcinations forming larger particles. Interestingly it is found that a variety of particle shapes are observed in the bimetallic catalysts while only spherical particles exist in both the Pt_{100}-MCM-C and Ni_{100}-MCM-C catalysts. Similar particle morphologies are also observed after catalytic reactions. The occurrences of the particles were infrequent. This may be due to the low quantity of metal incorporated into the support. However, the possibility of the formation of fine particles in the pores of the MCM-41 is not ruled out. Limitations of the TEM, limit observations at higher magnifications.

The shape distribution and average particle size of the metal particles in the catalysts after calcinations and hydrogenation reactions respectively are tabulated in Table 8.4 (a) and (b) respectively. As can be seen, both the Pt_{100}-MCM-C and Ni_{100}-MCM-C calcined catalysts are composed of spherical nanoparticles with average particle sizes of 1.6 $\pm$ 0.6 and 1.6 $\pm$ 0.9 nm correspondingly. In the Ni_{100}-MCM-C catalysts, particles which are well distributed on the MCM-41 support are small in size. This is unusual considering that Ni species such as its oxide is prone to aggregation due to its magnetic properties. Even so, this occurrence may be explained as due to the strong interaction between the metal species and the support. Previous works have

shown similar findings [5]. The low Ni content and high surface area of the support may have resulted in a large amount of the Ni species attached directly to the support. These findings correlates well with the H_2-TPR and H_2-TPD profiles reported above.

Table 8.4: Average particle sizes and distribution of particle shapes of the metallic phase in the PtNi catalysts (a) before and (b) after hydrogenation reactions.

(a)

Catalysts	Average Particle Size(nm) Spherical	Cubes	Cubes (%)	Spherical (%)
Ni_{100}-MCM-C	1.6 ± 0.9	-	-	100
$Pt_{10}Ni_{90}$-MCM-C	3.7 ± 1.3	6.7 ± 2.2	7.0	93.0
$Pt_{50}Ni_{50}$-MCM-C	10.4 ± 13.2	51.9 ± 20.6	15.9	84.1
$Pt_{90}Ni_{10}$-MCM-C	1.9 ± 0.4	17.1 ± 5.4	19.6	80.4
Pt_{100}-MCM-C	1.6 ± 0.6	-	-	100

(b)

Catalysts	Average Particle Size(nm) Spherical	Cubes	Cubes (%)	Spherical (%)
Ni_{100}-MCM-C	2.3 ± 0.7	-	-	100
$Pt_{10}Ni_{90}$-MCM-C	3.9 ± 1.8	13.6 ± 4.4	13.2	86.6
$Pt_{50}Ni_{50}$-MCM-C	1.8 ± 1.6	19.4 ± 10.5	10.0	90.0
$Pt_{90}Ni_{10}$-MCM-C	1.6 ± 0.3	16.2 ± 10.3	7.4	92.6
Pt_{100}-MCM-C	1.4 ± 1.3	-	-	100

The calcined bimetallic PtNi supported MCM-41 catalysts give rise to nanoparticles with different morphologies. Typical TEM images of the different morphologies are exhibited in Figure 8.4. In all the catalysts, mixtures of spherical and rectangular nanoparticles exist. The distribution of rectangular nanoparticles varies between 6 – 20 %. Average particle sizes of the rectangular particles are 17.1 ± 5.5, 51.9 ± 20.6 and 6.7 ± 2.2 nm for the $Pt_{90}Ni_{10}$-MCM-C, $Pt_{50}Ni_{50}$-MCM-C and $Pt_{10}Ni_{90}$-MCM-C catalysts respectively. Here, particle size

increased from 10 to 50 wt % of Ni content and then decreased with further increase in Ni content. A similar trend was also observed for the spherical nanoparticles. However, particles are much smaller in size. Average particle sizes of the spherical nanoparticles for the $Pt_{90}Ni_{10}$-MCM-C, $Pt_{50}Ni_{50}$-MCM-C and $Pt_{10}Ni_{90}$-MCM-C catalysts are 1.9 $\pm$ 0.4, 10.4 $\pm$ 6.3 and 3.7 $\pm$ 1.3 nm correspondingly.

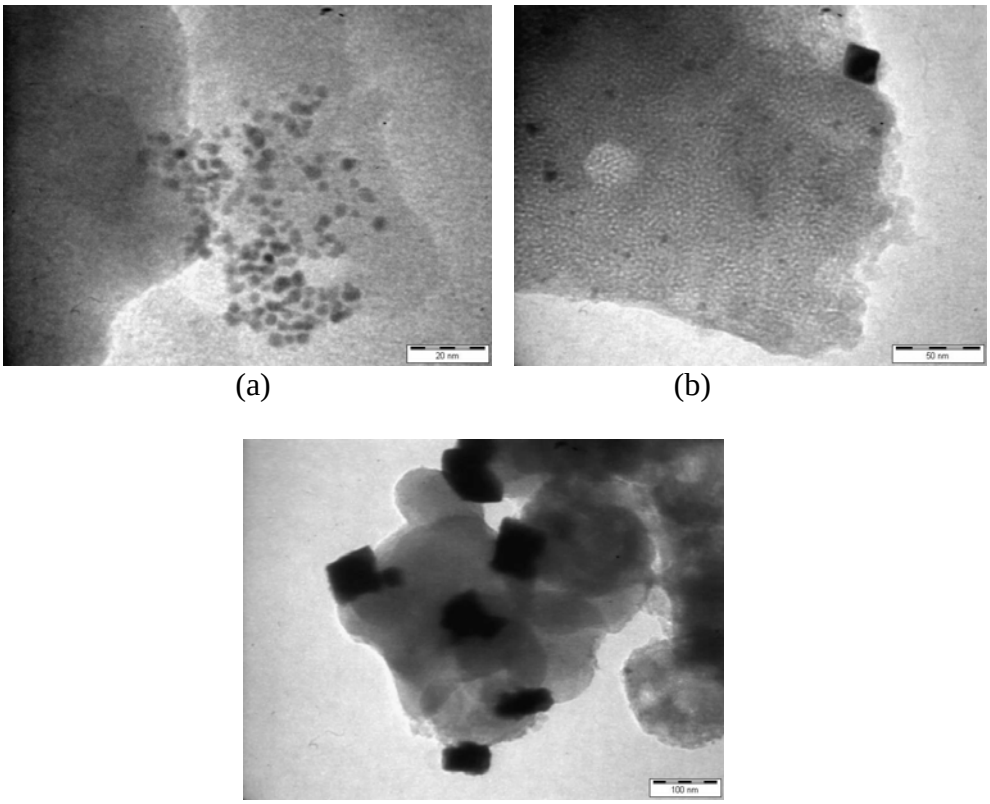

(a) (b)

(c)

Figure 8.4: Typical images of the various morphologies (a) spherical (b) mixtures of spherical and rectangular and (c) rectangular nanoparticles in the catalysts.

Upon activation and subsequent catalytic reactions, it is observed that the average metal particle sizes in both the Pt_{100}-MCM-C and Ni_{100}-MCM-C catalysts did not vary drastically when compared to those obtained before catalytic reactions. Average particle sizes of the metal phases are 1.4 $\pm$ 0.3 and 2.2 $\pm$ 0.7 nm respectively. For the Ni_{100}-MCM-C catalyst, this observation strengthens the belief that particles in this catalyst are strongly attached to the support via Ni^{2+} ions. This inhibits migration and subsequent aggregation of the metallic particles upon reduction or catalytic reaction. To demonstrate this, TEM equipped with EDX analysis was conducted on several areas of the support in the Ni_{100}-MCM-C catalyst where particles were not observed. In all the areas investigated, it was found that slight amounts of Ni were detected as shown in Figure 8.5(a). This proves that very fine Ni species are available on the MCM-41 support, probably in the form of ions. When the Pt_{100}-MCM-C catalyst was analyzed in the same way, such findings were not obtained. In contrast, Pt was only detected by EDX when particles are observed as in Figure 8.5(b). This suggests that Pt ions interacted less with the support.

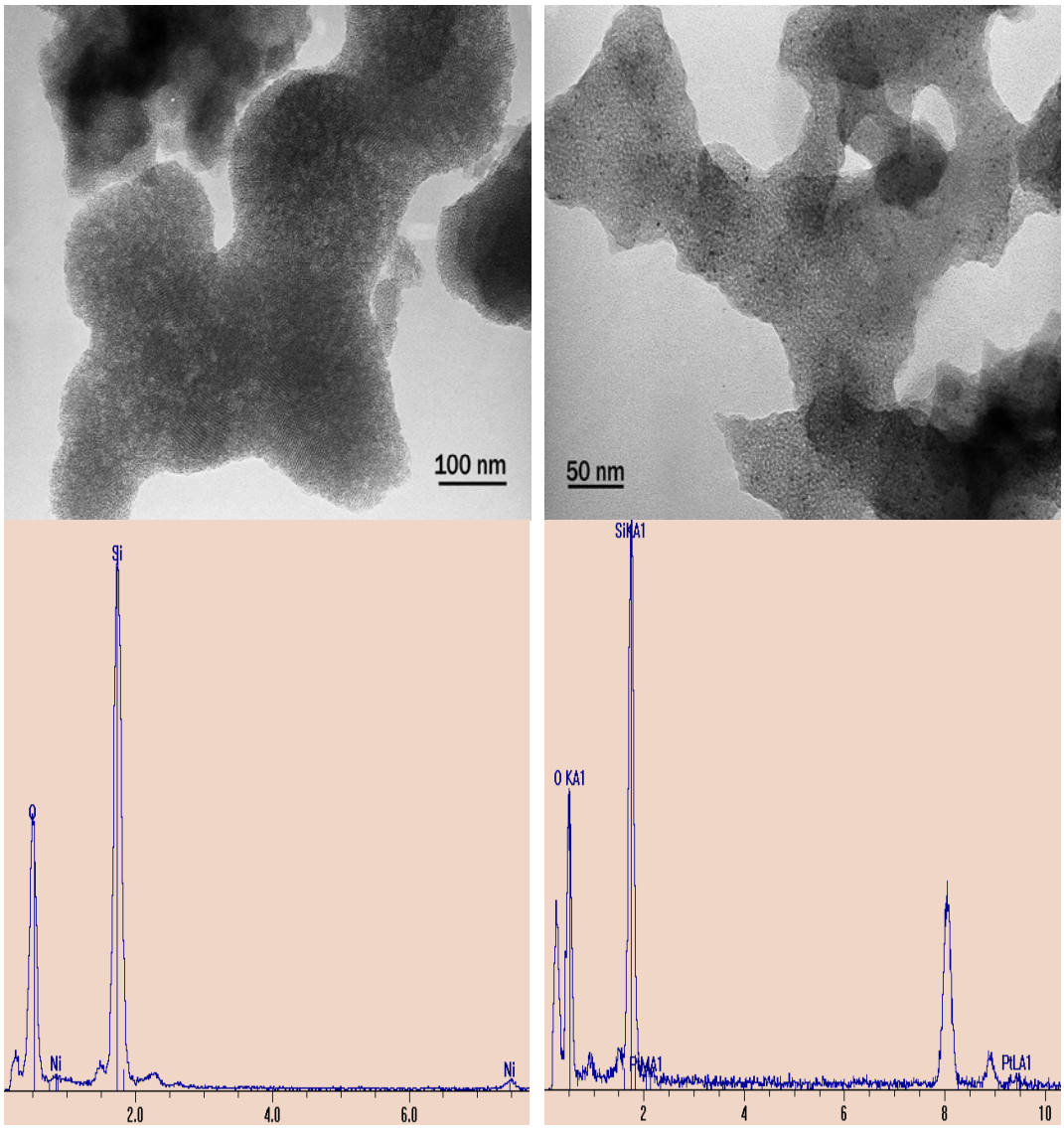

(a) (b)

Figure 8.5: TEM images of typical areas in the (a) Ni_{100}-MCM-C and (b) Pt_{100}-MCM-C catalysts as well as their corresponding EDX analysis.

In comparison to the monometallic catalysts, the bimetallic catalysts exhibit severe changes in the average particle sizes, though similar distributions in the particle shapes were observed. In this case the average particle sizes of the rectangular and spherical particles decreased to values in a range between 13.0 – 20.0 nm as well as 1.5 – 4.0 nm correspondingly, depending on the PtNi ratio.

This may be attributed to the large agglomerated species formed during calcinations, which fall apart forming smaller particles under a hydrogen flow or reductive atmosphere. This would particularly be the case for $Pt_{50}Ni_{50}$-MCM-C.

It is interesting to note that only the bimetallic catalysts exhibit particles with various morphologies. This could explain the shift in the XRD spectra of the $Pt_{90}Ni_{10}$-MCM-C catalyst relative to the Pt_{100}-MCM-C. To explain this observation the role of the Ni^{2+} ions in the system is considered. It is proposed that these ions either manipulate the decomposition kinetics of the PtO_2 by re-oxidizing the Pt atoms or seeds formed as temperatures are increased during calcinations or adsorb onto certain phases of the Pt nanocrystals. Either way, this causes the growth of the Pt particles to occur along certain surfaces, leading to the morphologies observed. Similar behavior have been observed by other researches who studied the effect of Fe^{3+} ions [23] and Ag^{2+} ions [24] on the morphology of Pt nanoparticles.

8.7 Catalytic Activity

The gas phase hydrogenation of benzene produced only cyclohexane, indicating that total hydrogenation occurred over the catalysts prepared. Profiles of the reaction rates as a function of temperature are illustrated in Figure 8.6. Under the conditions employed Ni_{100}-MCM-C exhibited no activity at all. This is expected even though the average particle sizes of the Ni nanoparticles formed after calcinations have an average diameter of 1.6 ± 0.9 nm. The inactivity of this catalyst can be attributed to the activation temperature and the strength of interaction between the metal and the support. The low activation temperature is insufficient to reduce the metal species which strongly interacts with the support

hence affects the metallic area available for the reaction to occur. This observation correlates well with the O_2-chemisorption and H_2-TPR analysis. Similar findings have been reported by Lewandowskov and co-workers [6].

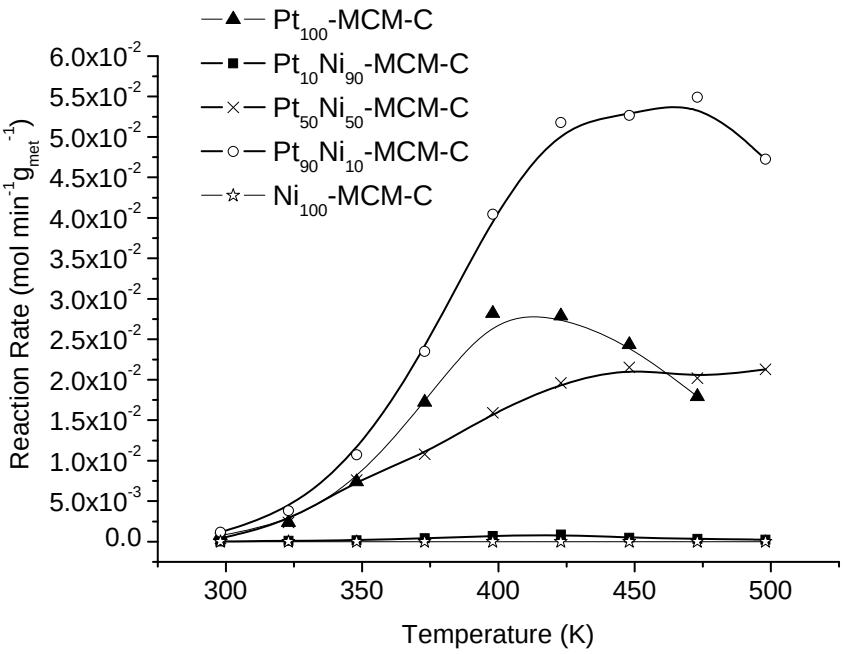

Figure 8.6: Profiles of the reaction rate of hydrogenation of benzene to cyclohexane for various PtNi catalysts supported on MCM-41 relative to the reaction temperature.

The increase of Pt content in the catalysts leads to an increase in the reaction rates. $Pt_{10}Ni_{90}$-MCM-C exhibited only a slight increase starting at approximately 350 K and reaching a maximum of 0.77 x 10^{-3} mol min^{-1} g_{met}^{-1} at 416 K before declining. In contrast, drastic enhancements in the reaction rates are seen when the Pt content is further increased. The $Pt_{50}Ni_{50}$-MCM-C and $Pt_{90}Ni_{10}$-MCM-C catalyst was found to be active even at 298 K. Here, reaction rates increased reaching a maximum of 21.03 x 10^{-3} mol min^{-1} g_{met}^{-1} and 53.65 x 10^{-3}

mol min^{-1} g_{met}^{-1} at 458 K and 452 K respectively. The reaction rates of the $Pt_{90}Ni_{10}$-MCM-C catalyst was found to be higher than that of Pt_{100}-MCM-C, which demonstrated a maximum reaction rate of 27.08 x 10^{-3} mol min^{-1} g_{met}^{-1} at 412 K. It is also interesting to note that the $Pt_{50}Ni_{50}$-MCM-C catalyst gave rise to reaction rates that were similar to that of Pt_{100}-MCM-C despite the fact that only 65.7 % of the catalyst existed in a reduced state and that only half the Pt content is available. These enhanced reaction rates can be explained as due to the anchoring effect of the Ni^{2+} ions that aides the formation of well dispersed Pt particles as reported above.

The turnover frequency (TOF) values were calculated to gain an insight on the number of benzene molecules converted to cyclohexane on a catalytic site per second. This is tabulated in Table 8.5. Inactivity prevented the determination of this value for the Ni_{100}-MCM-C catalyst. However, the calculated TOF value for the $Pt_{10}Ni_{90}$-MCM-C catalyst is 0.020s^{-1}. Interestingly, the $Pt_{50}Ni_{50}$-MCM-C and $Pt_{90}Ni_{10}$-MCM-C catalysts show lower TOF values when compared to the Pt_{100}-MCM-C catalyst. In these cases, the TOF value of Pt_{100}-MCM-C is approximately 0.030s^{-1} more than the $Pt_{50}Ni_{50}$-MCM-C and $Pt_{90}Ni_{10}$-MCM-C, though an enhanced reactivity was seen for the latter catalysts. Based on these findings it is obvious that the Pt sites in the Pt_{100}-MCM-C catalysts are more reactive than those available in the bimetallic catalysts. However, the improved reactivity of the $Pt_{50}Ni_{50}$-MCM-C and $Pt_{90}Ni_{10}$-MCM-C catalysts may be ascribed as due to the availability of a larger amount of reaction sites as shown by H_2-chemisorption studies.

Table 8.5: Percentage of conversion, specific rates and TOF values of the PtNi supported MCM-41 catalysts prepared with various PtNi ratios.

Catalysts	Maximum Conversion (%)	Max Specific Rate (x 10^{-3} mol min^{-1} g_{met}^{-1})	Temp. at Max. Specific Rate (K)	Specific Rate at 350 K (x 10^{-3} mol min^{-1} g_{met}^{-1})	TOF[a] at 350 K (sec^{-1})
Ni_{100}-MCM-C	-	-	-	-	-
$Pt_{10}Ni_{90}$-MCM-C	1.8	0.77	416	0.17	0.020
$Pt_{50}Ni_{50}$-MCM-C	42.3	21.03	458	7.62	0.089
$Pt_{90}Ni_{10}$-MCM-C	85.4	53.65	452	10.72	0.091
Pt_{100}-MCM-C	74.0	27.08	412	7.41	0.121

8.8 Kinetic Investigations

Kinetic investigations were carried out for the $Pt_{50}Ni_{50}$-MCM-C catalyst. Conversions were ensured to be less than 10 %. It is found that the E_a of the $Pt_{50}Ni_{50}$ catalysts is 24.4 kJ mol^{-1}. Comparison with previous works showed that this value is lower than that of both Pt and Ni monometallic supported catalysts which have been reported to be in the range 50.3 kJ mol^{-1} [25] and 36.5 – 96.0 kJ mol^{-1} [6, 26, 27] correspondingly. In addition, this value is less than half of that exhibited by Lu and coworkers [28] who studied the synthesis of PtNi supported γ-Al_2O_3 catalysts for the hydrogenation of benzene. In their work, an E_a value of approximately 56.8 kJ mol^{-1} was obtained. Furthermore, they reported that the catalyst did not promote the hydrogenation of benzene when carried out in a flow reactor. Though it is acknowledged that the difference in the total metal content and the PtNi ratio may have caused this variation in the activation energy, it is

shown that synergistic effects can still occur for the catalysts with moderate to high Pt content.

Experimental reaction orders were calculated based on the empirical kinetic model,

$$r = kP_H^{m}P_{Bz}^{n} \quad (1)$$

where *m* and *n* are the partial orders of hydrogen and benzene correspondingly and k is the rate constant. Experimental results indicate that reaction orders of hydrogen and benzene is 1.6 and -0.5 respectively. Plots of the reaction rate as a function of the partial pressure of benzene or hydrogen are shown in Figure 8.7. These reaction orders are consistent with previous works which report values ranging from 1.0 – 2.0 and -1.7 – 0.30 correspondingly [5, 29]. The negative order of benzene indicates that benzene is strongly adsorbed on the catalysts [5]. This is confirmed via TPSR studies whereby both reversibly and irreversibly adsorbed benzene exists on the catalyst upon reaction and subsequent purging in helium. It was found that as much as 1.11 x 10^{-4} mol g_{met}^{-1} was desorbed from the catalyst as reversibly adsorbed benzene. In the case of irreversibly adsorbed benzene, hydrogen was required to remove the strongly adsorbed benzene. This leads to the desorption of 1.88 x 10^{-5} mol g_{met}^{-1} cyclohexane. In addition, previous work on the hydrogenation of o-xylene at 418 K reported that such negative values for aromatic reaction orders signifies a competitive adsorption of hydrogen and the aromatic molecule on a catalyst surface [30]. Taking these factors into consideration, as well as additional assumptions such as hydrogen adsorbs dissociatively while benzene adsorbs molecularly on similar active sites, a mechanism for the reaction can be derived based on the following equations.

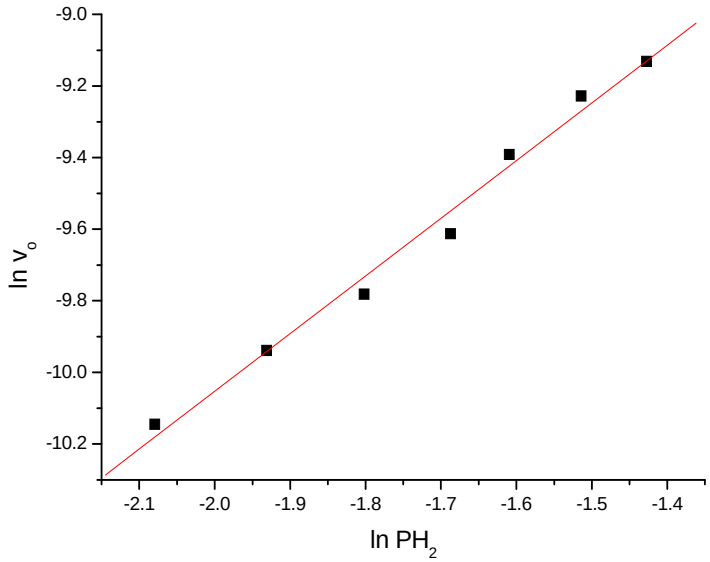

(a)

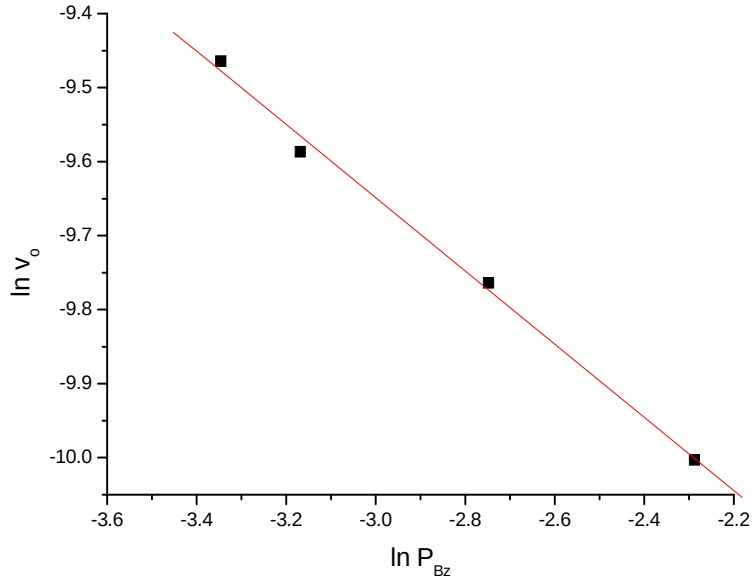

(b)

Figure 8.7: The dependence of the reaction rate on the partial pressure of (a) hydrogen (b) benzene.

$$H_2 + 2S \overset{K_H}{\leftrightarrow} 2\ H\text{-}S \tag{8.2}$$

$$C_6H_6 + S \overset{K_B}{\leftrightarrow} C_6H_6\text{-}S \tag{8.3}$$

$$C_6H_6\text{-}S + 3H\text{-}S \overset{K_E}{\leftrightarrow} C_6H_9\text{-}S + 2S \tag{8.4}$$

$$C_6H_9\text{-}S + H\text{-}S \overset{k}{\rightarrow} C_6H_{10}\text{-}S + S \tag{8.5}$$

$$C_6H_{10}\text{-}S + 3H\text{-}S \overset{fast}{\rightarrow} C_6H_{12}\text{-}S + 2S \tag{8.6}$$

$$C_6H_{12}\text{-}S \rightarrow C_6H_{12\ (g)} + S \tag{8.7}$$

This gives a Langmuir - Hinshelwood (L-H) expression as follows (Eq (8.8)):

$$r = \frac{kK_EK_BP_BK_H^2P_H^2}{(1 + K_BP_B)^2} \tag{8.8}$$

where k is the rate constant, K_H and K_B as well as P_H and P_B are the chemisorption constant and partial pressures of the hydrogen and benzene respectively and K_E is the equilibrium constant. The rate determining step (RDS) in this theoretical equation is the addition of the fourth hydrogen atom to an adsorbed benzene molecule. Plotting $P_HP_B^{1/2}/r^{1/2}$ as a function of P_B, results in a K_B and $kK_EK_H^2$ value of 44.83 and 5.01 x 10^{-3} respectively. A similar theoretical curve as the experimental was obtained when P_B is constant. However when P_H is constant, the theoretical curve was similar to the experimental data only at high partial pressures of benzene. This clearly indicates that a more complicated mechanism exists for these catalysts than described here.

8.9 Classical vs Non-classical Catalysts

The catalytic reactivity of catalysts prepared via classical methods using similar activation conditions as the catalysts prepared via non-classical methods were also investigated and compared to the non-classical catalysts synthesized at optimum conditions. Profiles of the specific rates as a function of temperature and the maximum specific rates of the catalysts are presented in Figure 8.8 and Table 8.6 respectively. Comparison of the profiles show that the reactivity of the catalysts prepared via classical methods increased slowly with reaction temperature, reaching a maximum at temperatures higher than 440 K. Further increase in the reaction temperatures led to a slight decrease in the reactivity of the catalysts in the temperature range studied. In contrast, the catalysts prepared via non-classical methods demonstrated a sharp increase followed by a decrease in the reaction rates which reaches near inactivity at approximately 500 K. Maximum reaction rates are observed at approximately 410 K.

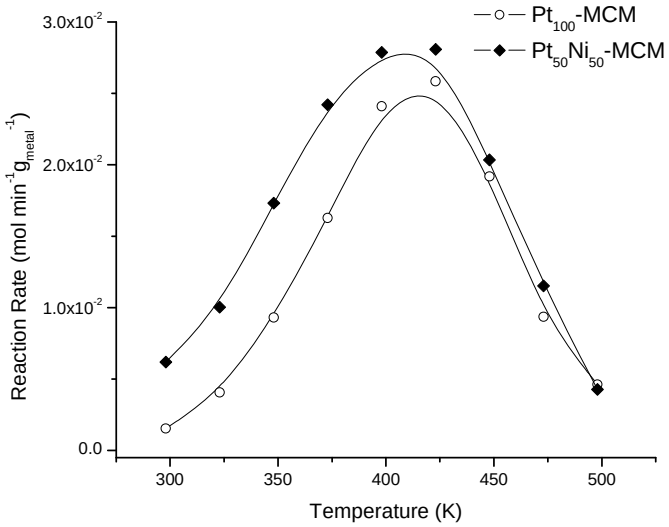

(a)

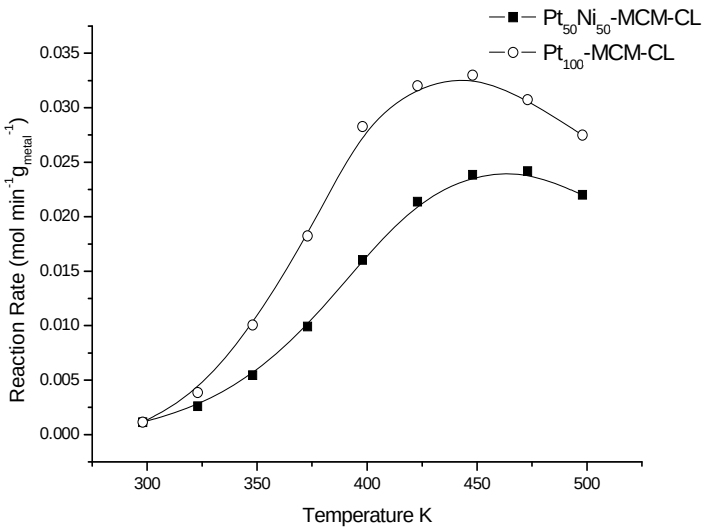

(b)

Figure 8.8: Hydrogenation of benzene profiles of the Pt_{100} and $Pt_{50}Ni_{50}$ catalysts prepared via (a) non-classical synthesized at optimum conditions and (b) classical methods.

Table 8.6: Specific rates of the $Pt_{50}Ni_{50}$ and Pt_{100} catalysts supported on MCM-41 prepared via classical and non-classical (synthesized at optimum conditions) methods. Catalysts activated at 473 K for duration of 15 minutes in 100 ml min^{-1} pure hydrogen.

Catalyst Denotation	Preparation Method	Specific Rate (x 10^{-3} mol min^{-1} g_{met}^{-1})	Temperature (K)
$Pt_{50}Ni_{50}$-MCM-CL	Classical	23.85	461
Pt_{100}-MCM-CL	Classical	32.59	441
$Pt_{50}Ni_{50}$-MCM	Non-classical	27.85	410
Pt_{100}-MCM	Non-classical	24.78	416

The variation in reactivity profiles as well as the temperature at which maximum reaction rates of the catalysts are achieved for the two methods, can be attributed to the pretreatment conditions of the catalysts. In terms of the reactivity profiles, the sharp deactivation observed in the catalysts prepared via non-classical methods may be due to the instability of the particles formed. This may be the result of the low temperature pretreatment conditions in contrast to the catalysts prepared via classical methods which were previously calcined at 773 K. The variation in the temperature in which maximum activity was observed for the classical and non-classical catalysts on the other hand, may be due to a difference in the surface geometry of the metal particles also as a result of the different pretreatment conditions. Even so, it is obvious that under similar activation conditions, the bimetallic catalysts prepared via classical methods exhibit similar reactivity with the PtNi catalysts prepared via non-classical methods. This can only be explained as due to the existence of a similar number

of active sites available in the catalysts, irrespective of the method of preparation employed.

8.10 Summary

To summarize, it is found that activation conditions in which optimum activity is obtained, for the PtNi bimetallic catalysts prepared via classical methods is at 373 K for 3 hours. The higher degree of reduction when the catalyst is activated at high temperatures, promotes aggregation that inevitably decreases catalytic reactivity. Studies of the PtNi catalysts with different ratios activated at low temperatures, demonstrated that the $Pt_{90}Ni_{10}$-MCM-C and $Pt_{50}Ni_{50}$-MCM-C catalysts gave rise to improved activity when compared to Pt_{100}-MCM-C. It is believed that this may be due to the anchoring effect of Ni^{2+} ions that result in well dispersed Pt particles. The contribution of the variation in particle morphology as well as alloying is not ruled out. However, no direct evidence was obtained to support the role of these two factors. Further, it is also found that catalysts prepared via classical and non-classical methods activated under similar conditions, showed similar reactivity.

8.11 References

[1] Z. B. Wang, G. P. Yin, P. F. Shi, J. Alloys Comp. 420 (2006) 126.

[2] E. Blosma, J. A. Martens, P. A. Jacobs, J. Catal. 165 (1997) 241.

[3] S. Lim, C. Wang, Y. Yang, D. Ciuparu, L. Pfefferle, G. L. Haller, Catal. Today 123 (2007) 122.

[4] J. Mikulova, J. Barbier Jr., S. Rossignol, D. Mesnard, D. Duprez, C. Kappenstein, J. Catal., 251 (2007) 172.

[5] R. Wojcieszak, S. Monteverdi, M. Mercy, I. Nowak, M. Ziolek, M. M. Bettahar, Appl. Catal. A: Gen., 268 (2004) 241.

[6] A. Lewandowska, S. Monteverdi, M. Bettahar, M. Ziolek, J. Mol. Catal. A: Chem., 188 (2002) 85.

[7] D. J. Kang, K. N. Kim, S. G. Kim, J. Mater. Sci. 40 (2005) 6283.

[8] A. Saadi, R. Merabti, Z. Rassoul, M.M. Bettahar, J. Mol. Catal. A: Chem., 253 (2006) 79.

[9] P. Kim, H. Kim, J. B. Joo, W. Kim, I. K. Song, Y. Yi, J. Mol. Catal. A 256 (2006) 178.

[10] J. C. Chaston, Plat. Met. Rev. 8 (1964) 50.

[11] T. Shima, J. Tominaga, Jpn. J. Appl. Phys. 42 (2003) 3479.

[12] J. Rynkowski, D. Rajski, I. Szyszka, J. R. Grzechowiak, Catal. Today, 90 (2004) 159.

[13] R. Lanza, P. Canu, S.G. Jaras, Appl. Catal. A: Gen., 348 (2008) 221.

[14] Y. Li, G. –H. Lai, R. –X. Zhou, Appl. Surf. Sci. 253 (2007) 4978.

[15] L. P. R. Profeti, J. A. C. Dias, J. M. Assaf, E. M. Assaf, J. Power Sources, 190 (2008) 525.

[16] R.-M. Jao, T.-B. Jao, and J.-R. Chang, J. Catal., 161 (1996) 222.

[17] M. Che, Z. X. Cheng, C. Louis, J. Am. Chem. Soc. 117 (1995) 2008.

[18] Y. I. Yermakov, B. N. Kuznetsov, I. A. Ovsyannikov, A. N. Startsev, S. B. Erenburg, M. A. Sheromov, React. Kinet. Catal. Lett. 8 (1978) 377.

[19] J. T. Miller, B. L. Mayers, M. K. Barr, F. S. Modica, D. C. Koningsberger, J. Catal. 159 (1996) 41.

[20] A. Punnoose, M.S. Seehra, I. Wender, Fuel Process. Technol., 74 (2001) 33.

[21] S. Mukerjee, S. Srinivasan, M. P. Soriaga, J. McBreen, J. Phys. Chem. 99 (1995) 4577.

[22] H. Yang, C. Coutanceau, J.-M. Léger, N. Alonso-Vante, C. Lamy, J. Electroanal. Chem., 576 (2005) 305.

[23] B. Lim, X. Lu, M. Jiang, P. H. C. Camargo, E. C. Cho, E. P. Lee, Y. Xia Nano Lett., 8 (2008) 4043.

[24] H. Song, F. Kim, S. Conner, G. A. Somorjai, P. Yang , J. Phys. Chem. B, 109 (2005) 188.

[25] S. D. Lin, M.A. Vennice, J. Catal., 143 (1993) 563.

[26] R. Molina, G. Poncelet, J. Catal., 199 (2001) 162.

[27] C. Miradatos, J.A. Dalmon, G.A. Martin, J. Catal., 105 (1987) 405.

[28] S. Lu, W. W. Lonergen, J. P. Basco, S. Wang, Y. Zhu, Y. Xie, J. G. Chen, J. Catal., 259 (2008) 260.

[29] P. Marécot, Appl. Catal., 74 (1991) 261.

[30] S. Smeds, T. Salmi, D. Murzin, Appl. Catal. A: Gen., 145 (1996) 253.

CHAPTER 9

CONCLUSIONS

9.1 Conclusions

In this research, PtNi supported silica catalysts were mainly synthesized via non-classical methods using $NaBH_4$ as the reducing agent. Various preparation techniques and reduction parameters were investigated. The main intention of these studies is to understand the formation and structure of the PtNi bimetallic particles on silica support (either crystalline silica or MCM-41) and their effect on the hydrogenation of benzene to cyclohexane. Besides that, for comparison, PtNi supported silica catalysts were also prepared via classical methods. In this case, pure H_2 gas was used as the reducing agent. The salient features of the catalysts are as follows.

1. In general, the results obtained demonstrate that when catalysts were prepared using $NaBH_4$ as the reducing agent, total reduction of the metal phases occur during the preparation stage for majority of the catalysts. This was shown via H_2-TPR analysis whereby any hydrogen consumption observed is mainly attributed to surface oxidation of the metallic phase which occurs during storage. This shows that in contrast to the classical methods, this synthesis method is effective in forming reduced metal particles at low temperatures.

This eliminates the necessity for calcinations and activation at high temperatures for long durations.

2. The co-precipitation (CP) as well as co- and step-impregnation (CI and SI) techniques were studied for the synthesis of Pt/Ni bimetallic particles on crystalline silica. All preparation techniques showed that higher reactivity was obtained for the bimetallic catalysts in comparison to the monometallic Ni catalysts. However, similar findings were not observed when the bimetallic catalysts were compared to the respective monometallic Pt catalyst. In this case, only the $Pt_{90}Ni_{10}$-CP as well as the $Pt_{55}Ni_{45}$-CI and $Pt_{92}Ni_{8}$-CI catalysts showed synergistic effects whereby an enhanced or similar reactivity to the corresponding monometallic Pt catalysts were seen. Results show that the catalytic trends for these catalysts were largely dependent on the surface properties and structure of the bimetallic phase. Based on XRD as well as TEM or SEM analysis with x-mapping, it was found that catalysts with an enhanced reactivity occur as alloys. Furthermore, XPS studies showed that in these alloys, surface segregation of Pt occurs.

3. As the formation of alloys is believed to improve catalytic reactivity, a comprehensive study on the synthesis of unsupported PtNi alloys was conducted. The effect of reduction temperature and oleic acid concentration were investigated to determine the conditions in which dispersed alloys were formed. Less aggregated PtNi alloy particles were obtained when the metal salts were reduced at 353 K with more than 0.2 M of oleic acid. Though these alloys were subsequently deposited onto the silica support, enhanced reactivity was not observed. In fact, all the bimetallic catalysts synthesized

via this technique showed a low catalytic reactivity. Analysis using H_2-TPD strongly indicated that surface segregation of Ni on these catalysts may have occurred, leading to the low catalytic reactivity. However, the inhibiting effect of oleic acid still covering the metallic particles even after activation may have contributed to the low reactivity.

4. Further studies on improving the catalytic reactivity of the catalysts were carried out by focusing on the reduction conditions of the metal salts. Three parameters were investigated and it was found that optimum reactivity was obtained when the metallic particles were synthesized at 273 K using 0.3 M of $NaBH_4$ and in a reduction medium of ethanol. TEM analysis revealed that these parameters influenced the morphology of the particles. Finer and better dispersed particles were obtained under these synthesis conditions.

5. A comparison between the catalysts synthesized using non-classical methods with that prepared via classical methods was also conducted. Under similar activation conditions, the bimetallic catalysts prepared via borohydride reduction gave a better reactivity when compared to that prepared via classical methods. Further studies on the catalysts prepared via classical methods activated to obtain optimum reactivity showed that the bimetallic catalysts exhibited finer dispersed particles in contrast to the monometallic Pt particles leading to the improved reactivity observed for several catalysts.

Discussion of the results obtained shows that explanation of surface and catalytic properties of materials prepared resides on the metal particles morphology which, in turn, depends in the mechanism of their formation. As a whole, this study showed that both alloyed and non-alloyed bimetallic catalysts can promote the enhancement of a catalytic reactivity.

1. Alloyed PtNi particles were formed when strong reducing agents were used in an aqueous media, as this allowed better contact between the metal salts. Under these synthesis conditions the influence of the type of support employed is less significant. The effect of the reduction conditions is more crucial as the nucleation and growth rates are affected upon varying the $NaBH_4$ concentration, temperature and medium in which reduction was carried out. This is mainly because the formation of the bimetallic particles occurs primarily in the colloidal state.
2. Further, when alloyed bimetallic particles are formed, it is important to ensure that surface segregation of Ni does not occur as this result in catalysts with a low reactivity. In contrast, better catalytic reactivity is observed when Pt segregation takes place. The environment in which the bimetallic particles are treated in, affects which metal segregates to the surface of the alloy. In the absence of oxygen species, Pt tends to segregate to the surface of the alloyed particles formed when heated. However, the presence of oxygen species (e. g. from oleic acid) promotes metal particles with a higher affinity towards oxygen, to the surface of the alloyed structures. In this case, surface segregation of Ni is seen.
3. This study has also shown that the formation of alloyed bimetallic particles were not a necessary requirement to obtain improved catalytic reactivity

when compared to the respective monometallic catalysts. Non-alloyed bimetallic particles can also exhibit such characteristics. This was shown for the Pt/Ni bimetallic nanoparticles supported on MCM-41 prepared via classical methods. This study demonstrated that reduction of the metal salts in a gas phase environment disables sufficient mixture of the metals involved, leading to the formation of monometallic particles. Here, considering that a support with a large surface area was employed, the Ni^{2+} ions acts as anchoring sites for the formation of fine Pt nanoparticles. This prepared a larger surface area available for reactions to occur upon low temperature activation.

9.2 Recommendations for Future Work

Considering that catalysts play a crucial role in every aspect of our lives and that though numerous studies have been conducted on supported bimetallic systems, very little is known on the design of PtNi bimetallic supported catalysts for hydrogenation reactions. It is therefore important that this work is researched further. The following are some suggestions for future work in this area:

- Fractals are known to exhibit unique characteristics. However, very limited work have been presented on how these structures especially those formed from more than one metal effects catalytic reactions. Therefore it is proposed that a thorough investigation is conducted on how to control the PtNi fractal morphology on supports as well as their influence on catalytic reactions.
- Finally, as non-classical methods have proved to be an efficient method in synthesizing totally reduced bimetallic particles, the need for long activation durations at high temperatures can be avoided. Hence, other reducing agents

such as hydrazine and alcohol reduction can be investigated for the synthesis of supported PtNi bimetallic particles. These reducing agents may enable a better control for the morphology in terms of size, of the alloyed particles formed.

LIST OF PUBLICATIONS AND PRESENTAIONS

Publications

1. **N. N. H. Abu Bakar**, M. M. Bettahar, M. Abu Bakar, S. Monteverdi, J. Ismail and M. Alnot, PtNi catalysts prepared via borohydride reduction for hydrogenation of benzene, J. Catalysis, 265 (2009) 63.
2. **N. N. H. Abu Bakar**, M. M. Bettahar, M. Abu Bakar, S. Monteverdi, J. Ismail and M. Alnot, Silica supported PtNi alloys prepared via co-precipitation method, J. Molecular Catalysis A, 308 (2009) 87.
3. **N. N. H. Abu Bakar**, M. M. Bettahar, M. Abu Bakar, S. Monteverdi and J. Ismail, The Effect of Preparation Parameters of MCM-41 Supported PtNi Catalysts and their Hydrogenation Properties, Catalysis Letters 130 (2009) 440.

Presentations

1. **N. H. H. Abu Bakar**, M. Bettahar, M. Abu Bakar, S. Montervedi, J. Ismail, Surface and Catalytic Properties of Supported PtNi Nanoparticles. *International Conference on Chemical Sciences*, 24th-26th May 2007, Yogyakarta, Indonesia.
2. **N. H. H. Abu Bakar**, M. M. Bettahar, M. Abu Bakar, S. Monteverdi and J. Ismail, Synthesis of PtNi Bimetallic Nanoparticles for Catalytic Application, *Europacat VII, 2007*, July 2007, Finland.
3. **N. H. H. Abu Bakar**, M. M. Bettahar, M. Abu Bakar , S. Monteverdi, and J. Ismail, Hydrogenation of Benzene over Silica Supported PtNi Catalysts Prepared via Co-impregnation Technique, *12th Asian Chemical Congress (12ACC)*, 23th-25th August 2007, Kuala Lumpur, Malaysia.
4. M. Abu Bakar, **N. H. H. Abu Bakar**, M. M. Bettahar, S. Monteverdi and J. Ismail, Effect of Different Preparation Techniques on the Activity of Benzene Hydrogenation, *Nanotech. Malaysia and Asia Nano Forum Summit 2007*, 29th Nov – 1st Dec 2007, Kuala Lumpur, Malaysia
5. M. M. Bettahar, **N. H. H. Abu Bakar**, M. Abu Bakar, S. Monteverdi and J. Ismail, Enhancing the Hydrogenation of Benzene via the PtNi-MCM Supported Catalysts, *Nanocatalysis: Fundamentals and Applications*, 9th-12th July 2008, Dalian, China.
6. **N. H. H. Abu Bakar**, M. M. Bettahar, M. Abu Bakar, S. Monteverdi and J. Ismail, PtNi Supported Silica Catalysis for Gas Phase Hydrogenation of Benzene. *14th International Congress on Catalysis*, 13th-18th July 2008, Seoul, Korea.
7. M. M. Bettahar, **N. H. H. Abu Bakar**, M. Abu Bakar, S. Monteverdi and J. Ismail, PtNi-MCM-41as Potential Catalysts for the Conversion of Benzene to Cyclohexane. *Europacat IX, 30th August-4th Sept 2009*, Salamanca, Spain.

APPENDIX

Flow Diagram of Study

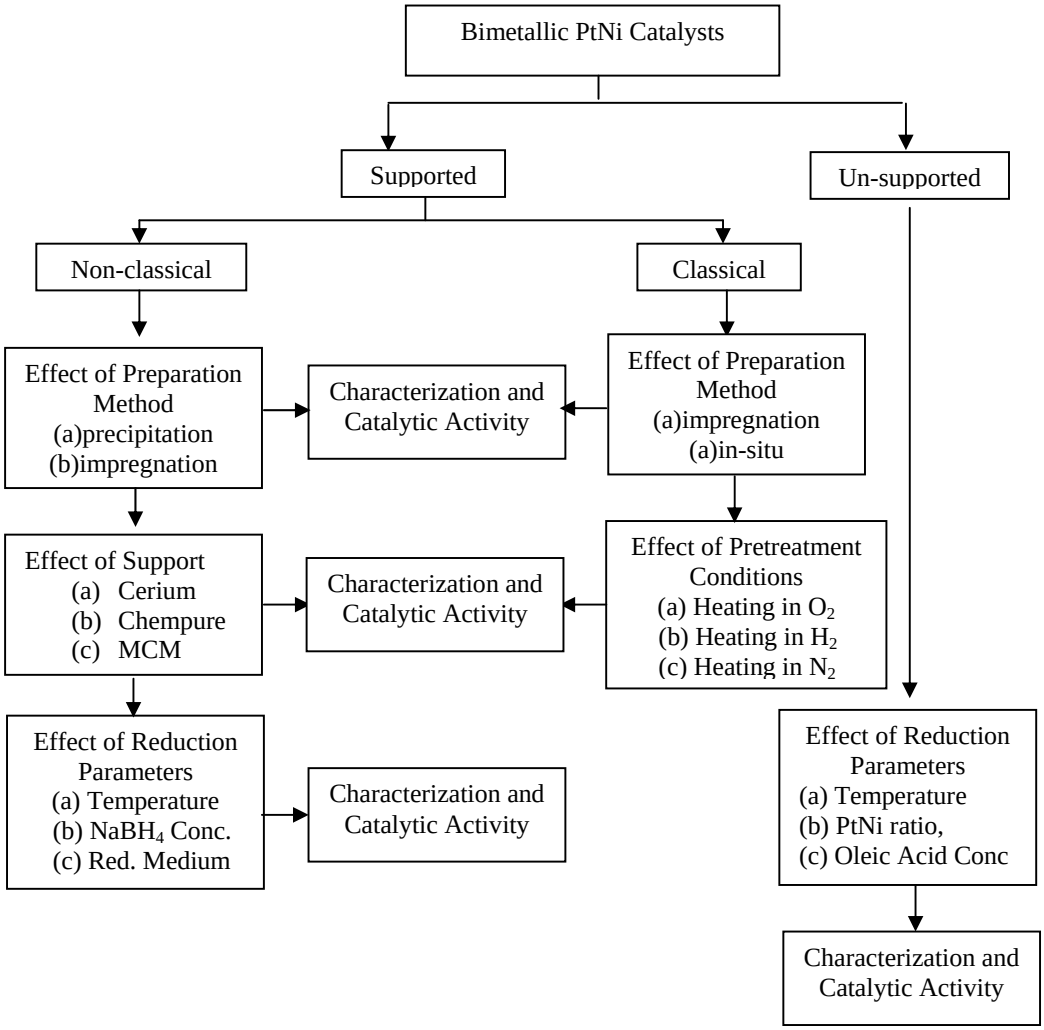

Flow Diagram of Catalyst Preparation Method

A) Preparation methods for non-classical catalysts without oleic acid

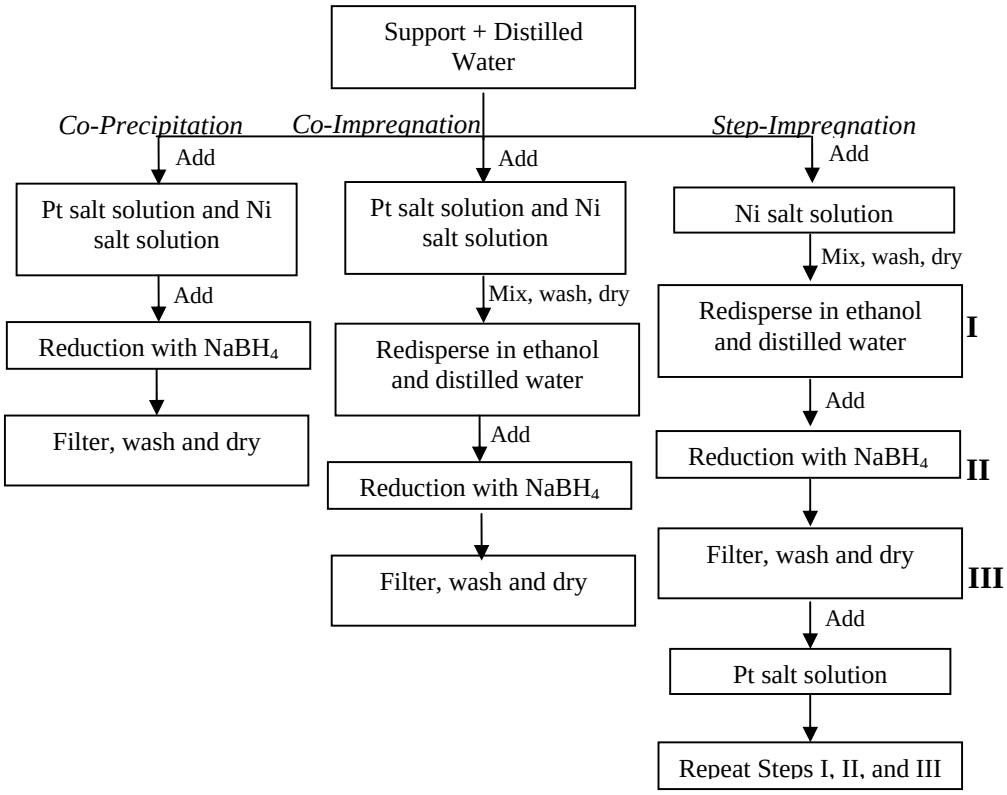

B) Preparation method for non-classical catalysts with oleic acid

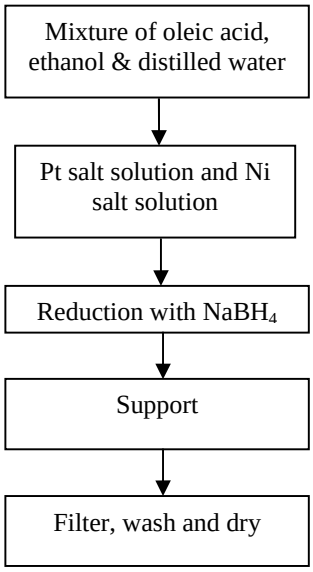
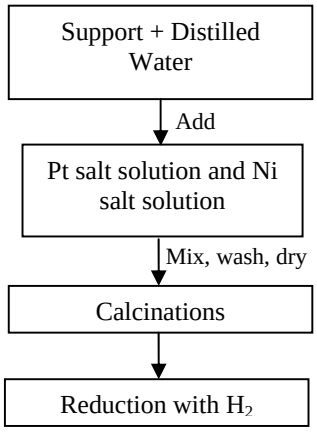
C) Preparation method for classical catalysts